



UNIVERSITÀ DI NAPOLI “FEDERICO II”

DOTTORATO DI RICERCA

XIX CICLO TRASPORTI

Comportamento dinamico e valutazione di sistemi di controllo attivo per una fusoliera di velivolo da trasporto con impiego di attuatori magneto-strittivi

Candidato
Ing Michele Iadevaia

Coordinatore Corso di Dottorato
Prof. Ing. Vincenzo Torrieri

Tutor
Prof. Ing. Leonardo Lecce

Napoli, Novembre 2007

ABSTRACT

This work presents the activities developed within the Research Project “MESEMA” funded by the European Commission. Structural dynamics, acoustics, active materials and active control systems represent the scientific topics of the project with the goal of designing and developing five systems integrating vibration transducers based on active components. Among these a noise & vibration control system using magnetostrictive actuators will be designed, developed and tested, with the goal of controlling noise & vibrations in a frequency range between 150 – 500 Hz. The primary noise & vibration excitations will be representative of a small/medium turboprop aircraft case. Final results of the task will be represented by a system made up of about 30 actuation/sensing devices connected to a aeronautical structure performing control of external disturbances as well as of the devices’ intrinsic non linearity. As experimental test article a fuselage mock-up of the ATR42/72 aircrafts family has been chosen available at the acoustic laboratory in the Alenia plant; due to its geometry and overall dimensions it well represents a fuselage section of a generic regional jet.

In the first chapter a general overview and state of art of Active noise control is presented. Active noise control (ANC) is achieved by introducing a canceling "antinoise" wave through an appropriate array of secondary sources. These secondary sources are interconnected through an electronic system using a specific signal processing algorithm for the particular cancellation scheme. ANC is an effective way to attenuate noise that is very difficult and expensive to control using passive means. It has application to a wide variety of problems in manufacturing, industrial operations, and consumer products. Many industrial companies and universities are currently engaged in ANC research and development.

The second chapter covers a general review of the MESEMA project. MESEMA, a technology oriented research program, builds upon the success of previous EU projects with devotion to accomplish the objectives of the aeronautics priority through designing, producing and testing “innovative transducer systems based on active materials“. Four fixed and rotary-wing aircraft companies accompanied by SMEs and university research institutes will take part in and benefit from the developments of primarily magneto-elastic transducers for high-torque actuation, vibration and noise reduction, electrical energy generation and structural health monitoring. Structural dynamics, energy conversion in active materials and control systems represent the scientific fundamentals of the project. The scientific and technological objectives are the results of a spontaneous evolution of the research activities developed during the last six years by the group which built the first consortium related to the European research program named “M.A.D.A.Vi.C.". That group focalized its activity on two main strictly correlated research paths: increasing the knowledge and creating a unique team of experts of “design and development of innovative actuation systems based on magnetostrictive materials”; customizing the expertise of this team for the analysis and solution of specific needs of the next generation aircraft in terms of actuation systems including driving electronics and control aspects.

The third chapter deal about the experimental and numerical modeling. The test-article reproducing a real fuselage sections, has been used in the “untrimmed configuration”, i.e. without interior furnishing and seats. The cylinder is closed at the two ends by heavy caps bolted to final flanges, and a proper spring system and fixture connection allow both vibration isolation and free longitudinal deformation of the fuselage section.

The experimental tests were aimed to extract modal parameters of both structure and acoustic volume in order to allow the numerical-experimental correlation and the updating of the model. The structural natural frequencies and modes shapes were extracted from the experimental measurements up to 300Hz, but it was not possible to classify all the extracted modes since above

120 Hz the local panels dynamics is dominant over the global mode shapes and the geometric description of the global modes becomes more difficult.

In designing the F.E. model, the author took in account the typical flexural wavefield behaviour of cylinders, including low frequency beam modes, intermediate frequency cylinder modes, and high frequency plate modes. In order to calculate the necessary maximum elements dimensions to reach an analysis frequency of about 1000 Hz, it has been necessary to determine the number of wavelengths around the circumference (m) and the number of wavelengths along the fuselage (n) correctly.

The numerical analysis results have been compared with those coming from experimental tests. The common results of modal testing is a set of modal parameters (resonance frequencies, damping and mode shapes), which characterise the linear dynamics of the structure. Different methodologies for the correlation analysis exist. Within this work the Modal Assurance Criterion (MAC) has been used: it compares all mode shapes in the numerical database with all mode shapes in the experimental database

The last chapter covers the Active control simulation. Two control strategies have been simulated: the first one consisting in an Active Structural Acoustic Control (ASAC) aimed to reduce interior noise by controlling the corresponding structural vibrations on the fuselage section; the second one consisting in an Active Noise Control (ANC) aimed to reducing directly interior noise actuating the structural components, but without attempting necessary to reduce vibrations levels

For what concerning the simulation of the actuators actions on the structure, the initial basic idea has been to focus on inertial actuators able to provide concentrated forces in their application point. As a consequence they have been modelled as single point force acting on the selected nodes of the F.E. model, neglecting their coupling with the dynamics of the overall fuselage structure. It has been chosen to optimize actuation locations and obtain required forces for each one of them contemporarily employing the well known optimization (pseudo-inverse).

Optimal control actuators placement employing genetic algorithms. In order to select among the many possible sets of control actuator configurations an optimisation activity was required. The used optimisation method is based on “genetic” algorithms: it is well known that they represent a quite fast, not deterministic approach for selection among many possible solutions of a problem whose effectiveness can be measured by a “score

Magnetostrictive control actuator characterisation and structural impedance correlation

In order to characterise the LPA actuator type in terms of force performances once installed on the fuselage section, a measurement campaign has been carried out at the Alenia Aeronautics plant in.

Laser vibrometer has been employed in order to measure the vibration spectra on the centre flange of the actuator as far as on its seismic masses. It is possible from these simple measurements to calculate the inertial force spectra provided by the actuator to the host structure.

Appendix A reports the activities carried out by Unina-DPA and LFME for selecting the optimal location of the actuator/sensor pairs with the use of Genetic Algorithms

Appendix B appendix reports the activities carried out by DII-SUN and LFME for selecting the most appropriate control algorithm for noise reduction.

ACKNOWLEDGMENT

The author wish to acknowledge and thank the MESEMA project consortium members. He also thank the European Community and the European Commission for the financial support of this activity under Contract N° AST3-CT-2003-502915.

He would also like to thank my supervisors Prof. Leonardo Lecce and Ernesto Monaco who guided me through some of the problems of the thesis. Finally I would like to thank the people who proof read this thesis.

TABLE OF CONTEST

ABSTRACT	2
ACKNOWLEDGMENT	4
TABLE OF CONTEST	5
LIST OF DIAGRAMS	8
LIST OF TABLES	10
NOMENCLATURE	11
GLOSSARY	12
1 STATE-OF-THE-ART IN ACTIVE NOISE CONTROL (ANC)	14
1.1 Introduction	14
1.2 Control algorithms	14
1.3 Early developments	15
1.4 Recent advances	16
1.5 Trends	20
2 PROJECT MESEMA	22
2.1 PROJECT OBJECTIVE (S)	22
2.2 Mesema Workplan	24
2.2.1 Introduction	24
2.2.2 Planning and timetable	24
2.2.3 Work package description	28
2.2.4 Relevance to the objectives of the Aeronautics and Space Priority	30
2.2.5 Potential Impact	33
2.3 Work package description	38
2.3.1 WP2 – Noise and Vibration Control	38
2.3.2 WP5 – Vibrational electrical energy (VIBEL)	42
3 THE TEST ARTICLE: EXPERIMENTAL AND NUMERICAL MODELLING	56
3.1 INTRODUCTION	56
3.2 EXPERIMENTAL MODAL ANALYSIS	56
3.2.1 APPROACH	57

3.2.2	FREE-FREE BOUNDARY CONDITIONS	58
3.2.3	INPUT SET-UP	59
3.2.4	CALCULATION OF THE FREQUENCY RESPONSE FUNCTION	60
3.2.5	TEST SETUP	60
3.2.6	EXCITATION	61
3.2.7	ACQUISITION	61
3.2.8	ANALYSIS	65
3.2.9	RESULTS	66
3.2.10	STRUCTURAL ELASTIC MODEL LEFT EXCITATION	66
3.2.11	STRUCTURAL ELASTIC MODE RIGHT EXCITATION	68
3.2.12	VALIDATION PARAMETERS	71
3.3	Frame Modal Hammer Test	75
3.3.1	APPROACH	75
3.3.2	INPUT SET-UP	76
3.3.3	CALCULATION OF THE FREQUENCY RESPONSE FUNCTION	77
3.3.4	TEST SETUP	77
3.3.5	EXCITATION	77
3.3.6	ACQUISITION	77
3.3.7	ANALYSIS	79
3.3.8	RESULTS	79
3.3.9	HAMMER TEST	80
3.3.10	CONCLUSION	82
3.3.11	DESCRIPTION OF THE NUMERICAL (F.E.) MODEL	84
	Mode	84
3.3.12	NUMERICAL MODAL ANALYSIS	88
3.3.13	NUMERICAL-EXPERIMENTAL CORRELATION	90
3.3.14	CONCLUSIONS	102
4	ACTIVE CONTROL SIMULATION	103
4.1	Control of noise on turbofan	103
4.2	Operating conditions of the noise control system	104
4.1	SETUP OF THE TEST ARTICLE	105
3.1.	PRIMARY EXCITATION	105
3.2.	ACTUATORS' INSTALLATION	106
4.2	SENSORS' INSTALLATION	108
4.3	CONTROL SYSTEM INSTALLATION	108
4.4	ASSESSMENT OF THE CONTROL CHANNELS BEHAVIOUR	111
4.4.1	Power amplifiers	112
4.5	EXPERIMENTAL CHARACTERIZATION	113
4.6	ACTUATORS' CHARACTERIZATION	113
4.7	PASSIVE CHARACTERIZATION OF THE TEST ARTICLE	115
4.7.1	Data Selection	116
4.7.2	Stabilization Diagram – Poles selection	117
4.7.3	List of modes	119
4.7.4	Validation of the selected modes	122
4.8	DYNAMIC MODEL IDENTIFICATION FOR CONTROL PURPOSES	127

4.9	TUNING OF THE CONTROL ALGORITHM	128
4.10	ACTUATORS' CONTROL LOOP	128
4.11	NOISE CONTROL LOOP	128
4.12	EXPERIMENTAL RESULTS	129
4.13	LOW LEVEL CONTROL RESULTS	129
4.14	HIGH LEVEL CONTROL RESULTS	130
5	CONCLUSIONS	134
	APPENDIX A – ACTUATOR/SENSOR PLACEMENT	135
	Optimal positioning approach proposed by LFME	135
	Calculation of the FRF's between the candidate sensors and actuators	135
	Description of the developed GA	137
	GA simulations and results	139
	Optimal positioning approach proposed by Unina-DPA	151
	Conclusions	156
	APPENDIX B – NOISE CONTROL ALGORITHM	156
	APPENDIX B - Noise control algorithm based on an expert system proposed by LFME	156
	Description of the Expert System	158
	ANN modelling of the structure	159
	The developed GA	161
	Simulation runs	164
	Noise control algorithm proposed by DII-SUN	171
	Experimental results with the test article	173
	Selection of final noise control algorithm	174

LIST OF DIAGRAMS

Figure 1-1: R&D Programs for noise and vibration control.....	36
Figure 2-1: <i>Response Points</i>	58
Figure 2-2: Input AutoPower.....	62
Figure 2-3: Driving Point FRF Function.....	62
Figure 2-4: <i>Driving Point Coherence Function</i>	63
Figure 2-5: Input AutoPower Spectrum	64
Figure 2-6: <i>Driving Point FRF Function</i>	64
Figure 2-7: Driving Point Coherence Function	65
Figure 2-8: Main Components of the Test Setup	66
Figure 2-9: Stabilization Diagram Polymax® method	67
Figure 2-10: Stabilization Diagram Polymax® method	68
Figure 2-11: Mode 47.749 Hz.....	70
Figure 2-12: Mode 57.527 Hz.....	71
Figure 2-13: Mode 61.469 Hz	71
Figure 2-14: Mac Left Excitation.....	72
Figure 2-15: Mac Right Excitation	73
Figure 2-16: Response Points	76
Figure 2-17: Input AutoPower.....	78
Figure 2-18: Driving Point FRF Function	78
Figure 2-19: Driving Point Coherence Function	79
Figure 2-20: Acquired points	80
Figure 2-21: Stabilization Diagram Polymax® method.....	80
Figure 2-22: Mode 133.628 Hz.....	81
Figure 2-23: Mode 151.364 Hz.....	82
Figure 2-24: Mode 165.619 Hz.....	82
Figure 2-25: <i>Original F.E.M. model</i>	84
Figure 2-26: <i>Modal density 2D</i>	85
Figure 2-27: <i>Frequency vs n and m</i>	87
Figure 2-28: <i>The new model structural F.E.M.</i>	87
Figure 2-29: <i>The fluid model.</i>	88
Figure 2-30: The coupling model fluid-structural.....	88
Figure 2-31 Mode 77.07 Hz.....	89
Figure 2-32 Mode 86.61 Hz.....	89
Figure 2-33 Mode 95.68 Hz.....	89
Figure 2-34 Mode 99.93 Hz.....	90
Figure 2-35: Mode 116.73 Hz.....	90
Figure 2-36 Experimental acquisition mesh and F.E. model	91
Figure 2-37: Exp_num modal analysis correlation	97
Figure 2-38: Detail of the springs	98
Figure 2-39: The springs on the global model.....	98
Figure 2-40: Exp_num modal analysis correlation	101
Figure 3-1: Full-scale mock-up used for testing of the noise control system.....	105
Figure 3-2: Optimal actuators location and channel numbers	106
Figure 3-3: Actuator couple mounted on a frame	107
Figure 3-4: Actuator mounted on a stringer	107
Figure 3-5: Accelerometer mounting description	108
Figure 3-6: Control system layout	109

Figure 3-7: Installation of actuators and sensors inside the fuselage.....	110
Figure 3-8: Installation of power and conditioning electronics.....	110
Figure 3-9: View of whole control system.....	111
Figure 3-10: Actuators mounting: frame configuration.....	113
Figure 3-11: Actuators mounting: stringer configuration.....	113
Figure 3-12: <i>Laser tests set-up</i>	114
Figure 3-13: <i>Laser measurement (seismic mass)</i>	114
Figure 3-14: <i>Comparison between actuator force spectra measured left: fuselage stringer mounted – right: laboratory measurement</i>	115
Figure 3-15 <i>Comparison between numerical and experimental fuselage structural impedances (inertance)</i>	115
Figure 3-16: Sum FRF and MIFs.....	117
Figure 3-17: Stabilization Diagram.....	119
Figure 3-18: Mode Shape at 51.08 Hz.....	120
Figure 3-19: Mode Shape at 51.88 Hz.....	121
Figure 3-20: Mode Shape at 61.64 Hz.....	121
Figure 3-21: Mode Shape at 122.14 Hz.....	122
Figure 3-22: <i>Example of synthesised FRFs</i>	124
Figure 3-23: Example of synthesised FRFs.....	125
Figure 3-24: Auto-MAC.....	127
Figure 3-25: <i>Identification result in a control point</i>	128
Figure 3-26: Complete control scheme.....	128
Figure 3-27: Actuator behaviour at different current: control off (blue), control on (red).....	130
Figure 3-28: Primary force field from specifications.....	131
Figure 3-29: Primary field from specs: control off (blue), control on (red).....	131
Figure 3-30: Random noise primary force field.....	132
Figure 3-31: Random noise primary field: control off (blue), control on (red).....	132
Figure 3-32: Vibration reduction with a random noise primary field: control off (blue), control on (red).....	133
Figure 3-33: Random noise in a co-located configuration: control off (blue), control on (red).....	133

LIST OF TABLES

Table 1-1: Work package list.....	27
Table 1-2: Participant list	29
Table 2-1: List of the Mode-Shapes.....	68
Table 2-2: List of the Mode-Shapes.....	69
Table 2-3: <i>List of the Mode-Shapes in the two tests</i>	70
Table 2-4: Mac Values	73
Table 2-5: List of the Mode-Shapes.....	81
Table 2-6: Structural natural frequencies [Hz] Numerical-Experimental comparison	84
Table 2-7: Grid points – acquisition points combination	91
Table 3-1: Components list of the final test bench	110
Table 3-2: Modal Frequencies and modal damping.....	120
Table A 1”Comparison Table between 400 and 126 candidate points.	147

NOMENCLATURE

GLOSSARY

MESEMA	European Founded Project: Sixth Framework Programme for Research and Technological Development: Magnetoelastic Energy Systems for Even More Electric Aircraft
M.A.D.A.Vi.C	European Founded Project: Sixth Framework Programme for Research and Technological Development”: Magnetostrictive Actuators for Damage Analysis and Active Vibration Control
M.E.S.A	European Founded Project: Sixth Framework Programme for Research and Technological Development
Uni-NA DPA	Università degli Studi di Napoli “Federico II” - Dipartimento di Progettazione Aeronautica
EURICE	European Research and Project Office GmbH
LPA-ZIP	Universität des Saarlandes (Saarland University)
DII-SUN	Seconda Università degli Studi di Napoli - Dipartimento di Ingegneria Dell’Informazione
ALA	Alenia Aeronautica S. p. A.
EADS-CRC	EADS Deutschland GmbH, Corporate Research Center
ZFL	ZF-Luftfahrttechnik GmbH
TACT	TACT Technology Ltd
CED	CEDRAT Technologies S. A.
CHALMERS	Chalmers Tekniska Högskola
ECD	EUROCOPTER DEUTSCHLAND GmbH
NIRDTP	National Institute of Research and Development for Technical Physics
KTH	Kungliga Tekniska Högskolan
LFME	Laboratory of Fluid Mechanics and Energy
MECEL	Mecel AB
NEWLANDS	Newlands Technology Ltd
PARAGON	Paragon Ltd.
USAL	University of Salford
WP1	Materials research and technology review
WP2	Noise and vibration control
WP3	Health monitoring
WP4	High-torque actuation
WP5	Vibration electrical energy (Vibel)
WP6	Dissemination and exploitation
WP7	Project management
FRF	Frequenci Response Function
FFT	Fast Fourier Function

MAC	Modal Assurance Criterion
LMS-CADA-x	Modal Analysis Software
FE	Finite Element
FEM	Finite Element Methods
EMA	Experimental Modal Analysis
HP	Hewlett-Packard
LMS	LMS International N.V. Leuven Belgium
MIFs	Modal Indicator Factors
LS	Least Square Difference Normalized
AVC	Active Vibration Control
GA	Genetic Algorithm
RNG	Random Number Generator
AVCS	
GASS	EU Founded project "A Generic Active Vibration Control System of Surfaces"
ANN	Artificial Neural Network
LFME	

1 STATE-OF-THE-ART IN ACTIVE NOISE CONTROL (ANC)

The chapter reviews techniques of active noise and vibration cancellation. Early developments and recent advances are surveyed including the theoretical background.

Some of the old and a myriad of new applications are referred to in the text.

1.1 INTRODUCTION

In general, the principle of active noise and vibration attenuation does not change, whatever system it is applied to. This principle postulates that when opposite noise and vibration fields are equal to the original ones, but in "anti phase", the two sounds will cancel each other by "destructive interference". An anti-noise or vibration is usually transmitted by a loudspeaker or a vibration transducer to the protected area in order to cancel there the existing unwanted noise/vibration. On the other hand, sounds to be heard, like speech, are subtracted from the canceled noise. These wanted sounds are reintroduced and remain at the end of the process undistorted within the domain of concern. Despite the fact that the use of destructive interference in acoustics was already understood in the last century (Rayleigh, 1877, # 264 and Tyndall, 1873, ch. 1), the earliest known exploitation of it in ANC is a French patent by Coanda (1932). However, a more technical approach is linked to an invention published shortly later, in 1933, and patented during 1936 by Paul Lueg, a doctor of philosophy and medicine.

Lueg outlines the principle: The unwanted sound is picked up by one or more microphones, their electrical signal feed, to one or more loudspeakers so that the sound wave produced is in "phase opposition" to the primary unwanted sound and cancels it. No physical argument was given explicitly in Lueg's patent. Later, the subject was developed into "active noise control" (ANC), which has now a precise theoretical and practical basis. Another early development is attributed to Bschorr (1969) for three patents about ANC, including noise elimination by an exact duplicate which is out of phase by 180° , and reduction of vibrating panels' noise radiation. Since then, the acoustics world everywhere has become flooded by publications and patents about active noise and vibration control. At present, the subject is still developing to a greater sophistication and efficacy. Although the principle is simple, the feasibility of implementation depends on the size of source, its radiation distribution, and the ability to generate and control electronically spatial and time characteristics of the primary field. To adjust auxiliary sources to a maximum noise reduction and compensate for the time variation of noise sources and their environment, real-time adaptive electronic systems have to be used. Rapid advances have recently brought these systems to some perfection, being cheaper and less clumsy as compared with the conventional passive solutions, in particular when the weight of the insulation is very important, and screening is impossible or too heavy.

Theoretically, the upper limit of ANC is the "zero option" defined by Doak (1988), which still necessitates effort and lengthy research, to yield a machine which does not radiate any noise. However, for "real life problems" a reasonable compromise and optimization may suffice in most cases.

1.2 CONTROL ALGORITHMS

ANC is based on minimizing the acoustic field in a definite domain. The signals of the unwanted steady or time varying noise are collected by microphones. They are then processed by an adaptive electronic system that defines the canceling signals to be radiated into the relevant domain by secondary sources (loudspeakers and shakers for sound and vibration).

Another way is the feed-forward control obtained by a prior knowledge of the acoustic signal which is recorded by an upstream detection microphone. The feedback control in ANC was first suggested by Olson and May (1953). This strategy is linked to the basic theory of information as suggested by Shannon (1949) and Wiener (1949), and the theories of feedback and feed forward systems, including the use of interfaces with electrical filters, such as FIR and IIR.

M. Jessel (1967) made an important contribution to the theory of cancellation of sound wave radiated from a given source distribution by an array of Huygens sources (monopoles and dipoles) distributed over a closed surface surrounding the primary sources. Jessel, Mangiante and Canevet developed the method further under the name JMC. See Uosukainen (1990) and Mangiante (1990).

Now the interest moves towards more complicated algorithms including adaptivity

(e.g. Kuo et al, 1994). A review about the subject is presented in the books Elliott and Nelson and by Tokhi and Leitch, both published during 1992. An additional paper with analytical clues about the subject was published by Elliott and Nelson (1993).

Here we note that active noise suppressing technologies, using electronic devices, can not be developed by one man's expertise, or at least require the following disciplines:

Theoretical acoustics, vibration control techniques, electro-acoustics, signal processing and control engineering.

1.3 EARLY DEVELOPMENTS

While the principles of ANC were correctly described already by Paul Lueg, the claimed possibility of practical application turned out to be beyond the scope of even some sophisticated electronic applications today. Twenty years after Lueg's application for a patent, the successful experiments done by Olson and May (1953) with their electronic sound absorber, marked the beginning of development of compact ear defenders in which the ear cavity is actively maintained at conditions of silence. This solution, which was patented by Olson (1953), represents protection at the receiver (Wheeler 1981, and Jones and Smith 1983). In parallel, Bykhovskii (1949), Hawley and Simshauser (1953) developed ANC headsets as the most straightforward ANC. Later, the subject was developed commercially by Hesselmann (1974), Veit (1976) and others to ANC headsets, using small microphone-loudspeaker systems within earcups.

Another local control strategy is ANC at the origin of the source (Bschorr 1970, 1971, 1973, Wurm 1974, Swinbanks 1976, 1985, Wanke 1976, Chaplin 1981, 1984, 1986, Hori et al. 1984, Kallergis 1990, and Geddes 1991). A large proportion of ANC development has been directed toward the control of noise in ducts, sources acting in free spaces, and sources within enclosures. Lueg's idea of ANC in ducts was developed later by Swinbanks (1972), Wanke (1972), Lawson-Tancred (1974), and the problem became more involved with electronics and design of electro-acoustic systems. Energetic issues and optimization were encountered in most of these works, and finally, the "time domain" aspect appeared to be of vital importance. Eghtesadi and Leventhall (1982) suggested a new approach to Active Noise Attenuation in ducts, using a monopole system. Up to that moment the current approach to active noise attenuation was based on two or three secondary sources. The monopole system had not been accepted due to lack of broad band attenuation and lack of stability. The new approach to the monopole defined as "Chelsea monopole", offered for the first time a theoretical solution. This new concept uses the upstream radiation from the secondary source as a compensating signal which adds to the primary source radiation. With a proper signal processing technique, it can maintain a full range attenuation. Although some difficulties due to departure from the ideal characteristics by such sources were reduced by using one secondary source, its frequency response was still a major problem. Trinder and Nelson (1983) introduced the application of "acoustical virtual earth" to attenuation of broad band noise in an open ended duct with no flow. Their simple technique included a feedback loop to derive the sound pressure to a minimum at a microphone placed close to a loudspeaker in the duct

wall. This produced reflected downstream traveling plane waves. The investigation of the loudspeaker's near field enabled identification of the optimum positioning of the microphone. The system is shown to be effective especially at the longitudinal duct resonances. The principal advantage of this technique is the simplicity of the control system which enables using low quality components, without the need for precision in design of the system phase response.

Attention was paid in the context of active control to noise in industry. A patent for reducing noise radiated by transformers, related more to environmental acoustics, was presented by Conover et al. (1957), while Brute de Remur (1960) developed ANC for a sound wave passing through an orifice in a baffle, which can be related to some degree to industrial noise. Self adaptive electronic echo cancellers were developed and patented separately during 1970 by Sondhi, and Kelly et al. This idea was applied in improving the acoustic impression in a room by cancellation of the cross-talk by Atal et al. (1966). Bschorr contributed to the early technology of ANC ideas about canceling propeller aircraft noise (1970) and other kinds of propellers' noise (1971),

He suggested an anti-sound source which acts also as a sensor. Bschorr (1978).

1.4 RECENT ADVANCES

The remarkable development in modern electronics has made active control schemes viable outside the laboratory. The ease with which difficult signal conditioning can be achieved with modern techniques has revolutionized the subject and stimulated a considerable research effort in recent years.

The most simple ANC which is the local active sound absorption, as was suggested by Olson and May, was followed by additional series of patents by Chaplin et al (1983), Swartz (1987), Peevers et al. (1985), Vermotel et al. (1988), Pass (1990), among others. Also, Ziegler (1990) came forward with a patent for sound attenuation for a personal seat. Today, ANC headsets are available from various companies. Reduction of noise in ducts by active control is being developed up to now. Hong et al. (1987) presented in 1984 a theory for the attenuation of tight-coupled attenuators, which constitutes a special form of the "Chelsea monopole" attenuator with almost zero microphone-loudspeaker spacing, along the direction of the duct axis. Practical and theoretical aspects of a tandem system is developed, using a two simple monopole attenuators cascade. The occurrence of different reflections from the duct walls is considered, and as a result sound radiation from a secondary source is not taken as plane wave. The tight coupled tandem attenuator can provide attenuation of 20 dB or more for more than three and a half octave bands from 30 to 330 Hz.

Curtis et al (1987) applied the technique of minimization of acoustic potential energy to control a harmonic reverberate sound field in a finite length duct, and compared the method with two others, namely, The "acoustical virtual earth", where the added source is driven so as to maintain the sound pressure null in front of itself; The second one is the "absorbing termination", where the secondary source is driven so that no reflection occurs. In the minimization of acoustic energy, the secondary source strength is obtained by equating the differential of the energy with respect to the source strength to zero. One major result is that optimal termination achieves the best possible reduction of acoustic energy in the enclosure. At the expense of a non-causal control system, this condition produces half the acoustic energy of that resulting from a purely absorbing termination. In controlling periodic excitations optimal termination is practical, but even if the excitation can be previewed, the added complexity may not justify, in random excitations, the increased performance. In the last case, an absorbing termination can be most practical. "Acoustical virtual earth" does not achieve as satisfactory reductions in acoustic energy over a band of frequencies. A practical strategy which achieves a reduction in acoustic potential energy of a harmonic reverberate sound field is the minimization of the sum of the squares of pressures at several locations.

Munjaj and Eriksson (1987) presented a one-dimensional standing-wave model of a

linear active noise control system in a duct and a closed-form expression for the filter transfer function, which reveals the real role of the auxiliary source, and the importance of the distance between the input microphone and the auxiliary source. It has been stated that the success of the system obviously lies in correct prediction of this transfer function. Scott et al. presented in 1989 a complete analytical model of active noise control in ducts, which allows for calculation of individual source power flows and downstream power flow as a function of source strengths and relative phase angles for finite size sources. The model for the finite size primary source in the plane of the duct cross section is evaluated for monopole and dual secondary source arrangements, with results that show that the mechanism of ANC in a duct cannot be properly understood if the primary source is omitted during analysis. On the other hand, suppression of sound power flow down a duct, by using a single or dual secondary source combines suppression of primary source power output and absorption of primary source energy by the secondary sources. Hence, use of the word "cancellation" to describe the mechanism of ANC in ducts is incomplete and misleading, and the term ANA which includes the word "attenuation" instead of "cancellation" is often used. The search for one-dimensional systems for quieting noise transmitted by duct has led to many patents, e.g. Ross (1981), Warnka (1984), Erikson (1987, 1989, 1991), Allie et al. (1988, 1989), Hamada et al. (1988), Takahashi et al. (1990), Dekker et al. (1990).

Three-dimensional effects of ANC in ducts are taken into account more recently. Mangiante (1990), who introduced the JMC algorithm into active control of ducts, and the twin papers by Stell and Bernhard (1994), which deal with minimizing three performance criteria, namely, sound pressure at a set of selected points, potential energy in a selected volume in the wave guide and acoustic power in the downstream region of the wave-guide, and the research on the response of different arrangements of secondary systems in the duct. e.g. Kuo et al. (1994) should be mentioned in this context.

It is much more complicated to achieve ANC over spaces of more than one dimension, and mostly only a local improvement is achieved even when several secondary sources are used. A comprehensive review paper by Ffowcs-Williams (1984) gives a thorough analysis of the energetics of anti-sound. He explains there that acoustic energy and power are quadratic measures of the sound field and do not therefore add linearly. Precisely how the energy balance is modified when a source of sound competes with an anti-source is to be determined after the linear field quantities have been evaluated by superposition. The results are not always in accord with intuition and a whole variety of behaviors can occur in different cases. Most often it is found that anti-sound suppresses the power-producing ability of the primary source. Sometimes an anti-noise source withdraws and consumes from a primary source much more acoustic power than the source could produce or radiate in free space; the secondary source then acts as a "sound sucker". Sometimes the ANC can prevent sound energy from escaping into an exterior field just by trapping it in an internal reservoir of ever increasing noise. In a large number of works, optimization techniques have been used to establish the maximum reduction in the controlled sound field. The technique essence is explained by Nelson et al. (1987). One selects the acoustical quantity of interest as a quadratic function of the strengths of the sources introduced to control the field. Thus one seeks a suitable quadratic measure (cost function) as the total power output from a given source distribution, the total acoustic energy in a region, or the sum of squared acoustic pressures at a number of positions in the field. Quantities such as these in terms of the secondary sources strength then permit identification of optimal secondary sources strengths which minimize the quadratic cost function considered. This lets unequivocal identification of how much the quantity of interest can be reduced by the action of the secondary sources, providing information for the engineer seeking to apply ANC. It enables an unambiguous evaluation of what can be achieved by acoustical consideration alone, before entering any examination of the means of achieving the control required.

Nelson et al. (1986) analyzed the free field of an optimized pair of monopole sources, with the power output as a cost function, and reached the following conclusions: In the low frequency limit, the secondary source strength is of the same order of magnitude and of opposite phase to that of the

primary source, such that the combination of sources reduces to that of the primary source. However, as source separation is increased relative to the wavelength, it is demonstrated that in order to achieve optimal results, it is beneficial to reduce the strength of the secondary source relative to that of the primary one. In addition, the secondary source must for certain distances be in phase with the primary source to achieve the minimum possible output power. When the secondary source is many wavelengths apart from a primary source, it can do only little to influence the effective radiation impedance seen at the primary source. Under such circumstances it is better to avoid secondary sources. An important aspect of these results is the time domain interpretation of the relationship between the primary and the secondary source strengths. In order to achieve optimal results, the secondary source must produce outputs "in anticipation" of the fluctuations in the primary source strength. The authors further analyze the maximum reduction in power output that can be obtained by using several point monopole sources to control the field of a number of primary monopole sources. It is shown in the low frequency limit that optimal sources arrangements do not necessarily reduce to classical types of inefficiently radiating source distributions. These results have been deduced from analysis in the frequency domain and it should be remembered that optimal results may only be achieved at the expense of secondary sources which act non-causally with respect to the primary sources (time domain). It is also shown that, for the numbers and arrangements of the secondary sources, significant reductions in power output may be obtained only if secondary sources are placed within a distance of one half wavelength apart from the primary source. However, it is possible to produce a substantial reduction in net sound power output with a relatively small number of secondary sources placed close to the primary source.

Another example of optimization of ANC is the work presented by Nelson et al. (1987) on the effect of sources within enclosures. They present an analysis of the effectiveness with which active methods can be used for producing global reduction in the pressure fluctuations amplitude of harmonically excited enclosed fields is presented. The total time-averaged acoustic potential energy is a measure of the most practical relevance in determining the global effectiveness of secondary sources of sound, since it leads naturally to a cost function based on the sum of the squared pressures sensed at a discrete number of locations. The first stage includes the case of a single primary source in a lightly damped rectangular enclosure when the frequency of sound is above Schroeder's cut-off frequency of the enclosure (high modal density).

It is assumed that the sound field there can be expressed as a sum of the modal contributions. Substantial reductions in the acoustic potential energy cannot be produced if the secondary sources are separated from the primary source by a distance which is less the half wavelength at the frequency of interest. The use of active control in sound fields of low modal density is based on the same theoretical basis. In this case appreciable reductions in the overall potential acoustic energy are achieved by introduction of a small number of added sources spaced at a distance greater than half a wavelength from the primary source, provided the system is being excited close to a lightly damped acoustic resonance. The location of secondary sources which gives optimal reductions is at the maxima of the primary sound field, where the major contributing modes all share the same relative phases. Minimizing the sum of the squared pressures at a number of discrete sensor locations can provide a good approximation to minimizing the total time averaged acoustic potential energy, if the sensors are placed at the maxima of the primary sound field. Positioning a sensor at a corner of a rectangular enclosure of a low modal density field ensures detection of single dominant modes, and thus results in a near optimal reduction.

Nelson et al. (1990) presented classical time domain methods for determining the performance limits of ANC systems that are constrained to act causally. Previous work on the subject has mostly used frequency domain formulations in order to establish the physical limitations of active methods. While entirely adequate for prediction of the performance of ANC systems designed to deal with deterministic primary fields, they not necessarily can be applied when the primary excitation is stationary and random in nature. The application of frequency domain techniques often yield results for optimal control strategy that requires from the secondary sources to act non causally with

respect to the primary sources. The first example considered is the minimization of the mean-squared acoustic pressure at a position in the field of a point monopole primary source by introduction of a point monopole, where the primary source radiates a stationary random signal. Active control of low frequency random sound in enclosure is then addressed. This theory is also used in a third example consisting a primary/secondary source pair that radiates in a free field. Further progress in the investigation of actively generated quiet zones was lately made by David et al. (1994). Finally, we mention here the general statistical approach which seeks to quantify the performance of well known active control strategies in enclosures, specifying mean value and variance about the mean, as adopted by Joseph et al. (1994). Echo cancellation in rooms was significant for "hands-free telephoning" - Berkley et al. (1974), Schiff (1987) and for removing howling instability, applying the room transfer function to the electronic compensating system - Christensen et al. (1978), Itoh (1986), Arasekietal (1987). Generally, there are many patents related to ANC in enclosed spaces, since it is crucial in the aircraft and car industries, where weight, cost and size penalties should be minimal. Patents about such ANC are available especially for reducing peaks of resonances and canceling repetitive sounds, using room acoustics techniques and adaptive elements. Manufacturers of cars and aircrafts are interested in such developments and encourage patents on the subject - for example: Olson (1961), Clarion Co. (1977), Seifert (1982), Lorenzini (1984), Nelson et al. (1983), Peevers et al. (1985), Warnaka (1985), Swartz(1987), Kuipers (1987), Elliott et al. (1987), Salikudin et al. (1987), Fuller (1987), Elliott et al. (1988), Freymann (1989), Pass (1990), Eriksson et al. (1991), Elliott et al. (1992), Hanada et al., (1994), Control algorithms were used already in active field control of auditoria and methods for handling loop gain to increase loudness, reverberance, spatial impression, etc. See, e.g. Kawakami et al.(1990). Maa (1994) has shown recently that the reverberant sound field in a room can be reduced as whole using an ANC system with both the pick-up microphone and the secondary loudspeaker in the corner region of the room.

Industrial applications involve most complicated sources. The unsteady burning in a turbulent flame is a process which produces both noise and associated unsteady light emission. Dines (1984) describes an interesting development in which quickly monitored light emission is used as a signal for the simultaneously produced noise of combustion. Other patents on the subject are by Roberts et al. (1987) & Margiarotty (1989). Improvement of flaws detection by reducing flow echoes was suggested by Huchens et al. (1989) and Gilbert (1989).

Berge et al. (1988) presented measurement results of ANC of two outdoor transformers' hum. An adaptive signal processor was used to generate 100 and 200 Hz tones in anti-phase with the transformer noise, at a single point some distance away from the transformer. The noise reduction obtained by the most suitable signal processing was in the range of 5-10 dB for equivalent and peak levels. The level reduction was up to 20 dB under certain conditions.

Applications have been reported by Elliott et al. (1988) on ANC of engine inside automobiles, and propeller induced cabin noise (1989).

The advance in microprocessors technology has made within reach many other applications in suppressing industrial and domestic machines noise within the spaces where they are located. For example, Nakanishi et al. (1991) helped Toshiba in offering a commercial ANC for a refrigerator and Hollowell et al. (1991) suggested an active vibration control system of an elevator. In last years the subject influences also medicine, and Kroll et al. (1987) patented an ANC device to reduce the masking effect of lung sounds during diagnostics of cardiac sounds. Eliminating acoustic noise created by medical diagnosis devices was suggested by Friedlander (1994).

Recent advances in Active Control of Vibrations include a series of patents concerning the creation of secondary vibrations, e.g. Harper (1994), going deeper and deeper into technological details.

1.5 TRENDS

ANC becomes an efficient way of noise reduction, where conventional passive protection methods fail. This mainly happens when the noise to be suppressed is at low frequency and includes distinct frequencies, where passive means cannot be used and when the primary signals include both the relevant sound and the intruding noise. In such cases a new approach different from the passive one, is needed for those repetitive sounds. On the whole, their control by active means is straightforward and offers a practical solution in cases where either low frequency solid-borne or airborne periodic noise exists. (Clarion Co 1976, Rose 1982, Crocker 1982, Seifert 1982, Lorenzini 1984, Chaplin 1978, 1979, 1983, 1984, 1986, Taylor, 1987). The ANC is an efficient device concerning repetitive, low frequency noise signals, which characterize propellers. This kind of noise can penetrate the cabins of the aircraft passengers and cause there a considerable inconvenience. Researchers such as Warnaka 1985, Nelson and Elliott 1983, 1987, 1988, Sallikudin 1987, Fuller 1987, Hill 1991, Gardner and Ziegler 1992, were interested in adaptive structural ANC. Some of them suggested use of an error microphones array. Consequently, many industries that are interested in the subject, develop and will develop in the future ANC units. Some of the leading companies involved in ANC are Bose, Nelson industries, Digisonix Division, ANVT, NCT and Contranoise. They have already elaborated definitely promising prototype devices, proving that the subject is ready for commercial use.

A relatively simple ANC unit is the "small zone silencer" and there are at least two categories for which its application has proven effective. One application is in the cavity between the ear and the ear piece in "earphone" type installations, and the other way is reduction of noise at the source. Algorithms for both local strategies are bound to further improve in the future.

ANC has deficiencies especially in time varying sound and vibration fields and when the domain has more than one dimension, and research workers try now to overcome those difficulties. See, for example, the algorithm for time varying signal prediction estimate maximize (EM) by Na Kam (1994).

A major development for preventing noise escaping from air-conditioning ducts and other kinds of wave guides occurs now and will go on including presentation of new theories and technologies.

The three dimensional problem is a most complicated one, and research reaches in this area a very high degree of sophistication. Yet the end cannot be seen, mainly as to the physical understanding and solution of such problems. An ANC solution that matches reality should consider fields created by real sources, such as combustion noises within interiors, and effects of high sound absorption by bodies and surfaces within the examined enclosure, where reflection of sound is scattered. This last problem of noise cancellation in rooms with sound absorbing surfaces was partly investigated by Rosenhouse and Sasaki (1995).

Structural vibration is often linear and occurs in a controllable frequency range, so that there is a natural application for these techniques. Such is the case with pulsate exhaust flow of internal combustion engines, large diesel generators, fans and exhaust units. One important line of progress is the application of active noise control in power plants. O'keefe (1994) shows that solutions by active noise control may improve also performance of machines, by eliminating some of the passive means, such as mufflers and absorbing materials. He also distinguishes between active devices for reduction of noise of few separate harmonics and broad band cancellation means. Both kinds of ANC units can function simultaneously.

The related field of Active Vibration Control is developing in parallel, as summarized by Soong (1990). It is based on algorithms built in a similar manner to those of the ANC, but the technology of vibrations cancellation is different from that of acoustic noise. It includes active tendon control, active mass dampers, aerodynamic appendages, hybrid active-passive systems etc. Finally, optimization procedures are used in order to get the best control system. In this context, superior algorithms are sought, such as the control algorithm with weighting matrix configuration, including reduction of the influence of time delay within stability regions, as suggested by Cheng and Tian

(1993). The new research trends include the use of piezoelectric actuators, magnetic bearings, electro-rheological fluids, micro-processing and hydraulics on one hand and nonlinear motions control and active control of chaotic vibrations on the other hand. Applications include active control of vibrations of vehicle suspensions, active isolation against earthquakes etc.. There is a remarkable development in systems of active control of vibrations including typical components of control systems as sensors, signal processors, actuators error detectors, e.g., Macdonald et al. (1993)

2 PROJECT MESEMA

MESEMA, a technology oriented research program, builds upon the success of previous EU projects with devotion to accomplish the objectives of the aeronautics priority through designing, producing and testing “innovative transducer systems based on active materials“. Four fixed and rotary-wing aircraft companies accompanied by SMEs and university research institutes will take part in and benefit from the developments of primarily magneto-elastic transducers for high-torque actuation, vibration and noise reduction, electrical energy generation and structural health monitoring. Structural dynamics, energy conversion in active materials and control systems represent the scientific fundamentals of the project. The scientific and technological objectives are the results of a spontaneous evolution of the research activities developed during the last six years by the group which built the first consortium related to the European research program named “M.A.D.A.Vi.C.”. That group focalized its activity on two main strictly correlated research paths: increasing the knowledge and creating a unique team of experts of “design and development of innovative actuation systems based on magnetostrictive materials”; customizing the expertise of this team for the analysis and solution of specific needs of the next generation aircraft in terms of actuation systems including driving electronics and control aspects.

The MADAVIC project permitted to create the expert team that was involved in the 5th FP research project named “M.E.S.A.”. This last project was much more “application oriented” than its precursor, focusing more and more on research applied to the very challenging needs of three main “end-users” belonging to the aircraft field. The MESA project has been concluded with excellent results since the vibrations control system tested on a laboratory specimen fully satisfies the requirements specified by the respective end-user (Alenia), and also the other two applications have been completed with the detailed design and the construction of two completely innovative actuation system prototypes. The follow-up of these first six years of research activities consisted in proposing for the next future to carry out a more complex project where the base research activities (enlarged to many active material types) still have a fundamental role and the main targets are represented by the design and development of five systems aimed at: reducing internal noise in helicopters and turbofan aircraft; examining the health status of aircraft structural components by measuring their dynamic structural responses; replacing the helicopter rotor blade pitch angle actuation systems with an innovative one based on active material members and a reduced number of components; transforming mechanical energy related to vibration fields within aircraft into electrical energy thanks to the inverse magnetostriction effect. These four objectives have, obviously, a common aspect that suggested their integration within this proposal: they all require the design and development of a dedicated transducers system (including control algorithms and driving electronics) providing dynamic displacement and force fields on a host structure or recovering mechanical energy related to those fields by converting it into an electrical one.

2.1 PROJECT OBJECTIVE (S)

The MESEMA project is a technology oriented research program mainly devoted to accomplish objectives of the aeronautics and space priority by implementing “innovative transducer systems based on active materials”. The objectives consist mainly in the design and development of five systems integrating vibration transducers based on active components. The main targets are represented by the design and development of five systems aimed at 1) reducing the level of disturbance noise in turbofan aircraft, and 2) in helicopters, 3) examining the health status of aircraft structural components, 4) replacing the helicopter rotor blade pitch angle actuation systems and 5) transforming mechanical energy related to vibration fields within aircraft into electric one. These five objectives have, a common aspect that suggested their integration within this project: **they all require the design and development of a dedicated actuation system (including control algorithms and driving electronics) providing dynamic displacement and**

force fields on a host structure. A brief description of the five applications and the related objectives is reported in the following.

Noise and vibrations control. Within the first activity (**Noise and Vibration Control on Turbofan Aircraft**) a noise & vibration control system using magnetostrictive actuators will be designed, developed and tested, with the goal of controlling noise & vibrations in a frequency range between 300 – 1000 Hz. The environmental noise & vibration excitations will be representative of a small/medium turbofan aircraft case. Final results of the task will be represented by a system made up of about 50 actuation/sensing devices connected to a system performing control of external disturbances as well as of the devices' intrinsic non-linearity. Within the second activity (**Vibration reduction on rotary wing aircraft**) the HDVA concept, developed within the MESA project, will represent the starting point for the design of devices fulfilling the vibration reduction requirements typical of rotary wing aircraft. Future helicopters will be expected to show vibration levels below 0.05g. The main objective of this task is to design, develop and test a complete hybrid (passive/active) control system including actuator(s) and sensor(s), power amplifiers.

Structural Health Monitoring (SHM) of aircraft fuselage components. The objective of this application is the development and testing of SHM systems based on the analysis of variations in structural dynamic responses induced by damages by means of dedicated neural network algorithms aiming at achieving a “recognition-based learning” system. **This activity will benefit from most of the actuation technologies that will be developed for the Noise and Vibration Control on Turbofan Aircraft.** The main target will be the implementation of a HM system based on the same “hardware” in terms of actuators and sensors but characterized by dedicated analysis algorithms in order **to develop and test innovative damage analysis approaches in a realistic environment at very low costs.**

High Torque Actuation for Rotor Blade Root Control. Present helicopters use complex primary control systems that allow the pilot to maneuver the helicopter by adjusting the rotor blade pitch angle and hence rotor forces and moments. This system is complex, heavy, because's drag, and requires periodical maintenance. The focus will be put on the search for a suitable electro-mechanical concept which can fulfill the high torque requirements of the envisioned application as well as the reliability level which is required for the primary control function of a helicopter. Within this task one or more concepts of actuation systems satisfying these requirements will be produced, including devices, power amplifiers and control systems. Furthermore a specific sub-task will be devoted to testing of each component as well as of the overall actuation system.

Vibration (elasto-magnetic) energy conversion using high efficiency giant magnetostriction alloys (VIBEL). The objective of the VIBEL technology is to recover part of the vibration energy losses into useful electrical energy thanks to elasto-magnetic energy coupling within giant magnetostriction Terfenol alloys. The MESEMA project will investigate and analyze the underlying physics of mechanical to electric magneto elastic energy conversion, providing the basis for efficient engineering exploitation of these effects. Several VIBEL prototypes will be adapted and optimized for electrical energy generation at selected positions onboard an aircraft and helicopter. The designs and their expected performances will be tested and evaluated together with the end-users.

2.2 MESEMA WORKPLAN

2.2.1 Introduction

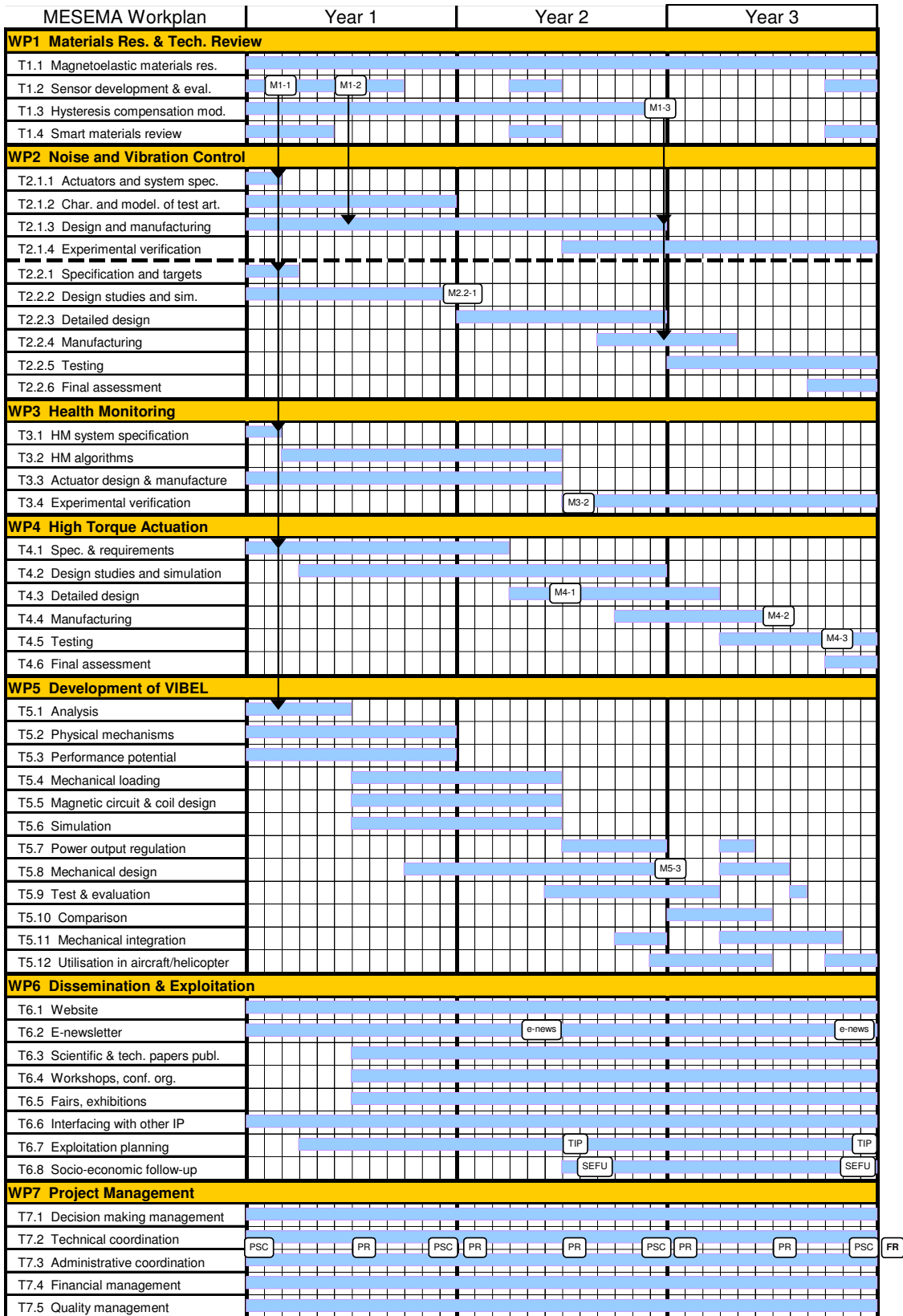
The work plan is divided into seven work packages (see *Work package list* on the following pages), the first of which focuses on the research aspect of magneto elastic materials and related technology. This work package feeds all of the technical development work packages (WP2 through WP5) with information regarding materials but also keeps the consortium abreast of the state of the art in the area of smart materials and structures. Moreover, WP1 also supplies WP2 and WP4 with the hardware development result—the hysteresis compensation module—for use in those two NVC applications.

WP2 is Noise and Vibration Control and houses two development activities, one for improving the cabin environment in turbofan aircraft by reducing noise levels through the application of magnetostrictive devices on the structural members (T2.1) and the second one involving the development of smart force generators for combating vibrations in the cockpit of helicopters (T2.2). WP3 is, relatively speaking, a small activity in the development of health monitoring (HM) algorithms for aeronautic systems incorporating active devices. This work represents an added value on two levels: firstly, the approach to be investigated involves the use of existing NVC devices for investigating the structural integrity; secondly, and a direct consequence of the first, is that the actuators and electronics integrated in the large-scale mock-up of WP2 can be implemented for the HM activities with little cost for additional hardware. WP4 involves the development of a high-torque actuation solution for root control of helicopter rotor blades—a large challenge demanding and promising innovative solutions. This actuation approach can solve the problem of Individual Blade Control (IBC) which is a proven method of reducing helicopter vibrations but also improving fuel efficiency. WP5 represents the latest innovation, the generation of electricity from the energy in vibrating structures. By their nature, such “Vibel” devices will also dampen vibrations and therefore offer a fruitful interaction with WP2.

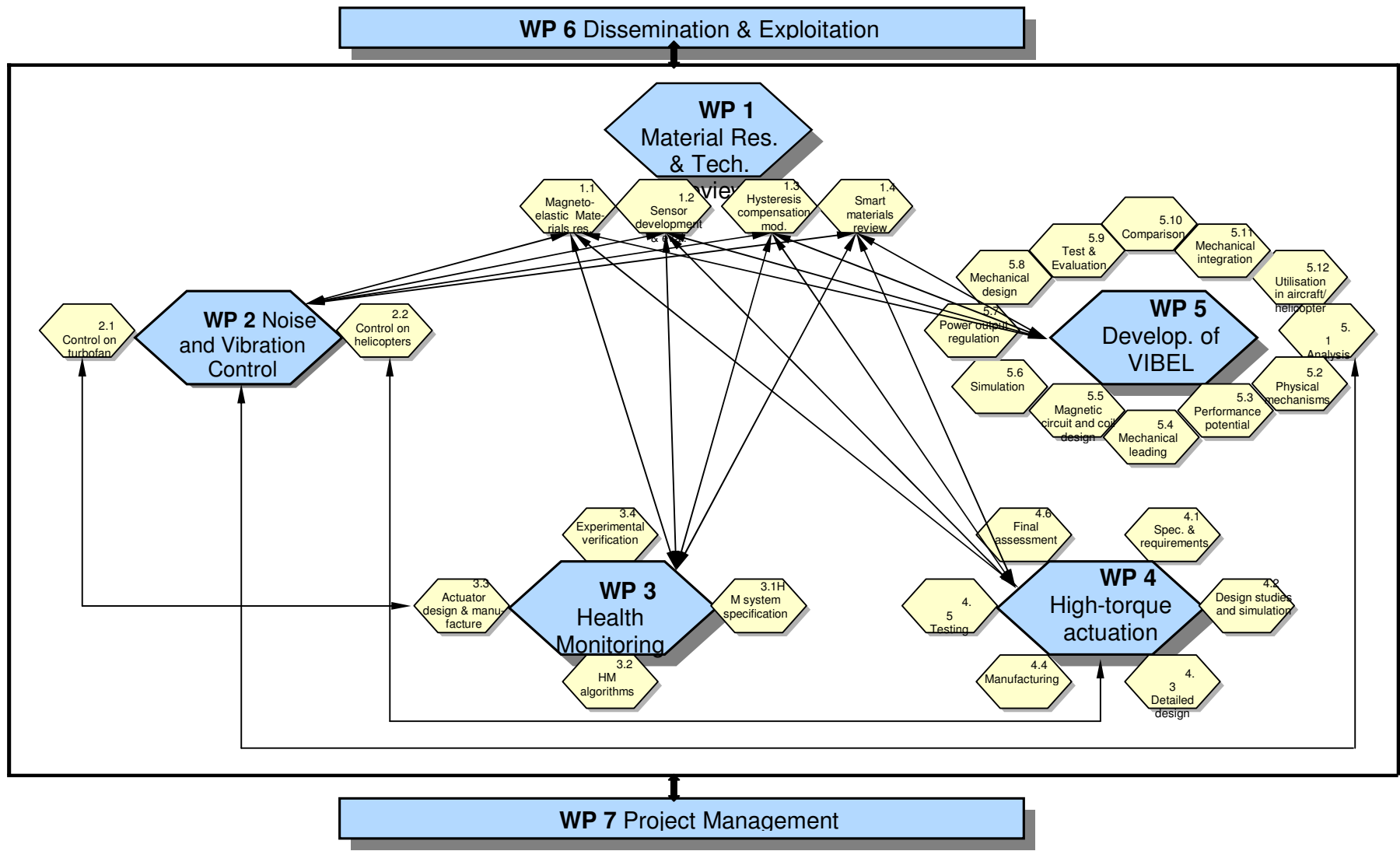
In following paragraphs a graph will present the main milestones timing, while contents of the milestones are reported within the single work packages descriptions.

2.2.2 PLANNING AND TIMETABLE

The project length is three years. In the next two pages a graphical description of the planning and timing of the work packages, as well as of the resources in terms of man-power is reported.



Scheme 2-1: Graphical presentation of work packages



Work-package No ¹	Workpackage title	Lead contractor No ²	Person-months ³	Start month ⁴	End month ⁵	Deliverable No ⁶
WP1	Materials research and technology review	3	81.0	0	36	D1.n
WP2	Noise and vibration control	4	273.9	0	36	D2.n
WP3	Health monitoring	1	36.0	0	36	D3.n
WP4	High-torque actuation	7	170.0	0	36	D4.n
WP5	Vibration electrical energy (Vibel)	8	135.5	0	36	D5.n
WP6	Dissemination and exploitation	9	63.0	0	36	D6.n
WP7	Project management	1	32.0	0	36	D7.n
	TOTAL		791.4			

Table 2-1: Work package list

¹ Work package number: WP1 – WPn.

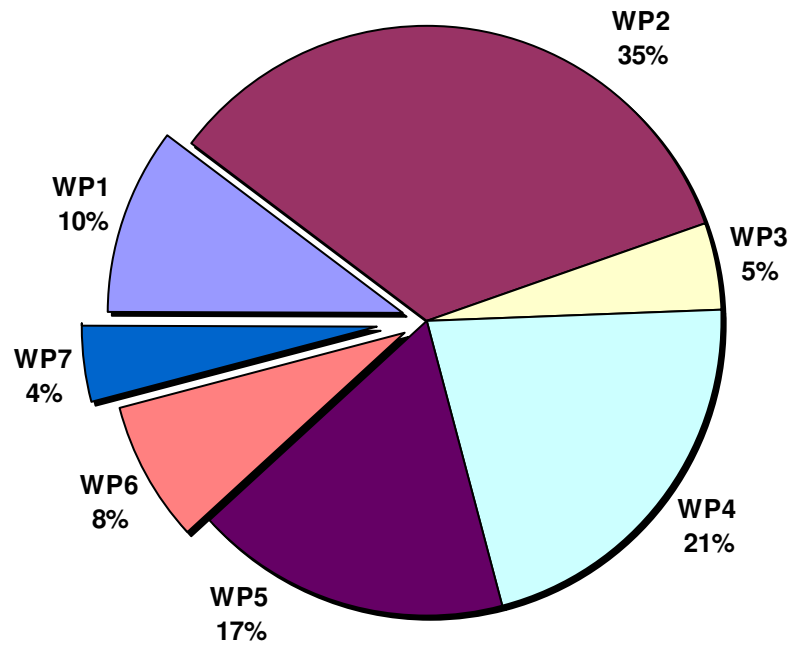
² Number of the contractor leading the work in this work package.

³ The total number of person-months allocated to each work package.

⁴ Relative start date for the work in the specific work packages, month 0 marking the start of the project, and all other start dates being relative to this start date.

⁵ Relative end date, month 0 marking the start of the project, and all ends dates being relative to this start date.

⁶ Deliverable number: Number for the deliverable(s)/result(s) mentioned in the work package: D1 - Dn.



Scheme 2-2: WorkPackage Description

2.2.3 WORK PACKAGE DESCRIPTION

Following is reported a description of activities, resources and milestones of each single Work Package. WPs presenting a more complex structure (2 and 4) have been organized in Tasks and Sub-tasks and each Task has been described separately.

Table 2-2: Participant list

List of Participants

Partic.Role*	Partic. no.	Participant name	Participant short name	Country	Date enter project**	Date exit project**
CO	1	Università degli Studi di Napoli "Federico II" - Dipartimento di Progettazione Aeronautica	Uni-NA DPA	I	month 1 (start of project)	month 36 (end of project)
CR	2	European Research and Project Office GmbH	EURICE	D	month 1 (start of project)	month 36 (end of project)
CR	3	Universität des Saarlandes (Saarland University)	LPA-ZIP	D	month 1 (start of project)	month 36 (end of project)
CR	4	Seconda Università degli Studi di Napoli - Dipartimento di Ingegneria Dell'Informazione	DII-SUN	I	month 1 (start of project)	month 36 (end of project)
CR	5	Alenia Aeronautica S. p. A.	ALA	I	month 1 (start of project)	month 36 (end of project)
CR	6	EADS Deutschland GmbH, Corporate Research Center	EADS-CRC	D	month 1 (start of project)	month 36 (end of project)
CR	7	ZF-Flugtechnik GmbH	ZFL	D	month 1 (start of project)	month 36 (end of project)
CR	8	TACT Technology Ltd	TACT	IRL	month 1 (start of project)	month 36 (end of project)
CR	9	CEDRAT Technologies S. A.	CED	F	month 1 (start of project)	month 36 (end of project)
CR	10	Chalmers Tekniska Högskola	CHALMERS	S	month 1 (start of project)	month 36 (end of project)
CR	11	EUROCOPTER DEUTSCHLAND GmbH	ECD	D	month 1 (start of project)	month 36 (end of project)
CR	12	National Institute of Research and Development for Technical Physics	NIRDTP	RO	month 1 (start of project)	month 36 (end of project)
CR	13	Kungliga Tekniska Högskolan	KTH	S	month 1 (start of project)	month 36 (end of project)

CR	14	Laboratory of Fluid Mechanics and Energy	LFME	GR	month 1 (start of project)	month 36 (end of project)
CR	15	Mecel AB	MECEL	S	month 1 (start of project)	month 36 (end of project)
CR	16	Newlands Technology Ltd	NEWLANDS	UK	month 1 (start of project)	month 36 (end of project)
CR	17	Paragon Ltd.	PARAGON	GR	month 1 (start of project)	month 36 (end of project)
CR	18	University of Salford	USAL	UK	month 1 (start of project)	month 36 (end of project)

*CO = Coordinator
CR = Contractor

** Normally insert “month 1 (start of project)” and “month n (end of project)”

These columns are needed for possible later contract revisions caused by joining/leaving participants

2.2.4 RELEVANCE TO THE OBJECTIVES OF THE AERONAUTICS AND SPACE PRIORITY

The aeronautics research work program is set against the two top-level objectives identified in the Strategic Research Agenda and the Vision 2020 Report:

- To meet society’s needs for a more efficient, safer and environmentally friendly air transport.
- To win global leadership for European aeronautics, with a competitive supply chain, including small and medium size enterprises.

The MESEMA project is focused on the satisfaction of both objectives through the development of systems for fixed and rotary wing aircraft; the common aspect unifying the proposal activities is the production of actuation systems based on active materials (magnetostrictive and/or others) working both as transducer of mechanical energy into electrical one and vice versa. This objective will bring to the implementation of :

- technologies and systems for a more-electric aircraft;
- systems for application of “smart” materials and structures aimed to structural weight reduction;
- concepts, technologies and systems to suppress noise and vibrations in fixed and rotary wing aircraft.
- smart maintenance systems including self-inspection;

The first two mentioned points (“smart” structures and systems for a more-electric aircraft) are the guide lines for the whole proposal also considering the partners’ consortium characteristics: the core group has been working on smart materials since

more than six years creating the main group of experts of magnetostriction and its applications to aeronautics in Europe. The group has expanded within the last research project “MESA” including industrial partners coming from aeronautic world (Alenia and ZFL) and is still expanding for this project considered more challenging than the previous ones: the big challenge comes from the fact that the “know-how” acquired during the last years is this time focused on specific application suggested by aeronautic industrial partners (including this time EADS and Eurocopter). The systems that will have to be developed within the project must, as a consequence, respond to requirements of selected applications, solving problems for which a solution is not available at the moment or replacing existing systems with new “smart” ones that should permit to reduce weight and/or components number, simplify maintenance or improve aircraft internal comfort.

Furthermore within the MESEMA project the requirements obtained by three leading industries of the European aeronautics field should find fulfillment through the synergy between academic research centers and small or medium size enterprises; this characteristic will permit a diffuse “know-how” exchange between universities, SME active in high-technology field and big industries, contributing to expand the competitiveness of the involved partners in the global aeronautics market as well as in its supply chain. It is now possible to get into detail of how each specific project’s application addresses the mentioned objectives of the aeronautics priority.

Reducing noise and vibrations in turbofan aircraft has a direct influence on “strengthening competitiveness”, addressing in particular “smart” systems for weight reduction and cabin environment improvement. The results of the project are expected to reinforce the competitiveness of European aircraft industry, since the selected solution can give a positive contribution to a real improvement in aircraft comfort perception of passengers. The active control system that will be developed and assessed on an ordinary metallic structure throughout the project, will be flexible thanks to the potential performances of magnetostrictive actuators, and will allow its use with no extra weight on-board of next generation turbofan aircraft, whose structures will be made using new metallic alloys, which will be much lighter.

Vibrations attenuation within helicopters will have influence on points (structural weight reduction) and cabin environment of the strengthening competitiveness objective of aeronautic priority. The aim of this application is in fact to replace and, mostly, improve performances of the vibrations reduction systems now employed reducing as first direct consequence the overall weight and the number of components of the system itself. Additionally, this application has to be seen also in close relation with the Integrated Program “Friendcopter” addressed in 1.3.2.1.A #5 “Integration of technologies.

Structural Health Monitoring of aircraft fuselage components addresses directly point of “strengthening competitiveness” priority as well as point. The proposed approach, in fact should satisfy requirements of smart maintenance systems supporting failure tolerance and structural integrity assessment of ageing aircraft. Furthermore, an effective “smart” maintenance system could permit a reduction of redundancies of structural components on next generation aircraft reducing as a consequence the overall weight.

The proposed approach for **High Torque Actuation for Rotor Blade Root Control** yields two major advantages over current helicopter control systems:

(a) Weight reduction, simplification and lower power consumption compared to the conventional (swash plate type) control system of helicopters

(b) Inclusion of benefits that come with the integration of IBC within the same control system.

The implications of (a) are a reduction of the aircraft operating cost through reduced maintenance costs of the less mechanically complicated control system and the over-all power savings through a lower equipment weight and lower power take up. It further helps to substitute hydraulic systems (today's primary control boosters and IBC actuators) by electrical ones yielding to the desirable more-electric aircraft. The benefits associated with (b) have been demonstrated in several IBC flight and wind tunnel test campaigns and shall now be realized with minimal weight penalty compared to the IBC systems used so far. The capability of IBC allows to reduce vibrations below 0.05g for better cabin environment. Additionally, the reduction of external noise in the order of 5 to 6dB has been repeatedly demonstrated through application of IBC using a small IBC authority of about 1° blade pitch. More noise reduction in the range of 8 to 10dB and even beyond can be reached with an increased IBC authority. This, too, has been demonstrated in wind tunnel campaigns. Further, the aircraft operating cost will be reduced through the improved efficiency of the rotor at higher forward speed through the application of 2nd harmonic blade pitch control. Values in the range of 4 to 9% have been measured for different helicopter types. An additional aspect concerns the reduction of the aircraft development cost. The inclusion of a flexible active vibration suppression system (i.e. IBC) right from the beginning of the design phase prevents the necessity of any tedious and expensive retrofit solution as it often became necessary in the past. Many helicopters had to be modified after the first flight due to immense vibration levels they produced. A well known example for this is the helicopter UH-60. This helicopter uses a "shaft extender" to reduce vibrations resulting from rotor fuselage interaction and bifilars to counteract rotor in-plane vibrations. Currently, further anti-vibration means are fitted to the fuselage. The total mass of anti-vibration means is about 200kg for this helicopter. Since vibrations are a major driver for the immense maintenance effort, the reduction of vibrations will also reduce the maintenance and operating costs. This statement is underlined by results of a Sikorsky and a Westland study.

The novel aspect to be considered here are not the benefits of IBC itself but the integration of such a system with the primary control enabled by the new control system architecture with IBC capability.

Therefore, both above mentioned objectives strengthening competitiveness (1.3.1.1) and improving environmental impact with regard to emissions and noise (1.3.1.2) are directly addressed by such a novel control system. The objectives of 1.3.1.2 stated in the work program specifies an external noise reduction of 6dB in the short term and 10dB in the long term for helicopters. The novel control system with IBC integrated will clearly reach that specification. In addition, this concept not only helps to reach the vibration target of 0.05g specified for the environmentally friendly helicopter described under "Integrated Focused Downstream Research" of the work program, but also to reach the specified fuel consumption reduction of 20%. This latter target can not be reached by an optimization of engines or an improved aerodynamically designs of the fuselage etc. alone. This will require new control concepts as outlined in WP4. Since hydraulic solutions with complex systems in the rotating system have proven not feasible, the

successful realisation of this idea is directly linked to the success of a suitable high performance electrical actuation system. In this respect, WP4 will contribute to improve the environmentally friendliness of helicopters.

The reduction of noise and vibration levels will improve the public acceptance of helicopters.

Finally **vibration (elasto-magnetic) energy conversion using high efficiency giant magnetostriction alloys (VIBEL)** introduces an innovative concept to the «More Electrical Aircraft's» objective of global value to power preservation and generation. By recovering, what today are mechanical loss energy onboard aircraft and re-entering it as electrical power into the aircraft system, fuel and weight will be saved for each flight. Furthermore, as vibrations are present over most of the aircraft structure, the Vibel could be used for distributed power generation reducing cabling, weight and complexity in the aircraft. For improving cabin environment and passenger comfort, the Vibel contributes by its capability to absorb noise and vibration energies by converting them into electrical and useful power. As a consequence, also in this case many aspects of “strengthening competitiveness” priority could be fulfilled like maintenance, weight reduction, cabin environment, breakthrough technologies for on-board systems). Furthermore, reduced fuel consumption can affect aircraft emissions, addressing as a consequence the “environmental impact improvement” priority.

In conclusion is possible to assert that the proposal is perfectly in agreement with the “open upstream research” guidelines for aeronautics, since it addresses to specific priorities and applications but still developing base research on smart materials and the related aspects (magnetostrictive and piezoelectric materials, electro-rheological and magneto-rheological fluids, hysteresis compensation, fibre optics).

Small and medium size enterprises cover a fundamental role within the project activities being the most involved in the design and production of the main project's products (actuators). This role could bring as added value the possibility of patenting very innovative devices increasing as a consequence their competitiveness in the global aircraft supply chain market.

2.2.5 POTENTIAL IMPACT

It was becoming clear in aeronautics before the 11 September attacks that 2001 was going to be bumpier than predicted. Immediately after the dramatic events most aerospace analyst described the aeronautical industry “uncertain, unpredictable, and unforecastable”. The aircraft deliveries, estimated for 2003, are roughly 150 units. This value is the total number of aircraft by European and U.S. industries. This forecast immediately highlights the importance of having competitive products. In fact, aerospace companies are constantly facing domestic and global competition, and they need intelligence to keep informed about market trends, competitor strategies, changes in the industry, new available technology. Staying competitive means anticipating industry actions in time to respond them. *The aerospace industry, with its volatile market swings, needs competitive intelligence to survive in the global marketplace* – Aerospace America Magazine December 2002 Issue. Hence, in aeronautics some key parameters for enhancing aircraft competitiveness are: weight reduction, overall efficiency

(aerodynamics and structures), maintenance costs. This proposal addresses these fundamental aspects by using “smart” technologies. In U.S.A. there are already ongoing programmes which are carrying out first prototypes based on smart/adaptive structures, for example:

- Honeywell is continuously introducing in the market new systems for the damage detection and identification in aircraft;
- Boeing, in DARPA and NASA funded efforts to reduce vibration and noise and improve aerodynamic performance, has completed model-scale wind tunnel tests and is working on a full-scale bench demonstration of an active-twist rotor blade for the CH-47 - in other activities Boeing is bench testing a set of four full-scale blades incorporating on blade smart material devices;
- The University of Maryland, in collaboration with Penn State and Cornell, completed the Army-sponsored Innovative Smart Technologies on Quiet Rotorcraft program by developing smart-rotor concepts;
- Boeing and Virginia Tech designed and tested distributed vibration devices for aircraft interior noise reduction based on vibration absorbers;
- Funded by the Army Aviation Applied Technology Directorate, engineers at Bell Helicopter, Midè Technology, and Starboard Innovations demonstrated a number of adaptive structures concepts for helicopter vibration control, including an adaptive wing-fuselage isolator for tilt-rotor aircraft and two adaptive/active cargo floor isolation systems using a distributed adaptive stiffness approach and an active x-frame piezoactuators.

All above-mentioned activities will have a significant impact on American products and demonstrates the need: of interdisciplinary consortium and of new technologies based on smart materials. According to these general needs this proposal is focused on the development of enhanced devices based on magnetostrictive materials and/or active ones and furthermore it involves main European experts on this particular topic. This approach fits the objective of increasing competitiveness but is innovative too. In fact it tries to maximize skills of some European partners on magnetostrictive materials.

The improvement of whole aircraft efficiency obviously has social effects too. With reference to the selected applications in aeronautics the social importance of increasing the “damage tolerance” aspects and comfort on-board for passengers and crew is quite evident. The expected potential impact on application basis is summarized here:

High Torque Actuation for Rotor Blade Root Control - The redesign of the conventional helicopter control system architecture would be a break-through towards both: the fly-by-wire and the more-electric aircraft. As long as swash plate based control systems are used fly-by-wire stops short of the initial goal to substitute heavy mechanical linkages by wires or glass fibers. For fixed wing aircraft “fly-by-wire” has been realized in many aircraft, but not for helicopters. Only the NH-90, which is not in service yet, uses this technology, but still uses almost the same mechanical effort, since a swash plate arrangement is used.

As long as the classical swash plate architecture is preserved the major part of the control path mechanics can not be removed and fly-by-wire on the helicopter yields only minor effects compared to the realization in fixed wing aircraft. Primary and individual blade control have both successfully been realized with hydraulic power supply, mostly using the concept of blade root control, where the complete blade is rotated about its span

wise axis via a hinge at the blade root. The power density of hydraulic components still outperforms the electrical devices. However, many attempts have been undertaken to use the flexibility of electrical actuators to provide “on-blade” rotor control (e.g. trailing edge flaps or variable twist). In all these cases smart electrical actuators will be imbedded in the blade to change the blade geometry. But, none of these concepts will reach the amplitudes required to realize the primary control function and will be restricted to the small amplitudes of the IBC function.

Thus, the provision of a capable electric blade control system will directly help the helicopter to duplicate the success story of fly-by-wire for fixed wing aircraft. As shown by the example of Airbus, a novel advantageous technology can help to improve competitiveness versus the American and growing Asian helicopter manufactures. The designs of these competitors tend to be more conservative, which helps to capitalize on a technological advantage. This activity also fits into the worldwide trend to use unmanned aerial vehicles for commercial and military applications. These vehicles will even stronger benefit from more electric based systems.

Within Europe, this type of innovative project helps to balance the prospects of system and subsystem suppliers as ZFL on one hand and the large system integrators and manufactures as Eurocopter on the other hand. ZFL as an “end-user” in this project intends to pick up the results of the proposed program, transfer them into a commercial valid product.

ECD will check the capabilities and investigate the certification of such a flight control system under the required safety regulations and the impact on the helicopter. A flight test campaign could be carried out to substantiate the predicted performance and prove its commercial feasibility. For ZFL the extension of its activities beyond the traditional transmission design stabilizes its position as an innovative system supplier with a widened know-how basis.

Noise and Vibrations Control in Fixed and Rotary Wing Aircraft – The reduction of interior noise and vibrations has two main effects, i.e. comfort and fatigue improvements. Both aspects have a strong appeal on potential markets. In fact NVC requirements are becoming more and more stringent since the proposed targets need high capabilities in a wide frequency band vs.: a) increase of passenger riding comfort; b) less severe vibratory environment for equipment; c) less structural fatigue problems; d) decrease of physical stress of pilot; e) realization of jet-smooth ride in helicopters.

For this reason a big effort has been already spent in the European Union for achieving the design of lighter and quieter aircraft as shown in the following figure. Most of the funded projects were focused in the methodological approaches or on the evaluation of a comfort index.

Therefore this proposal is well fitted in the whole context of R&D programs for noise and vibrations and it is envisaged that the activity in MESEMA will benefit from some outcomes of previous projects and will recovery a technological gap in actuation systems for active noise and vibration control.

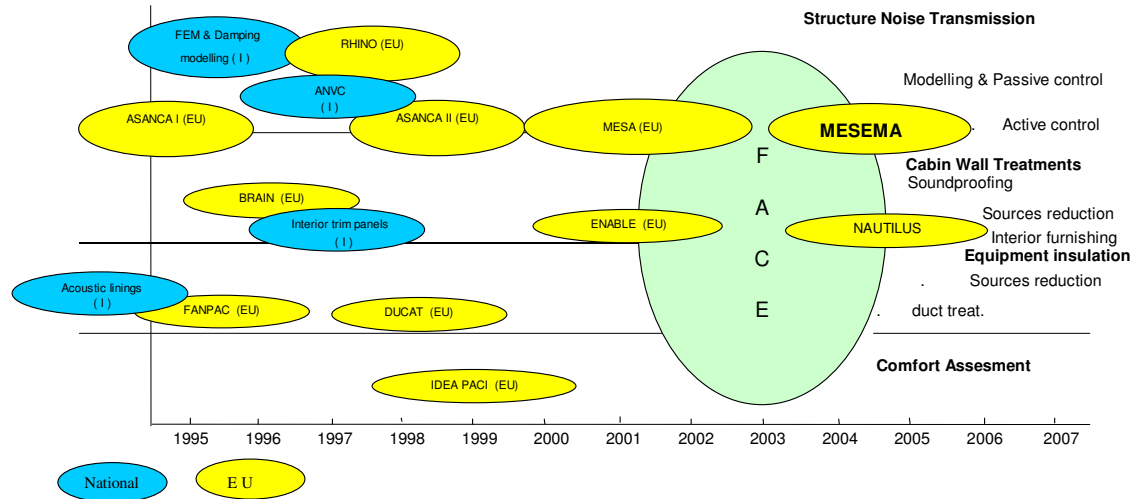


Figure 2-1: R&D Programs for noise and vibration control

Moreover, even if large research efforts are on-going investigating active noise control solutions over wide frequency bands, particularly in the U.S.A., this project has a strong innovative character, since it represents the first approach to the development of a complex active control system via magnetostrictive actuation, which has a specific target in the low to medium frequency region. Other approaches, which try to combine active control at lower frequencies with passive performance of the active medium at higher frequencies, being far more complex, appear to have a long way to run, notwithstanding the relevant research activities already started some years ago.

Structural Health Monitoring of Aircraft Fuselage Components – Nowadays aircraft design is based on “damage tolerance” approach. According to this methods structural damages can occur but they must be monitored (for example in terms of crack propagation speed) in order to avoid dangerous structural breaks. For this reason some key components are doubled in aircraft. The damage tolerance philosophy has overcome the critical aspects of “fail safe” and “safe-life” design methodologies but it requires an accurate health monitoring program and it introduces some weight penalties due to the duplication of some components. In the last years in Europe and in U.S.A. the maintenance fleet costs were roughly around 50 billions of Euros. These costs are even increasing due to the ageing factor of fleet. Most of aircraft in operation that are older than 20 years were designed according to a shorter operative life. Therefore, in aeronautics, a smart system able to check the structural integrity has a significant impact on safety and economic aspects. In fact, a continuous check by using smart devices could avoid long time consuming inspection and substitutions of structural elements scheduled on statistic information.

Vibration Energy Conversion using High Efficiency Giant Magnetostriction Alloys (VIBEL) - Providing a new means of generating electrical power on aircraft while at the same time improving fuel efficiency is of great strategic importance for aerospace technology and transport. Utilising the aircraft vibrations as source for electrical power opens up new approaches and ways of thinking in the design of aircraft electrical systems. The VIBEL concept is truly new and innovative and provides the basis for a completely new type of electrical power generators. A new market segment and range of products can be created. The VIBEL technology will open a new segment in the power

generation market, extending beyond aerospace into a new manner for more efficient energy use and electrical power generation. Economical and environmental benefits the society are clear and obvious. The new business opportunities from this new and patented technology to Europe are rich and the product itself represents a prestigious contribution from Europe to a more ecological society with positive consequences to quality of life in Europe. The development of the VIBEL technology requires the multidisciplinary competencies across Europe already mobilised through the MADAVIC and MESA programs. The continued development of a European Terfenol competence structure is of vital importance for the magnetoelastic technologies development to the European aerospace industry.

The above sections of this paragraph have already highlights some projects linked to this one. With reference to technological aspects and actuation system developments further links are:

- MESA G4RD-CT 1999-00035, development of magnetostrictive actuators for the shape control of helicopter blades, vibration damping of turboprop aircraft, actuators for electric movement of control surfaces;
- SMARTOOL GRD2-2000-30314, in which CEDRAT is developing high forces piezoelectric actuators and electronics for the vibration damping of machine tools;
- PIEZODIAGNOSTIC G1RD-2001-00659, in which CEDRAT is developing piezoelectric actuators and electronics for the health monitoring of large structures;
- In a co-operation with ONERA, CEDRAT is involved in the development of actuators and active structures for shape control. The project aims at combining piezo and composite materials to get active structures combining large deformations with low weight. This project is partly funded by DGA (Ministry of Defence), partly private investment;
- Integrated Programme “Friendcopter” addressed in 1.3.2.1.A #5 “Integration of technologies”.

The MESEMA consortium will benefit from results of previous MESA project and from expertise achieved by some consortium partners in other programs.

As far as the dissemination and exploitation topic is concerned the proposal is already organised by paying attention to the needs of end-users. Therefore, the results should fit immediately industrial interests. Nevertheless, the proposal has a workpackage (WP6) devoted to the exploitation and dissemination of results. The leader of WP6 is CEDRAT. CEDRAT has an important activity in terms of promotion of its research results as regard its Active Materials Applications (AMA), such as Smart Actuators, and will applied it with this project. Scientific papers are produced at a rate of more than 1 per AMA research engineer and per year. Participation to fairs and business international meetings are performed at the rate of about 10 per year. The CEDRAT web site (<http://www.cedrat.com>) receives 50,000 accesses per month. CEDRAT is certified for training and provides both training courses (mainly followed by SMEs) and transfers of technologies (toward large companies). This dissemination policy is possible without problem of industrial properties, because CEDRAT applies for patents before publishing. With reference to exploitation, some partners of the project could be customer of CEDRAT actuators. New targeted companies are easily contacted through the National

Civil Aircraft Agencies or through specialised fairs. The market for aircraft smart actuators to be addressed by CEDRAT in the project is presently estimated of 10,000 units per year in the world. Considering an acceptable value of 1kEuro/unit, the world market is at least 10Million Euro per year. As Cedrat is a company having a world distribution, it can address this world market by gaining 10% of it. This would lead to a production of 1000 units per year and an income of 1Million Euro per year. Preliminary exploitation timing is a qualification & industrialisation phase with pilot customers during 2-3 years after the project end and then an industrial start.

2.3 WORK PACKAGE DESCRIPTION

Following is reported a description of activities, resources and milestones of each single Work Package. WPs presenting a more complex structure (2 and 4) have been organised in Tasks and Sub-tasks and each Task has been described separately.

2.3.1 WP2 – NOISE AND VIBRATION CONTROL

Workpackage number		2		Start date or starting event:				Mo0	
Participant short name:	Uni-NA DPA	Eurice	LPA-ZIP	<u>DII-SUN</u>	ALA	EADS-CRC	ZFL	TAC T	CED
Person-mon	32	-	56	64.5	42.5	26.5	0	-	29
TOTAL	Chalmers	ECD	NIRDTP	KTH	LFME	Mecel	New-lands	Para gon	USAL
273.9	-	16	-	-	7.4	-	0	-	-

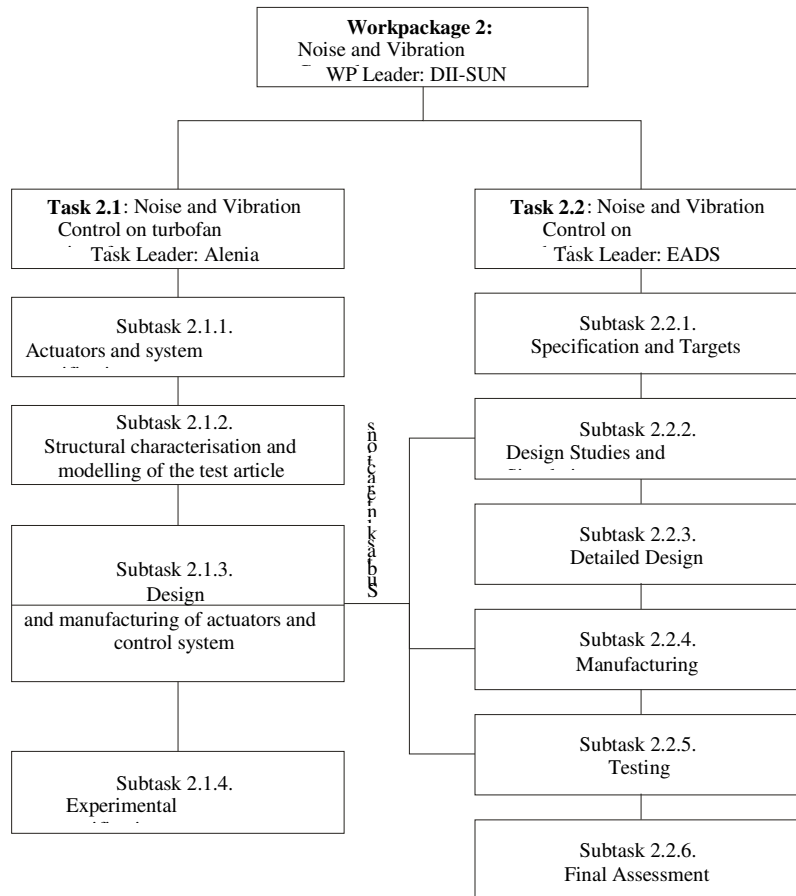
2.3.1.1 Objectives

Work package 2 is devoted to noise and vibration reduction for aircraft. Two different aircraft types, namely fixed wing and rotary wing aircraft, are addressed in the work package, the differences being both in the nature of the structure to be considered and on the effect to be controlled. The activities of WP2 have also strong links with the other work packages, since the choice of materials for actuators and sensors will connect WP2 to WP1, the actuators manufactured in WP2, with embedded sensors, will also be used in WP3, hysteresis compensation techniques and power amplifiers studies are needed in WP4.

2.3.1.2 Description of work

WP2 is divided into two major tasks, the first for the turbofan aircraft, and the second for the helicopter. Each task is divided in turn in logical sub-tasks, with partial time overlap. The sub-tasks are composed by different work steps.

The structure of the work package is shown in the following figure.



Scheme 2-3: Work package Flow

2.3.1.3 Description of work

WP2 is divided into two major tasks, the first for the turbofan aircraft, the second for the helicopter. Each task is divided in turn in logical sub-tasks, with partial time overlap. The sub-tasks are composed by different work steps.

TASK 2.1: NOISE AND VIBRATION CONTROL ON TURBOFAN AIRCRAFT

Workpackage number			2		Start date or starting event:			Mo0		
Participant short name:	Uni-NA DPA	Eurice	LPA- ZIP	<u>DII-</u> <u>SUN</u>	ALA	EADS- CRC	ZFL	TACT	CED	

Person-months:	32	-	33	60	42.5	0	0	-	5
TOTAL	Chal- mers	ECD	NIRDTP	KTH	LFME	Mecel	New- lands	Paragon	USAL
179.9	-	0	-	-	7.4	-	0	-	-

2.3.1.4 Objectives

The first topic deals with noise reductions for turbofan aircraft, where the noise is a broadband disturbance with frequency range between 300-1000 Hz, resulting from the turbulent boundary layer. This noise will be characterized and simulated in an experimental set-up consisting of a full scale fuselage mock-up available at Alenia plant. Magnetostrictive actuators will be considered, with embedded fiber optics conferring those self-sensing capabilities. Microphones will also be used both for performance evaluation and for control, allowing the use of mixed feedback-feed forward control strategies. Also passivity-based active control approached will be investigated. 30 to 50 magnetostrictive actuators will be designed and manufactured, along with power amplifiers, controlled by a network of DSP, and the actuator location will be optimized. The actuator performances will be critically compared vs. piezoelectric solutions.

2.3.1.5 Description of work

T2.1.1: Actuators and system specification [Mo0- Mo2], [2.5 PM]
Partners: Alenia [1 PM], Uni-NA DPA [1.5 PM]

The definition of requested force and displacement actuator outputs, along with the actuators, sensors and amplifiers operating frequency range will be defined, with reference to the goal of controlling noise and vibrations in a frequency range between 300 – 1000 Hz. The industrial partner (Alenia) will define the specs, while Uni-NA DPA will translate them in specs for each component of the devices (amplifiers, actuators, sensors) to be produced.

T2.1.2 Structural characterization and modeling of the test article [Mo0- Mo12], [26.6 PM]

Partners: Alenia [10 PM], Uni-NA DPA [6 PM], DII-SUN [6 PM], LFME [4.6 PM]

This sub-task is devoted to the mathematical preliminary description of all the aspects of the application, namely modeling of the structure in the frequency of interest. This will be accomplished both by modal analysis and by amplitude measurements, according to the relevant frequency regions. A model of the structure will be deduced and its parameters identified based on experimental measurements, so as to obtain a model of the structure useful for simulation and control design purposes. Based on preliminary actuator design and on the results and experience from MESA project, the actuator will be modeled and inserted into a MATLAB/SIMULINK simulator for control design (subtask 2.1.3) and performance evaluation. Sensors will also be considered and modeled. The location of the actuators will be defined, based on optimality criteria, i.e. maximizing controllability and observability indices, in order to guarantee highest effectiveness of the actuator. In this subtask, also the optimization of the number of actuator/sensor pairs will be tackled, by means of genetic algorithms. The result will be

the definition of number and location of the actuators on the test article. The sub-task is articulated in the following phases:

Experimental modal analysis of the test article, [Alenia, Uni-NA DPA]

Modeling and identification for control purposes, [DII-SUN, LFME]

Definition of acoustic and vibration excitation, [Alenia, Uni-NA DPA, DII-SUN]

Sensor definition, with self-sensing capabilities [DII-SUN]

Sensor/Actuator optimal placement, [DII-SUN, LFME]

Noise and vibration amplitude measurements under final excitation conditions, [Alenia, Uni-NA DPA, DII-SUN].

T2.1.3 Design and manufacturing of actuators and control system [Mo0- Mo24],
[83.8 PM]

Partners: Alenia [1 PM], Uni-NA DPA [6 PM], LPA-ZIP [33 PM], DII-SUN [36 PM], CED [5 PM], LFME [2.8 PM]

This is the sub-task devoted to production of the components for the solutions to the problem. In these sub-task 30-50 actuators, controllers and amplifiers are designed and produced.

It is assumed that the new performance requirements will demand at the very least a scaling of the MESA DVA concept but perhaps even an entirely new concept in order fulfill the new requirements concerning smaller size, lower weight, higher and wider operating frequency band. Finite Element Modeling will be applied to estimate the device performance before prototype manufacturing. If feasible, more than one manufacturing method will be explored to optimize on device performance or cost. Presumably more than one prototype device will be manufactured and characterized before a final design is selected. Moreover, the actuator produced will be dynamically characterized and experimentally identified. The hysteretic behavior of the device will be modeled in order to deduce an inverse model for hysteresis compensation. In the past LPA-ZIP and DII-SUN have developed successful hysteresis compensation algorithms currently being commercialized and further developed them within the MESA project. The LPA-ZIP algorithms are noted for their quality and high-speed. The proposed work shall result in a stand-alone hardware device characterized by high performance specially suited for noise and vibration control problems. For the controller design, ANVC on a turbofan requires broadband disturbances rejection capabilities. This can be accomplished by resorting to adaptive feed-forward control and robust feedback control strategies, able to reject unmodeled dynamics and system uncertainties, developed by DII-SUN and partially employed in the MESA project. Moreover, any robust feedback technique requires co-located sensor/actuator pairs, in order to confer passivity properties to the controlled structure. This goal can be accomplished by embedding fiber optic sensors (Bragg fiber gratings) into the magnetostrictive actuator. Fiber Bragg gratings are small (sized down to 1 mm length and 150 microns diameter) lightweight and with maximum sensitivity of 1 micro strain. For the power amplifier, compact and lightweight amplifiers will be developed. If feasible, the amplifier unit will be designed such that a single channel can be mounted onto or very close to the magnetostrictive actuator device. The characteristics of the electrical supply system available in the aircraft will be taken into consideration. More than one prototype amplifier will be produced and characterized before a final design is selected. Finally, in order to co-ordinate the large number of actuators foreseen for Task 2.1 application, communication capabilities will be considered for the final DSP

boards, and real-time automation communication protocols will be implemented, producing controller network solution. The activities of the subtask are articulated according to the following sequence.

- Preliminary actuators and amplifiers design (LPA-ZIP, DII-SUN, Alenia)
- Prototype actuators and amplifiers detailed design (LPA-ZIP, DII-SUN)
- Prototype actuators and amplifiers manufacturing (LPA-ZIP)
- Actuators intrinsic characterization (LPA-ZIP, DII-SUN, Uni-NA DPA)
- Actuators and amplifiers manufacturing (LPA-ZIP)
- Comparison between different actuator solutions (piezo, magnetostr.) (CED, Alenia)
- Control logic design (DII-SUN)
- Manufacturing of DSP boards (DII-SUN)
- Simulations of installed actuators performance (Uni-NA DPA, Alenia, DII-SUN)
- Optimization of actuators position (Uni-NA DPA, Alenia, DII-SUN)
- Controller network and distributed control systems design (DII-SUN, LFME)

T2.1.4 Experimental verification [Mo19 – Mo36], [67 PM]

Partners: Alenia [30.5 PM], Uni-NA DPA [18.5 PM], DII-SUN [18 PM]

In the last sub-task of this activity, the actuators produced in the first 18 months are mounted on the structure and the effectiveness of the proposed strategy experimentally assessed. In a first phase 4-5 prototypes of controllers, actuators and amplifiers will be tested on reduced, although significant, Alenia mock-up. Next, feedback to subtask 2.1.3 will result and the production of the remaining devices enabled. Finally, a conclusive verification and final assessment will be carried out on the full-scale Alenia test article. The work steps are the following.

- Definition of tests specification (Uni-NA DPA, Alenia)
- Active noise control testing preliminary phase by using first actuators and controller prototypes (Uni-NA DPA, Alenia, DII-SUN)
- Final active noise control verification (Uni-NA DPA, Alenia, DII-SUN)

2.3.1.6 Milestones and expected result

- M2.1-1 (Mo1) Choice of actuator concept based on specs for turbofan
- M2.1-2 (Mo20) Selection of final actuator, amplifiers and sensors for turbofan
- M2.1-3 (Mo24) Selection of final control strategy and control hardware for turbofan

2.3.2 WP5 – VIBRATIONAL ELECTRICAL ENERGY (VIBEL)

2.3.2.1 Objectives

In all vehicle systems a part of the produced energy is transformed into mechanical vibration energy losses. The very high energy density and magneto elastic coupling of Terfenol together with its metallic properties makes it possible to achieve VIBEL

generator power to weight and size ratios higher than those of conventional rotating generators. Moreover Terfenol is by far the best material for mechanical to electrical energy power conversion. The objective of the VIBEL technology is to recover and reconvert some of the vibration energy losses into useful electrical energy. The technical principle of the VIBEL is elasto-magnetic energy conversion using high efficiency giant magnetostriction Terfenol alloys. To define the optimal integration of magneto elastic electrical power generation into an aircraft and helicopter system and to test and evaluate its performance and benefits.

The three main aspects of this work are:

- To investigate and define the design fundamentals of the Vibel mechanic-electrical generator to provide the basis for design and construction of Vibels optimized for different mechanical energy input profiles and electrical energy output requirements.
- To investigate and analyze the availability, distribution and power profile of mechanical vibrational energy on an aircraft and helicopter.
- To investigate and analyze the new opportunities for distributed, electrical power supply on an aircraft and helicopter and to specify the requirements on a complete Vibel system integration into the vehicle's electrical system, considering also how decentralized energy supply could make electrical wiring on aircraft less complex offering reduced weight and increased safety.

2.3.2.2 Description of work

The WP5 is divided into 12 Tasks. They have been designed to be almost consecutive from a logical point of view, a part from some small overlapping considered to ensure a smooth passage from a work phase and the following one.

The first three tasks mostly are related to basic research activities concerning materials physics, analysis of vibration paths in aeronautics vehicles and performance potential investigations. Following the design and manufacture phase will start that will be strictly correlated to the following testing of the built prototypes on dedicated test-benches. The last task is dedicated to a critical assessment of potentialities of built for their employ on next generation fixed and rotary wing aircrafts.

2.3.2.3 Task 5.1: Analysis of overall distribution and availability of mechanical dynamic / vibrational energy across an aircraft /helicopter structure

2.3.2.3.1 Objectives

To investigate and analyze the availability, distribution and power profile of mechanical vibrational energy on an aircraft and helicopter.

2.3.2.3.2 Description of work

Task 5.1: Analysis of overall distribution and availability of mechanical dynamic / vibrational energy across an aircraft /helicopter structure [11.3 PM],

Leader: Uni-NA DPA

Partners: Uni-NA DPA [2 PM], LFME [1.8 PM], Paragon [5.5 PM], EADS [0.5 PM], ZFL [0.5 PM], ALA [1 PM]

Uni-NA DPA will co-ordinate this investigation and in collaboration with LFME analyzes as well as presents the result. Mechanical energy distribution maps of aircraft and helicopter structures will be produced and will provide a basis for the Vibel design work.

Paragon will develop an Evolutionary based algorithm for the optimization of the selection of the optimal Vibel locations inside the aircraft. This optimization algorithm will take into account the vibratory pattern inside the aircraft and the available types of Vibel power generators (different sizes, weights, vibration threshold, etc) and will provide the optimal configuration of vibration locations and relevant power generator type per location that will provide the maximum power (taking into account weight constraints).

EADS will provide information of vibrational energy power and distribution across an aircraft and helicopter. ZFL will extract and supply vibration data from helicopter flight tests for various sensor positions, helicopter loading and speeds defining the vibration spectrum of the flight envelope. These vibration data supplied in time history format can be used for laboratory testing of the Vibel on a shaker. The vibration spectra will be analyzed with respect to frequency content and acceleration amplitudes.

2.3.2.3.3 Milestones and expected result

Definition of available mechanical input and desirable electrical output energy levels

2.3.2.4 Task 5.2 The physical mechanisms of the mechanic-magnetic work cycle

2.3.2.4.1 Objectives

To perform basic research activities concerning materials physics within magnetostrictive materials.

2.3.2.4.2 Description of work

Task 5.2 The physical mechanisms of the mechano-magnetic work cycle [7 PM],

Leader: TACT

Partners: TACT [3 PM], USAL [4 PM]

TACT and USAL will work together to understand in detail the mechano-magnetic energy conversion cycle. As Terfenol so far in principle solely has been used for actuators it has become clear that very little is really understood about energy conversion in the inverse direction. Issues like magneto elastic coupling factor and energy density could well have other importance for a generator as for an actuator and actual limits of energy transferable per work cycle must be investigated. The input of mechanical energy as axial and/or radial stress loading on the magneto elastic material is of vital consequence to maximum energy transfer as well as the mechanical load of the Vibel seen by the airframe structure. Optimal magnetic bias levels relative to operating conditions should result from in-depth understanding of the work-cycle as well as when and how mechanical pre-stress should be applied.

2.3.2.5 Task 5.3 Investigation and evaluation of Terfenol and other magnetoelastic materials as to their performance potential in a Vibel

2.3.2.5.1 Objectives

To perform performance potential investigations for the new concept devices (VIBEL) to be developed in the following Tasks.

2.3.2.5.2 Description of work

Task 5.3 Investigation and evaluation of Terfenol and other magneto elastic materials as to their performance potential in a Vibel [17 PM],

Leader: USAL

Partners: USAL [6 PM], NIRDTP [8 PM], Mecel [3 PM]

USAL will concentrate their studies on Terfenol alloys and will make a complete investigation and analysis of all Terfenol materials available on the world market as well as any obtainable research samples. Determination of magnetic, magneto elastic as well as mechanical, including robustness and fatigue life, properties will be performed. Analysis of alloy microstructures and its consequences to material performance and durability will be carried out using the wide range of imaging techniques available at USAL.

NIRDTP will focus on other than Terfenol magneto elastic materials and will give an overview of these materials, their main properties and expected performance potential for mechano-magnetic energy conversion. Materials to be considered include amorphous, nanocrystalline and MSME alloys. The relation between required electrical power levels and alloy type suitability will be analyzed and mapped. Demonstration devices based on particularly interesting alternative alloys will be built and tested.

Mecel and KTH will collaborate to provide high mechanical loading testing arrangements covering meaningful mechanical frequency intervals and will participate in the testing and user aspects analysis of test results.

2.3.2.6 Task 5.4 Mechanical loading of the magneto elastic material

2.3.2.6.1 Objectives

To investigate and define the design fundamentals of the Vibel mechano-electrical generator to provide the basis for design and construction of Vibels.

2.3.2.6.2 Description of work [Mo7- Mo18]

Task 5.4 Mechanical loading of the magneto elastic material [5 PM],

Leader: TACT: Partners: TACT [2 PM], Mecel [1 PM], USAL [2 PM]

TACT and USAL will use the understanding of the mechano-magnetic work cycle and the magneto elastic properties of Terfenol to study the implication of different mechanical loading strategies for the operation and performance of a Vibel device.

Mecel will investigate possible methods for realizing different mechanical loading situations and their implications to the Vibel characteristics as a mechanical structural loading for the end users. The probably very important but practically difficult to create radial pre-stressing of Terfenol will require innovative thinking and extensive testing.

An emphasis will be placed on finding pre-stress methods providing good reproducibility and stability of the mechanical loading combined with industrial production techniques.

2.3.2.7 Task 5.5 Magnetic circuit and coil design including eddy current and hysteresis considerations

2.3.2.7.1 Objectives

To design magnetic circuit and coil of Vibels, taking in account eddy currents and hysteresis phenomena.

2.3.2.7.2 Description of work [Mo7- Mo18]

Task 5.5 Magnetic circuit and coil design including eddy current and hysteresis considerations [8 PM],

Leader: KTH;

Partners: KTH [4 PM], CED [2 PM], Mecel [2 PM]

KTH and CED have extensive and long term experience in magnetic circuit design including selection of soft and hard magnetic materials for Terfenol systems. Likewise eddy current lamination considerations are well understood. Now this knowledge base will be applied to the new challenges of mechano-magnetic energy conversion in the Vibel design.

Mecel will co-ordinate the magnetic system design and provide design requirements for coil output energy and voltage levels under different electrical loading conditions. Mecel will also participate in the adaptation to the electrical voltage output regulator.

2.3.2.8 Task 5.6 Simulation of Vibel designs for optimal performance and expected energy conversion levels

2.3.2.8.1 Objectives

To investigate and define the design fundamentals of the Vibel mechano-electrical generator to provide the basis for design and construction of Vibels.

2.3.2.8.2 Description of work

Task 5.6 Simulation of Vibel designs for optimal performance and expected energy conversion levels [20.8PM],

Leader: CED;

Partners: CED [3 PM], EADS [1 PM], KTH [8 PM], LFME [1.8 PM], Chalmers [4 PM], Mecel [3 PM]

KTH has developed unique simulation programs for high power to the limits simulation of Terfenol actuators. The simulations are based on a large, empirical data base on Terfenol to performance limits. KTH intends now to adapt the simulation program to mechano-electrical energy conversion to study and evaluate Vibel design options and expected performance levels.

CED has been involved in the development of the Atila software active material complete system designs and has also several fields modeling software in their product range. CED will complement and collaborate with KTH to make Vibel simulations as complete and multi-expected as possible.

EADS will simulate and compare different piezo-vibel designs with the focus on effectively coupling a Vibel to the vibrating structure and to provide sufficient power to operate a set of wireless sensors.

LFME will develop GA based algorithms for optimizing the Vibel energy conversion performance.

CHALMERS will develop model-based non-linear programming algorithms for determining optimal performance of Vibel mechano-electrical generators with the highest demand to energy conversion and will make comparison with the results of optimization obtained by GA.

Mecel will co-ordinate the Vibel design inputs to the simulation and participate in the analysis and evaluation of the simulation results. Mecel will also bring the technical consequences of the simulation results back into the Vibel design and initialize design modifications as well as the re-entries into an iterative design - simulations optimization process.

2.3.2.9 Task 5.7 Electrical power output regulation

2.3.2.9.1 Objectives

To investigate and define the design of electric circuitry for power output regulation.

2.3.2.9.2 Description of work

Task 5.7 Electrical power output regulation [5 PM],

Leader: Mecel

Partners: Mecel [3 PM], TACT [2 PM]

Mecel will co-ordinate this activity being responsible for the construction of the Vibel prototype(s). Mecel has expertise in automotive power regulation systems design and fabrication.

TACT will provide design input information on the role and importance of Vibel electrical load impedance relative to the mechano-magnetic work cycle and the characteristics of the mechanical energy input - which has been defined and extensively studied by TACT.

EADS-CRC will provide necessary data for circuitry design.

2.3.2.10 Task 5.8 Mechanical design of the Vibel

2.3.2.10.1 Objectives

To investigate and define the mechanical design of the devices

2.3.2.10.2 Description of work

Task 5.8 Mechanical design of the Vibel [27.5 PM],

Leader: Mecel

Partners: Mecel [10 PM], Chalmers [12 PM], EADS [3.5 PM], Newlands [2 PM]

Mecel will build the Vibel prototypes and will study different design options ensuring optimal stress loading of the Terfenol element and overall Vibel mechanical stability ensuring maximum unit life.

Inputs from the aerospace partners on vital aspects of the Vibel mechanical design will be actively gathered and will be given special consideration in the design of the Vibel.

Chalmers will develop methodology and software for designing optimal Vibel mechano-electrical generators based on global model-based optimization approach and will perform computational analysis supporting the Vibel design work.

EADS will provide their simulation expertise to optimize the coupling of the Vibel to the driving mechanical structure and will build a miniaturized prototype piezo-Vibel according to the most promising of the designs investigated in subtask 5.6.

Newlands will contribute their experiences from building commercial Terfenol loudspeakers.

2.3.2.10.3 Task 5.9 Test and evaluation of the Vibel mechanical to electrical energy conversion performance

2.3.2.10.4 Objectives

To test and evaluate the Vibel mechanical to electrical energy conversion performance.

2.3.2.10.5 Description of work

Task 5.9 Test and evaluation of the Vibel mechanical to electrical energy conversion performance [17.8 PM],

Leader: LFME;

Partners: LFME [1.8 PM], Uni-NA DPA [2 PM], Mecel [7 PM], EADS [1 PM], TACT [1 PM], Newlands [2 PM], LPA-ZIP [3 PM]

LFME will co-ordinate the Vibel testing applying defined mechanical energy input profiles and measuring the electrical power output. Optimal energy conversion working points will be searched and conversion ratios, output voltage and current measured.

Uni-NA DPA will supply vibrational energy power spectra corresponding to actual Vibel locations proposed by the aerospace partners. Uni-NA DPA will also measure the mechanical energy input into the Vibel during the testing to verify the actual energy input.

Mecel will provide the main mechanical test arrangement and the mechanical energy source as well as the Vibel prototype integrated into the test structure.

KTH will measure the electrical energy output under different loading conditions and will, together with TACT, contribute to the analysis and evaluation of the magneto elastic energy conversion.

EADS will provide sophisticated experimental facilities and extensive experience acquired during the last decade in PZT testing and characterization.

Newlands will offer a test set-up involving a very, large Terfenol vibrational actuator.

LPA-ZIP will experimentally investigate the Vibel potential of magnetostrictive DVAs produced in the MESA project as well as those produced in WP2.

2.3.2.10.6 Milestones and expected result

M5-3 Mo24 Complete Vibel unit manufactured and ready for testing

2.3.2.11 Task 5.10 Comparison between magneto elastic and piezoelectric continuous, high power mechano-electric energy conversion

2.3.2.11.1 Objectives

To study and analyze the comparison between magneto elastic and piezo performance profiles for their implications to Vibel products and marketing strategies

2.3.2.11.2 Description of work

Task 5.10 Comparison between magneto elastic and piezoelectric continuous, high power mechano-electric energy conversion [8 PM],

Leader: EADS

Partners: EADS [2 PM] CED [3 PM], TACT [2 PM], Mecel [1 PM]

As magneto elastic and piezoelectric technologies are generally driven by two separate technical communities often knowing too little about the virtues of the other technology it is important for relevant and sound arguments of a new active material technology such as the Vibel to include an activity of comparison.

EADS will contribute their experiences with piezoelectric generators supplying electronic circuitry and the data acquired on the piezo-Vibel.

CED are strongly involved in piezoelectric technology development but has also worked extensively with Terfenol and other magneto elastic materials, also in several EU projects.

TACT has worked on Terfenol and amorphous magneto elastic technology development since many years creating a large number of patents and technical development projects. TACT also works with one company constructing very small electrical power sources driven by mechanical vibrations.

Therefore CED, EADS and TACT will jointly analyze the analogies and differences between magneto elastic and piezoelectric electrical power generation attempting to capture the benefits, drawbacks and optimal utilization of the two materials in this application.

Mecel will study and analyze the comparison between magneto elastic and piezo performance profiles for their implications to Vibel products and marketing strategies.

2.3.2.12 Task 5.11 Mechanical integration of the Vibel in the aircraft / helicopter structure

2.3.2.12.1 Objectives

To evaluate the Vibel integration into the airframe structure.

2.3.2.12.2 Description of work

Task 5.11 Mechanical integration of the Vibel in the aircraft / helicopter structure [2.5 PM],

Leader: LFME;

Partners: LFME [1 PM], Mecel [1.5 PM]

LFME will co-ordinate the activity of Vibel integration into the airframe structure. Furthermore, LFME will particularly study the utilisation of controlled aerodynamic structural flutter in combination with the Vibel for emergency electrical power generation.

Mecel will take responsibility for adaptation of the Vibel design to be suitable to the chosen airframe integration location.

2.3.2.13 Task 5.12 Utilisation of the Vibel electrical power source in the electrical system of the aircraft / helicopter

2.3.2.13.1 Objectives

To test the Vibel electrical power source in the system of the aircraft/helicopter.

2.3.2.13.2 Description of work [Mo24- Mo36]

Task 5.12 Utilisation of the Vibel electrical power source in the electrical system of the aircraft / helicopter [5.6 PM], Leader: LFME;

Partners: EADS [3 PM], LFME [2.6 PM]

EADS will build a demonstrator of a totally wireless sensor module supplied by an attached vibel and transmitting data wireless to the receiver. Such a sensor could for example be located in the rotor of a helicopter (e.g. icing detection). EADS will also map other potential uses of the Vibel in onboard electrical systems and the benefits foreseen.

LFME will collaborate to create an optimal emergency electrical power Vibel-flatter system defining both the electrical power consumers to be supplied in various emergency situations as well as the most suitable locations of Vibel-flatter electricity generators on the aircraft structure. An analysis of the electrical power generation capabilities offered by the Vibel technology with respect to the needs of electrical power across an aircraft will be made and an assessment of the possible benefits and new opportunities offered by the Vibel technology. The role of the Vibel in achieving a More Electrical Aircraft will be reviewed in the light of this novel, simple and powerful device.

2.3.2.13.3 Milestones and expected result

M5-4 Mo36 Vibel tests and performance + value analysis completed M36

3 THE TEST ARTICLE: EXPERIMENTAL AND NUMERICAL MODELLING

This part presents numerical and experimental activities developed by the University of Naples, department of aeronautical engineering, within the Research Project funded by the European Commission within the 6th FP named MESEMA. Aim of the chapter is the description of the numerical and experimental activities performed in order to characterize the vibro-acoustic behavior of a partial turboprop fuselage section available in the Alenia plant in Naples and selected as WP2.1 test-article.

The validated numerical model will represent the reference for all the simulations that will be performed by the Partners involved into development of control algorithms and system. Only the structural experimental modal analysis is described and the related correlation between experimental and numerical modal analysis results.

3.1 INTRODUCTION

This part presents numerical and experimental activities developed by the University of Naples, Department of Aeronautical Engineering, within the WP2.1 of the MESEMA Research Project.

Aim of the numerical activities is to select the structural elements to be controlled for optimizing the performance of the control approach as well for obtaining an estimation of required control forces values when the fuselage is loaded by a typical primary field. This numerical investigation will permit the involved partners to carry out the guidelines for the actuator design in terms of required specifications. In fact, according to some topological constraints (general dimensions, max allowed mass, etc.) this study will also issues the requirements of the actuators in terms of forces vs. frequency in order to cancel the primary noise field by treating in the most convenient way the selected fuselage structural components. The related experimental activities have been performed on a fuselage barrel provided by Alenia acquiring vibro-acoustic responses up to 800 Hz with a broad band primary noise.

In order to choose the best modeling solution among those developed the numerical analysis results have been compared with those coming from experimental tests and the models have been updated.

3.2 EXPERIMENTAL MODAL ANALYSIS

Among the MESEMA Project WP2.1 activities the ATR 42 fuselage test case has to be characterized in terms of modal parameters and vibro-acoustic behavior. There is, in fact, the need to create an experimental modal model in order to define the requested force and displacement actuator outputs; these informations along with the actuators, sensors and amplifiers operating frequency range will then be defined, with reference to the goal of controlling noise and vibrations in a frequency range between 300 – 1000 Hz.

In the Alenia Acoustics department the Atr42 fuselage test case was suspended with a special structure to simulate the free-free conditions. Two shakers were used to excite the structure and accelerometers were positioned on the skin of the fuselage in correspondence of the frames or stiffeners.

The structure was excited by shakers using a random signal. It was impossible to use a multi input multi output technique due to the restriction of the acquisition system. So the structure was excited with two shakers in two different runs. The structure was divided in thirteen acquisition sections and on each sections 34 responses points were acquired. The ATR 42 floor is also acquired. A four by six acquisition grid was created..

Single direction accelerometers were positioned. The software used to pilot the shaker and to acquire accelerometers signal is the LMS Cada-x v.3.3.05 software. It is an integrated software that can manage all the acquisition process, save the data and analyze them using different modal technique.

3.2.1 APPROACH

The tests pertaining to the first part (the elastic mode-shapes) have been performed by computing the frequency response functions between many points of the structure, each with reference to a fixed position of the excitation point. Nextly the position of the excitation point has been changed and the frequency response functions, for the same positions, have been acquired. This approach should eliminate the probability of hidden mode-shapes, after a careful selection of the excitation points.

The main steps for such test are therefore:

1. Selection of the excitation and acquisition points
2. Evaluation of the frequency response function. This task is accomplished, in our case, by the LMS/CADA-X software running on an HP Workstation
3. Modal parameters identification using the proper algorithms programmed inside the CADA-X software.

The third step may be completed without the structure, since it is only a software analysis; therefore the fuselage test case is necessary only for the first two items.

- The excitation signal used during these tests has been a Random Excitation, produced by the HP 3560x front-end. The signal was generated and pilot by the LMS-Cada-X software. The software can control the generation and acquisition process. The following two different excitation points have been used:
- Frame 5 of the Atr test case, left part;
- Frame 5 of the Atr test case in correspondence of the floor skin connection right part;

For all these configurations of the excitation points, 454 (frequency response functions have been acquired. During these tests the fuselage test case has been isolated

from the ground, in fact the fuselage is suspended using a special structure as Figure 3-1 **Errore. L'origine riferimento non è stata trovata.** shows

Photo 3-1 shows the points positions on the different part of the fuselage in the modal tests.

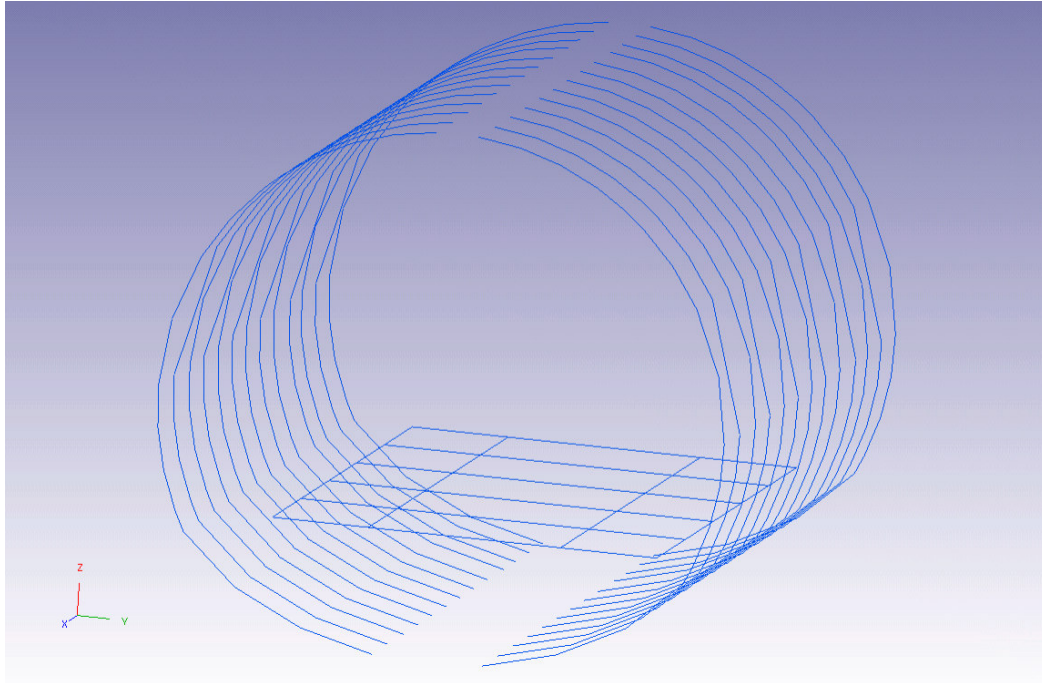


Figure 3-1: *Response Points*

3.2.2 FREE-FREE BOUNDARY CONDITIONS

The free-free conditions are realized: The fuselage test case is closed on both sides with two heavy structures (Caps). The ended parts of the fuselage are screwed on these caps. The caps are connected to the external frame with three vertical springs. Photo 3-1 shows how the free-free conditions were realized.



Photo 3-1: Fuselage Test Case

3.2.3 INPUT SET-UP

A Bruel & Kjaer shaker was used as generator force unit in the ground vibration tests.



Photo 3-2: Shaker on the Left Fuselage Side

A mechanical system was designed and built to lift the shaker. (Photo 3-2 and Photo 2-3) The system has the capability to move the shaker along the vertical axis. The mechanism has also two screws in order to have a micrometric position system. The

shaker is connected to the structure through four soft springs. The use of the springs is necessary to isolate the shaker from the ground and to introduce a free-free boundary condition to the shaker.



Photo 3-3: Shaker on the Right Fuselage Side

Photo 3-3 shows the excitation point position in excitation test.

3.2.4 CALCULATION OF THE FREQUENCY RESPONSE FUNCTION

The frequency response functions are computed directly inside the HP Workstation by the CADA-X modal software. The two signals, from the structure to the computer, come from the impedance head installed between the sting of the dynamic exciter and from a Endevco Type 61-100 accelerometer running on the structure.

For any other reference, it is worthwhile to refer to the proper manuals of the CADA-X system, worldwide diffused software for the modal testing monitor and identification, [xx].

3.2.5 TEST SETUP

A short description of the test set-up follows, completed with a block diagram of the main devices used. This set-up may be subdivided in the following three main blocks:

- Excitation
- Acquisition
- Analysis

The instrumentation used in the experiment is:

- Integrated Acquisition/generation system installed on HP 715/50 Workstation connected to eight acquisition channels and one generation channel HP 3560x frontend.
- The software that manages the Acquisition/generation system is LMS Cada-X ver. 3.3.05 product by LMS Interanational Belgium.
- Shaker Bruel & Kjaer Type 4805 shaker are piloted by Bruel & Kjaer amplifier Type 2707.
- Impedence Head B&K Type 8202 connected to B&K Type 2635 charge amplifier
- Accelerometers Endevco Type 61-100.

3.2.6 EXCITATION

The excitation has been obtained through an electro-dynamic exciter (Bruel & Kjaer), driven by a random signal produced by Hp 3560x Front-end. Such signal was synchronized with the acquisition by the software itself, generating the driving signal in the 0÷512 *Hz* frequency range which reached the exciter after the amplification of a power amplifier. A piezoelectric B&K Type 8202 impedance head has been mounted between the exciter and the structure in order to detect the real force entering the structure and the acceleration in the same point. A charge amplifier B&K Type 2635 provided the necessary power supply and signal conditioning for such sensor.

3.2.7 ACQUISITION

The structural response has been measured with Endevco Type 61-100 accelerometers properly located on the structural components of the fuselage under test. As for the impedance force gauge, also this signal has been amplified and conditioned before reaching the workstation for the next steps.

Figure 3-2, Figure 3-3, and Figure 3-4 show an example of the Autopower function, the driving point FRF and driving point coherence function acquired during the left side excitation.

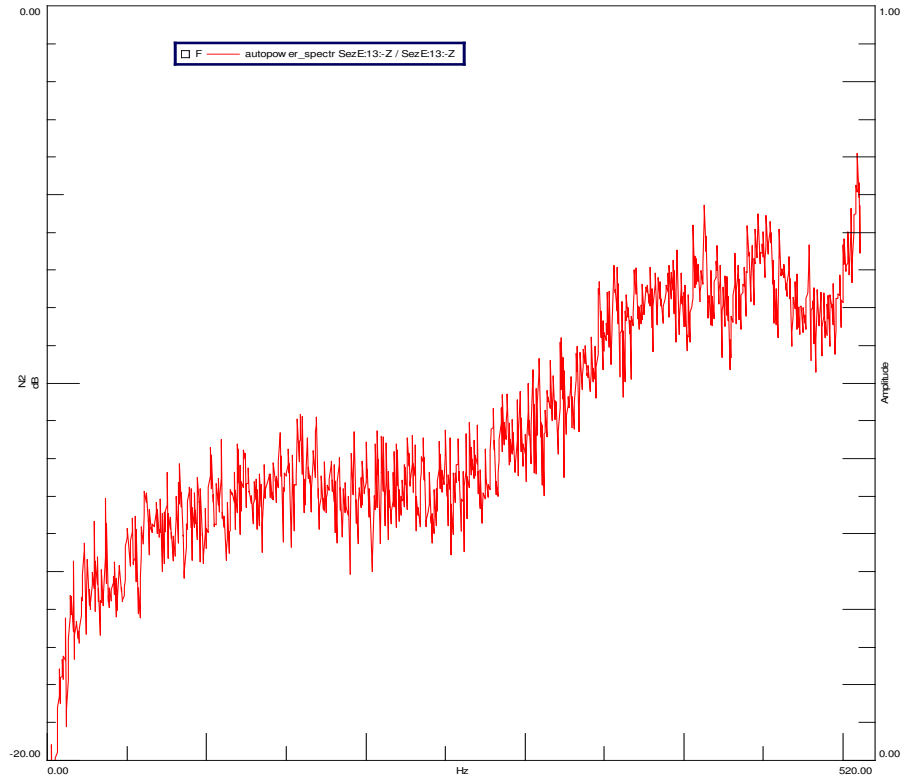


Figure 3-2: Input AutoPower

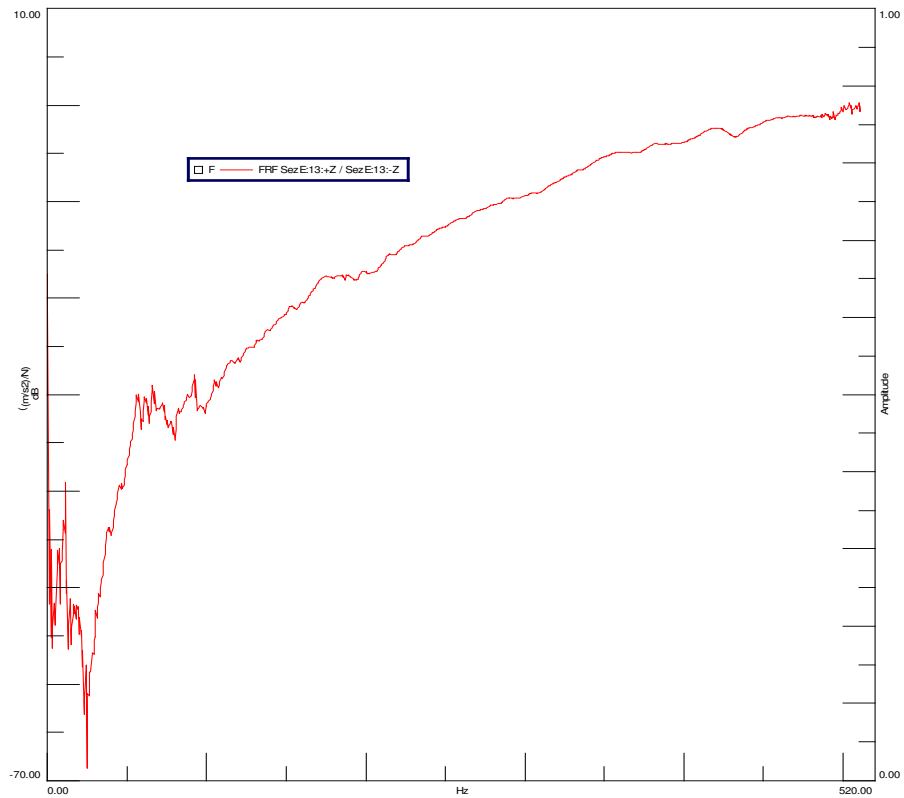


Figure 3-3: Driving Point FRF Function

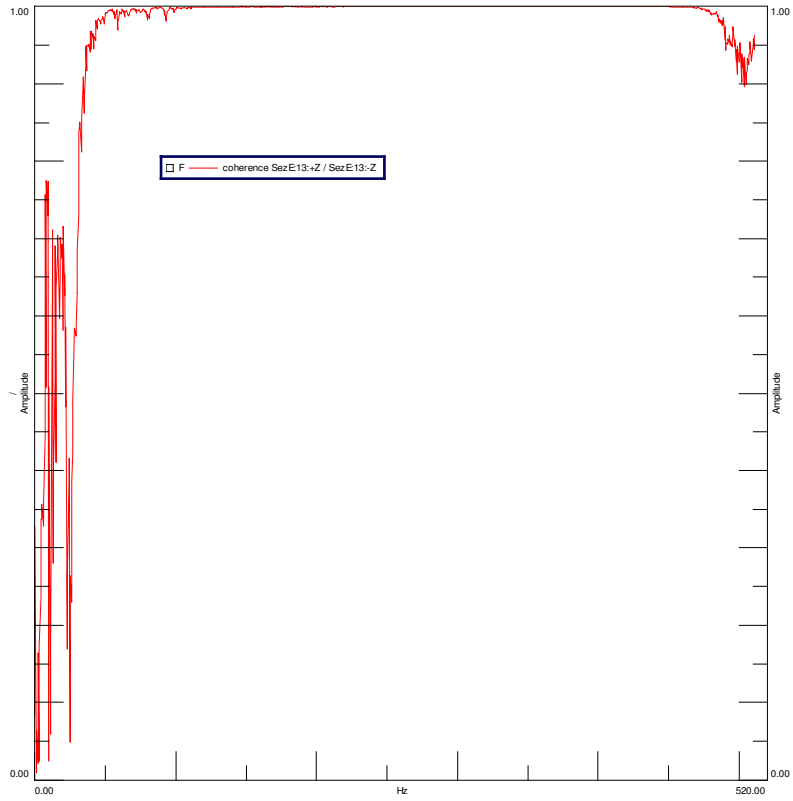


Figure 3-4: Driving Point Coherence Function

Figure 3-5, Figure 3-6 and Figure 3-7 show an example of the Autopower function, the driving point FRF and driving point coherence function acquired during the right side excitation.

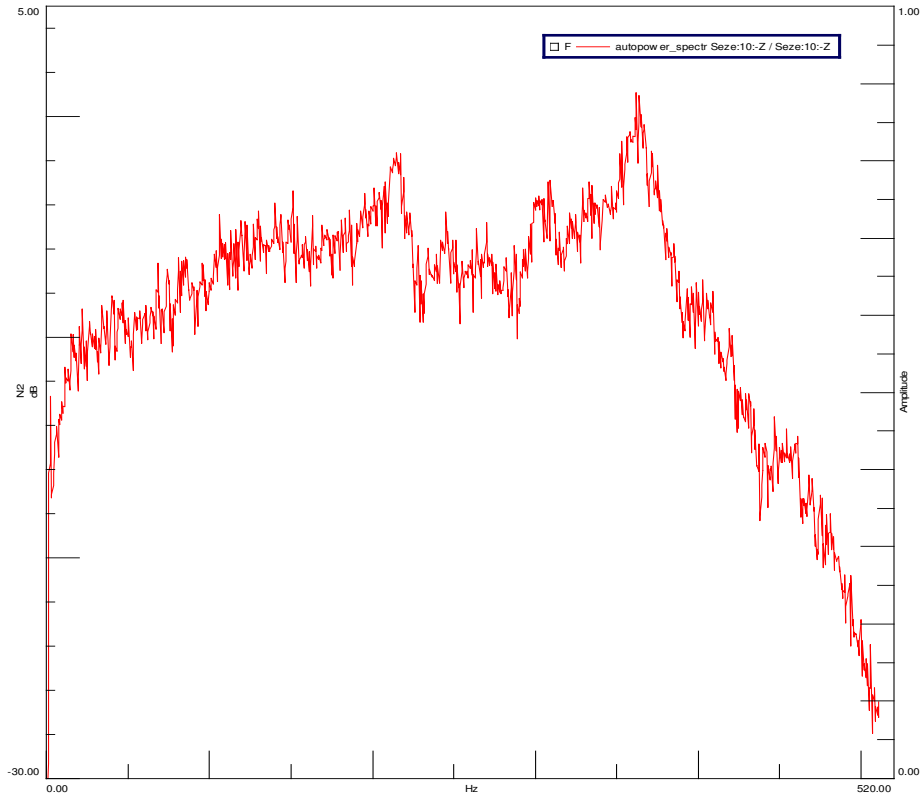


Figure 3-5: Input AutoPower Spectrum

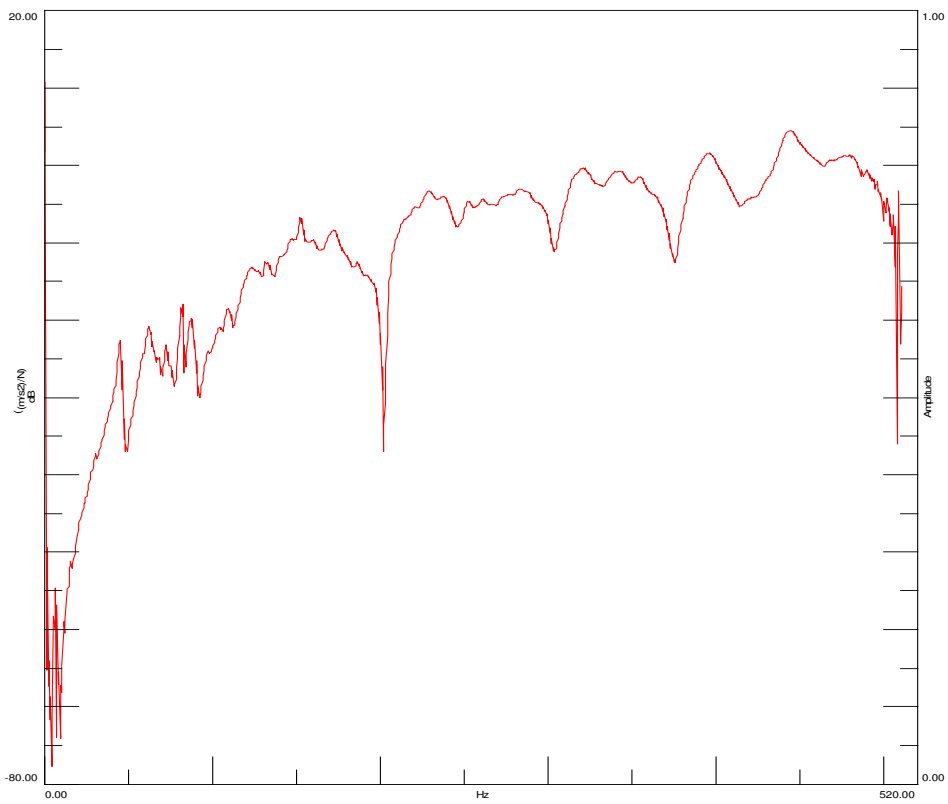


Figure 3-6: Driving Point FRF Function

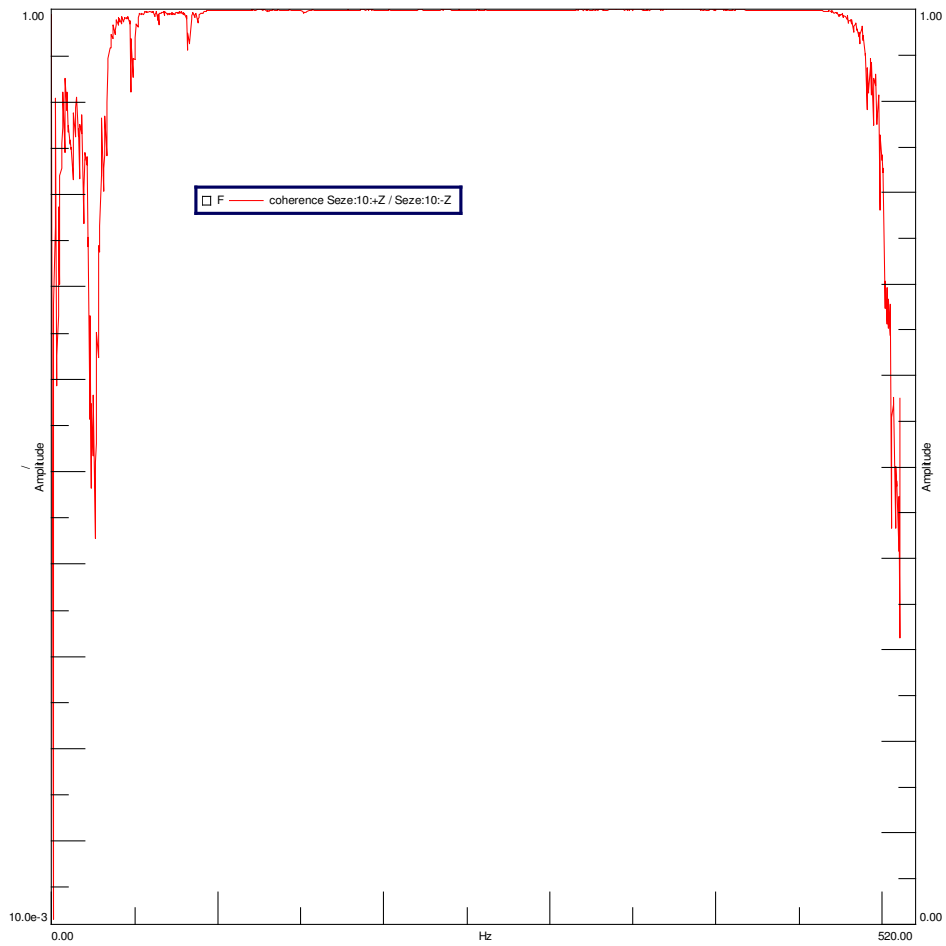


Figure 3-7: Driving Point Coherence Function

3.2.8 ANALYSIS

The software CADA-X provides the subsequent steps for the analysis and the extraction of the modal parameters. Therefore the input and the output signals are digitalized and, using an FFT algorithm, converted into the frequency domain for the computation of all the estimators available in this domain (frequency response function, coherence, and so on).

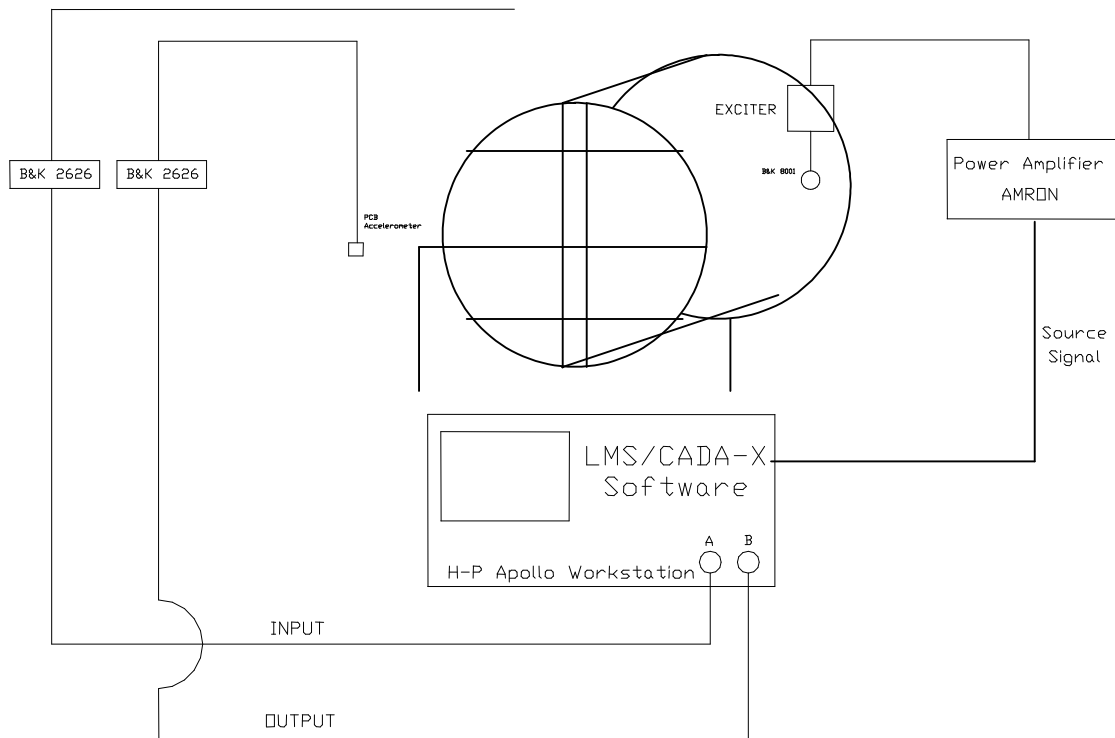


Figure 3-8: Main Components of the Test Setup .

3.2.9 RESULTS

The results obtained from the analysis of the modal analysis tests on the ATR42 fuselage Test Case are presented. These results are relative to the identification of the natural frequencies, damping factors and to a description of the modal behaviour of the test case, trying to identify the main structural components most probably responsible for the vibration at that specific frequency.

3.2.10 STRUCTURAL ELASTIC MODEL LEFT EXCITATION

The structural elastic mode-shapes have been identified using the complete left excitation point.

Figure 3-9 shows the stabilization diagram in the extracting mode parameter procedure using the LMS Polymax® method.

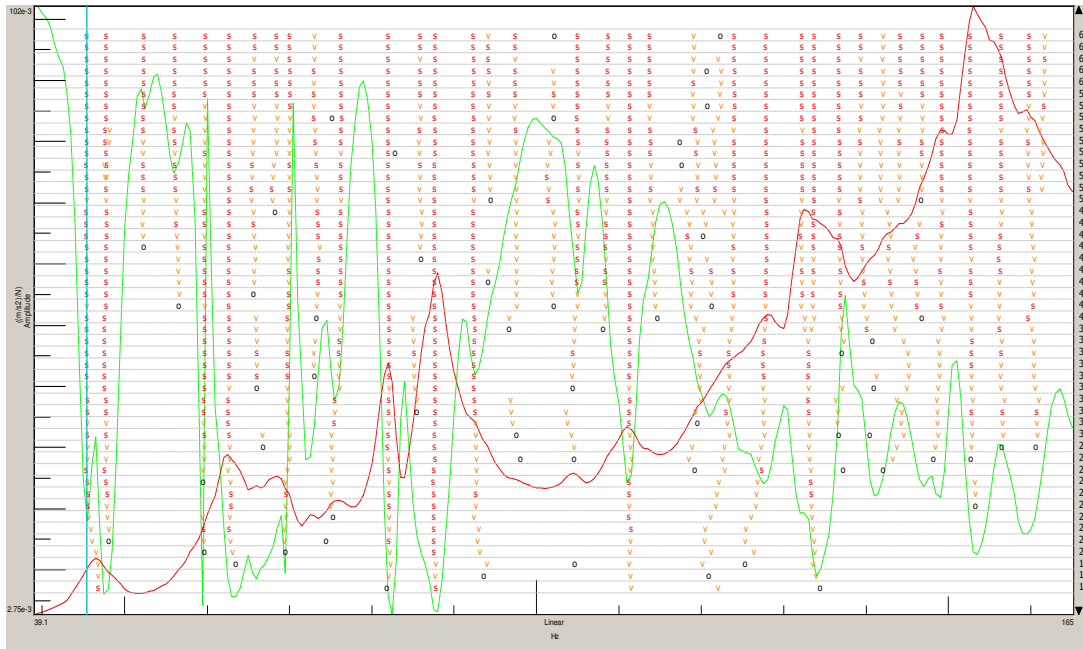


Figure 3-9: Stabilization Diagram Polymax® method

Table 3-1 shows the results obtained from the left excitation, in the table are reported the list of the extracted pole with the geometric description of the mode itself.

Not all the modes are reported because above 120 Hz the local panel dynamics is predominant over the global mode shapes and the description is more difficult.

Mode Id. (Fig.)	Frequency	Damping	Desc fig	Description
Figure 3-11	47.433	0,05	2,1	Anti Simm Bending Floor
Figure 3-12	57.521	0,09	3,0	Three Cylinder Lobe
Figure 3-12	61,522	0.10	1,1	Bending Floor
Figure 3-12	68.275	2.80	3,0	Three Cylinder Lobe
	74.658	0.86	1,1	Anti Simm Bending Floor
	75.993	1.24	3,0	Three Cylinder Lobe
	78,430	0.78	2,2	Anti Simm Bending Floor
	85.979	1.20	4,0	Four Cylinder Lobe
	88.507	1.51	4,0	Four Cylinder Lobe
	91.101	0.53	3,0	ThreeCylinder Lobe UP, One Down
	93.268	0.53	4,1	Four Cylinder Lobe, One longitudinal
	95,908	1.30	4,1	Four Cylinder Lobe, One longitudinal
	100.363	1.33	2,1	Anti Simm Bending Floor
	103.981	0.84	5,1	Five Cylinder Lobe, One Long.
	106.196	1.03	4,2	Four Cylinder Lobe, One longitudinal
	109.961	0.67	3,1	Three Up side Cylinder Lobe
	113.597	0.67	4,2	Four Cylinder Lobe, Two longitudinal
	115.604	1.33	4,2	Four Cylinder Lobe, Two longitudinal
	120.901	0.69	4,2	Four Cylinder Lobe, Two longitudinal
	127.897	1.16		Four Cylinder Lobe, Two longitudinal
	131.950	0.22	4,3	Four Cylinder Lobe, Three longitudinal
	138.240	0.24		Central Cylinder Lobe

	145.801	0.45	2.1	Anti Simm Bending Floor
	148.312	0.60	4,2	Four Cylinder Lobe, Two longitudinal
	149.809	0.27	4,2	Four Cylinder Lobe, Two longitudinal

Table 3-1: List of the Mode-Shapes.

3.2.11 STRUCTURAL ELASTIC MODE RIGHT EXCITATION

The structural elastic mode-shapes have been identified using the complete right excitation point.

Figure 3-10 shows the stabilization diagram in the extracting mode parameter procedure using the LMS Polymax® method.

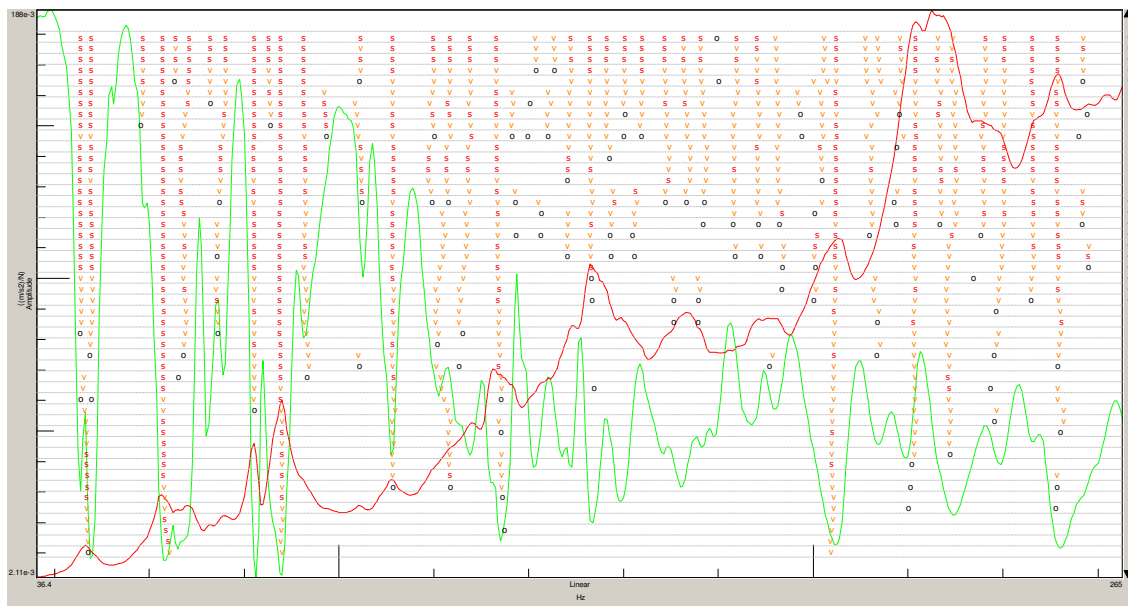


Figure 3-10: Stabilization Diagram Polymax® method

Errore. L'origine riferimento non è stata trovata. shows the results obtained from the left excitation, in the table are reported the list of the extracted pole with the geometric description of the mode itself.

Not all the modes are reported because above 120 Hz the local panels dynamics is predominant over the global mode shapes and the description is more difficult.

Mode Id. (Fig.)	Frequency	Damping	Desc fig	Description
Figure 3-11	47.749	2.15	2,1	Anti Simm Bending Floor
Figure 3-12	57.527	1.67	3,0	Three Cylinder Lobe
Figure 3-13	61.489	1.85	1,1	Anti Simm Bending Floor

Figure 3-12 Errore. L'origine riferimento non è stata trovata.	75.844	0.96	3,0	Three Cylinder Lobe
	78.448	0.78	2,1	Anti Simm Bending Floor
	82.593	0.60	4,0	Four Cylinder Lobe
	85.999	1.22	4,0	Four Cylinder Lobe
	88.561	1.56	4,0	Four Cylinder Lobe
	91.172	0.58	3,0	ThreeCylinder Lobe UP, One Down
	93.263	0.53	4,1	Four Cylinder Lobe, OneLongitudinal
	96.002	1.28	4,1	Four Cylinder Lobe, Longitudinal
	100.394	1.47	2,1	Anti Simm Bending Floor
	103.759	0.82	5,1	Four Cylinder Lobe, One longitudinal
	106.172	1.08	5,1	Four Cylinder Lobe, One longitudinal
	109.685	0.76	3,1	Three Up side Cylinder Lobe
	113.528	0.57	4,2	Four Cylinder Lobe, Two longitudinal
	115.625	1.27	4,2	Four Cylinder Lobe, Two longitudinal
	120.987	0.63	4,2	Four Cylinder Lobe, Two Longitudinal
	128.044	1.09	4,2	Four Longitudinal, Two Longitudinal

Table 3-2: List of the Mode-Shapes.

From the analysis of the mode shape and from the analysis of the data the right excitation gives better results in terms of mode shape, frequency.

Table 3-3 reports and compare the pole extracted in both the excitations.

Right Ex	Left Ex	Description	Diff %
47.749	47.433	Anti Simm Bending Floor	0,66
57.527	57.521	Three Cylinder Lobe	0,01
61.489	61,522	Bending Floor	-0,01
75.844	75.993	Three Cylinder Lobe	-0,19
85.999	85.979	Four Cylinder Lobe	0,02
91.172	91.101	ThreeCylinder Lobe UP, One Down	0,07
93.263	93.268	Four Cylinder Lobe, One longitudinal	-0,005
96.002	95,908	Four Cylinder Lobe, One longitudinal	0,01
100.394	100.363	Anti Simm Bending Floor	0,03
106.172	106.196	Anti Simm Bending Floor	-0,02
109.685	109.961	Three Up side Cylinder Lobe	-0,25
113.528	113.597	Four Cylinder Lobe, Two longitudinal	-0,06
115.625	115.604	Four Cylinder Lobe, Two longitudinal	0,01
120.987	120.901	Four Cylinder Lobe, Two longitudinal	0,07

128.044	127.897	Four Cylinder Lobe, Two longitudinal	0,11
---------	---------	--------------------------------------	------

Table 3-3: List of the Mode-Shapes in the two tests

The following figures show some of the modal shapes extracted from the modal analysis data. They are related to modes printed in the Table 3-3.

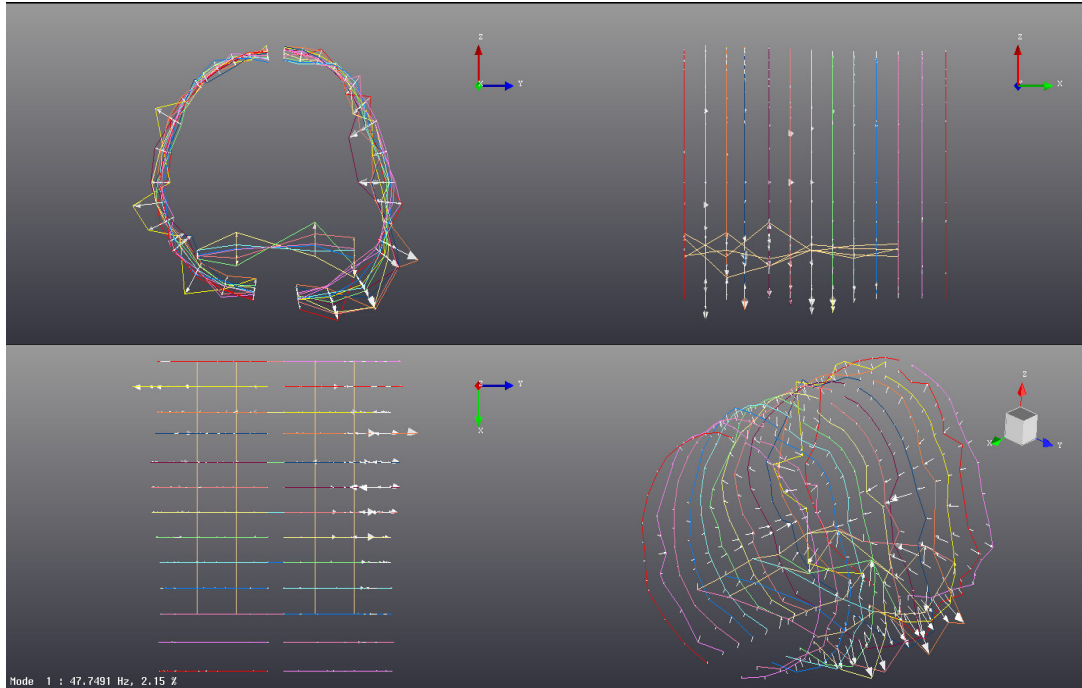


Figure 3-11: Mode 47.749 Hz

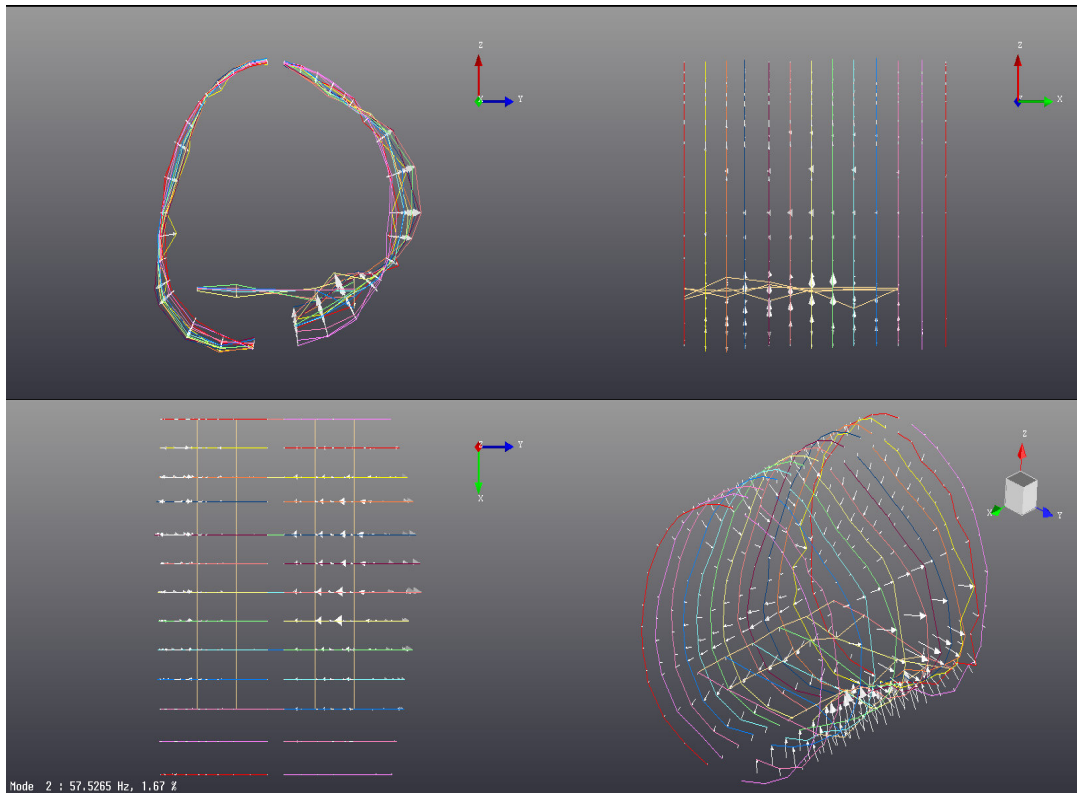


Figure 3-12: Mode 57.527 Hz

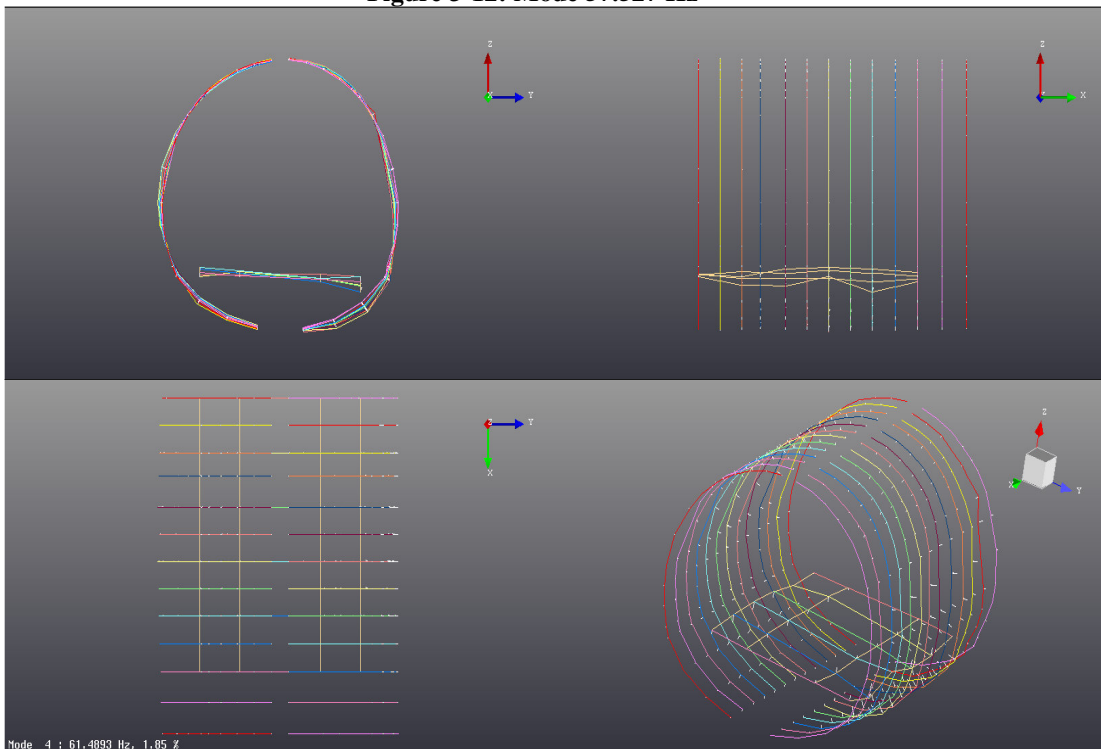


Figure 3-13: Mode 61.469 Hz

3.2.12 VALIDATION PARAMETERS

The mode shapes are extracted from the two analysis are validated using the MAC factor.

The MAC (Modal Assurance Criterion) is the scalar vector of the mode shape. It is a square symmetric matrix with the diagonal terms equal to one. Values in the upper or lower part of the matrix close to one indicates that the two mode shape are linear dependent.

The mode shape extracted from the left data are not well defined and the quality is poor compared to the right data

The MAC non diagonal data related to the left test are not zero and many of them are close and bigger than 0.5. Instead the MAC matrix related to the right test shows better results but It indicates that the mode 10 at 82.595 Hz is similar to the mode 13 at 91.174Hz

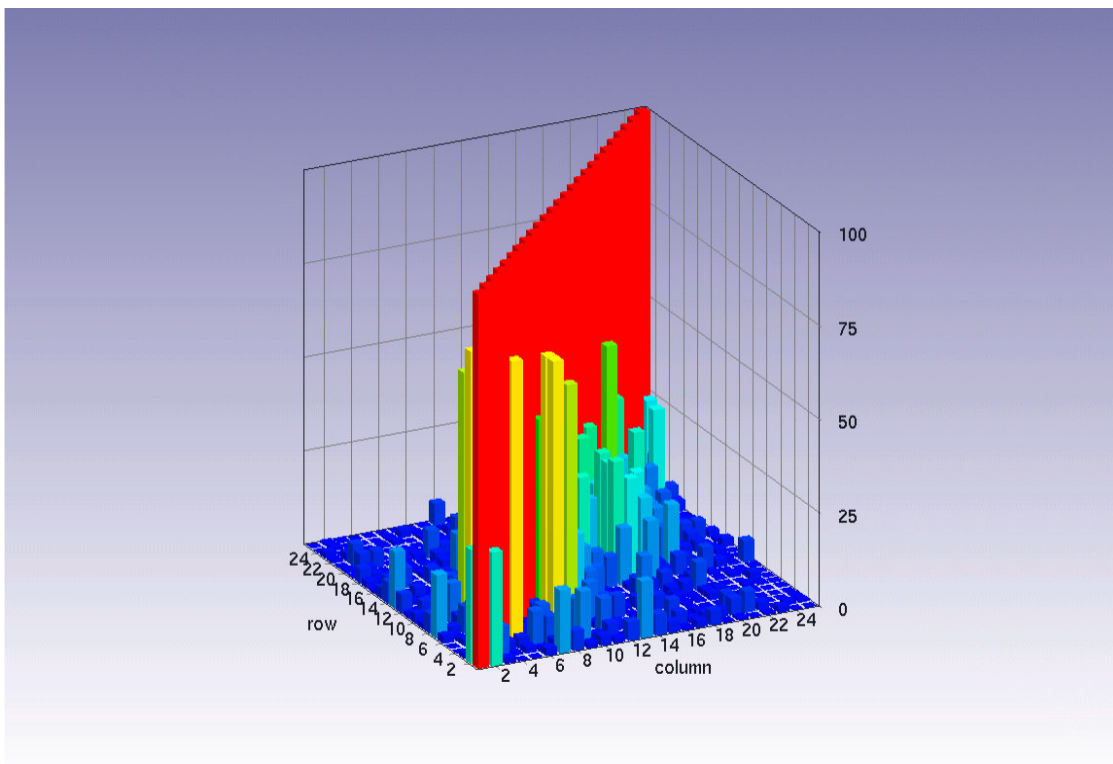


Figure 3-14: Mac Left Excitation

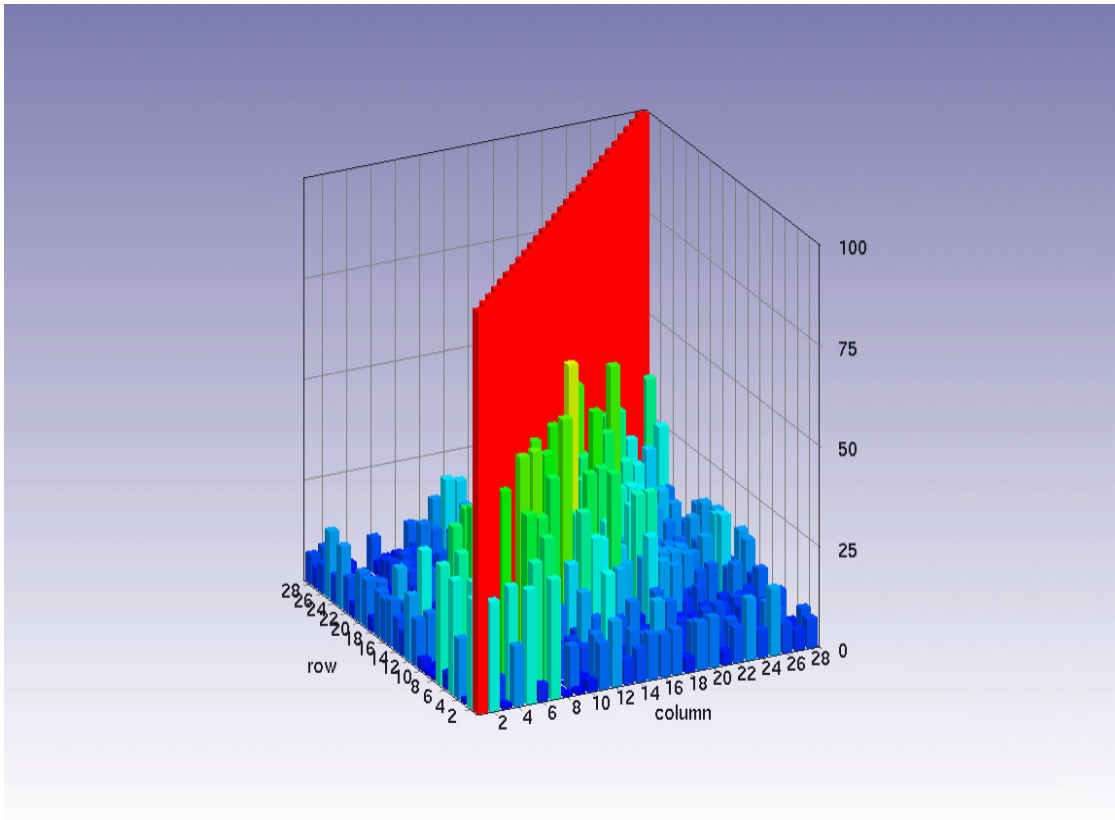


Figure 3-15: Mac Right Excitation

Left Ex.	Hz	Right Ex.	Hz	Diff.	MAC %
2	48.20	1	47.76	0.93	60.1
3	57.53	2	57.53	-0.01	88.9
4	59.45	3	59.45	-0.00	99.1
5	61.53	4	61.50	0.05	91.0
6	65.04	5	64.84	0.30	84.8
8	68.29	6	68.27	0.03	91.3
9	69.90	7	69.90	0.00	98.6
12	76.00	8	75.85	0.20	69.6
13	78.43	9	78.45	-0.02	62.9
14	82.62	10	82.59	0.03	92.4
15	85.99	11	86.01	-0.02	86.4
16	88.52	12	88.59	-0.08	87.6
17	91.10	13	91.17	-0.08	77.7
18	93.27	14	93.26	0.01	71.0
19	95.92	15	96.01	-0.10	81.7
20	100.37	16	100.40	-0.03	70.5
21	103.89	17	103.76	0.13	60.5
22	106.20	18	106.18	0.02	75.4
23	109.96	19	109.69	0.25	73.7
24	113.60	20	113.53	0.06	60.0
25	115.66	21	115.63	0.02	82.3

Table 3-4: Mac Values

Table 3-4 shows the Mac values extracted from the Right and Left Excitation Analysis.

The Mac values are higher than 80% in most cases. It shows that the results have high quality and they can be used in the father analysis.

3.3 FRAME MODAL HAMMER TEST

Due to the high modal density of the structure a part of fuselage was investigated with the hammer modal analysis technique.

The nodal analysis on complete fuselage shows that the modes can be clearly identify in the frequency range 0-120/140 Hz. Above this frequency range the system shows an high modal coupling behavior and local modal phenomena starts to be expressed.

This second test has the main goal to:

- Identification of frame mode shapes
- Creation of a modal model of a small part of the fuselage

The modal model that come out from this second test can help the design of the actuator and give information to the control people in the design of the active control system that pilot the actuator.

The acquisition FRF procedure is similar to that followed in the previous test, but instead to use an electrodynamic shaker to generate the frame input displacement, an instrumented hammer is used.

This particular transducer is similar to a normal hammer, but and the end of its head it has a force piezoelectric transducer that is able to valuate the force developed during the impact.

3.3.1 APPROACH

The tests pertaining to the first part (the elastic mode-shapes) have been performed by computing the frequency response functions between several excitation points and one reference points on the structure. Nextly the position of the excitation point has been changed and the frequency response functions, for the same positions, have been acquired. This approach should eliminate the probability of hidden mode-shapes, after a careful selection of the excitation points.

The main steps for such test are therefore:

1. Selection of the excitation and acquisition points
2. Evaluation of the frequency response function. This task is accomplished, in our case, by the LMS/CADA-X software running on an HP Workstation
4. Modal parameters identification using the proper algorithms programmed inside the CADA-X software.

The third step may be completed without the structure, since it is only a software analysis, therefore the fuselage test case is necessary only for the first two items.

In the test 72 (frequency response functions) have been acquired. During these tests the fuselage test case has been isolated from the ground, in fact the fuselage is suspended using a special structure as Figure 3-16 shows

Figure 3-16 shows the points positions on the different part of the fuselage in the modal tests.

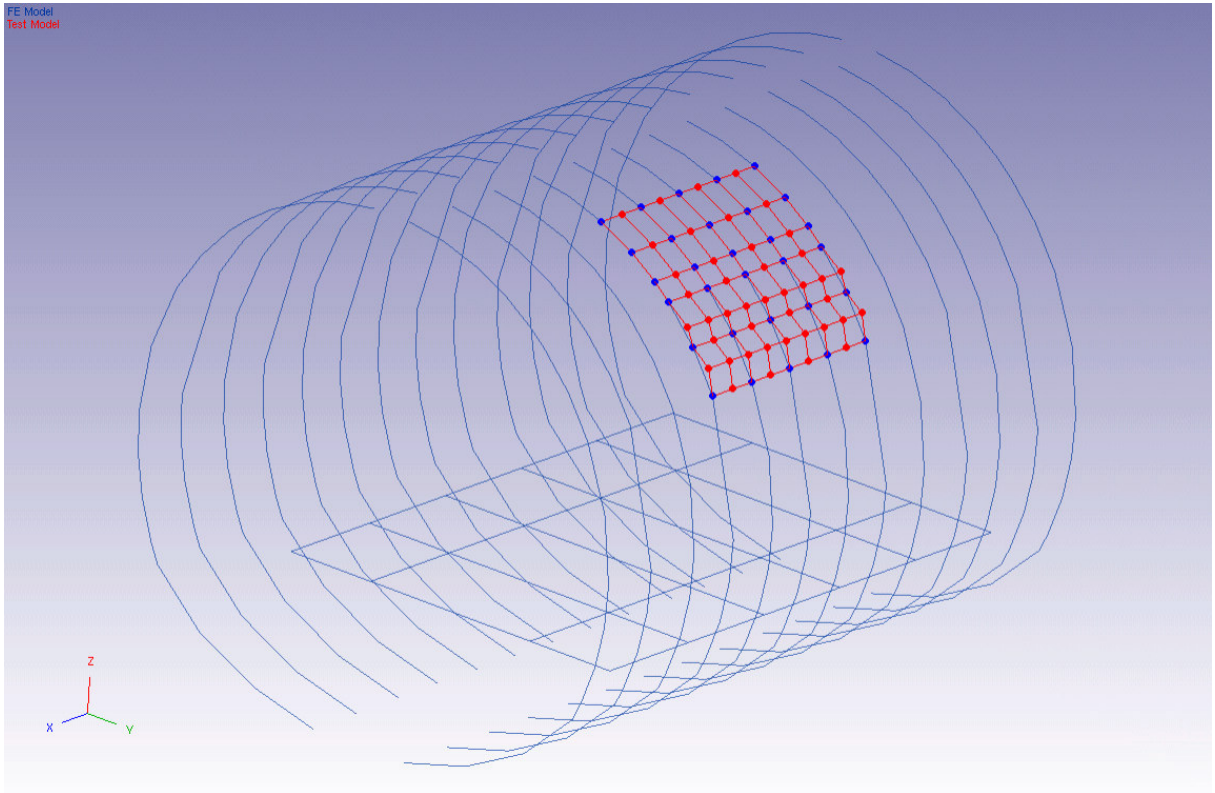


Figure 3-16: Response Points

3.3.2 INPUT SET-UP

A PCB Model 086C03 hammer was used as generator force unit in the frame modal test.



Photo 3-4: Hammer used in the test

The fuselage was positioned in the same way of the previous test: free-free condition was created for the fuselage.

A 9X8 acquisition grid points was created.

The technique used in this test was the roving hammer test.

Only one accelerometer was positioned on the acquisition grid. The hammer roves on the grid. After each acquisition the operator move the hitting acquisition point. Each acquisition is maenad on 10 hits.

3.3.3 CALCULATION OF THE FREQUENCY RESPONSE FUNCTION

The frequency response functions are computed directly inside the HP Workstation by the CADA-X modal software. The two signals, from the structure to the computer, come from the hammer head and the Endevco Type 61-100 accelerometer positioned on the structure.

For any other reference, it is worthwhile to refer to the proper manuals of the CADA-X system, worldwide diffused software for the modal testing monitor and identification, [xx].

3.3.4 TEST SETUP

A short description of the test set-up follows, completed with a block diagram of the main devices used. This set-up may be subdivided in the following three main blocks:

Excitation

Acquisition

Analysis

The instrumentation used in the experiment is:

- Integrated Acquisition/generation system installed on HP 715/50 Workstation connected to eight acquisition channels and one generation channel HP 3560x frontend.
- The software that manages the Acquisition/generation system is LMS Cada-X ver. 3.3.05 product by LMS Interanational Belgium.
- PCB Model 086C03 hammer.
- Accelerometers Endevco Type 61-100.

3.3.5 EXCITATION

The excitation has been obtained through PCB Model 086C03 hammer. The hammer roves on the grid. After each acquisition the operator move the hitting acquisition point. Each acquisition is maenad on 10 hits.

3.3.6 ACQUISITION

The structural response has been measured with Endevco Type 61-100 accelerometers properly located on the structural components of the fuselage under test. As for the hammer force gauge, also this signal has been amplified and conditioned before reaching the workstation for the next steps.

Figure 3-17, Figure 3-18 and Figure 3-19 show an example of the autopower function, the driving point FRF and driving point coherence function acquired during the left side excitation.

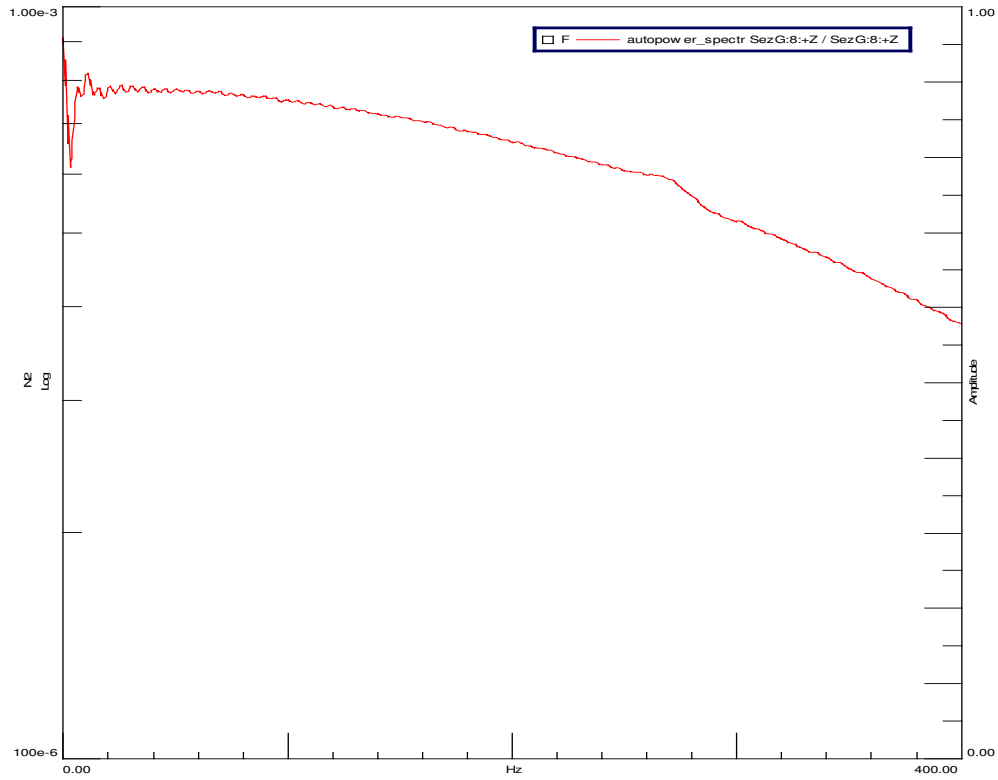


Figure 3-17: Input AutoPower

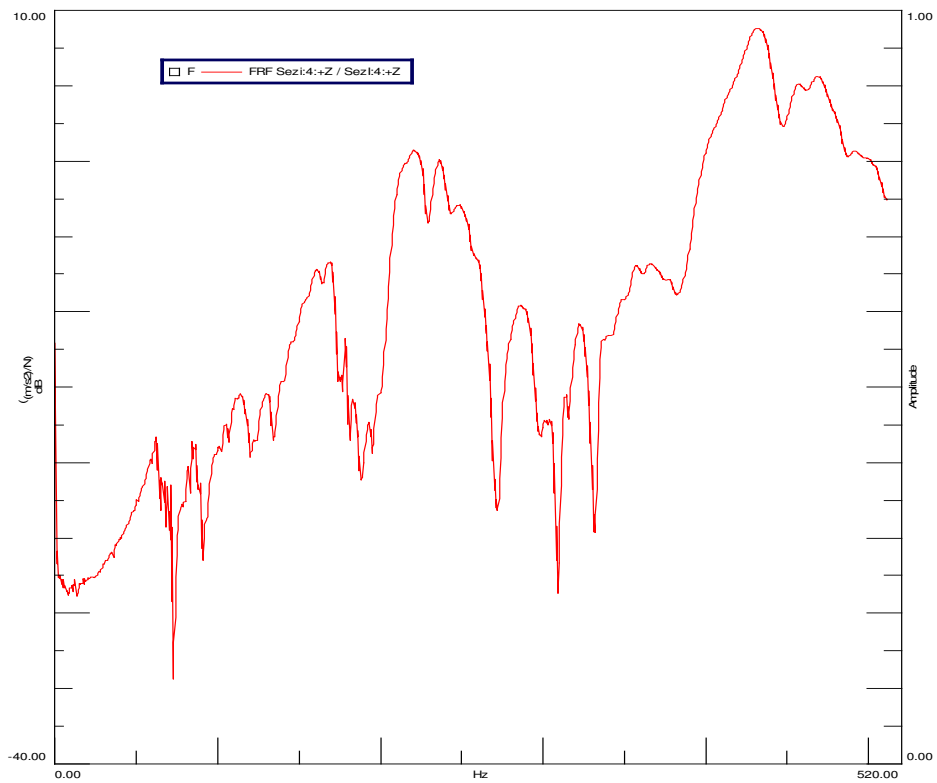


Figure 3-18: Driving Point FRF Function

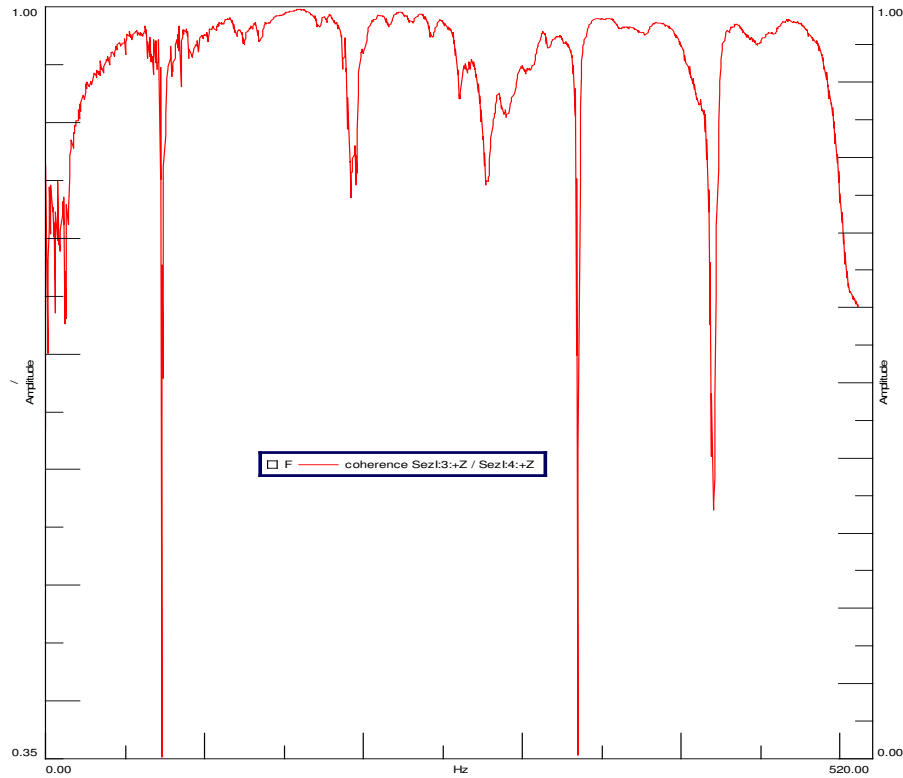


Figure 3-19: Driving Point Coherence Function

3.3.7 ANALYSIS

The software CADA-X provides the subsequent steps for the analysis and the extraction of the modal parameters. Therefore the input and the output signals are digitalized and, using an FFT algorithm, converted into the frequency domain for the computation of all the estimators available in this domain (frequency response function, coherence, and so on).

3.3.8 RESULTS

The results obtained from the analysis of the modal analysis tests on the ATR42 fuselage Test Case are presented. These results are relative to the identification of the natural frequencies, damping factors and to a description of the modal behaviour of the test case, trying to identify the main structural components most probably responsible for the vibration at that specific frequency.

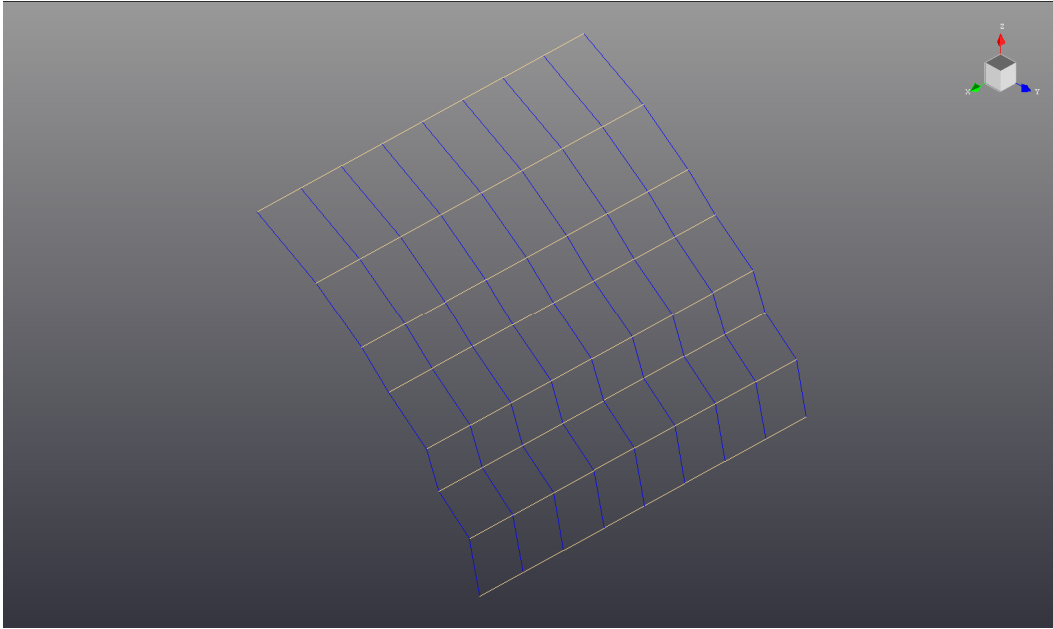


Figure 3-20: Acquired points

Figure 3-20 shows the acquisition grid in the hammer test. All the Frame are connected by blue lines instead the correnti are connected by brown lines.

3.3.9 HAMMER TEST

The structural elastic mode-shapes have been identified using the complete left excitation point.

Figure 3-21 shows the stabilization diagram in the extracting mode parameter procedure using the LMS Polymax® method.

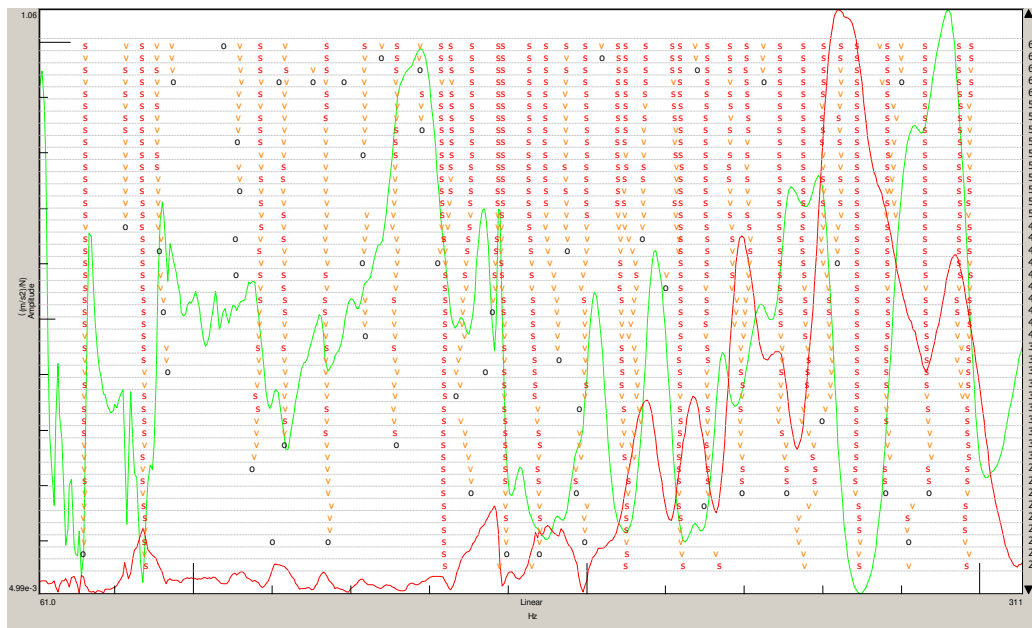


Figure 3-21: Stabilization Diagram Polymax® method

Table 3-5 shows the results obtained from the left excitation, in the table are reported the list of the extracted pole with the geometric description of the mode itself.

Not all the modes are reported because above 120 Hz the local panels dynamics is predominant over the global mode shapes and the description is more difficult.

Mode Id. (Fig.)	Frequency	Damping	Mode Id. (Fig.)	Frequency	Damping
Figure 3-23	133.628	0.85		236.423	0.87
Figure 3-23	151.364	0.90		240.953	1.08
Figure 3-24	165.619	0.98		249.105	1.23
	170.808	1.23		255.046	1.40
	177.473	0.52		260.049	1.03
	185.306	1.88		264.310	0.60
	189.302	1.11		268.696	2.27
	194.478	0.75		276.351	1.29
	199.911	1.37		286.140	1.18
	207.898	1.27		294.716	1.28
	209.973	1.70		297.606	1.10
	214.566	0.98			
	222.517	1.12			
	230.619	1.61			

Table 3-5: List of the Mode-Shapes.

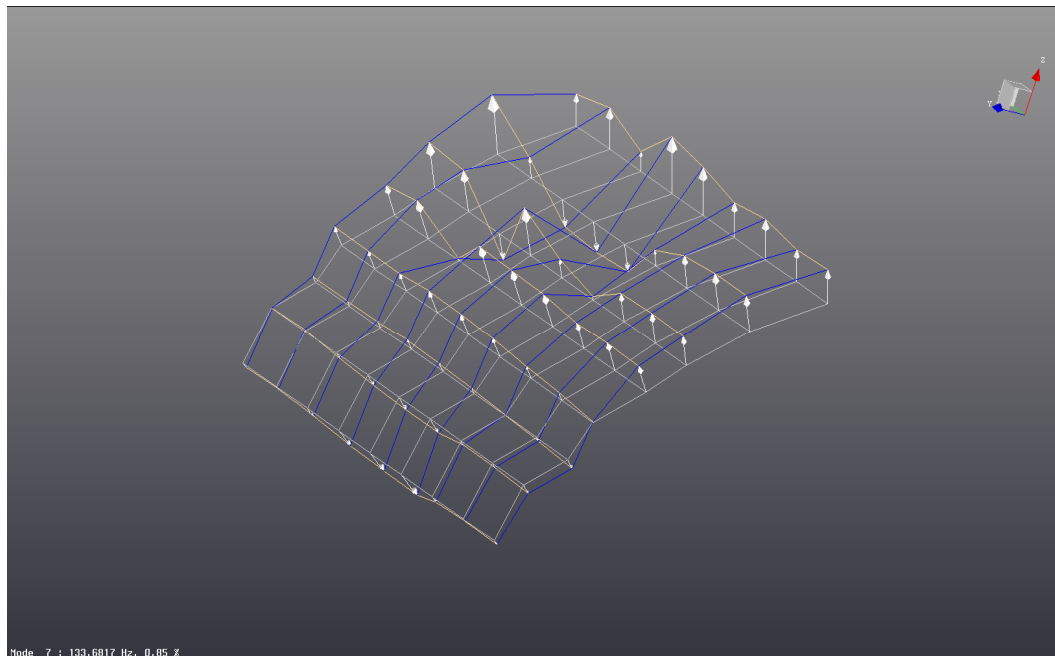


Figure 3-22: Mode 133.628 Hz

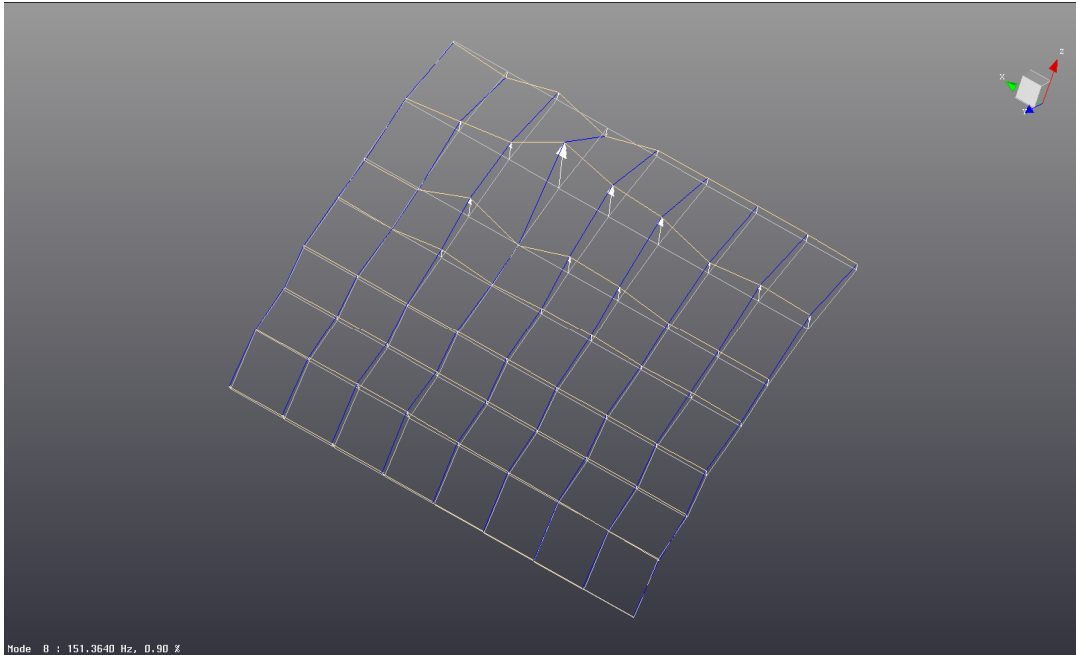


Figure 3-23: Mode 151.364 Hz

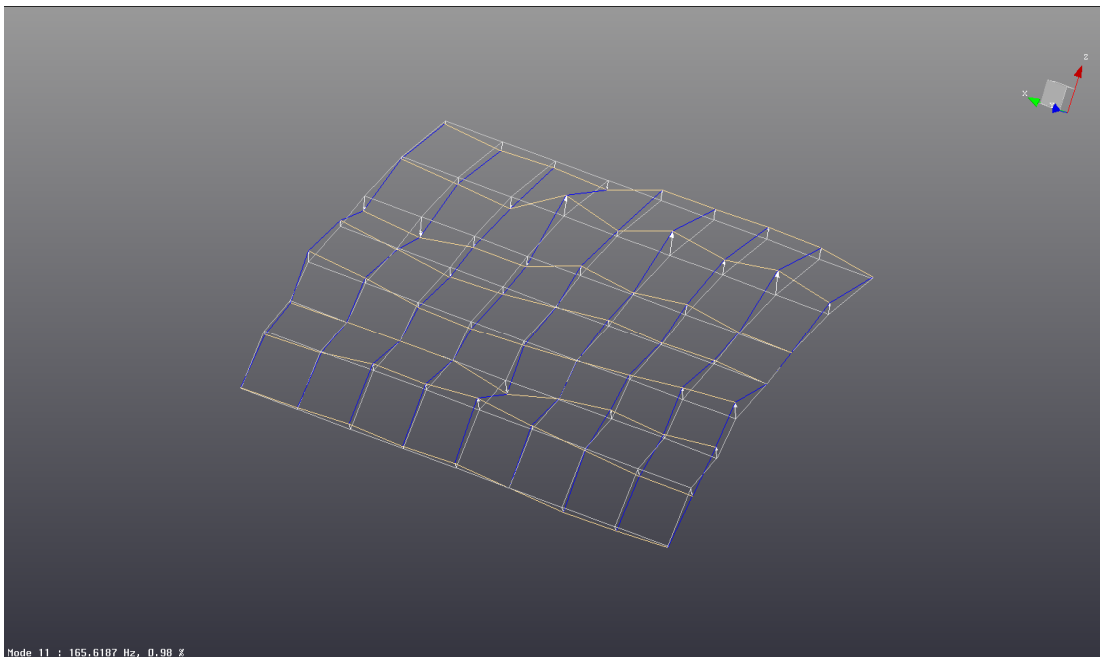


Figure 3-24: Mode 165.619 Hz

3.3.10 CONCLUSION

The hammer modal analysis shows that above 130 Hz the frames and xxx have a good dynamic response and they participate to the fuselage structural response.

The fuselage dynamics shows local contribution of frames and xxx in the 130-300 Hz band.

It is possible to see that some modes different in frequency are close in shape. This is a typical phenomena of high modal damping and high modal density structure. It is possible to speak of global mode shape in a small frequency band. That means that there are several modes at different frequencies but with the “same” shape.

3.3.11 DESCRIPTION OF THE NUMERICAL (F.E.) MODEL

In a previous research program Alenia realized a finite element model reproducing the overall mock-up consisting of seven frames, thirty stiffeners and the two end caps. The model is made by 2076 grid points and by 3207 elements (Figure 3-25), and the maximum dynamic analysis frequency has been valuated around 150 Hz.

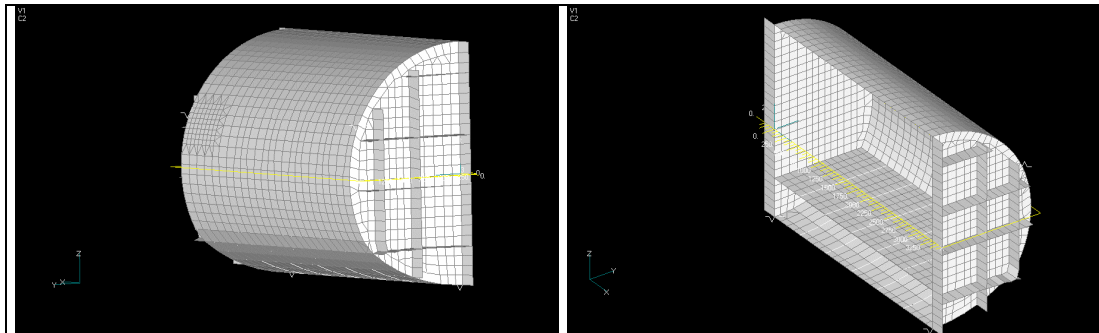


Figure 3-25: Original F.E.M. model

The numerical results of the F.E. model previously described and the experimental results obtained on a laboratory full scale fuselage section have been used to try to obtain a significant and reliable comparison (Table 3-6) ⁷.

MODE	2-D F.E. Model (frame)	3-D Half Model (six bays)	Experimental
0.2 A	17.30	17.20	60.60
0.2 S	20.98	30.15	71.40
0.3 A	49.58	53.63	81.00
0.3 S	79.15	82.66	85.10
0.4 A	92.94	92.91	87.70
0.4 S	131.74	115.73	101.16
0.5 A	141.15	101.63	110.84
0.5 S	154.40	124.22	128.28

Table 3-6: Structural natural frequencies [Hz] Numerical-Experimental comparison

In order to increase the maximum analysis frequency of the Alenia's model until at least 800 Hz, the authors took in account the typical flexural wavefield behaviour of

⁷ L.Lecce, F.Marulo, A.Paonessa, A.Sollo, "Acousto-structural coupling by FEM on a full scale aircraft fuselage section with experimental comparison", *Proc. of CMEM '89 Conference*, Capri – ITALY, May 1989.

cylinders, including low frequency beam modes, intermediate frequency cylinder modes, and high frequency plate modes (Figure 3-26). The transition from beam to cylinder modes occurs at the first free bending mode of the ring cross-section. The transition from cylinder to plate modes occurs at the ring frequency $\omega_r = c_L / a$ where c_L is the material longitudinal wavespeed and a is a radius of pipe.

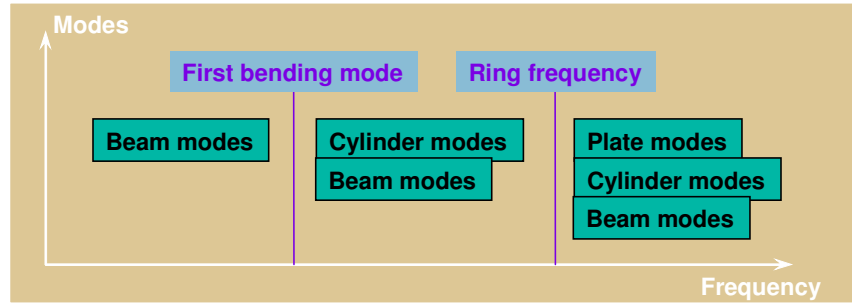


Figure 3-26: Modal density 2D

The total modal density of the cylinder is then the sum of the beam, cylinder, and plate modes. The beam modes is given from the equation:

$$n(f) = \frac{c_B}{2 \cdot L} = \frac{\sqrt{2 \cdot \pi \cdot f \cdot \chi \cdot c_L}}{2 \cdot L} \quad [1]$$

The cylinder modal density for a cylinder of radius a , length L , and wall bending radius of gyration χ is obtained from the dispersion relation:

$$\left(\frac{\omega \cdot a}{c_L}\right)^2 = \frac{\sigma^4}{(\sigma^2 + m^2)} + \left(\frac{\chi}{a}\right)^2 \cdot [(\sigma^2 + m^2)^2 - 2 \cdot m^2 + 1] \quad [2]$$

where m is the number of wavelengths around the circumference and $\sigma = n \cdot \pi \cdot a / L$ with n being the number of half-wavelengths along the pipe length.

It is very difficult to develop an expression for the modal density in all cases.

Also, in its present form, equation (3) does not adequately represent simple beam bending motion ($m=1$) at low frequencies. Therefore, it is better to use a formulation developed by Heckl⁸ which separates the cylinder modes and plate modes into two formulations.

The cylinder modes are obtained from the low-frequency asymptote ($\omega \ll c_L / a$) to the approximate dispersion relation:

⁸ L. Cremer and M. Heckl, "Structure-Borne Sound" - 2nd Ed. – Edited by Springer-Verlag (1988).

$$\left(\frac{\omega \cdot a}{c_L}\right) = \frac{\sigma^2}{(\sigma^2 + m^2)} + \left(\frac{\chi}{a}\right) \cdot (\sigma^2 + m^2) \quad [3]$$

A convenient curve fit for the supplement cylinder modal density is then :

$$n(\omega)_{cyl} = \frac{L \cdot a}{\pi \cdot \chi \cdot c_L} \cdot \frac{1}{\sqrt{\frac{c_L}{\omega \cdot a} + \frac{\omega \cdot a}{c_L}}} \quad [4]$$

The high-frequency plate modes can be added using the curve fit:

$$n(\omega)_{plt} = \frac{L \cdot a}{2 \cdot \chi \cdot c_L} \cdot \frac{1}{\sqrt{1 + \left(\frac{c_L}{\omega \cdot a}\right)^4}} \quad [5]$$

In order to calculate the necessary maximum elements dimensions to reach an analysis frequency of about 1000 Hz, it has been necessary to determine the number of wavelengths around the circumference and the number of wavelengths along the fuselage correctly.

From the equation (4), considering $\omega = 2 \cdot \pi \cdot f$ it is possible to obtain the following relationship:

$$f(n, m) = \left[\frac{\left(\frac{n}{\pi \cdot a \cdot L}\right)^2}{\left(\frac{n}{\pi \cdot a \cdot L}\right)^2 + m^2} + \left[\frac{hr}{\sqrt{12}} \cdot \frac{1}{a} \cdot \left[\left(\frac{n \cdot \pi \cdot a}{L}\right)^2 + m^2 \right] \right] \right] \cdot \left[\frac{\sqrt{\frac{E}{\rho \cdot (1 - \nu^2)}}}{2 \cdot \pi \cdot a} \right] \quad [6]$$

Plotting the obtained relationship, it is possible to characterize the maximum value of n and of m in order to avoid spatial aliasing problems within analyses up to 1000Hz.

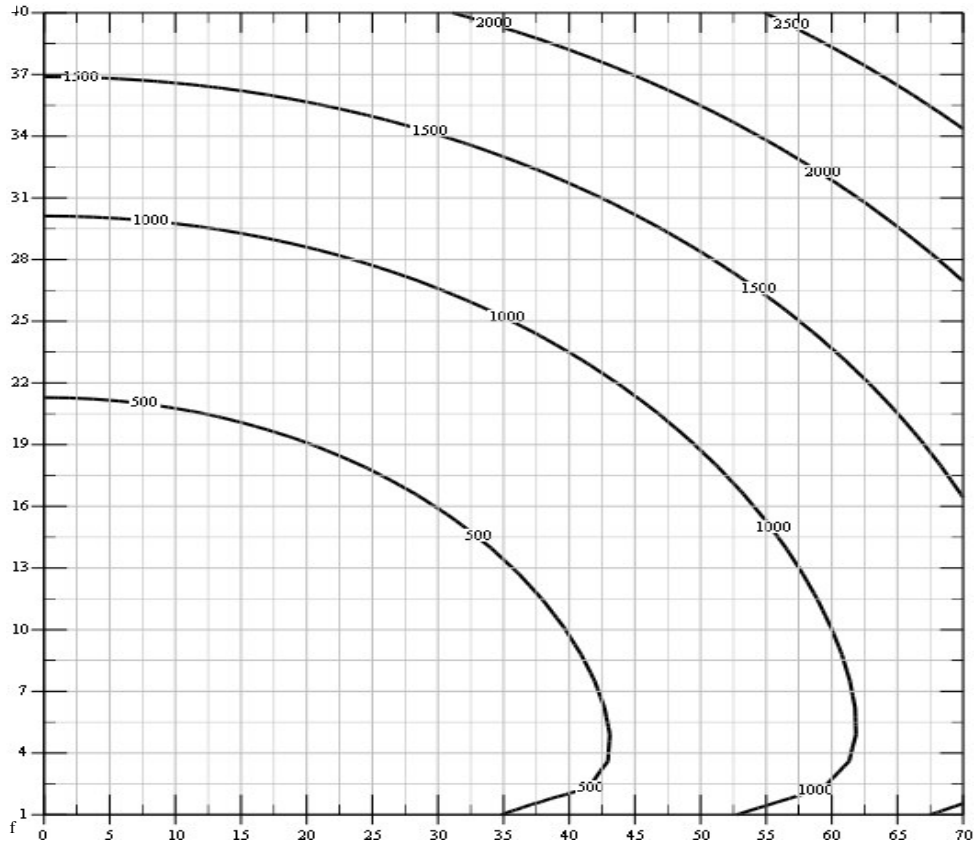


Figure 3-27: Frequency vs n and m

Considering the values of n and of m from the preceding relationship, the structural part of the new F.E. model is composed by 21576 grid points and 27452 elements.

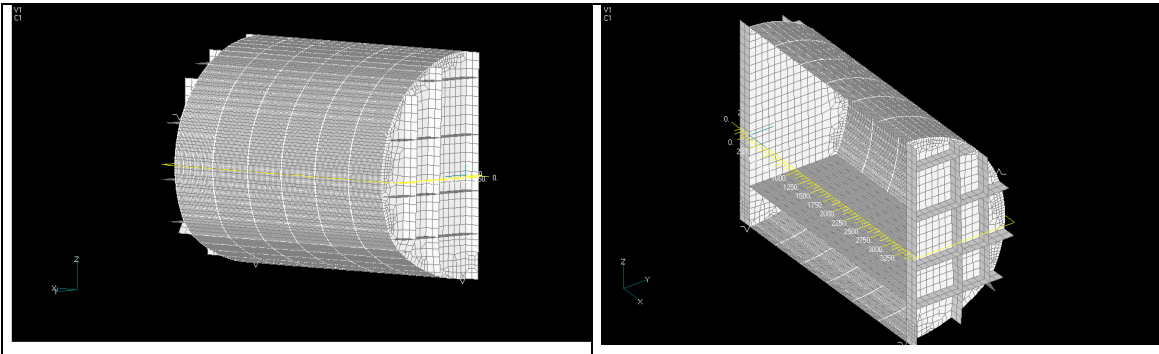


Figure 3-28: The new model structural F.E.M.

After realized the structural model, the fluid part representing the cabin's interior air volume has been modeled still dimensioning the "acoustic" mesh in order to permit maximum analysis frequencies of the acoustic model up to 1000Hz. The fluid part of the model consisted in 80275 grid points and 70560 elements.

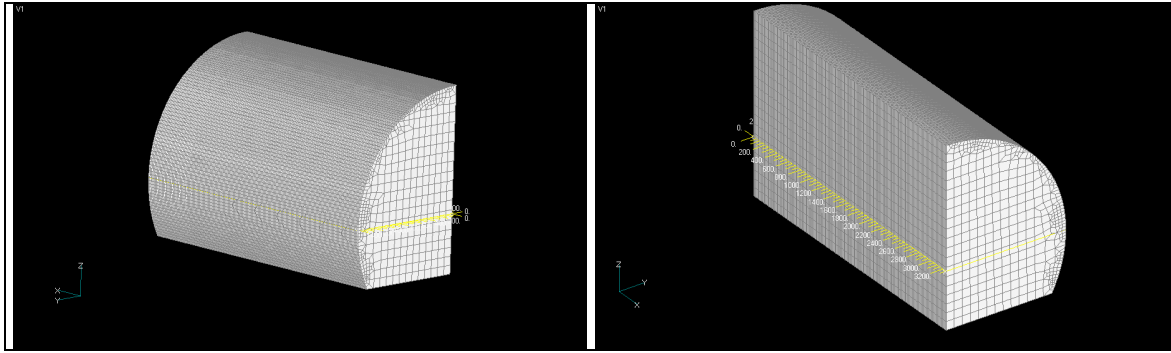


Figure 3-29: *The fluid model.*

Finally acoustic and structural models have been coupled to simulate the fluid-structure interaction. The structure has been modeled with existing one-dimensional elements CBAR and two-dimensional elements CQUAD4. While the fluid has been modeled with existing three-dimensional elements: CHEXA, CPENTA, and CTETRA. These elements can assume the properties of irrotational and compressible fluids suitable for acoustic analysis or other types of analyses governed by the three-dimensional wave equation. The interface between the fluid and the structure has been modeled so that the grid points of the fluid are coincident with those of the structure (matching mesh).

The complete model is composed by 101899 grid points and 98102 elements

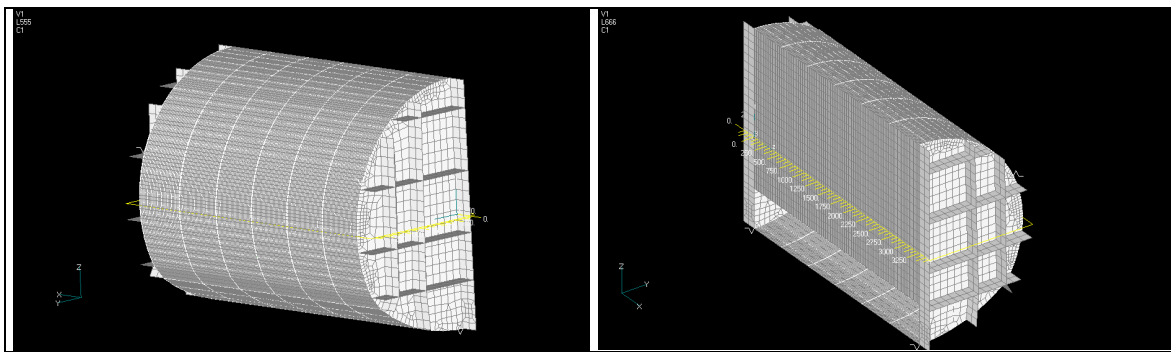


Figure 3-30: The coupling model fluid-structural

3.3.12 NUMERICAL MODAL ANALYSIS

The results obtained from the modal analysis on the finite element model of the ATR42 fuselage are presented. These results concern the identification of the natural frequencies, and the description of the modal shapes.

The following figures show some of the modal shapes extracted from the modal analysis.

Not all the modes are reported because above 120 Hz the local plate dynamics is predominant over the global mode shapes and the description is more difficult.

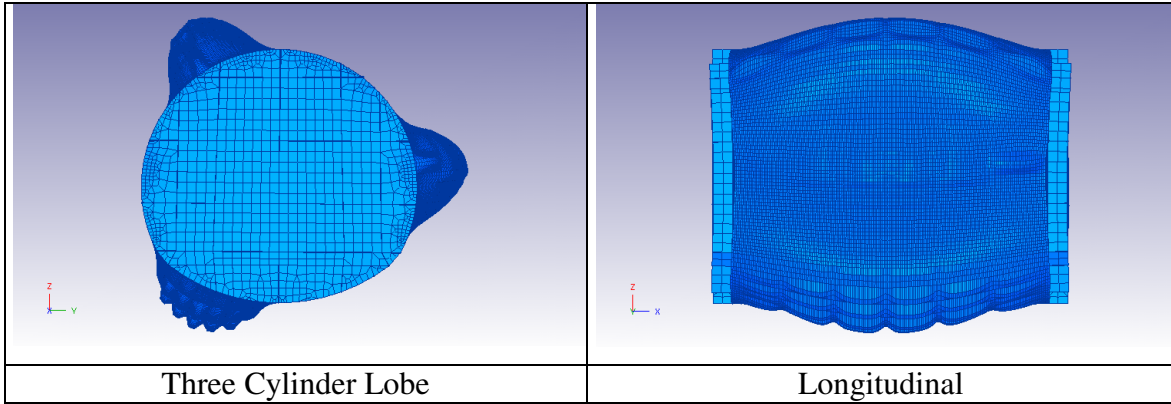


Figure 3-31 Mode 77.07 Hz

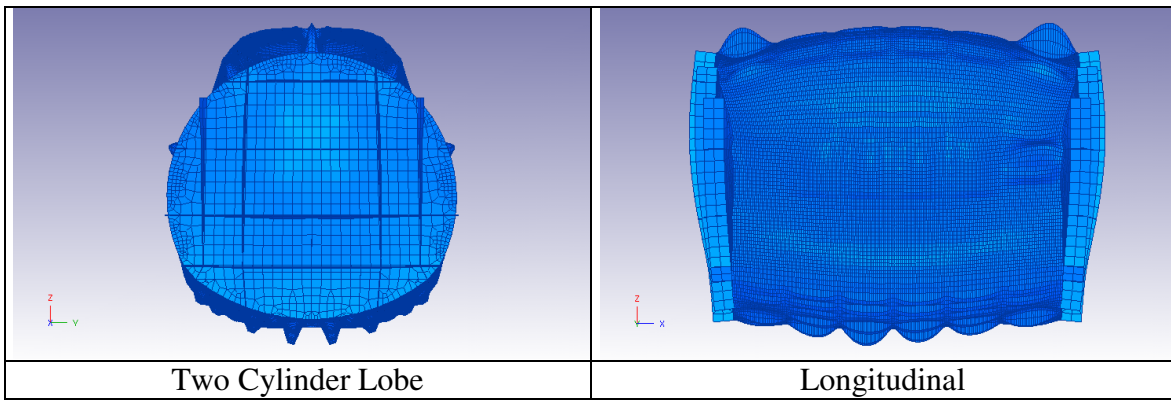


Figure 3-32 Mode 86.61 Hz

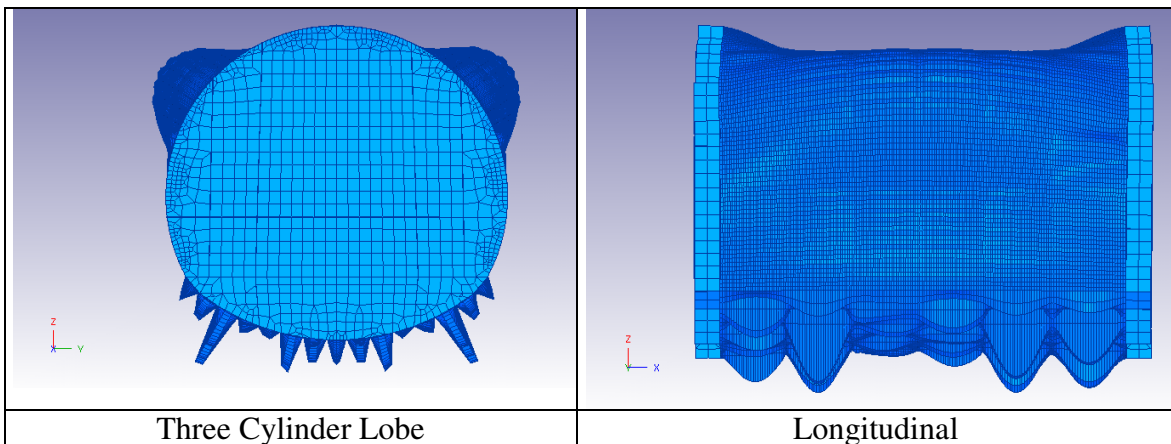


Figure 3-33 Mode 95.68 Hz

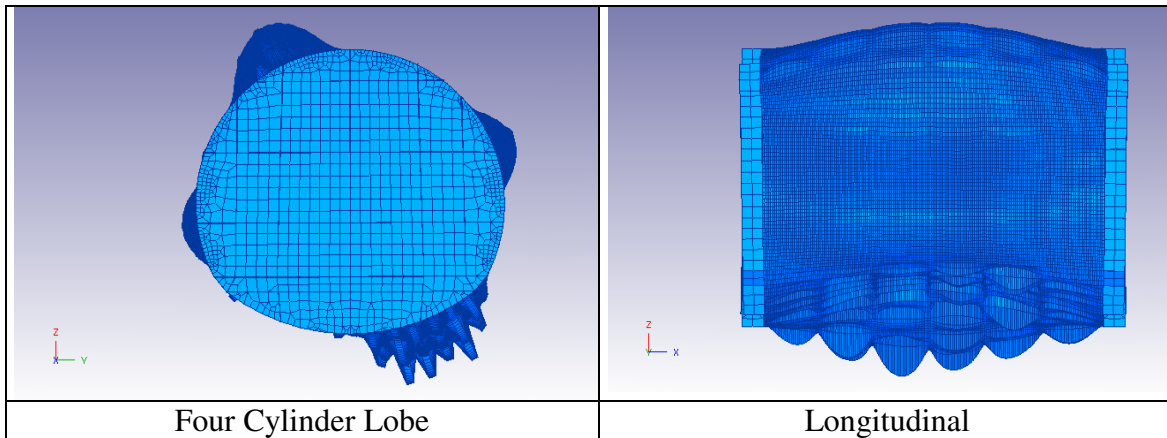


Figure 3-34 Mode 99.93 Hz

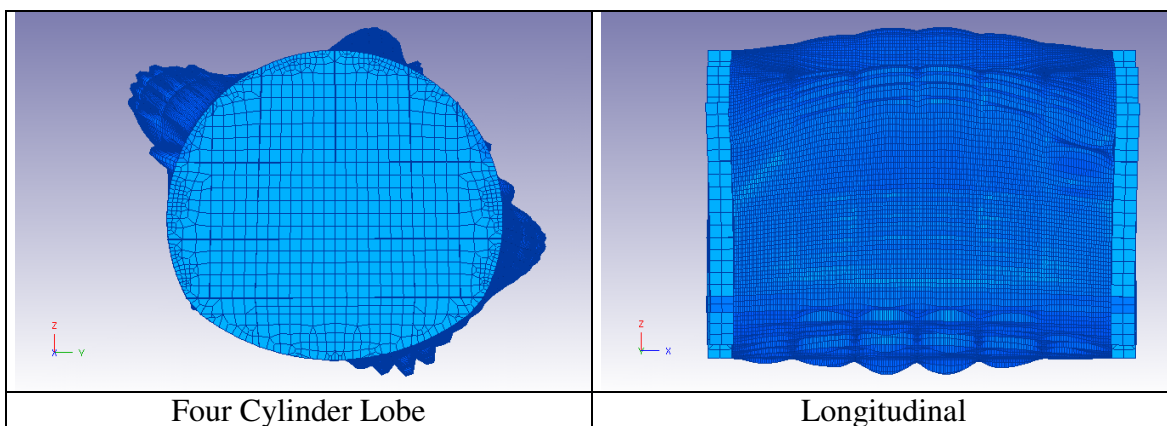


Figure 3-35: Mode 116.73 Hz

3.3.13 NUMERICAL-EXPERIMENTAL CORRELATION

In order to choose the best modeling solution the model analysis results have been compared with those coming from experimental tests. The correlation has been carried on taking in account results of numerical and experimental modal analysis performed.

The common results of modes analysis and modal testing is a set of modal parameters (resonance frequencies, damping and mode shapes), which characterize the linear dynamics of the structure. Ideally, the two techniques should yield the same results. In practice, however, they rarely do. Correlation analysis is a technique to quantitatively and qualitatively examine the correspondences and differences between analytically and experimentally obtained modal parameters.

Different levels of correlation analysis exist. They range from visual comparison of the mode shapes to the calculation of correlation coefficients that are calculated from the weighted relative differences between modal parameters.

Since correlation analysis is based on two sets of modal data, one experimentally obtained and another analytically, it must be verified if the same global coordinate systems are used. If not, it is necessary to perform scaling, translation and rotation operations on one or both databases in order to obtain consistent data.

Next figure presents the experimental acquisition mesh (238 points) superimposed on the F.E. model after the necessary translations and rotation were made.

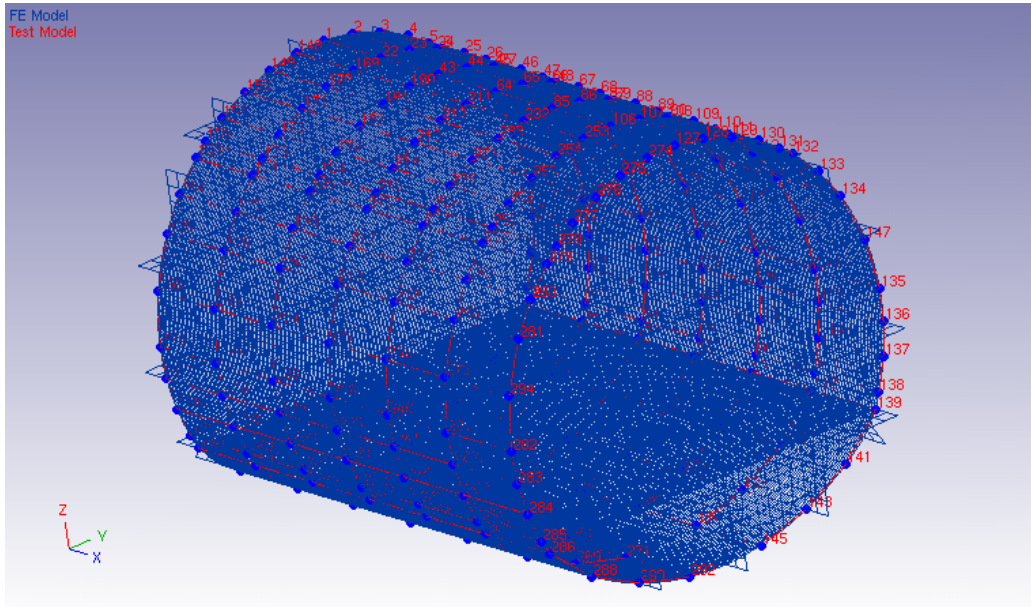


Figure 3-36 Experimental acquisition mesh and F.E. model

A table relating the nodes from the finite element model with the measurements points has been created by comparing their location in space. This has been done by mapping the grid points on the F.E. model and computing the distances among all node/acquisition points combination. The combinations characterised by the shortest distance have been chosen.

Table 3-7: Grid points – acquisition points combination

Combination	Node	Point	Distance (mm)	48	2840	70	0
1	173	253	0	49	2898	248	0
2	204	106	0	50	2957	112	0
3	332	235	0	51	3015	113	0
4	335	232	0	52	3221	185	0
5	406	88	0	53	3266	279	0
6	407	85	0	54	3268	277	0
7	453	213	0	55	3272	274	0
8	551	66	0	56	3280	255	0
9	683	190	0	57	3285	258	0
10	708	169	0	58	3300	236	0
11	813	43	0	59	3303	237	0
12	841	22	0	60	3308	239	0
13	899	172	0	61	3312	211	0
14	928	148	0	62	3318	214	0
15	1015	25	0	63	3332	191	0
16	1044	1	0	64	3337	192	0
17	1253	215	0	65	3341	193	0
18	1270	194	0	66	3352	170	0
19	1361	176	0	67	3356	171	0
20	1376	196	0	68	3362	174	0
21	1419	216	0	69	3365	175	0
22	1435	195	0	70	3372	153	0
23	1478	218	0	71	3391	252	0
24	1528	217	0	72	3409	219	0
25	1581	259	0	73	3415	210	0
26	1604	260	0	74	3422	198	0
27	1661	262	0	75	3435	284	0
28	1752	261	0	76	3441	242	0
29	1838	240	0	77	3447	221	0
30	1865	241	0	78	3465	264	0
31	1950	199	0	79	3469	222	0
32	1958	220	0	80	3472	201	0
33	2076	177	0	Combination	Node	Point	Distance (mm)
34	2134	178	0	81	3477	181	0
35	2229	180	0	82	3488	225	0
36	2232	68	0	83	3495	288	0
37	2261	47	0	84	3496	267	0
38	2274	200	0	85	3498	246	0
39	2492	29	0	86	3514	271	0
40	2522	49	0	87	3522	250	0
Combination	Node	Point	Distance (mm)	88	3529	229	0
41	2574	204	0	89	3535	206	0
42	2609	69	0	90	3539	208	0
43	2637	48	0	91	3554	166	0
44	2655	183	0	92	4058	115	0
45	2725	71	0	93	4231	114	0
46	2746	162	0	94	4434	93	0
47	2787	269	0	95	4492	94	0

96	4667	52	0	144	10036	54	0
97	4695	73	0	145	10047	34	0
98	4869	30	0	146	11031	78	0
99	4927	31	0	147	11107	197	0
100	5072	33	0	148	11826	156	0
101	5130	53	0	149	12004	120	0
102	5201	254	0	150	12008	99	0
103	5508	57	0	151	13032	124	0
104	5595	36	0	152	13052	103	0
105	5682	15	0	153	13071	82	0
106	5797	256	0	154	13083	59	0
107	5880	257	0	155	13092	61	0
108	6000	122	0	156	13132	19	0
109	6116	101	0	157	13403	187	0
110	6608	38	0	158	13499	276	0
111	6790	238	0	159	14773	179	0
112	7019	132	0	160	15859	107	0
113	7028	130	0	161	16436	109	0
114	7048	127	0	162	16583	110	0
115	7075	108	0	163	17483	91	0
116	7096	111	0	164	18233	227	0
117	7147	89	0	165	18295	87	0
118	7152	90	0	166	18527	86	0
119	7167	92	0	167	19024	243	0
120	7171	64	0	168	19220	65	0
121	7196	67	0	169	21427	26	0
122	7236	44	0	170	24022	263	0
123	7244	45	0	171	24126	50	0
124	7251	46	0	172	25195	273	0
125	7291	23	0	173	25286	9	0
126	7299	24	0	174	26439	189	0
127	7320	27	0	175	27804	40	0
128	7328	28	0	176	27933	282	0
Combination	Node	Point	Distance (mm)	Combination	Node	Point	Distance (mm)
129	7376	6	0	177	28190	231	0
130	7401	234	0	178	29343	32	0
131	7539	233	0	179	31547	80	0
132	7793	137	0	180	32014	96	0
133	7990	212	0	181	34697	283	0
134	8067	105	0	182	34773	285	0
135	8108	72	0	183	34780	265	0
136	8124	63	0	184	34814	244	0
137	8135	51	0	185	34916	202	0
138	8831	141	0	186	34922	223	0
139	9044	95	0	187	35262	116	0
140	9060	74	0	188	35274	158	0
141	9417	173	0	189	35277	159	0
142	10011	117	0	190	35381	157	0
143	10027	75	0	191	35387	168	0

192	35958	126	0
193	35959	155	0
194	35962	154	0
195	36053	151	0
196	36074	150	0
197	36083	149	0
198	36263	275	0
199	36362	278	0
200	36392	281	0
201	36397	280	0
202	36420	294	0
203	36633	160	0
204	36653	164	0
205	36758	292	0
206	36915	290	0
207	37425	42	0
Combination	Node	Point	Distance (mm)
209	38435	84	0
210	38963	286	0
211	40083	131	0
212	41673	136	0
213	41695	138	0
214	41810	118	0
215	41857	145	0
216	41896	97	0
217	42012	55	0
218	42026	76	0
219	42307	139	0
220	42805	11	0
221	42811	12	0
222	42855	10	0
223	42870	21	0
224	43147	8	0
225	43153	7	0
226	43187	4	0
227	43214	3	0
228	43220	2	0
229	43286	129	0
230	43292	128	0
231	43483	134	0
232	43489	133	0
233	43527	147	0
234	43536	135	0
235	43832	13	0
236	43878	17	0
237	44435	143	0
238	44770	5	0

Since the FE model in general will contain much more degrees of freedom than the experimental one, the numerical normal modes can be truncated to eliminate all data for which no experimental counterpart exists.

Several methods exist to compare analytical and experimental mode shapes. Visual inspection is a very effective but time consuming way. Numerical mode shape correlation techniques like the Modal Assurance Criterion and Eigenvector orthogonality⁹ can be used to automatically check all possible mode shape pairs and compute a quantity that expresses the level of correlation. From these quantities a mode shape pairing table can be derived.

Within this work the Modal Assurance Criterion (MAC) has been used: it compares all mode shapes in the numerical database with all mode shapes in the experimental database. The following equation is used:

$$MAC(\{\psi_n\}, \{\psi_e\}) = \frac{|\{\psi_n\}^T \{\psi_e\}|^2}{(\{\psi_n\}^T \{\psi_e\})(\{\psi_e\}^T \{\psi_n\})}$$

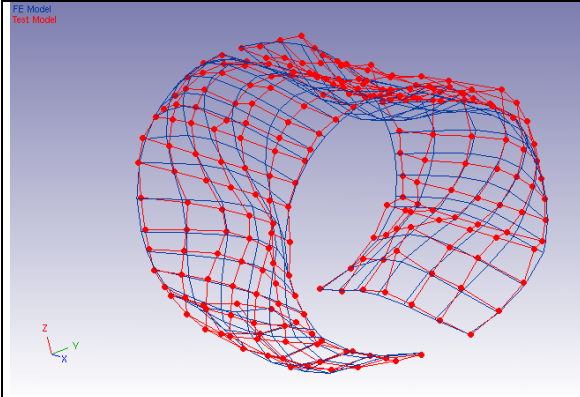
where $\{\psi_n\}$ and $\{\psi_e\}$ are respectively the numerical and experimental eigenvectors we want to correlate. It should be noted that MAC-values are calculated by multiplying numerically and experimentally obtained modal displacements at paired node/point locations on the structure.

Following are reported the experimental and numerical natural frequencies selected to carry on the correlation analysis using the results of the model where the grid points of the external frames are linked with the grid points of the heavy caps.

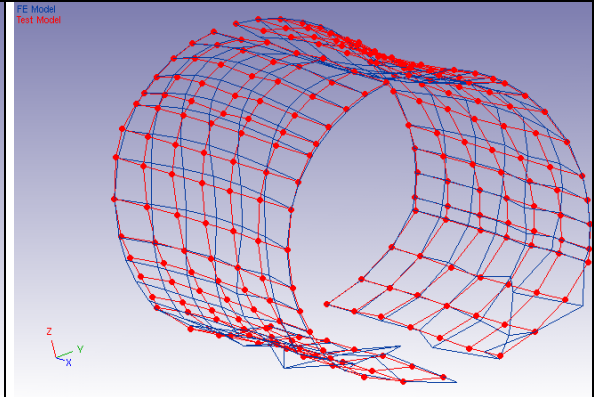
F.E.A. natural frequency	Hz	E.M.A. natural frequency	Hz	Diff. (Hz)	M.A.C.
5	77.07	4	61.94	24.44	66.4
8	86.84	6	68.2	27.32	32.1
18	91.13	15	91.86	-0.8	36.4
22	95.28	13	86.04	10.74	34.1
23	95.68	12	82.62	15.8	37.3
24	95.89	11	79.04	21.32	30.5
29	98.54	7	70.29	40.2	46.6
50	116.73	20	109.44	6.67	33.4

Following is also possible to compare visually the experimental and numerical mode shapes:

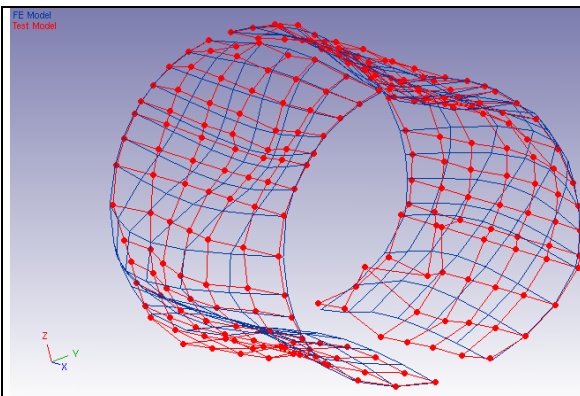
⁹ “Dynamic Design Solutions NV - FEMtools – Theoretical Manual, July 2001 ”



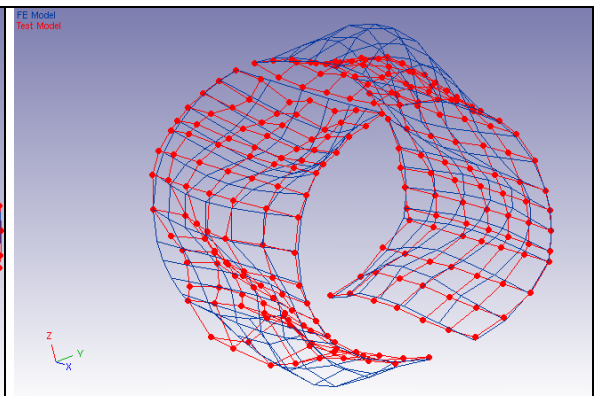
F.E.A. 77.07 – E.M.A. 61.94



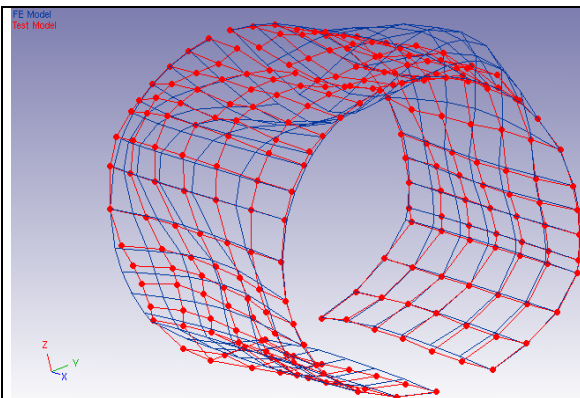
F.E.A. 86.84 – E.M.A. 68.2



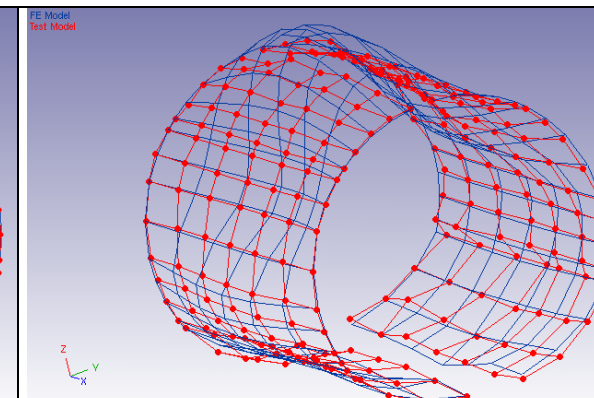
F.E.A. 91.13 – E.M.A. 91.86



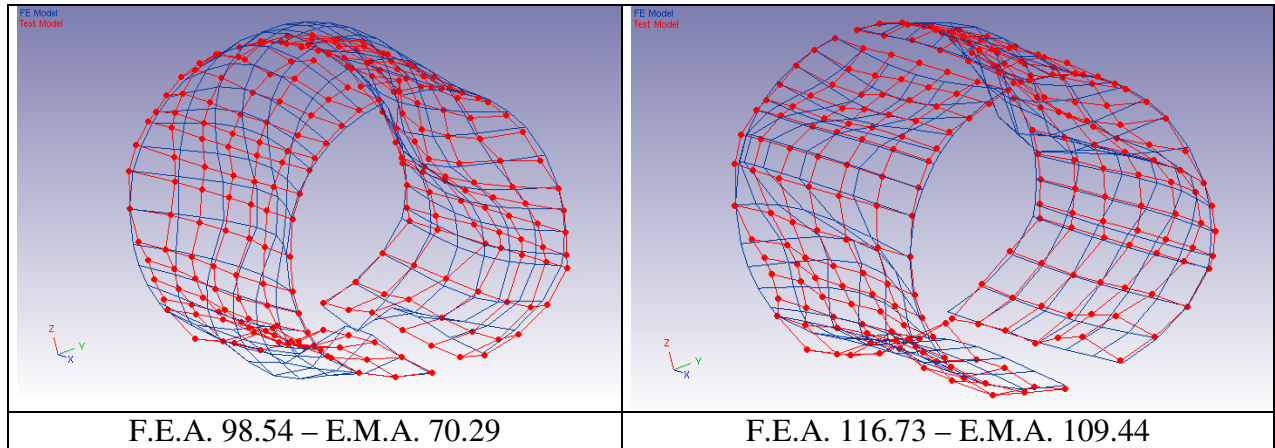
F.E.A. 95.28 – E.M.A. 86.04



F.E.A. 95.68 – E.M.A. 82.62



F.E.A. 95.89 – E.M.A. 79.04



In the next figures the correlation of the experimental-numerical frequencies couple is presented: if a good correlation was achieved the points representing the frequency couples should stay very close to the red line (angular coefficient = 1).

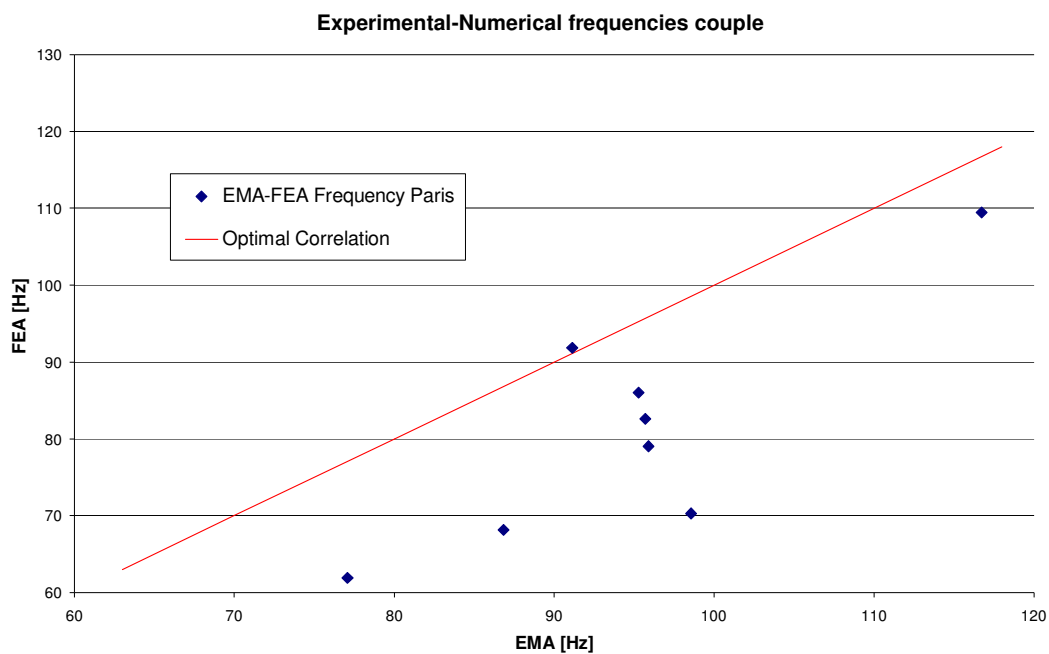


Figure 3-37: Exp_num modal analysis correlation

It is possible to notice how the initial model doesn't well represent the dynamic behavior of the real structure for what concerns the natural frequency parameter, because the experimental-numerical frequencies couple are quite far from the midline of the x-y plane.

The poor correlation between numerical and experimental modal parameters brought to the decision of updating the original model modifying the links between the grid points of the external frames and the grid points of the heavy caps. This approach obviously came from a very detailed analysis of the exp. and num. mode shapes that often differed one from the each other in the mentioned areas. Within the original model the nodes on

the external frames and the corresponding ones on the end caps where merged (the links were considered “perfect” with an infinite stiffness!). The experimental modal analysis demonstrated that this configuration did not represent the real behavior of the connections between the fuselage section and the end caps, for this reason it was decided to modify the model.

In detail it was chosen to consider one “evolution” of the original model, consisting in linking the grid points of the external frames with the grid points of the heavy caps through spring elements (named CELAS in MSC/NASTRAN).

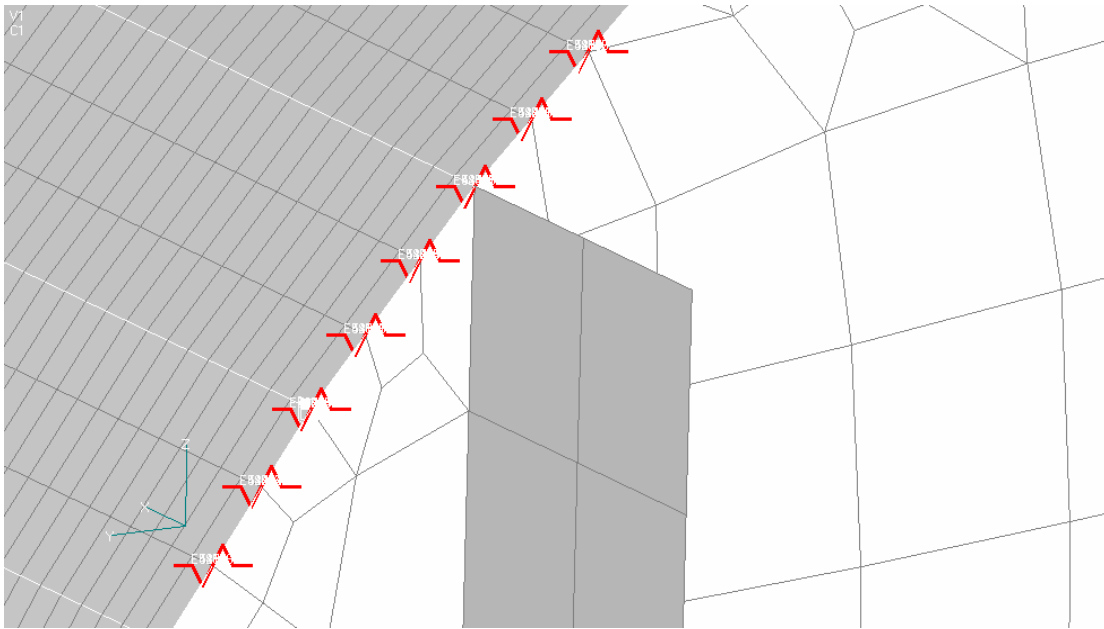


Figure 3-38: Detail of the springs

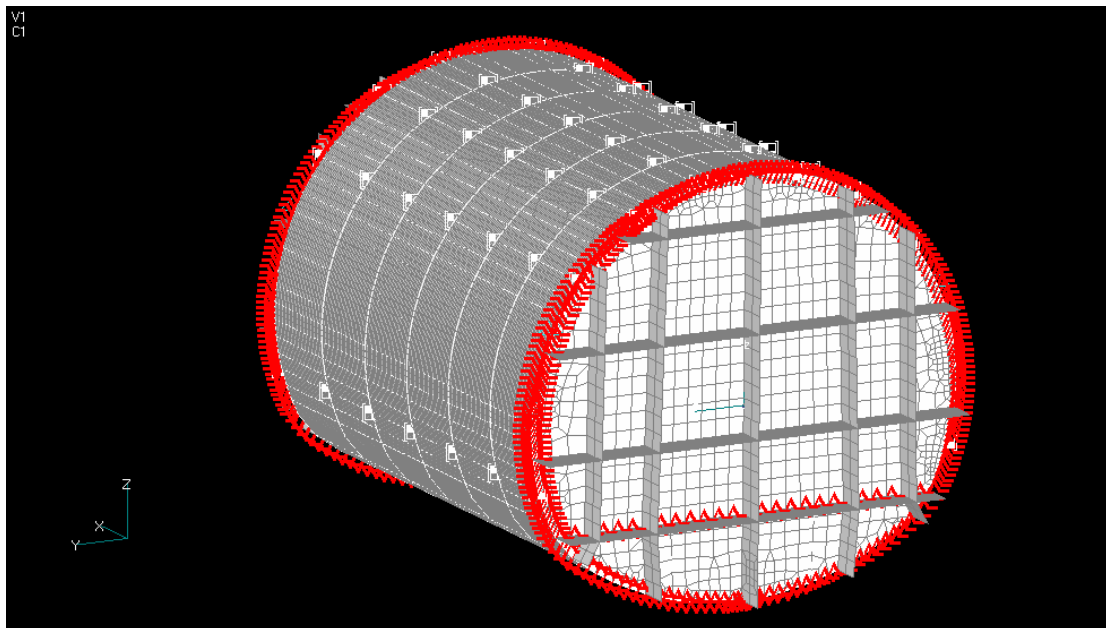


Figure 3-39: The springs on the global model

In order to determine stiffness coefficient of the springs, it was required to assign a value of attempt, and perform a “sensitivity analysis” by the mean of sensitivity coefficients. A differential sensitivity coefficient is the slope of the response R_i with respect to parameter P_j , computed at a given state of the parameter. When this differential is computed for all selected responses with respect to all selected parameters, the sensitivity matrix [S] is obtained:

$$[S] = S_{ij} = \left[\frac{\delta R_i}{\delta P_j} \right]$$

where:

i: 1..N Responses
j: 1..M Parameters

Each row of the sensitivity matrix corresponds with a response R_i , each column with a parameter P_j . The sensitivity matrix is a rectangular matrix.

The sensitivity analysis brought to the decision of updating the presented model by modifying the stiffness coefficient of the springs. The objective of model updating is to adjust the values of selected parameters such that a reference correlation coefficient is minimized. The correlation coefficients should all be zero in case of perfect correlation. In order to achieve quickly and reliably the correlation results a commercial software has been employed. It provides six pre-defined correlation coefficients (CC) that are computed from the difference between selected reference responses and actual values.

$$CC_{TOT} = CC_{ABS} + K_1 CC_{MAC} + K_2 CC_{MDISP} + K_3 CC_{MASS}$$

where:

CC_{TOT} Sum of all other CC_s

CC_{ABS} Average value of weighted absolute relative differences between predicted and reference resonance frequencies

CC_{MAC} Average value of weighted margin of the actual MAC-values for selected experimental modes

CC_{MDISP} Average value of weighted relative differences between predicted and reference mode shape components

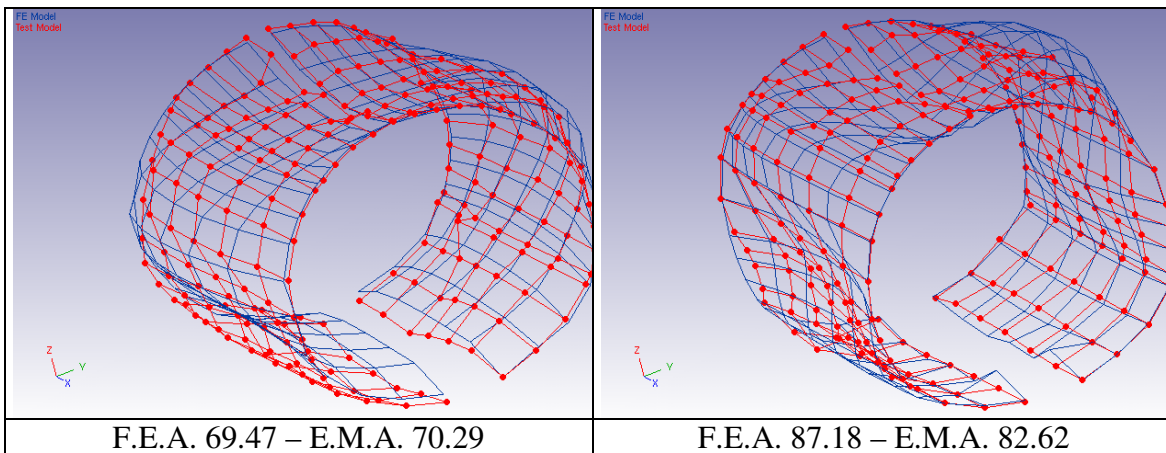
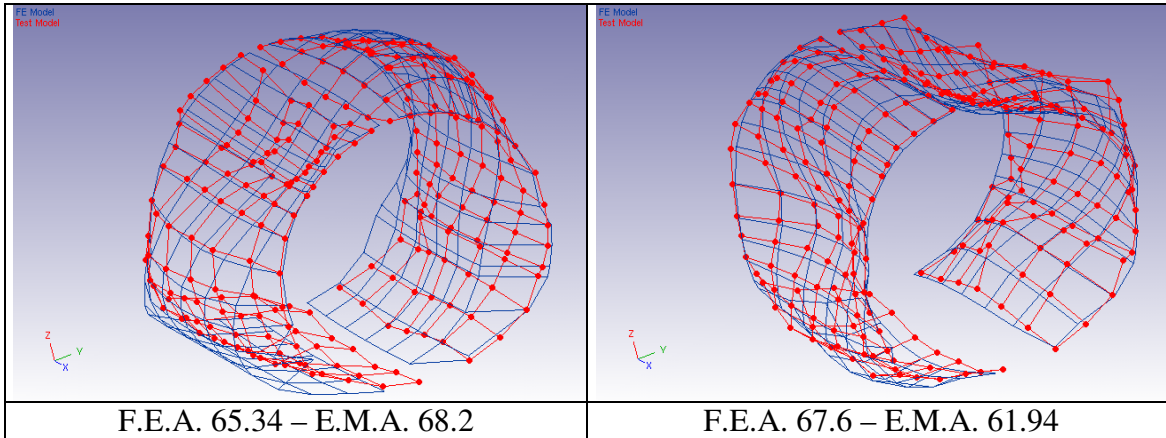
CC_{MASS} Average value of weighted relative differences between predicted and reference mass

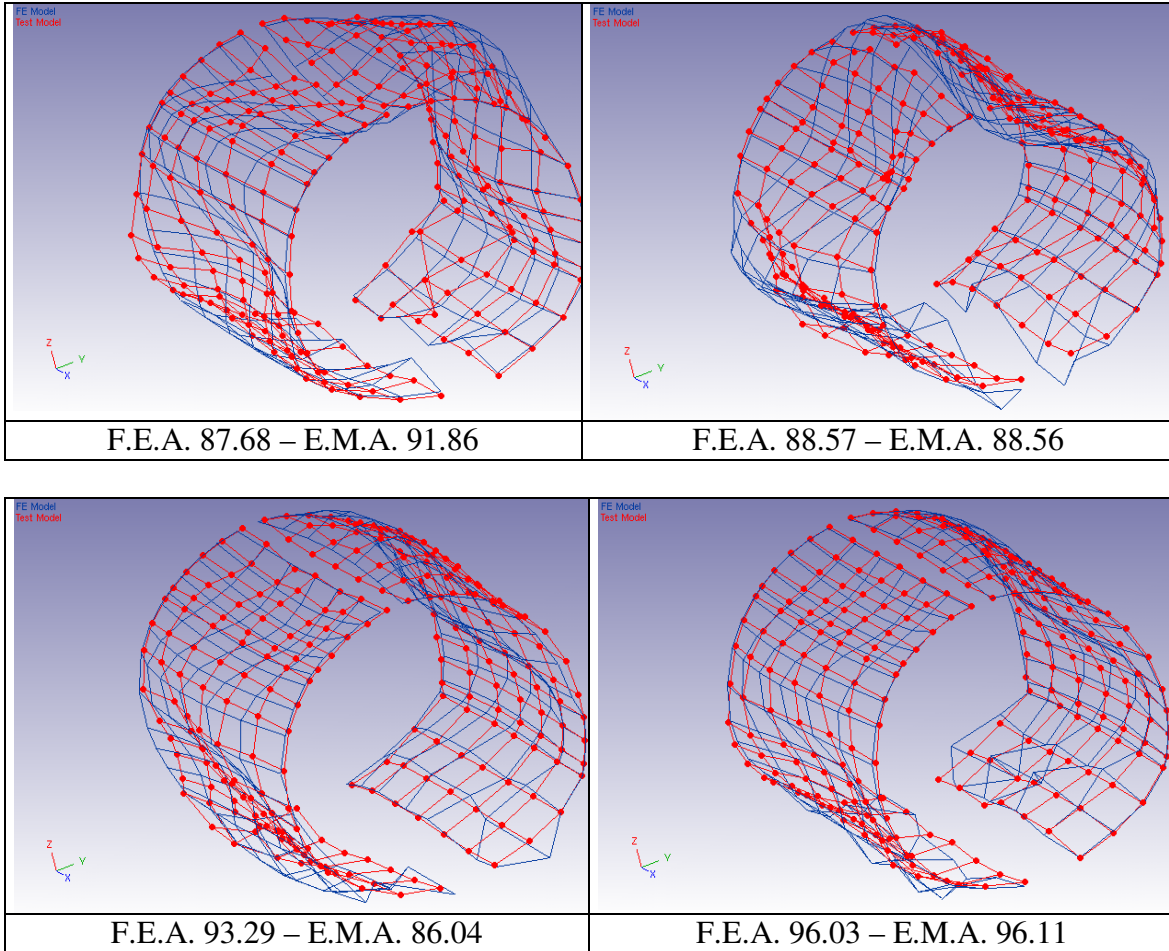
They are used in the model updating module as the objective function that is minimized using an iterative procedure. Following are reported the experimental and numerical natural frequencies selected to carry on the correlation analysis using the results of the model where the grid points of the external frames are linked with the grid points of the heavy caps through the spring elements. These results have been achieved after fifty updating iterations of the stiffness of the springs.

F.E.A. natural frequency	Hz	E.M.A. natural frequency	Hz	Diff. (Hz)	M.A.C.
6	65.34	6	68.2	-4.2	43.3
7	67.6	4	61.94	9.15	76
8	69.47	7	70.29	-1.15	40.6

15	87.18	12	82.62	5.52	43.2
16	87.65	15	91.86	-4.59	47.8
19	88.57	14	88.56	0.01	44.6
27	93.29	13	86.04	8.42	30.4
31	96.03	16	96.11	-0.09	39.5

Following is also possible to compare visually the exp.-num. mode shapes pairs





In the next figure the correlation of the experimental-numerical frequencies pairs is presented after the updating procedure.

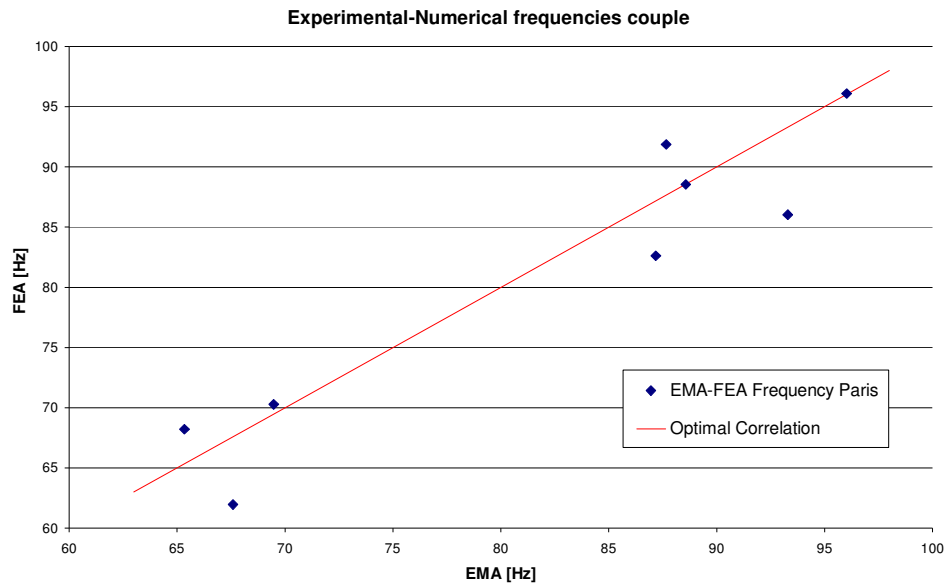


Figure 3-40: Exp_num modal analysis correlation

It is possible to notice how the updated model, presents higher M.A.C. values and lower values of the difference between numerical and experimental frequencies than the original ones. This last parameter is in this case particularly relevant since, due to the cylindrical geometry and to the very complex panels dynamics in the medium frequency ranges (from 100Hz), it is almost impossible to get very high M.A.C. values, apart from the very first “global” mode shapes.

3.3.14 CONCLUSIONS

These activities performed during the first task of the MESEMA Project aimed to the numerical and experimental characterization of the vibro-acoustic behavior of the selected test-article (a full scale turboprop fuselage section). The coupled structural-acoustic F.E. model has been described as far as the experimental modal analysis set-up and results. Furthermore the correlation between numerical and experimental modal parameters by the mean of a sensitivity analysis brought to an updated numerical model that now is able to well represent the real structural dynamic behavior of the test article. This model will now represent the reference for the next activities related to the simulations of the control system. Finally the vibro-acoustic experimental acquisition have been completed.

4 ACTIVE CONTROL SIMULATION

This chapter reports the activities carried out for the final testing phase of the noise control system for turbofan aircraft within the Research Project funded by the European Commission within the 6th FP named MESEMA.

Aim of the report is the description of the experimental results obtained by implementing the broadband noise control system on a full-scale fuselage section of the commercial aircraft ATR-42 available in the Alenia plant in Pomigliano d'Arco (NA) and selected as WP2.1 test-article.

The document presents all the activities that were necessary to setup the final experiment, starting from the installation of actuators, power amplifiers and sensors to the setup of the control system network which includes both conditioning and computational electronics.

The results of the experimental testing phase have been assessed with the end-user and the conclusion is a possible interest of Alenia in licensing the noise control system.

The document contains also two appendices reporting the main research activities concerning the selection of the optimal location of the actuators and sensors and the selection of the most suitable control algorithm.

4.1 CONTROL OF NOISE ON TURBOFAN

This part reports the activities concerning the final testing phase performed by the following partners within the WP2.1 of the MESEMA Research Project:

- Second University of Naples (DII-SUN)
- University of Naples (Unina-DPA)
- Saarland University (LPA-ZIP)
- Alenia Aeronautica (Alenia)

It is worth remarking that the results presented later on in the document would have never been obtained without the strong effort spent in the first three years of the project on a number of related activities already documented in past deliverables but which is worth recalling here together with the main contributing partners:

- Specification of requirements for noise control on turbofan: (Alenia, Unina-DPA)
- Structural characterization: (Unina-DPA, Alenia, DII-SUN, LFME)
- Selection of optimal actuator location: (Unina-DPA, LFME)
- Actuators and power electronics design and manufacturing: (LPA-ZIP)
- Final control algorithm design and implementation: (DII-SUN)

The goal of Task 2.1 is to reduce the interior noise caused during the cruise flight by the turbulence of the external air flow, in a broad frequency range up to 500 Hz.

4.2 OPERATING CONDITIONS OF THE NOISE CONTROL SYSTEM

- the spectrum of the primary force field is broadband and completely unknown to the control system (this is to simulate the variation of the actual primary field with the different flight conditions)
- the points where the primary force field is applied to the structure are not known (this is to simulate that the actual primary field is applied in a distributed way)

As decided at the beginning of the project, a structural control approach has been pursued and therefore the actuators are placed on structural elements, i.e. frames and stringers and accelerometers are used to monitor the structural behavior as well as optical sensors (Bragg gratings) integrated in the actuators to sense their internal state. In detail, the actuators have to be placed on the structural elements which predominantly contribute to the produced acoustic field, i.e.

- actuators placed along the frames for controlling the noise at low frequencies (below 200 Hz)
- actuators placed on the stiffeners for controlling the noise at high frequencies (above 200 Hz)

Two appendices have been included in this report to document the main research activities which led to the selection of the actuator location (appendix A) and of the final noise control algorithm (appendix B).



the suspension system



shakers for primary field generation

Figure 4-1: Full-scale mock-up used for testing of the noise control system

4.1 SETUP OF THE TEST ARTICLE

In Figure 4-1 the segment of ATR-42 fuselage selected as test rig is depicted. The structural configuration of the test article, described in detail in previous paragraph, simulating a free-free boundary condition is obtained using a suspension system and two heavy caps fixed at the two ends of the fuselage section.

3.1. PRIMARY EXCITATION

Two shakers were used to excite the structure with a primary force field suitably selected by Unina-DPA and Alenia to best simulate the noise conditions inside the cabin of a turbofan aircraft during cruise flight and caused by the turbulence of the external air flow. To this purpose the two shakers were positioned on the skin of the fuselage close to the zone where the wings are attached to the fuselage itself (Figure 4-1).

The shakers were also equipped with a couple of load cells in order to estimate the structural impedance.

3.2. ACTUATORS' INSTALLATION

As mentioned, two possible mounting options were forecasted for each actuator, namely a frame mounting and a stringer mounting.

Considering the spectrum of the primary field and the possible candidate locations within the two central bays of the fuselage, the partners involved selected the optimal location for 30 actuation points marked with green spots in Figure 4-1 **Errore. L'origine riferimento non è stata trovata.**, where the blue numbers refer to the node numbers of the FEM used to select the location (nodes 39 and 102 correspond to the shakers location).

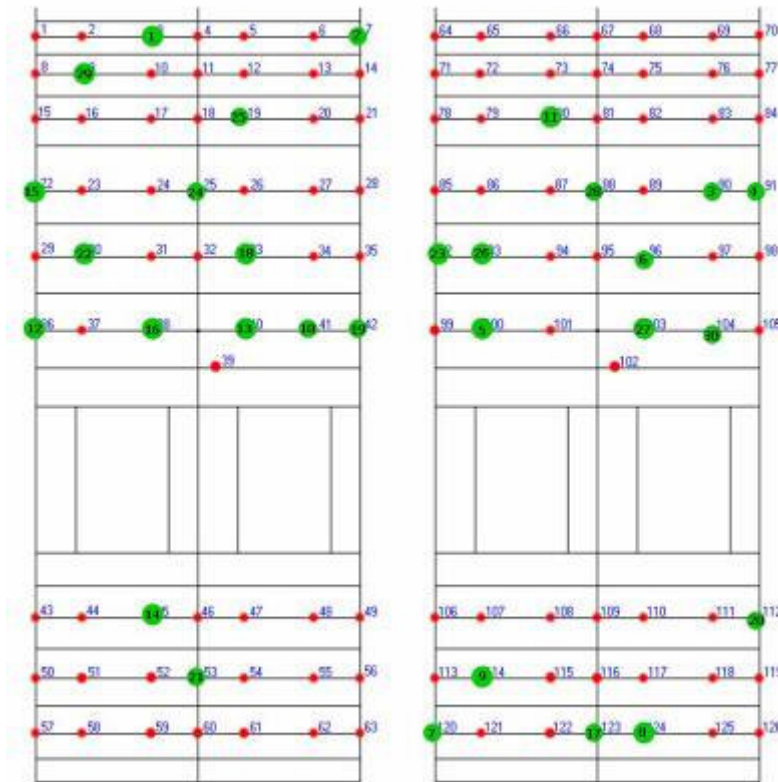


Figure 4-2: Optimal actuators location and channel numbers

For the details of the approach followed to select the optimal location the reader is referred to Appendix A.

As suggested by the experience gained from the installation tests of the first prototypes of the actuators, the frame mounting was particularly difficult for the small space available to the tools necessary for the installation operations. This issue, together with the necessity to stiffen the mounting flange of each actuator couple, required a modification to the original actuator design, which was the main source of delay in actuators' delivery.

The resulting modification designed by LPA-ZIP required also a modification to the optical fiber installation procedure, which eventually required the use of suitably

manufactured spacers (provided by LPA-ZIP) and this was the second source of delay in the actuator installation (see the following section for more details on sensor installation).

Its worth remarking that for each actuator pair to be mounted on a frame, an offset displacement of a few centimeters with respect to the original forecasted location was necessary to actually install the devices due to the intersection between the two structural members that limited the space available to the actuators (see Figure 4-3).

Once the actuators were received by DII-SUN; the optical sensors were integrated and all the actuators were installed by DII-SUN in collaboration with Alenia together with all the accelerometers. A typical stringer mounting is reported in Figure 4-4 before accelerometer installation.

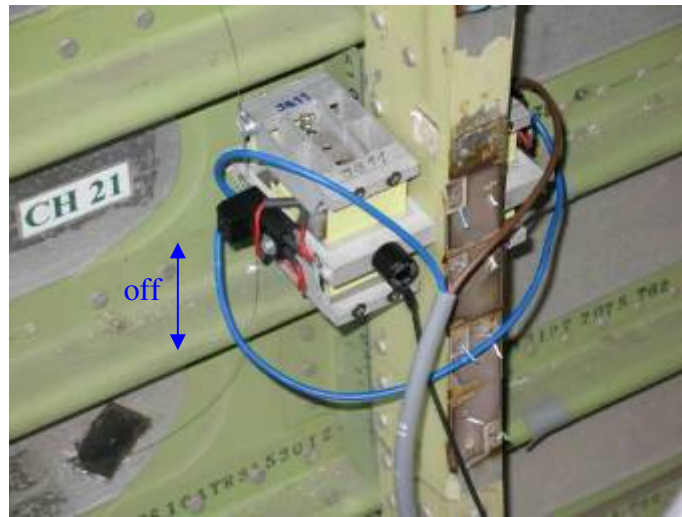


Figure 4-3: Actuator couple mounted on a frame

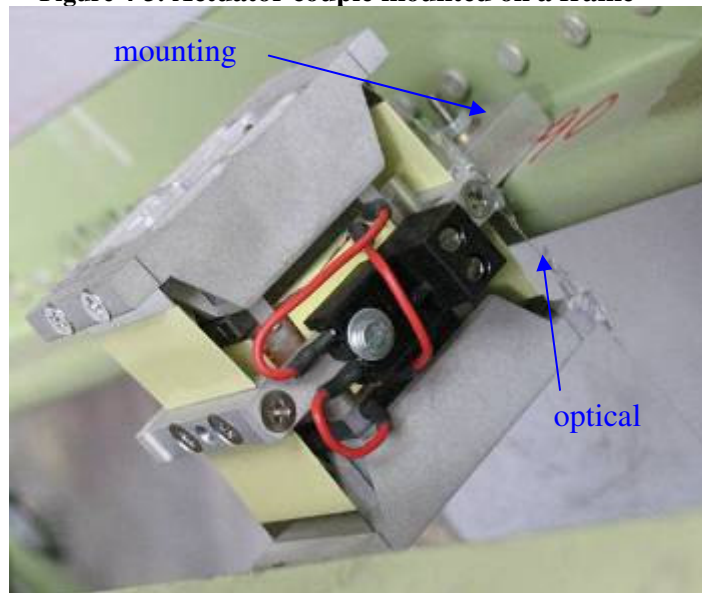


Figure 4-4: Actuator mounted on a stringer

4.2 SENSORS' INSTALLATION

Bragg gratings: the optical sensors have been installed on each actuator before mounting this on the fuselage according to the procedure documented in the Deliverable D1.2-1 of Workpackage 1 (see Figure 4-4 for a detail of an optical sensor integrated in a stringer actuator).

Accelerometers: since a co-located control strategy was selected, the accelerometers were fixed directly on each actuator by using M3 threaded rods specially manufactured by LPA-ZIP to be suitably integrated into the actuators stiffening frames. For instance, Figure 4-45 reports the mounting solution for the actuators to be mounted in pairs.

Material: M3 threaded rod

Bearbeiter: Chris May
Telefon: -4188

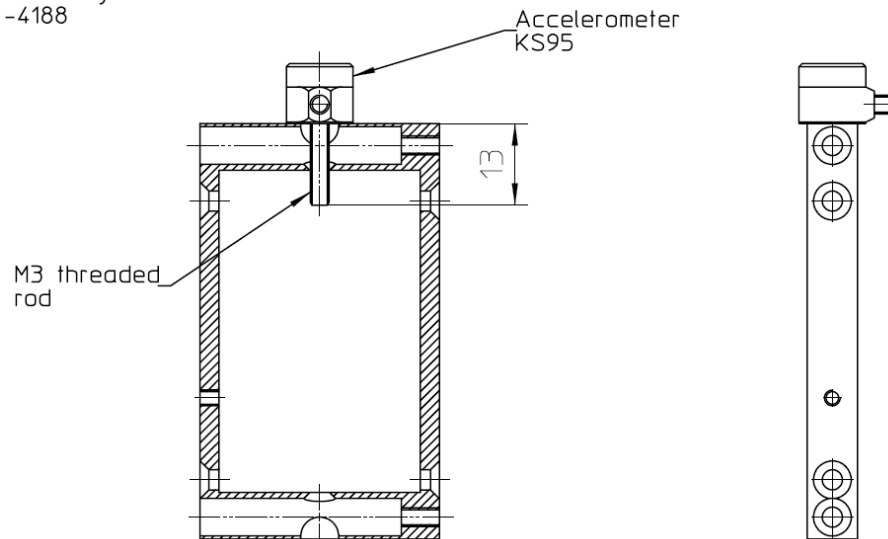


Figure 4-5: Accelerometer mounting description

The accelerometers, selected by Alenia experts, are the KS95.100 model by Metra Meß- und Frequenztechnik (MMF) with a sensitivity of 100 mV/g, a dynamic range of 60 g, a bandwidth of 40 kHz and a weight of 3.2 g (without the cable).

Microphones: four measurement microphones (1/2" BSWA TECH mod.MP201 + ICP Microphone Preamplifier BSWA TECH mod. MA201) have been installed in a transverse section of the fuselage with the aim of measuring the noise field in different points which were selected at locations close to the passengers head when seated, so as to evaluate the effects of the noise control system on the cabin comfort.

4.3 CONTROL SYSTEM INSTALLATION

DII-SUN has cabled the whole ATR-42 fuselage in collaboration with Alenia and has arranged the emplacement of the control system components. In particular, inside the

fuselage, for each control channel a power bipolar cable has been laid for the control input, an accelerometer cable for the high level control and a couple of fibres for the low level control (a detailed description of the control system is reported in Appendix). Moreover a BNC/BNC cable has been laid for each microphone. All the cables coming out of the fuselage have been connected to the conditioning electronics in a rack unit accordingly. An OROS system for data acquisition in the frequency domain has been used both to evaluate performances using the signals of the microphones and to generate the input signals to the shakers' amplifiers for primary disturbance field generation. Figure 4-4 shows the layout of all implemented connections and Figure 4-4 reports the list of all components used in the control system installation. Figure 4-4 and Figure 4-4 show some pictures of the experimental installation both inside and outside the fuselage.

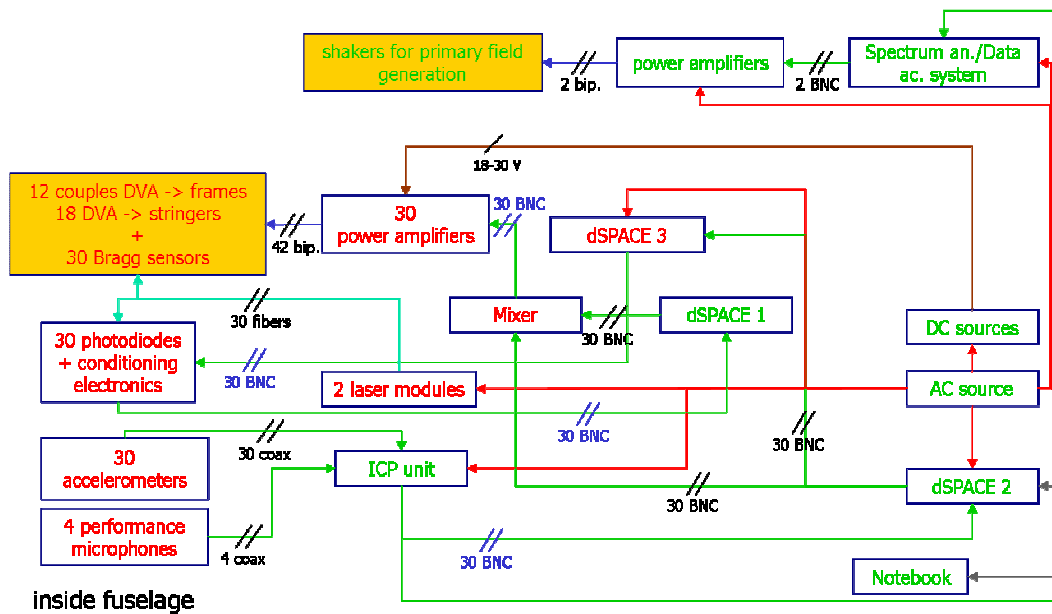


Figure 4-6: Control system layout

Component	Nr.	Provider
Final actuators	42	LPA-ZIP
dSPACE 1	1	Unina-
Power amplifiers	30	LPA-ZIP
Accelerometers	30	Alenia
BNC-BNC cables	210	Alenia
Bipolar cables	30	Alenia
ICP unit (16 channels)	2	Alenia
Bipolar DC power cables	4	Alenia
DC power source	2	Alenia
AC power cables and adapters	12	Alenia
Accelerometers coaxial cables	30	Alenia
Shaker + amplifier	2	Alenia
Microphones	4	Alenia
Microphones coaxial cables	4	Alenia
Spectrum an./Data acq. system	1	Alenia
Bragg sensors	30	DII-SUN
Laser modules	2	DII-SUN
Photodiodes	30	DII-SUN

Conditioning electronics	2	DII-SUN
dSPACE 2	1	DII-SUN
Notebook	1	DII-SUN
dSPACE 3	1	DII-SUN

Table 4-1: Components list of the final test bench

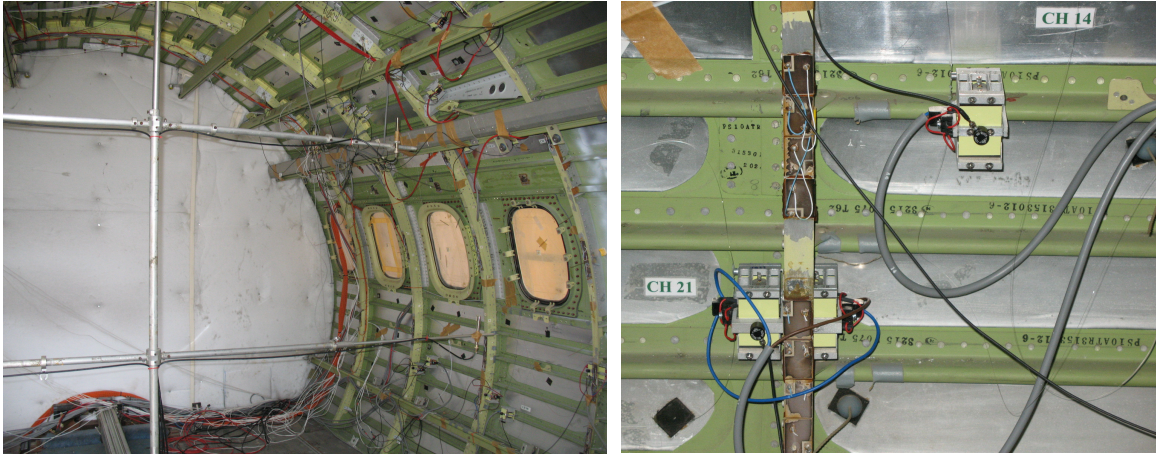


Figure 4-7: Installation of actuators and sensors inside the fuselage

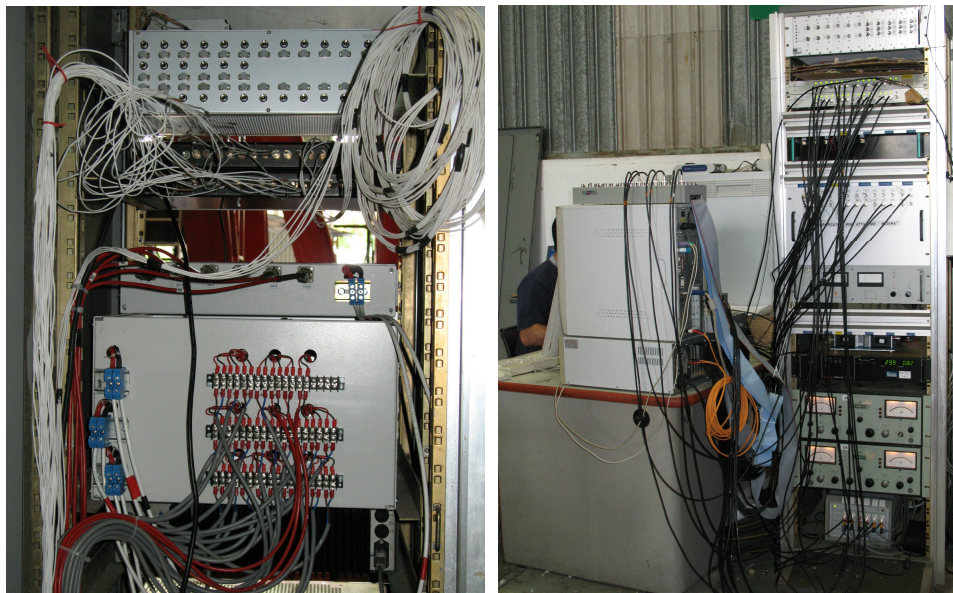


Figure 4-8: Installation of power and conditioning electronics



Figure 4-9: View of whole control system

4.4 ASSESSMENT OF THE CONTROL CHANNELS BEHAVIOUR

The assessment of control channels behavior has been carried out during three days spent at Alenia by Chris May (LPA-ZIP) investigating and correcting the performance of actuator channels. Prior to the visit, DII-SUN had identified 13 of the 30 channels with medium to strong harmonic distortion in the acceleration signals when driving with a sinusoidal control signal. Strong clipping of the actuator driving current was found to exist on all of these channels. When driving with the 6-channel analogue amplifier 11 of these channels exhibited acceptable acceleration behavior with respect to harmonics.

Miscellaneous problems were encountered on certain channels as recorded below. At the end of the week, only CH12 was considered to be still KO, whereby CH24 and CH28 were labeled OK-

- CH04 - loose electrical contact at coil on actuator #38 (resoldered)
 - poor contact of accelerometer cable connector (tightened)
 - acceleration signal was unclean although the acceleration signal from neighbouring actuator 6 was clean
 - one side of Bragg sensor optical fibre broken during investigations (reflection mode may still be feasible)
 - mechanical contact between actuator flanges and shear tie rivet (alleviated by filing)
 - actuator pair rematched by tuning to 125 Hz
 - higher than average electrical resistance of 3.3 Ohm measured
- CH12 - mechanical contact between moving mass and cable tie adapter (adapter removed)
 - actuator pair rematched by tuning to 103 Hz
 - washers make uneven contact in corner of frame and shear tie components (corrected by filing washers)

- poor connection of accelerometer and its cable (improved by tightening)
- high-impedance (8 MOhm) electrical short detected in actuator (not repaired)
- mechanical contact between flange and shear tie rivet at skin
- CH14 - acceleration signal OK despite high-impedance electrical short detected in actuator (not repaired)
- CH15 - lower than average electrical resistance of 1.8 Ohm measured
- CH24 - flange bent by original mounting against shear tie rivet (flange replaced)
 - high-impedance (90 kOhm) electrical short detected in actuator (repaired)
 - noise from accelerometer cable connector (tightened)
 - actuator pair rematched by tuning to 114 Hz
 - source of remaining medium harmonic distortion not identified;
- CH28 - source of remaining medium harmonic distortion not identified;

4.4.1 POWER AMPLIFIERS

The supply voltage at the amplifiers was measured to be 29.6 V. All channel loads were measured with respect to DC resistance and inductance as well as tested for electrical short to ground. Due to the long power cables connecting the amplifiers inside the test hall with the actuators inside the mock-up, the DC resistance of each channel was increased by about 1.1 Ohm and the inductance by about 50 μ H with respect to the case where amplifiers would be mounted in the mock-up close to the actuators. In the case of the amplifier on CH03, the current clipping behavior disappeared when driving a short circuit directly at the output of the amplifier, while shorting the load in front of the actuator still resulting in current clipping. Driving CH03 with the amplifier from CH06 did not result in clipping, verifying that some amplifiers are sufficiently dimensioned for the load and others are inadequate.

E-mail and telephone communication with Benedikt Holz and Thomas Würtz of ZIP lead to the shipment of 11 additional amplifiers with about 10% power increase on Friday, May 25th and arrival at Alenia on Tuesday, May 29th. These amplifiers and the 6 analogue amplifier channels shall replace the inadequate amplifiers and should lead to acceptable acceleration signals as indicated by the experiments using the 6-channel analogue amplifier. Back-up solutions include mounting the amplifiers close to the actuator loads within the mock-up or limiting the current signal amplitude to a value where clipping does not occur.

The 14 V DC power supply to the 6-channel analogue amplifier was found to be the source of spikes in the accelerometer and current measurement signals. These seemed to be purely electrical disturbance with little to no relevance for the structural acceleration.

The conclusion of this work lead to the result that only 21 out of the 30 available control channels were actually working in a proper way resulting in an expected performance worse than the originally forecasted.

4.5 EXPERIMENTAL CHARACTERIZATION

Once the control system experimental set-up has been installed a characterization of the structural test article (fuselage mock-up) as well as of the installed actuators was necessary in order to:

- 1) Verify that the actuators performances in terms of force spectra were in line with the specifications issued within the Task 1 of WP2.1;
- 2) Characterize passively the fuselage mock-up, as already done within Task 1 for validating the numerical model, in order to verify and (if possible) quantify the perturbations that actuators installation added to the overall structural dynamic behavior;
- 3) Characterize passively the fuselage mock-up at control points locations for control purposes, in order to obtain a realistic model to implement into the outer control algorithm.

Following is a short description of the three activities that, due to relevant delays that affected the production and installation of the control actuators, have been carried out within less than two months instead of the original forecasted timeframe.

4.6 ACTUATORS' CHARACTERIZATION

In order to characterize the LPA actuator type in terms of force performances once installed on the fuselage section, a measurement campaign has been carried out at the Alenia Aeronautics plant in Pomigliano d'Arco (NA). Several actuators have been installed both in single (stringer) and coupled (frame) configurations – see next pictures.

Laser vibrometer has been employed in order to measure the vibration spectra on the centre flange of the actuator as far as on its seismic masses. It is possible from these simple measurements to calculate the inertial force spectra provided by the actuator to the host structure: from the laboratory characterization of the devices resulted that the overall inertial force, $F(\omega)$ can be obtained scaling the seismic mass acceleration, $a(\omega)$ by a factor of 0.15:

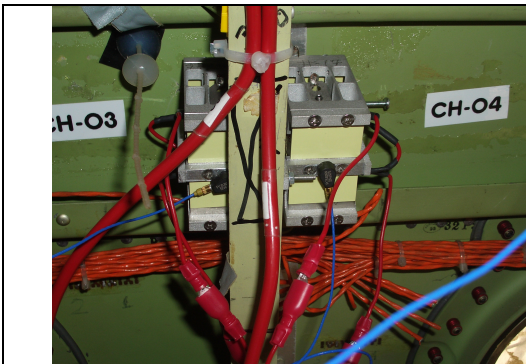


Figure 4-10: Actuators mounting: frame configuration

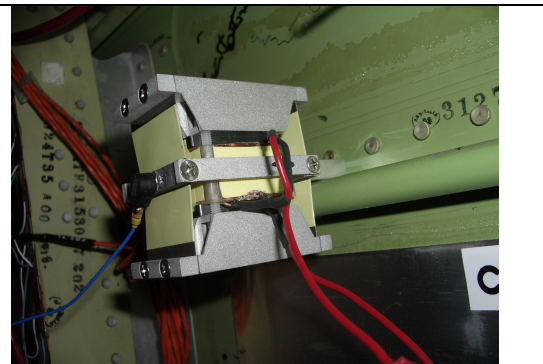


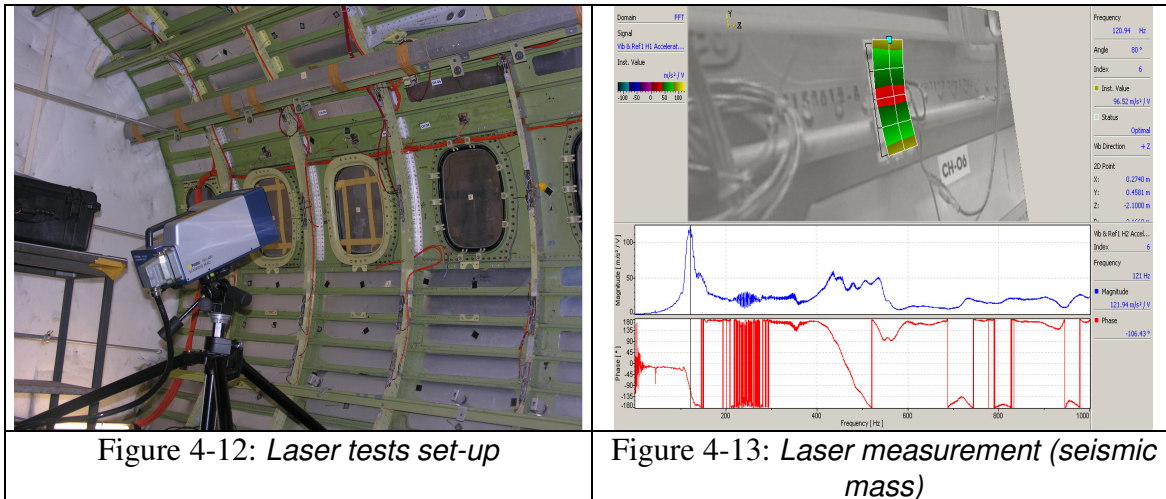
Figure 4-11: Actuators mounting: stringer configuration

$$F(\omega) = a(\omega) * 0.15$$

provided that [a]=[m/sec²] and [F]=[Newtons].

At the same time, once the force spectra is known, it is also possible to estimate the direct structural impedance of the host structure in the point where the actuator is connected to; provided that the central flange can be considered rigid up to about 1000Hz, it is possible to assume that the acceleration measured on the central flange of the actuator is equal to the one of the connection point with the host structure. By dividing that acceleration by the inertial force $F(\omega)$ measured as described above it is possible to evaluate the impedance (inertance) of the host structural in the points where the actuators are applied.

Next figures show the test set-up (laser vibrometer) and a picture of the measurements carried on.



In next figure the amplitude force spectra of the actuator in the stringer mounting configuration is reported. It is possible to notice its resonant behaviour around 100Hz with a peak force value of about sixteen Newtons; out of the seismic flanges resonance domain the force values present a dependence from the dynamic coupling between the actuator and its host structure, but result very close to the spectra measured during laboratory characterization (fixed point) of a device of the same typology carried out at University of Saarland.

Finally local impedances of the fuselage section evaluated by the mean of the numerical (FEM) model have been compared with one calculated by the procedure described above. Figure 27 presents this comparison. It is possible to notice the magnitude order differences between structural impedances of point located on frames (1,56,25) and those located on stringers (12, 31,37); the experimental impedance presented in the graph is related to a stringer measurement point. Provided force spectra can be considered in good agreement with the actuators requirements; furthermore the measured inertance is in good agreement with those obtained by the F.E. model; differences at higher frequencies can be considered again due to the damping material added on the real fuselage mock-up whose effect was not included into the F.E. model.

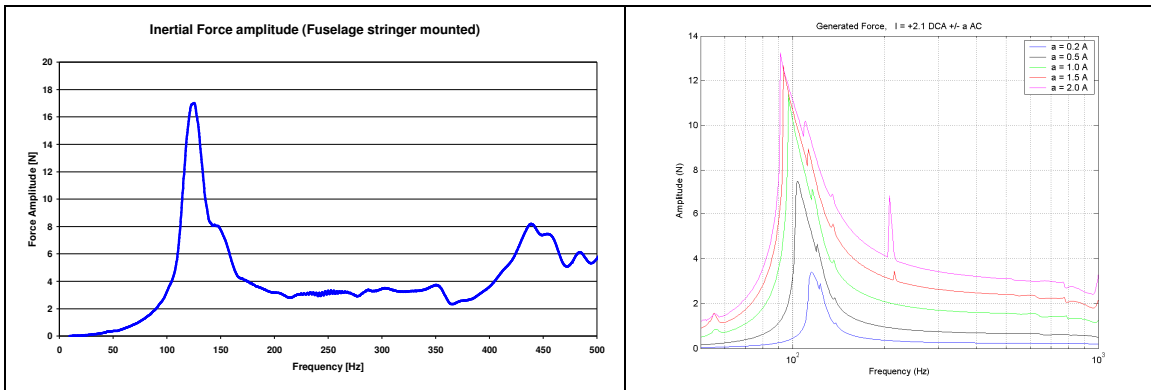


Figure 4-14: Comparison between actuator force spectra measured left: fuselage stringer mounted – right: laboratory measurement

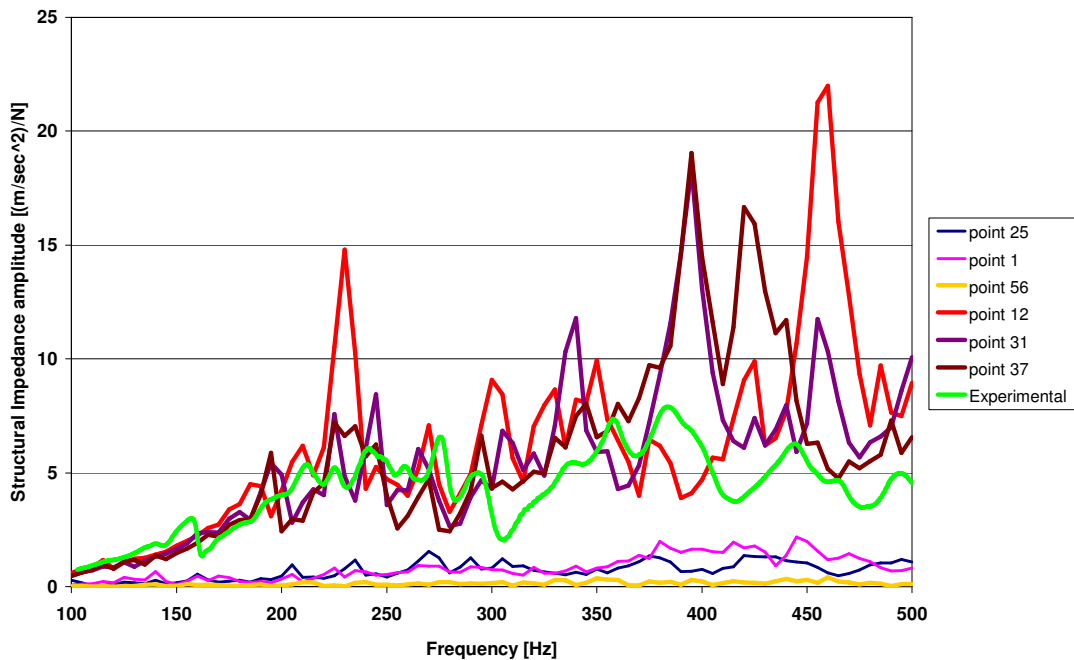


Figure 4-15: Comparison between numerical and experimental fuselage structural impedances (inertance)

4.7 PASSIVE CHARACTERIZATION OF THE TEST ARTICLE

Once all the control actuators had been installed on the fuselage section a new passive characterization of the test article (experimental modal analysis) was required in order to assess the shifts of its natural frequencies respect to the first passive characterization carried out during the requirements specification task. The target of the first passive characterization was mainly to validate the numerical F.E. model of the test article employed for calculating the control actuators specifications (see D2.1-1). The target of

this second passive structural characterization was to quantify the unavoidable shifts of natural frequencies happened to the fuselage section due mostly to:

- Local small impedances of control actuators connected to the fuselage structure;
- Differences in the constraint configuration of the mock-up due to the particular solution adopted for cylinder suspension trough two end caps bolted.

In order to understand the importance of even small differences in the structural dynamic behavior of the structure to be controlled it must recall that positioning configuration and performances of the control actuators were designed employing as main tool the numerical model validated by the first dynamic characterization: each modification happened to that “baseline” should reflect in reduced performances of the control system even if characterized by a certain degree of robustness.

The passive characterization has been carried out by the same approach of the first one by LMS (as subcontractor of Alenia) and UNI-Na DPA. The involvement of LMS, that is also the developer of the tool employed for the modal analysis, permitted to have a further validation of the methodologies and of the results obtained during the Task 1 activities.

Following a description of the methodologies and a summary of the results of this activities is reported.

4.7.1 DATA SELECTION

The software LMS Test.Lab provides the subsequent steps for the analysis and the extraction of the modal parameters. The first step is to select the group of FRF's to be used to identify the modal parameters.

In order to have a global indicator of all the responses of the system, a summed FRF is computed. In the Figure 16 is shown the Sum of the FRFs and also two Mode Indicator Functions (MIFs)

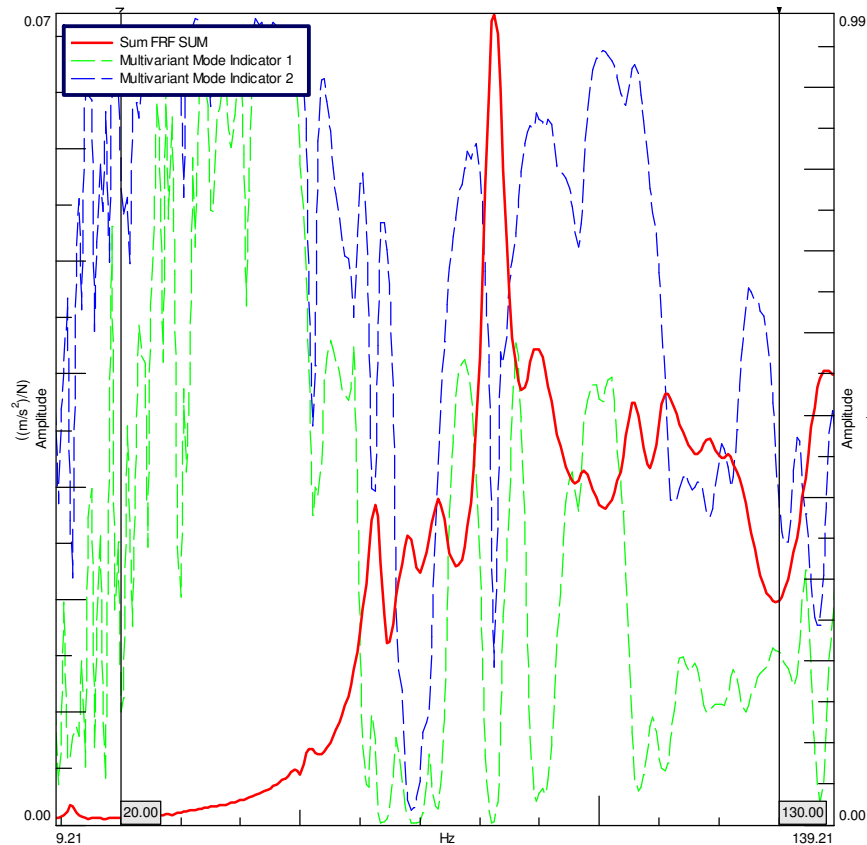


Figure 4-16: Sum FRF and MIFs

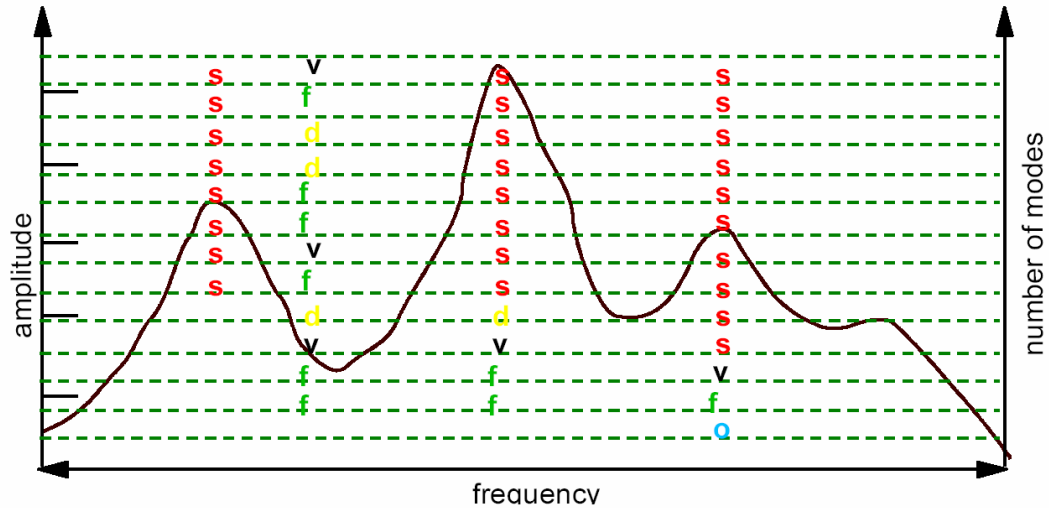
Mode Indicator Functions (MIFs) are frequency domain functions that exhibit local minima at the natural frequencies of real normal modes.

The number of MIFs that can be computed for a given data set is equal to the number of input locations that are available. The so-called primary MIF will exhibit a local minimum at each of the structure's natural frequencies. The secondary MIF will have local minima only in the case of repeated roots. Depending on the number of input (reference) locations for which data is available, higher order MIFs can be computed to determine the multiplicity of the repeated root. So a root with a multiplicity of four will cause a minimum in the first, second, third and fourth MIF for example

In the Figure 16 it's possible to notice that at the frequency 69Hz both MIF1 and MIF2 are close to zero, this suggests 2 repeated roots, in fact, 2 different modes will be identified: Mode 4 : 68.389 Hz, 1.57 % and Mode 5 : 69.803 Hz, 2.56 %.

4.7.2 STABILIZATION DIAGRAM – POLES SELECTION

A crucial step for the experimental modal analysis is the calculation of the stabilization diagram.



In the stabilization diagram are shown the poles, means both frequency and damping, with increasing complexity of the model.

Physical intuition would lead you to expect that estimates of frequency and damping corresponding to true structural modes, should recur (in approximately the same place) as the number of modes is increased. Computational modes will not reappear with identical frequency and damping. The optimal number of modes that can be calculated for use can then be seen, as those modes for which the frequency and damping values of the physical modes do not change significantly. In other words, those which have stabilized.

In the Figure 4-17 is shown the stabilization diagram concerning the structure under test.

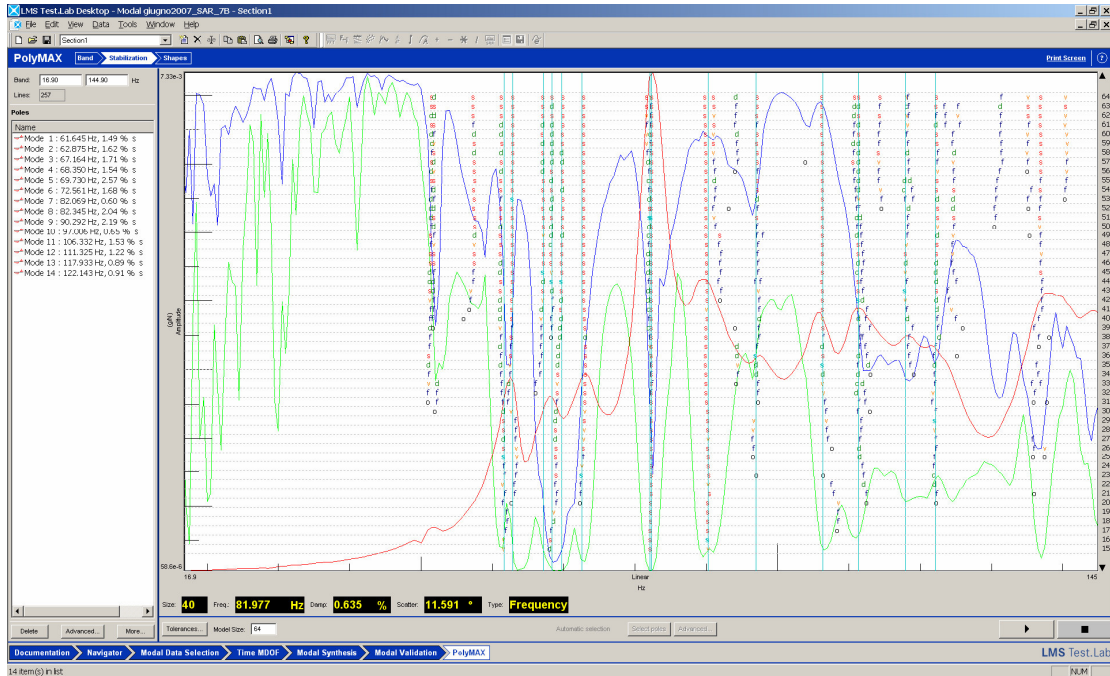


Figure 4-17: Stabilization Diagram

In order to select the best group of modes the user can use also some advanced automated tool like the LMS Test.Lab Automatic Modal Parameter Selection (AMPS). This tool is an intelligent rule-based technique to analyze the stabilization diagram by selecting only the physical poles, that was developed based on the observation of skilled engineers.

One of the biggest advantage of this tool is a ‘user independent modal identification’; that ensure consistent analyses obtained from different people using the same setup and measurement.

4.7.3 LIST OF MODES

Using the procedure described it has been possible to identify the following structural modes:

<i>Modes: freq and damping</i>
<i>Mode 1 : 51.085 Hz, 1.05 %</i>
<i>Mode 2 : 51.888 Hz, 0.99 %</i>
<i>Mode 3 : 61.645 Hz, 1.49 %</i>
<i>Mode 4 : 62.875 Hz, 1.62 %</i>
<i>Mode 5 : 67.164 Hz, 1.71 %</i>
<i>Mode 6 : 68.350 Hz, 1.54 %</i>
<i>Mode 7 : 69.730 Hz, 2.57 %</i>
<i>Mode 8 : 72.561 Hz, 1.68 %</i>
<i>Mode 9 : 82.069 Hz, 0.60 %</i>

<i>Mode 10 : 82.345 Hz, 2.04 %</i>
<i>Mode 11 : 90.292 Hz, 2.19 %</i>
<i>Mode 12 : 97.006 Hz, 0.65 %</i>
<i>Mode 13 : 106.332 Hz, 1.53 %</i>
<i>Mode 14 : 111.325 Hz, 1.22 %</i>
<i>Mode 15 : 117.933 Hz, 0.89 %</i>
<i>Mode 16 : 122.143 Hz, 0.91 %</i>

Table 4-2: Modal Frequencies and modal damping

From the graphical representation of the shape for each mode are shown.

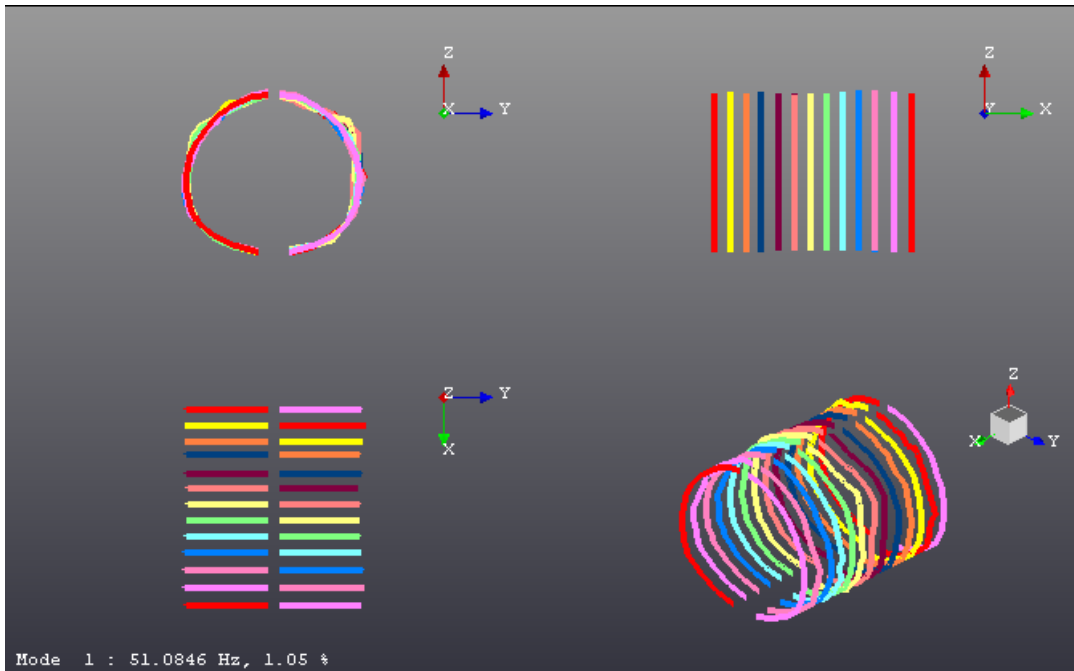


Figure 4-18: Mode Shape at 51.08 Hz

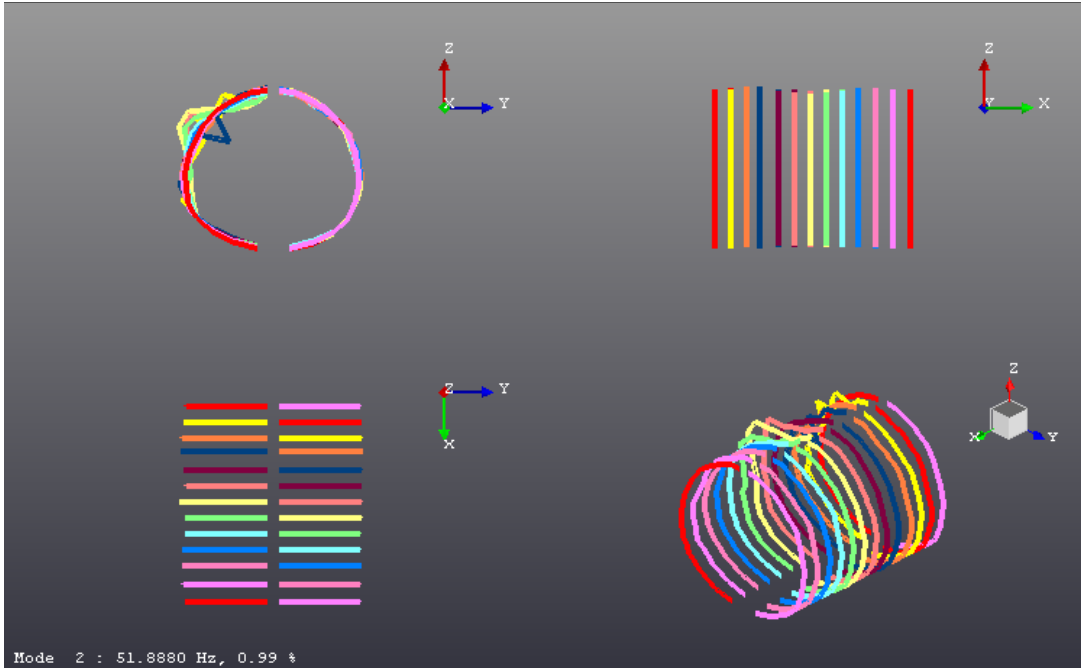


Figure 4-19: Mode Shape at 51.88 Hz

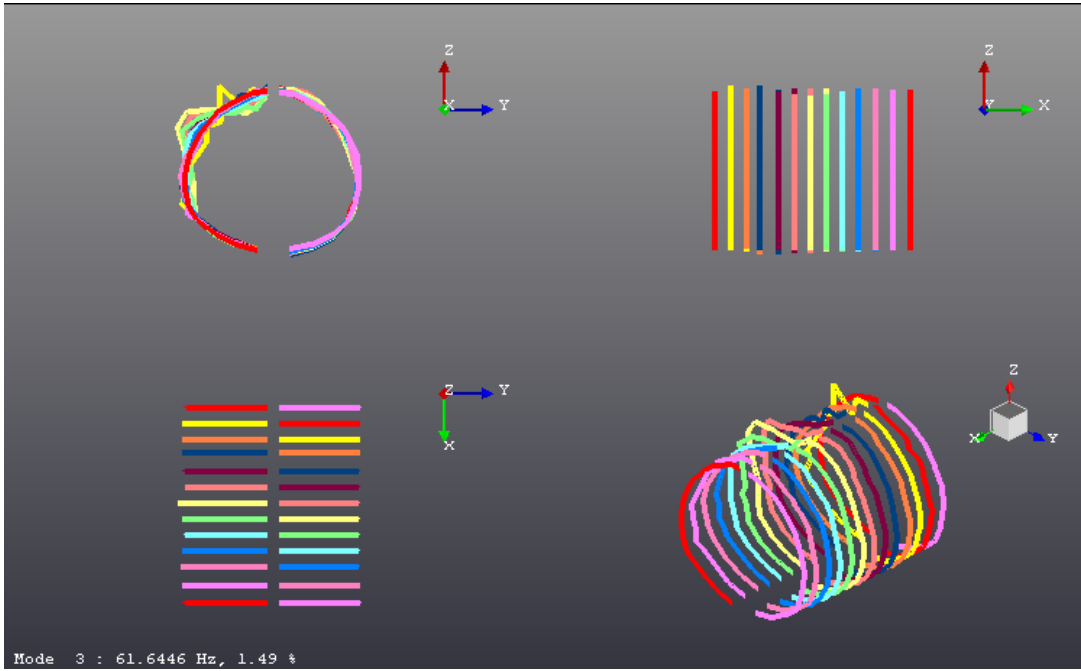


Figure 4-20: Mode Shape at 61.64 Hz

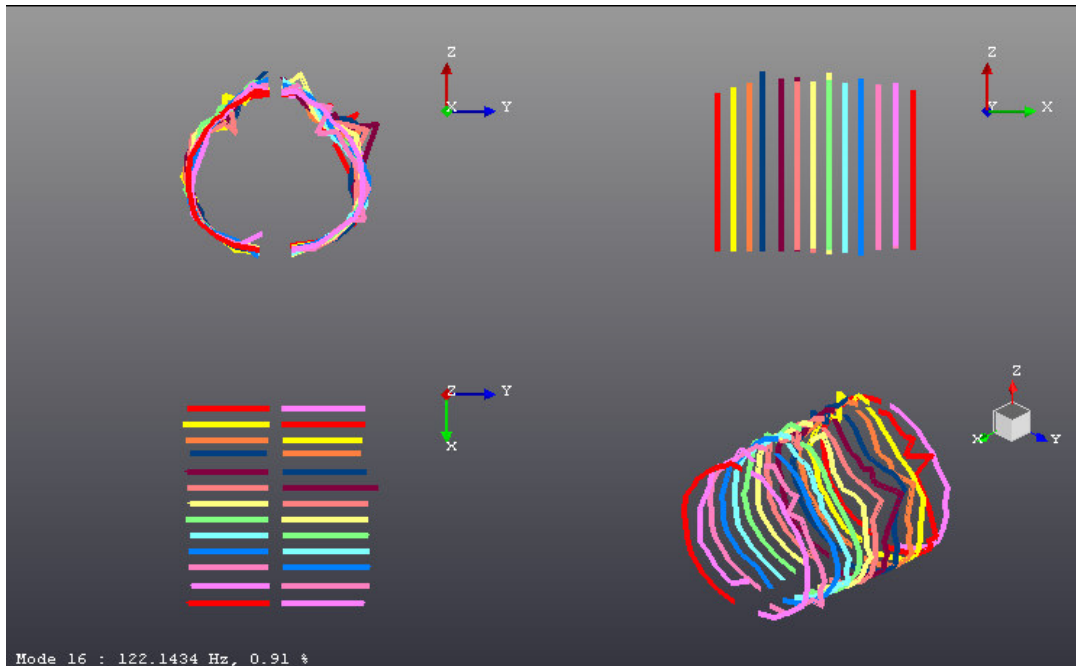


Figure 4-21: Mode Shape at 122.14 Hz

4.7.4 VALIDATION OF THE SELECTED MODES

In order to give high confidence on the results, it's worth to use some Validations Tools.

There are many way to better understand if a mode is 'structural' or 'computational' like *Synthesised FRF*, *Auto-Mac*, *Cross-Mac*, etc...

The check called *Synthesised FRF* is a comparison between measured and synthesized FRFs The FRFs are synthesized as follow:

$$[H(j\omega)] = \sum_{r=1}^N \left(\frac{\langle \psi \rangle_r \langle L \rangle_r}{(j\omega - \lambda_r)} + \frac{\langle \psi \rangle_r^* \langle L \rangle_r^*}{(j\omega - \lambda_r^*)} \right) + [UR] - \frac{[LR]}{\omega^2} \quad \text{or}$$

$$[H(j\omega)] = \sum_{r=1}^N \left(\frac{Q_r \langle \psi \rangle_r \langle \psi \rangle_r}{(j\omega - \lambda_r)} + \frac{Q_r^* \langle \psi \rangle_r^* \langle \psi \rangle_r^*}{(j\omega - \lambda_r^*)} \right) + [UR] - \frac{[LR]}{\omega^2}$$

where:

$[H(j\omega)]$ is the frequency response matrix

λ_r is the system poles for mode r

$\langle \psi \rangle_r$ is the mode shape r

$\langle L \rangle_r$ is the modal participation factor vector for mode r

Q_r is the modal scale factor for mode r

$[UR]$ is the upper residual

$[LR]$ is the lower residual

It is also possible to obtain correlation and error values relating to the measured and synthesized FRFs

$$\text{Correlation} = \frac{\left| \sum_i (S_i \times M_i^*) \right|^2}{\left(\sum_i (S_i \times S_i^*) \right) \left(\sum_i (M_i \times M_i^*) \right)}$$

with

S_i = the complex value of the synthesized FRF at spectral line i

M_i = the complex value of the measured FRF at spectral line i

And the LS error is the least square difference normalized to the synthesized values

$$\text{LS error} = \frac{\sum_i (S_i - M_i) \times (S_i - M_i)^*}{\sum_i (S_i \times S_i^*)}$$

In Figure 4-22 and Figure 4-22 are shown some examples of comparisons between FRF measured (red) and synthesised (green).

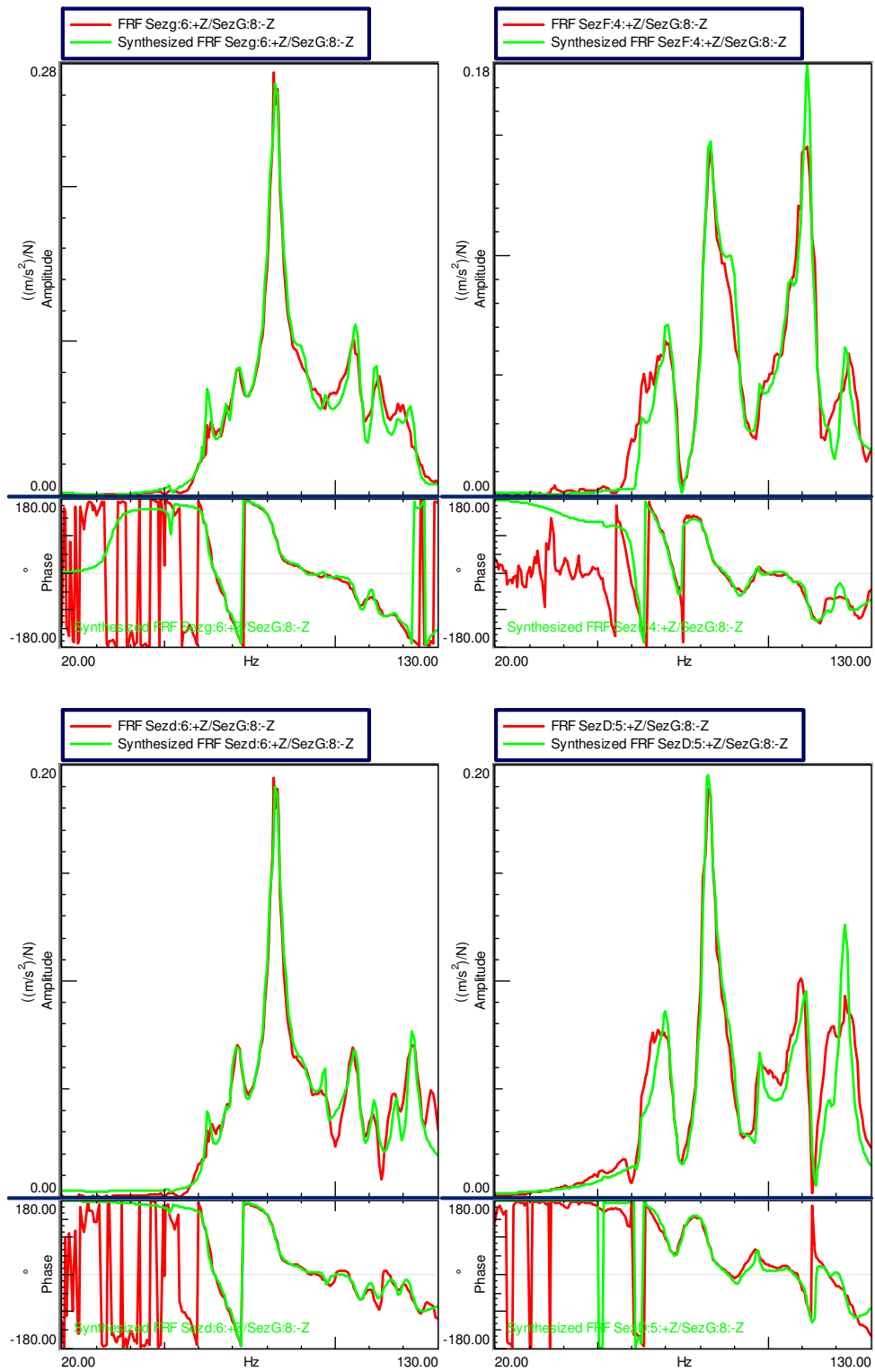


Figure 4-22: Example of synthesised FRFs

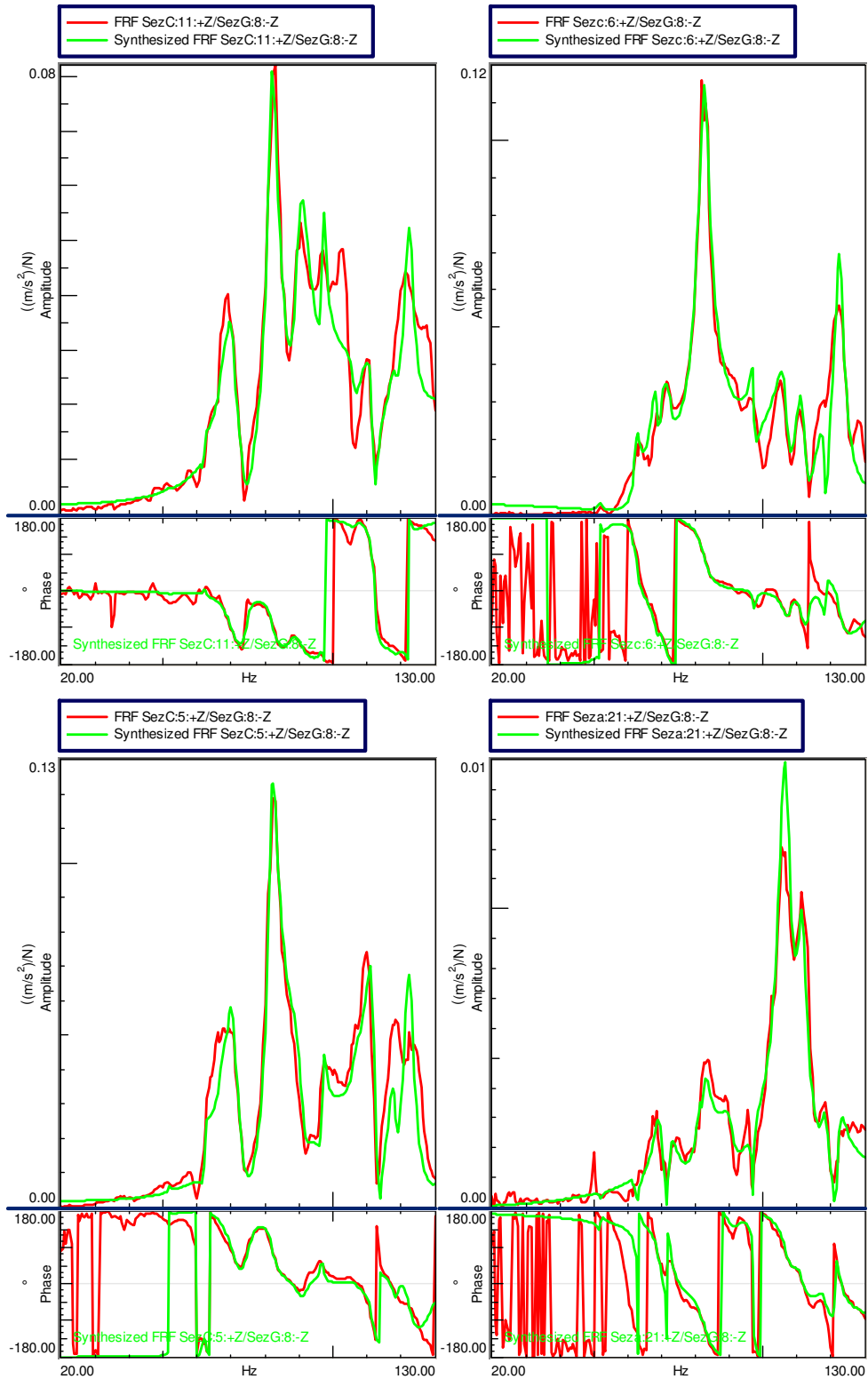


Figure 4-23: Example of synthesised FRFs

The *Modal Assurance Criterion (MAC)* is a mathematical tool to compare two vectors. It can be used to compare modal mode shape information.

The MAC expresses a degree of confidence for this calculation:

$$MAC_{xy} = \frac{|(X)^* [W] (Y)|^2}{((Y)^* [W] (Y)) ((X)^* [W] (X))}$$

[W] is the weighting matrix (most often the unity matrix).

If a linear relationship exists between the two complex vectors X and Y, the MAC value will be near to one. If they are linearly independent, the MAC value will be small (near zero).

In a more general way, the MAC concept can be applied on two arbitrary complex vectors. This is useful in comparing two arbitrary scaled mode shape vectors since similar mode shapes have a high MAC value.

Modal Assurance Criterion values can be used to compare two modal models obtained from two different modal parameter estimation processes on the same test data for example or to investigate the validity of the estimated modes within the same modal model. The MAC between two mode shape vectors, and, is defined as:

$$MAC((\psi_r), (\psi_s)) = \frac{|(\psi_r)^* (\psi_s)|^2}{((\psi_r)^* (\psi_r)) ((\psi_s)^* (\psi_s))}$$

When comparing mode shapes, the MAC values for corresponding modes should be closed to 100 %.

In Figure 36 is shown the graphical representation of the Auto-Mac of the modes identified. The MAC is called Auto-MAC when only one set of modes is used.

This is very useful to check the accuracy of the experimental wireframe. In case of few measurement points the result will be that different modes will have similar shapes and consequently high MAC value (problem know also with the name of *spatial aliasing*).

In case a good experimental wireframe has been used, the modes will result not linear dependant and consequently low MAC values are expected.

In Figure 2-1Figure 4-24 the main diagonal of the matrix is equal to 100% because shows the MAC between a mode with the same mode; all the other bars should be near to zero because the structural modes are linear independent. High MAC values between two different modes it's a warning for the *spatial aliasing*.

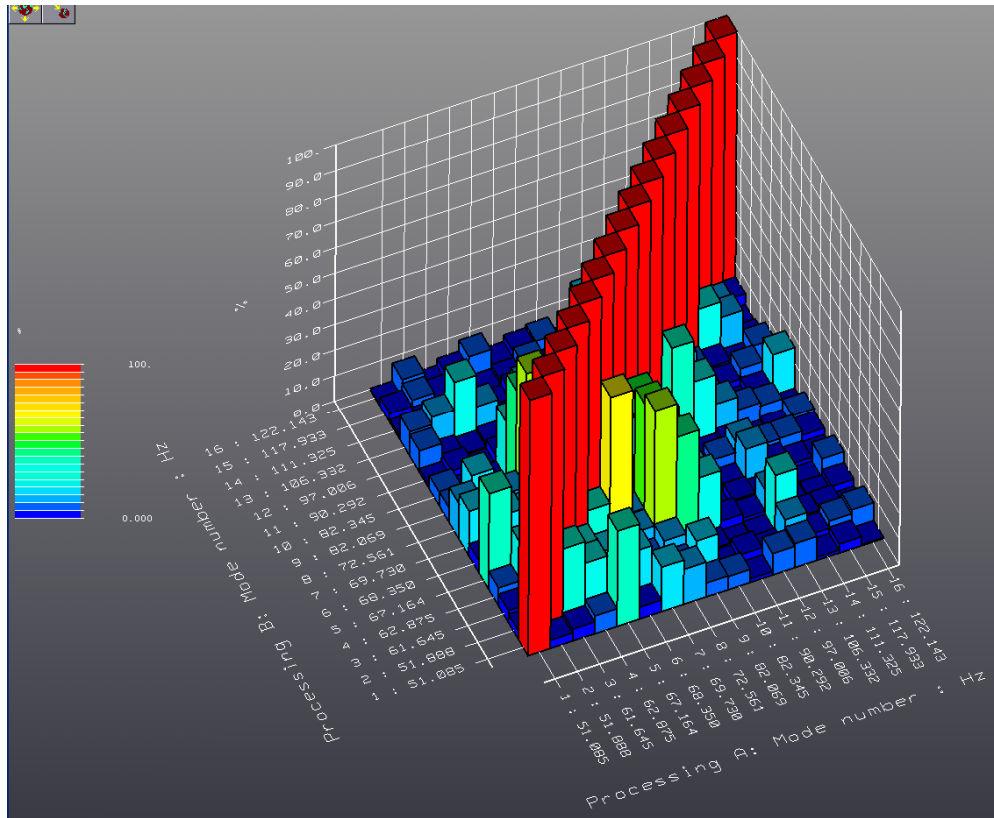


Figure 4-24: Auto-MAC

4.8 DYNAMIC MODEL IDENTIFICATION FOR CONTROL PURPOSES

The dynamic model for control purposes has been identified according to the identification procedure proposed by DII-SUN and reported in the Deliverable D2.1-2. As an example, an experimental result for a control point of the structure is reported in Fig. 10. The identified dynamic model has been used in the subsequent phase for the design of the noise control algorithm as detailed in Appendix B.

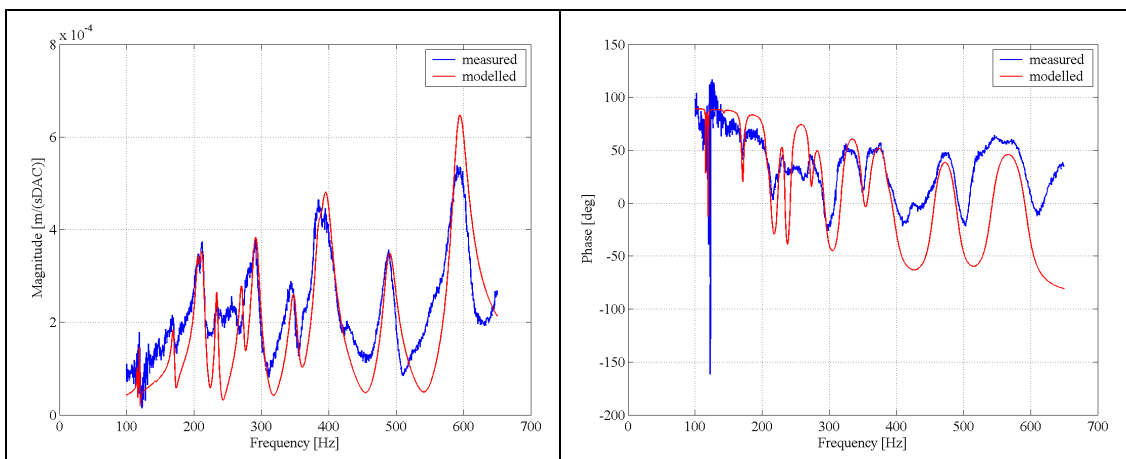


Figure 4-25: Identification result in a control point

4.9 TUNING OF THE CONTROL ALGORITHM

As reported in Appendix B, the selected control algorithm designed by DII-SN is based on a two-level control concept (see Figure 4-26). A low level control has been developed for the linearization of the actuator behavior and then a high level control has been designed for the active noise control. Further details can be found in Appendix B.

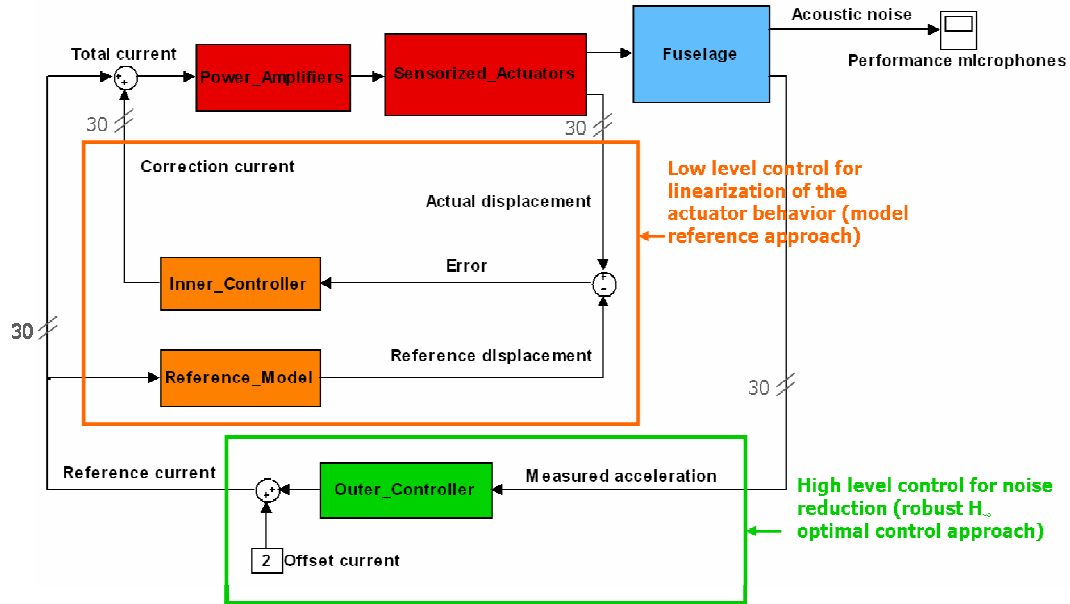


Figure 4-26: Complete control scheme

4.10 ACTUATORS' CONTROL LOOP

Even though satisfying the demanding requirements, final actuators present a strong nonlinear behavior, in particular the resonant frequency shifts with respect to the amplitude of the input current. Therefore, the low level control has been designed for the linearization of the actuator behavior so as to fix the resonant frequency. In fact, such a behavior makes the actuator hardly usable due to the significant phase shift variation depending on the input signal. The optical sensor has been usefully exploited to measure the position of the moving mass of the actuator and to implement a reference model control, which aims at imposing a desired linear behavior to the controlled device.

4.11 NOISE CONTROL LOOP

The high level control loop has been designed according to a robust H_∞ optimal control approach with the primary objective of reducing the noise inside the fuselage. In particular, this procedure is based on an experimentally identified linear dynamic model,

with the actuators current as input and the accelerometers signal as output. It is evident that the results of the low level control are of fundamental importance for letting this approach feasible, since it is based on the assumption of linearity.

4.12 EXPERIMENTAL RESULTS

The experimental presented hereafter have been evaluated both for the low level control loop and for the high level control loop, comparing the control-on case to the control-off one.

4.13 LOW LEVEL CONTROL RESULTS

In Figure 4-27, the blue lines represent the actuator frequency response function measured at three different input currents without the low level control. In the same figure, it is possible to see the positive effects of the low level control on the actuator behavior since the red lines represent the same FRFs measured with the control loop activated, and they all exhibit the same resonant frequency, resulting in a phase shift almost insensitive to the input current amplitude.

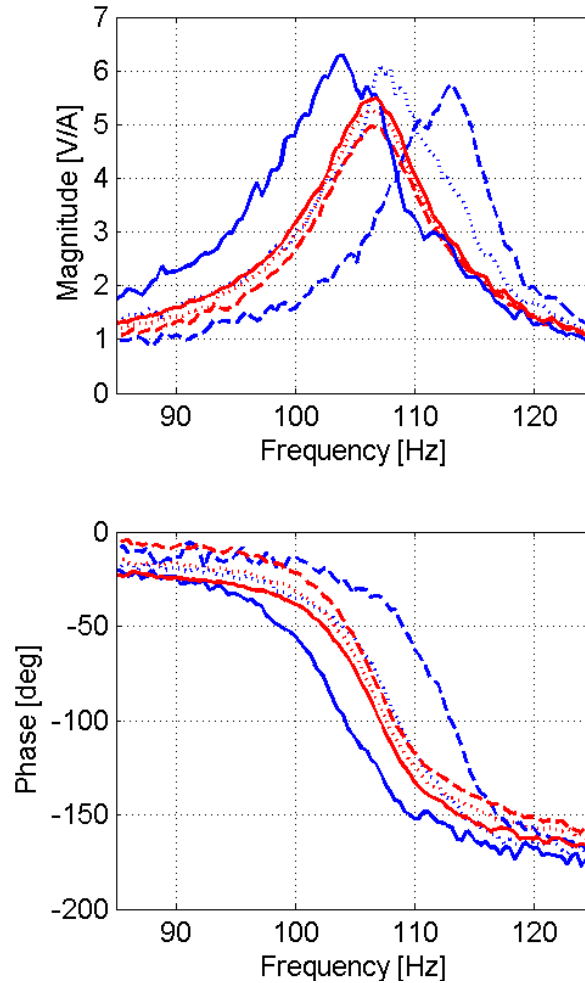


Figure 4-27: Actuator behaviour at different current: control off (blue), control on (red)

4.14 HIGH LEVEL CONTROL RESULTS

The effectiveness of the active noise control system has been tested in different conditions. First of all, it is important to state that since the total number of working control channels was limited to 21 and only 4 couples have been mounted on the frames, low controllability of frequencies below 150 Hz is expected and therefore, in agreement with the end-user, a primary force fields at a medium frequency range [200,600] Hz was selected. The spectrum of this primary force field as measured by one the two load cells installed on the shakers is reported in Figure 4-28.

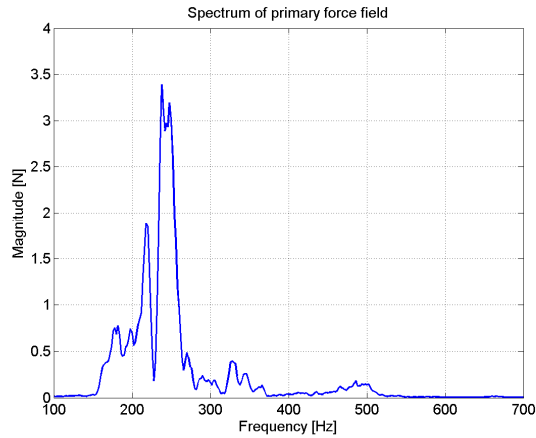


Figure 4-28: Primary force field from specifications

A first set of experiments has been made with this primary disturbance field generated from two symmetric shakers as requested from the specs. The performances of the control loop, measured from the microphones #1 and #2, are shown in Figure 4-29. Errore. L'origine riferimento non è stata trovata. Also, a 3.7 dBA reduction of the overall levels of SPL has been measured.

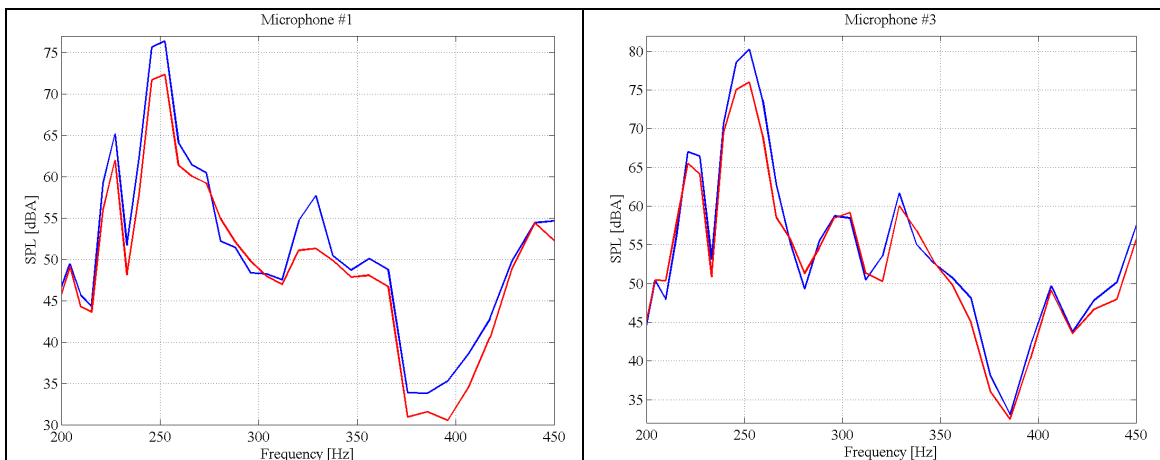


Figure 4-29: Primary field from specs: control off (blue), control on (red)

A second experiment has been performed by applying as disturbance field a random noise from 200 Hz to 600 Hz, whose spectrum is reported in Figure 4-30.

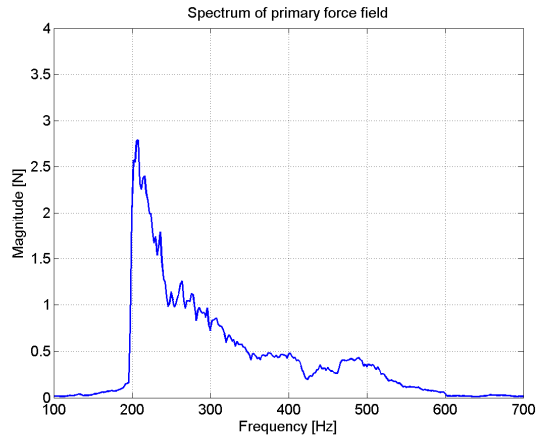


Figure 4-30: Random noise primary force field

The SPL measured in this case are reported in **Errore. L'origine riferimento non è stata trovata.**, with a 2 dBA reduction of the overall levels.

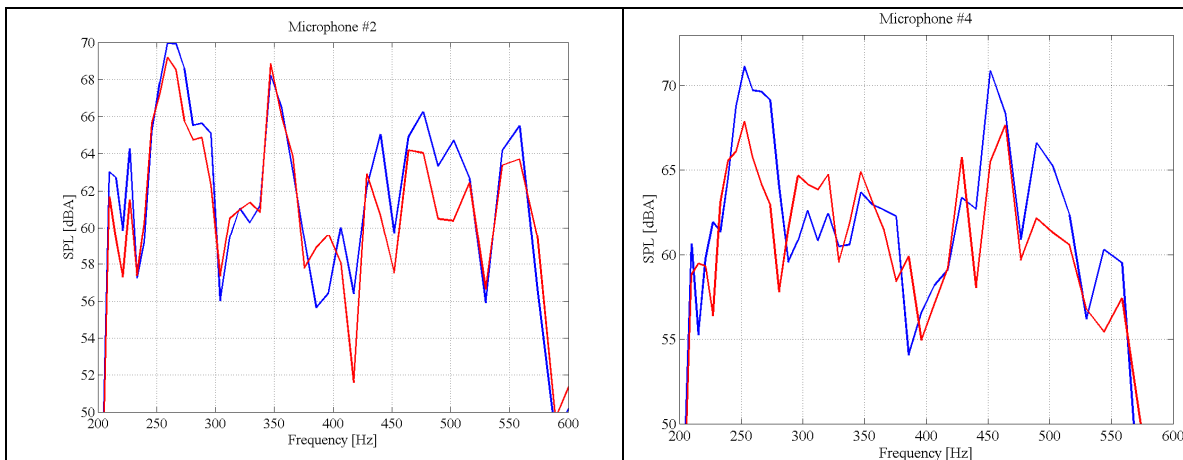


Figure 4-31: Random noise primary field: control off (blue), control on (red)

In the same case, the effect of the control algorithm in terms of vibration reduction has also been evaluated and the results are reported in **Errore. L'origine riferimento non è stata trovata.**, showing an average reduction of 9 dB with several peaks of 40 dB. In the same figure, the control current of one of the actuators is reported too, showing how the full range ([0,4] A) is exploited.

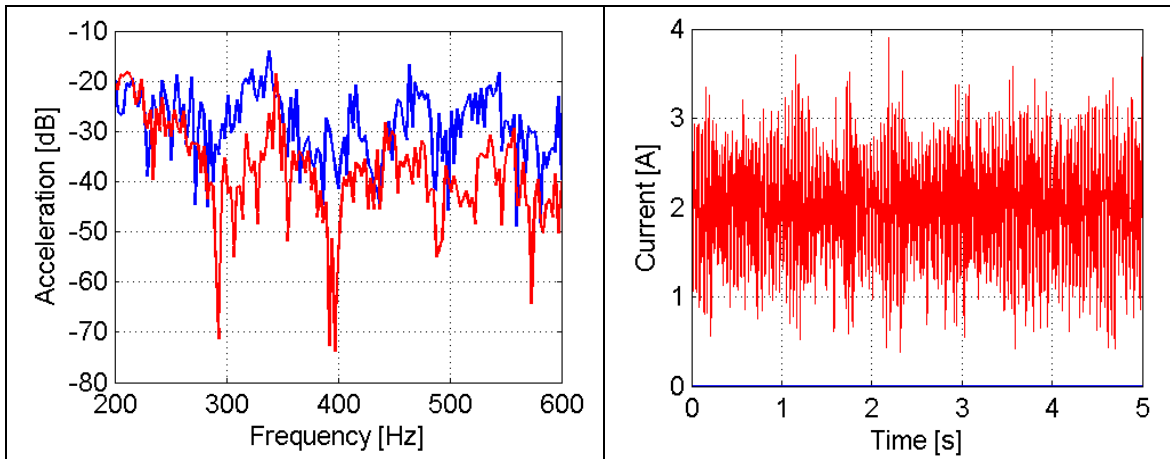


Figure 4-32: Vibration reduction with a random noise primary field: control off (blue), control on (red)

Finally, in order to test the capabilities of the control algorithm in counteracting the effects of the disturbance independently of the actuator location, an experiment has been carried out to simulate ideally placed actuators. In this asymptotic case, a 4.3 dBA reduction of the overall levels has been measured when a random noise disturbance has been applied directly in the control points. The spectra of the SPL measured by two performance microphones are reported in Figure 4-33.

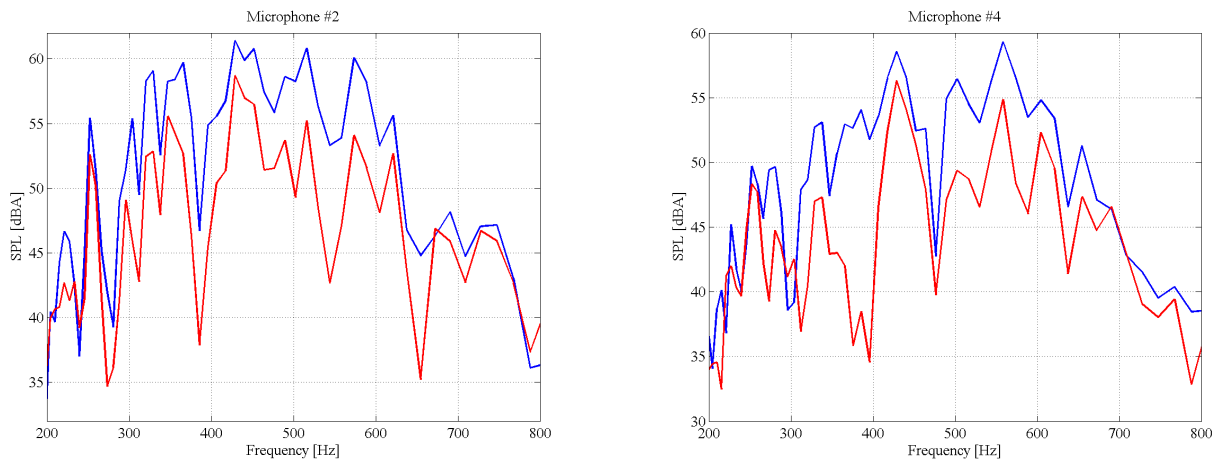


Figure 4-33: Random noise in a co-located configuration: control off (blue), control on (red)

5 CONCLUSIONS

This activities performed during the first year of the MESEMA Project aimed to the numerical and experimental characterization of the vibro-acoustic behavior of the selected test-article (a full scale turboprop fuselage section). The coupled structural-acoustic F.E. model has been described as far as the experimental modal analysis set-up and results. Furthermore the correlation between numerical and experimental modal parameters by the mean of a sensitivity analysis brought to an updated numerical model that now is able to well represent the real structural dynamic behavior of the test article. This model will now represent the reference for the next activities related to the simulations of the control system. Finally the vibro-acoustic experimental acquisition have been completed.

The main results achieved in Task 2.1 of the MESEMA project can be summarised in terms of

Innovative devices:

- Magnetostrictive Auxiliary Mass Damper with Bragg sensor
- Light Hybrid Amplifier
- as well as
- Innovative concepts
- Identification procedure for dynamic model of flexible structures
- Optimization procedure for actuator location
- Control algorithm for noise and vibration control

The experiments clearly showed that the proposed noise control system can actually reduce the overall levels of a broadband noise inside the cabin and also the vibration levels of the structural elements of the fuselage is significantly reduced on a wide range of frequencies.

The end-user Alenia considers the obtained results in terms of noise reduction inside the cabin worth of further investments with the aim of improving the performance for an actual exploitation of the system.

Of course, the performance of the system could be further improved, e.g.

- by increasing the number of actuators (only 21 control channels have been successfully used out of the 30 originally forecasted)
- by a new optimization of their location usefully exploiting the acquired measurements when the control is active
- by further optimizing their installation on the frames

APPENDIX A – ACTUATOR/SENSOR PLACEMENT

This appendix reports the activities carried out by Unina-DPA and LFME for selecting the optimal location of the actuator/sensor pairs with the use of Genetic Algorithms.

OPTIMAL POSITIONING APPROACH PROPOSED BY LFME

The optimization procedure makes use of the Frequency Response Functions (FRFs) between the sensors and the actuators, calculated by the Finite Element (FE) model of the ATR-42 fuselage developed by UniNa-DPA. Optimal positions for a candidate set of 400 points uniformly distributed over the whole structure have been derived for low and broadband excitation using 10, 20 and 30 sensor/actuator pairs respectively.

After the placement of the first actuator prototypes on the fuselage, some problems have arisen concerning the availability of some specific positions. Finally the new constraints for the actuator candidate position have been delivered by Unina-DPA. The not accessible positions, due to the presence of several subsidiary structural components are depicted in Fig. A 1.

The contribution at hand presents the results for the optimal position of the sensor/actuator pairs under the new constraints.



Fig. A 1: Photos of the mounting “constraints”

CALCULATION OF THE FRF’S BETWEEN THE CANDIDATE SENSORS AND ACTUATORS

The FRFs required for the calculation of the performance of the AVC system were calculated by the updated FE model developed by UniNa-DPA in NASTRAN. The direction of the actuator force has been assumed vertical to the surface, radial to the fuselage. 124 candidate positions were selected over the two middle bays. The distribution of the grid points selected is shown in Fig. A 4.

Apart from the FRFs between the candidate sensors and actuators, accelerations, generated by two primary excitations, in all sensors were also calculated. These patterns are shown in Fig. A 2 and Fig. A 3 being of broad-band and of low frequency components, respectively. The excitations were introduced as nodal forces at the locations where the wings are connected with the fuselage.

Furthermore, in order to investigate the noise produced inside the fuselage, acoustical FRF's between the actuators and 32 positions uniformly distributed inside the fuselage (Fig. A5) have been calculated.

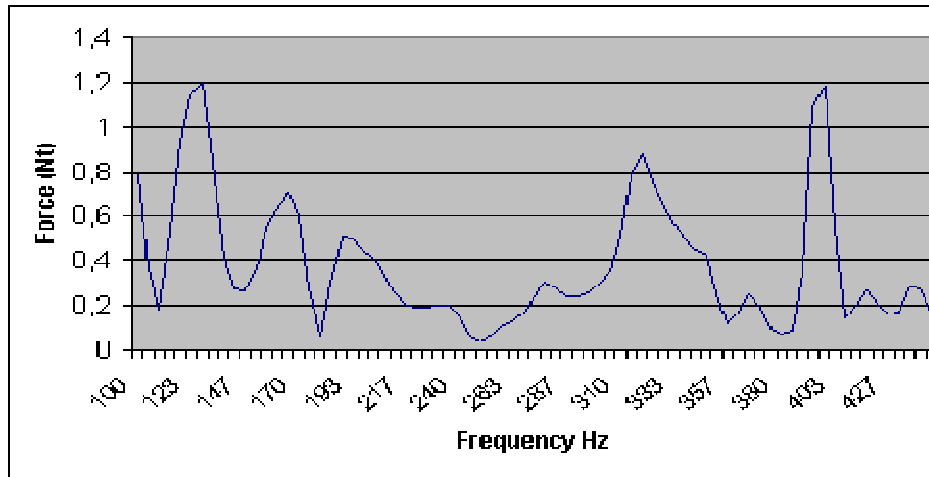


Fig. A 2: Broad band excitation.

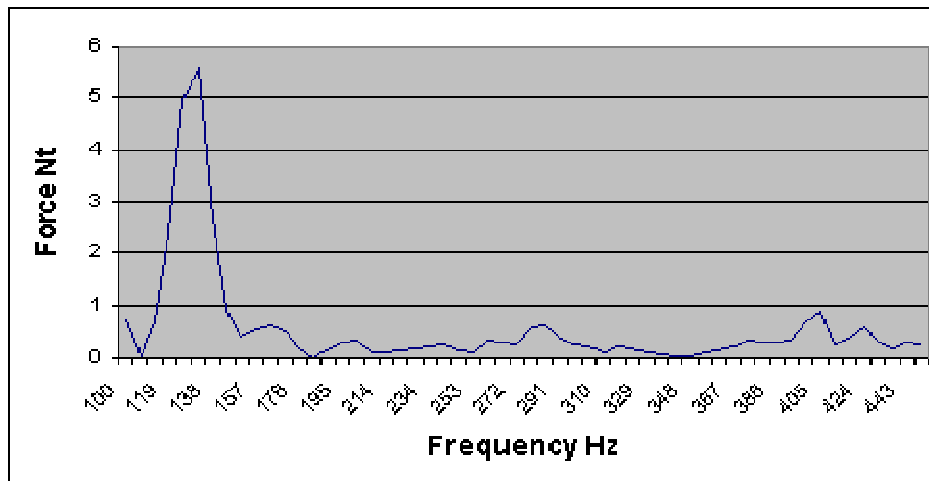


Fig. A 3: Low frequency excitation.

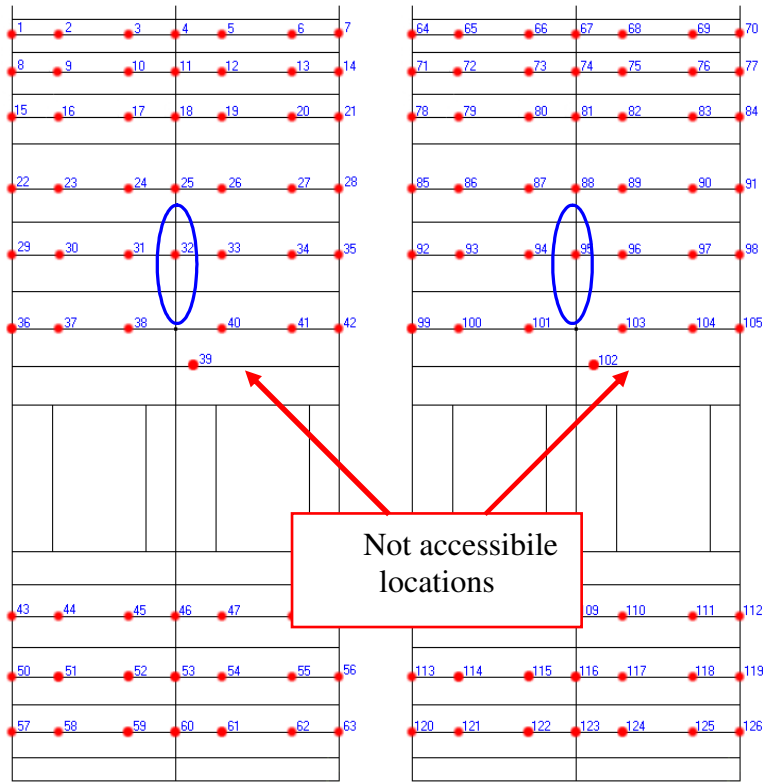


Fig. A 4: Left and right partial sections of the 2 middle bays.

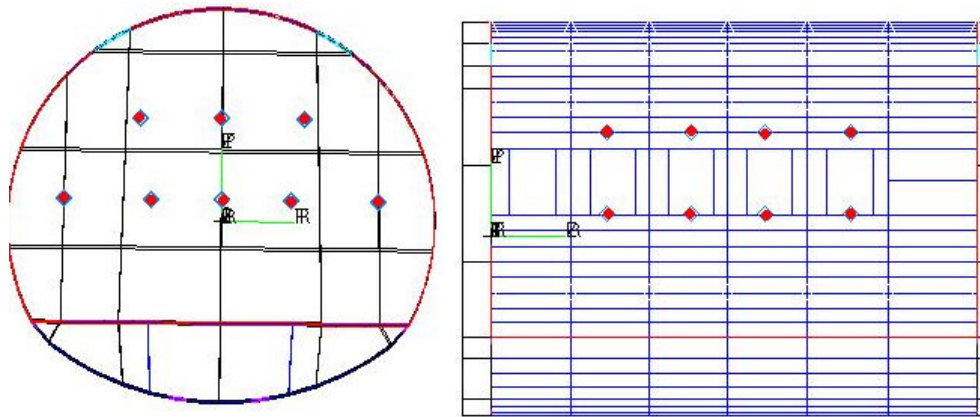


Fig. A 5: Microphone positions inside the fuselage.

DESCRIPTION OF THE DEVELOPED GA

The present optimization problem is a combinatorial one. The optimal combinations of M sensor/actuator locations out of the M_{max} available ones, have to be determined. During the Frequency Response Function (FRF) generation, the sensor/actuator locations were given a code number from 1 to M_{max} .

In the development of a GA for any optimization problem, the parameter space should be coded in such a way that a string (array consisting of integers) is formed. This string contains all the independent variables of the problem that has to be optimized. For the GA developed for the given problem, it was decided that the strings would consist of the number of pairs M . In this step, the constraint that a code number cannot appear more than once in the same string was imposed. In this way, it would be ensured that no more than one sensor/actuator pair could be positioned in the same location.

Following this coding, each string would correspond to only one Active Vibration Control System (AVCS) consisting of M sensor/actuator pairs.

Each of the strings comprising the GA population was created in as follows:

The sensor/actuator string was created using a Random Number Generator (RNG). M integers in the space $[1 \text{ Mmax}]$ were selected in random. Special care was given that an integer already selected could not be selected again during the creation of the same string (due to the constraint of the previous paragraph). Each of these random integers was placed in a string position, giving birth to a complete string.

This procedure was applied as many times as the number of strings consisting the population of the GA.

The fitness function

In order to define the optimal actuator forces the efficient Least Squares technique has been selected.

Assuming that the AVCS consists of K sensors and N actuators ($K > N$) the optimal forces F_{opt} to the N actuators of the AVCS, may be calculated by:

$$F_{opt} = -(H^H \cdot H)^{-1} \cdot H^H \cdot p \quad (\text{A.1})$$

where:

$H(i,j)$ is the matrix with the frequency response functions between the sensor i and the actuator j .

P is the acceleration vector at the K sensors.

$(\cdot)^H$ denotes the conjugate transpose.

In our problem at hand the AVCS comprises M sensor/actuator pairs out of M_{max} possible pair positions. From equation (1) the optimal forces to the $M-1$ actuators (the actuator of the last pair is neglected in order to be consistent with the assumption that sensors are more than the actuators) are calculated. Next the average acceleration reduction (S) of the AVCS is calculated by the formula:

$$S = \log_{10} \frac{\left[\sum_{i=1}^{M_{max}} (p_0(i))^2 \right]}{\left[\sum_{i=1}^{M_{max}} (r(i))^2 \right]} \quad (\text{A.2})$$

where :

$p_0(i)$ is the acceleration at the sensor of the i^{th} sensor/actuator pair produced by the primary excitation.

$r(i)$ is the residual acceleration at the sensor of the i^{th} sensor/actuator pair after the application of the F_{opt} at the actuators.

The average acceleration reduction S of the equation (2) is used as the fitness function in the proposed Genetic Algorithm.

GA SIMULATIONS AND RESULTS

Several runs of the developed GA were performed for different AVC system configurations as in sections IV and V in the first contribution of 2.1.2. More specifically, the GA was applied for configurations of 10, 20 and 30 pairs of sensors/actuators. Simulations have been carried out for both the low frequency primary excitation and the broadband (high frequency) primary excitation. The optimal pair placement in the case where the low frequency or broadband primary excitation is used is named “placement 1” and “placement 2” respectively.

In Fig. A 8 ,A11,A14,A17,A20 and A23 the average SPL of the 32 microphones is presented. As a consequence of the acceleration reduction the sound pressure is also reduced especially in low frequencies.

In Fig. A6 the convergence of the GA algorithm for the “placement 1” case, using 10 pairs is presented. A significant increment can be noticed after the first 50 generations. The maximum forces used by each actuator for the case of “placement 1” using 10 pairs are presented in Fig. A7. The maximum force needed is about 5 Nt. The In Fig. 8 the results for 10 pairs and low frequency excitation are presented. Using placement1 a significant reduction of the SPL is noticed in the range between 100 and 230 Hz. At 100 Hz a reduction up to 20 dB has been achieved. Nevertheless above 230 Hz the results don't show any significant improvement. Similar results have been achieved using placement2”.

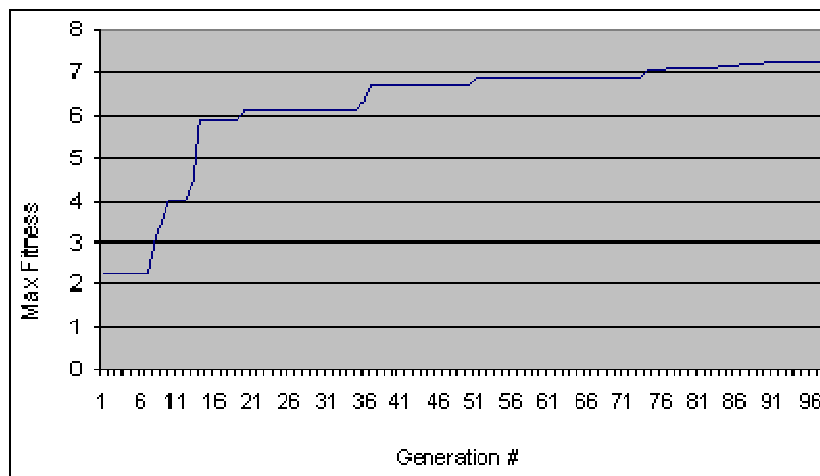


Fig. A 6: Maximum Fitness for 10 pairs using the low frequency primary excitation.

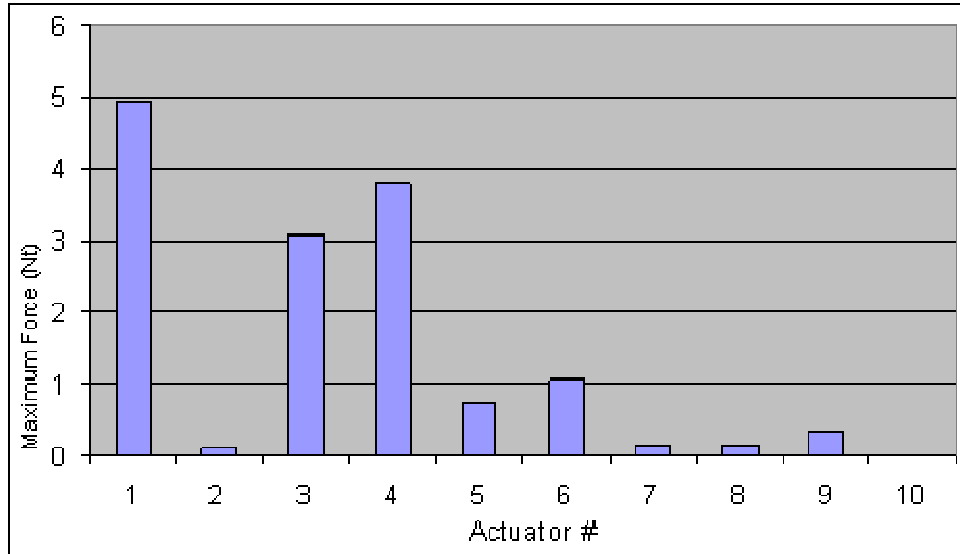


Fig. A 7: Magnitude of the maximum forces for 10 pairs , using the low frequency primary excitation.

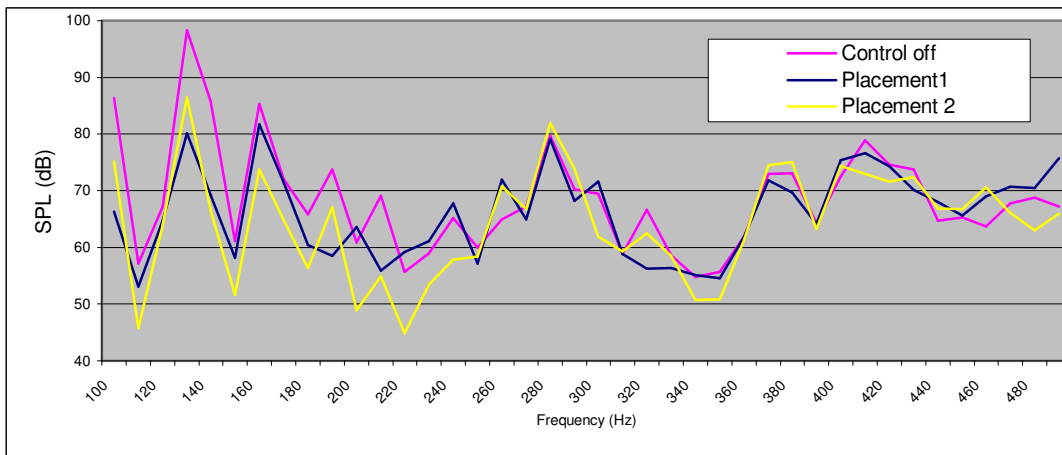


Fig. A 8: Average SPL in all microphones (32) with and without control for 10 pairs, using the low frequency excitation.

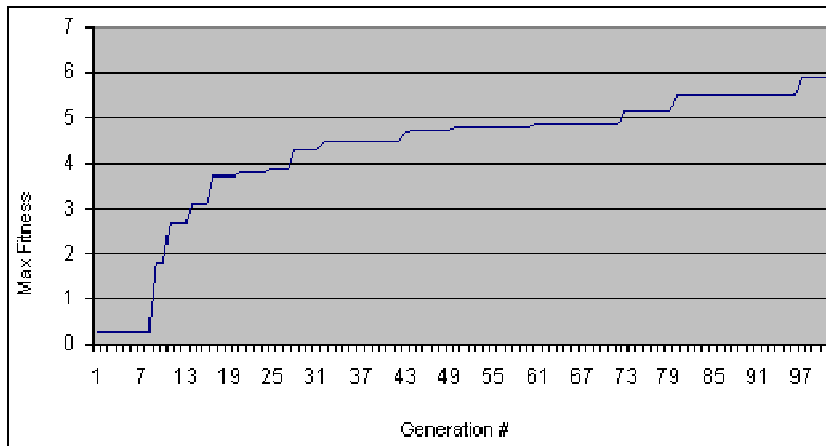


Fig. A 9: Maximum Fitness for 20 pairs using the low frequency primary excitation.

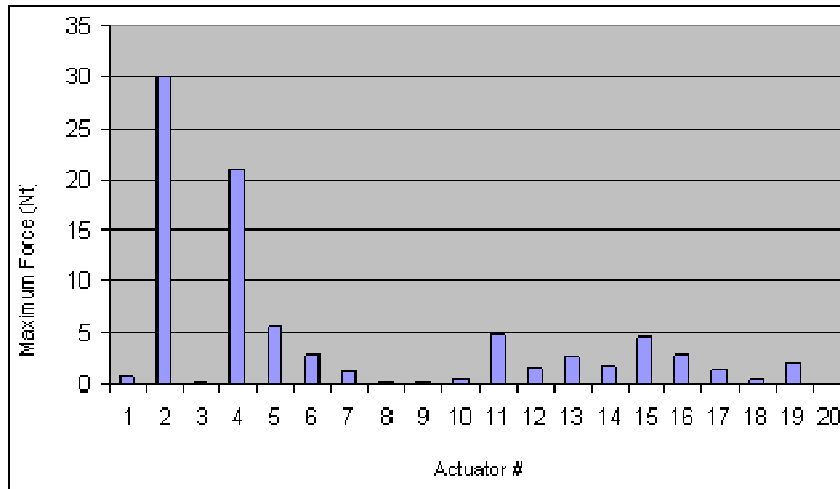


Fig. A 10: Magnitude of the maximum forces for 20 pairs, using the low frequency primary excitation.

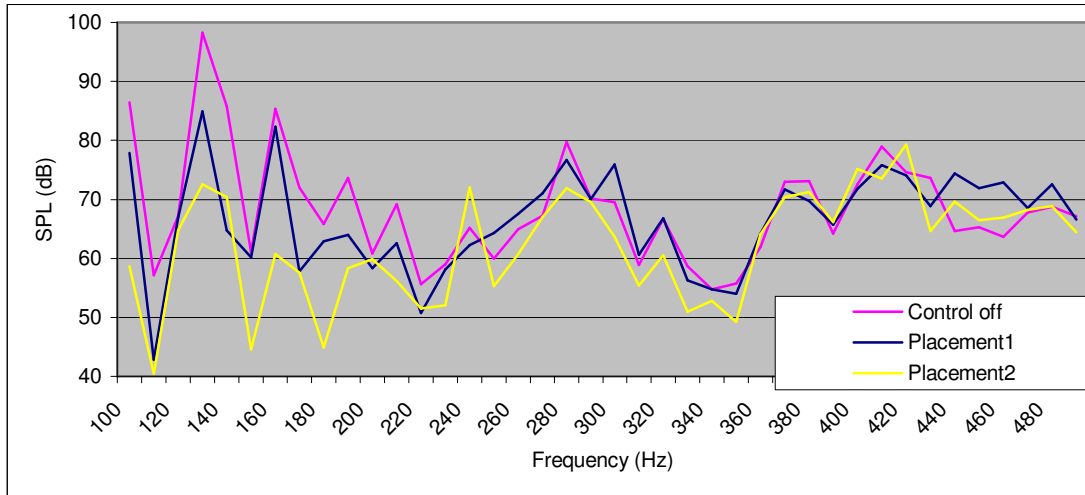


Fig. A 11: Average SPL in all microphones (32) with and without control for 20 pairs, using the low frequency excitation.

The convergence of the GA algorithm for the “placement 1” case, using 20 pairs is presented in Fig. A9. The maximum forces used by each actuator for that case are presented in Fig. A10. The maximum forces are of the same order of magnitude as in the 10 pairs, except two actuators that are activated with 20 and 30 Nt respectively. The noise reduction results are presented in Fig. A11. Using placement1 and comparing the results with the previous case (10 pairs) no significant changes have been noticed. On the contrary using “placement2” a significant improvement of the SPL reduction is noticed in the range between 100 and 240 Hz. More specific at 100 Hz a reduction near to 30 dB has been achieved. Nevertheless above 230 Hz the results don’t show any significant improvement.

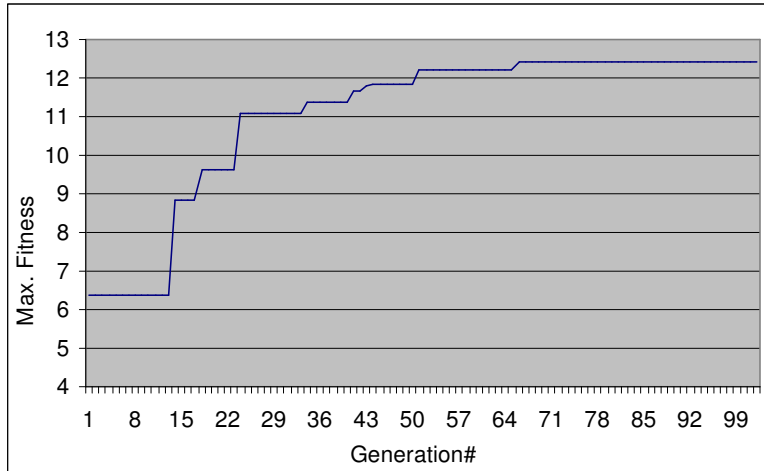


Fig. A 12: Maximum Fitness for 30 pairs using the low frequency primary excitation.

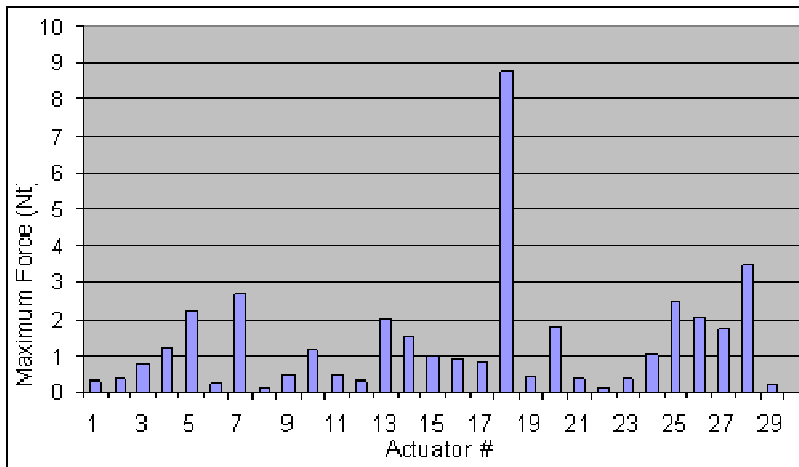


Fig. A 13: Magnitude of the maximum forces for 30 pairs , using the low frequency primary excitation.

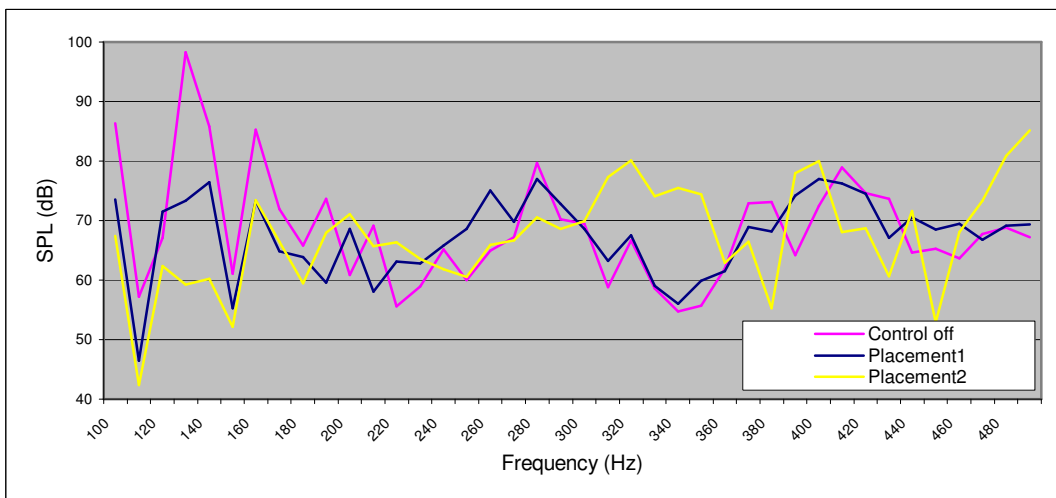


Fig. A 14: Average SPL in all microphones (32) with and without control for 30 pairs, using the low frequency excitation.

The convergence of the GA algorithm for the “placement 1” case, using 30 pairs is presented in Fig. A12. After the 70th generation the fitness has been reached an optimum value with no further increment. The maximum forces used by each actuator for that case are presented in Fig. A13. The values are in the range between 0 and 3,5 N except one actuator that activates using a maximum force of about 8,5 N. In Fig. A14 the noise reduction results are presented. Using placement1 the improvement is significant at low frequencies in the range between 100 and 210 Hz. Beyond 220 Hz no significant changes have been noticed. Using “placement2” a significant improvement of the SPL reduction is noticed in the range between 130 and 220 Hz. More specific at 140 Hz a reduction up to 35 dB has been achieved. Nevertheless above 200 Hz the results don’t show any significant improvement. On the contrary in the range between 300 and 360 Hz the SPL has been increased.

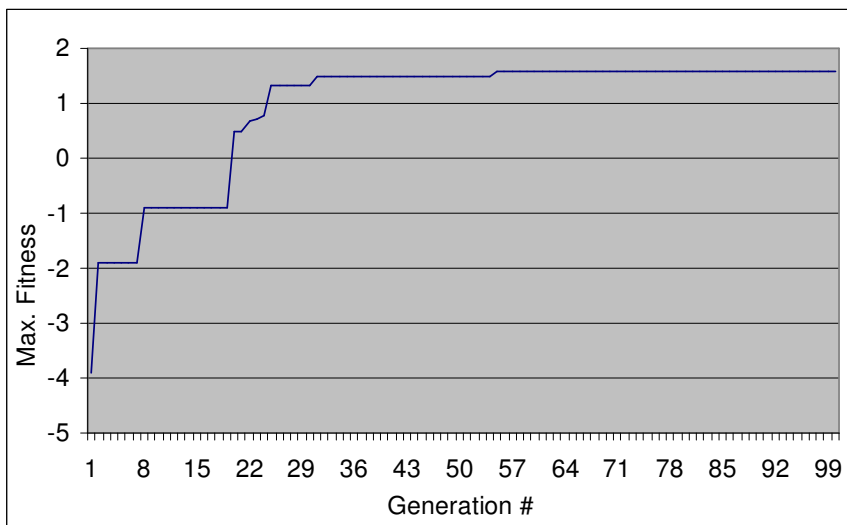


Fig. A 15Maximum Fitness for 10 pairs using the broadband primary excitation.

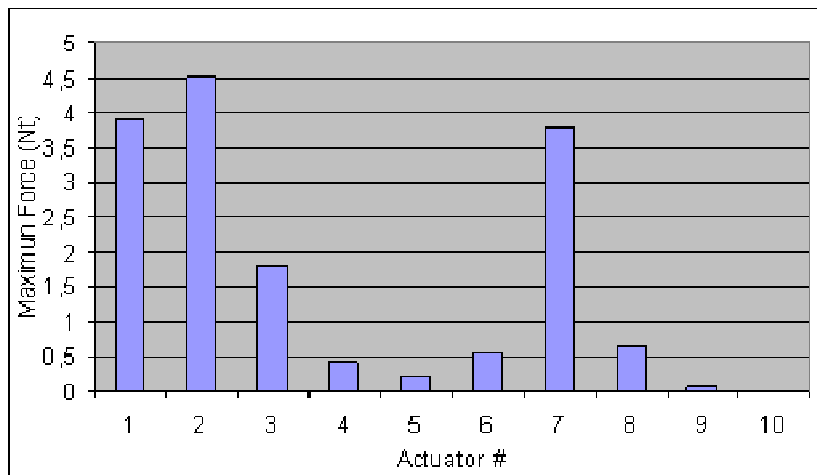


Fig. A 16: Magnitude of the maximum forces for 10 pairs, using the broadband primary excitation.

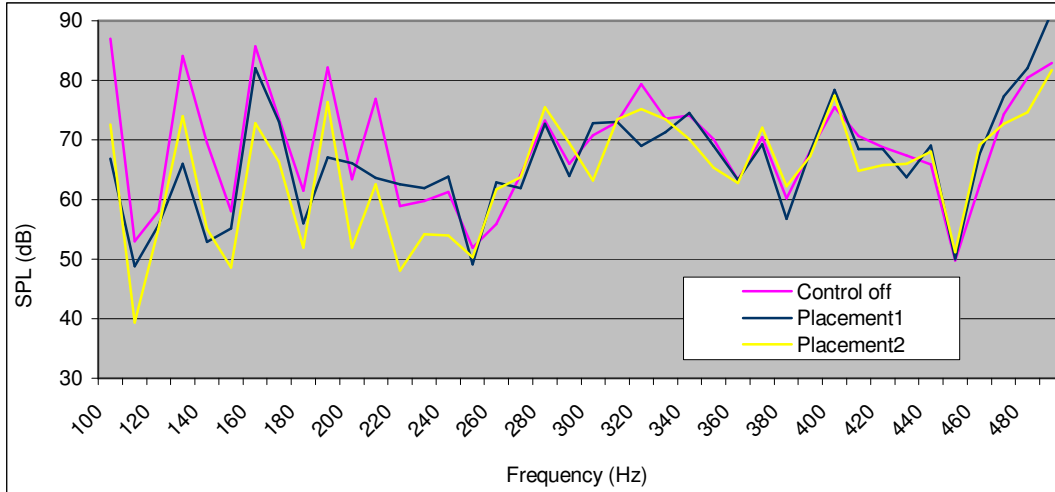


Fig. A 17: Average SPL in all microphones (32) with and without control for 10 pairs, using the broadband frequency excitation.

The convergence of the GA algorithm for the “placement 2” case, using 10 pairs and broadband frequency excitation is presented in Fig. A15. After the 30th generation no significant improvement can be noticed. Regarding the maximum force needed it has been found about 4,5 N (Fig. A16). In figure 17 the noise reduction results are presented. Using “placement2” a significant reduction of the SPL is noticed in the range between 100 and 260 Hz. More specific 110 Hz a reduction up to 15 dB has been achieved. Above 260 Hz the results don’t show any significant improvement. A little worst results have been achieved using “placement1”.

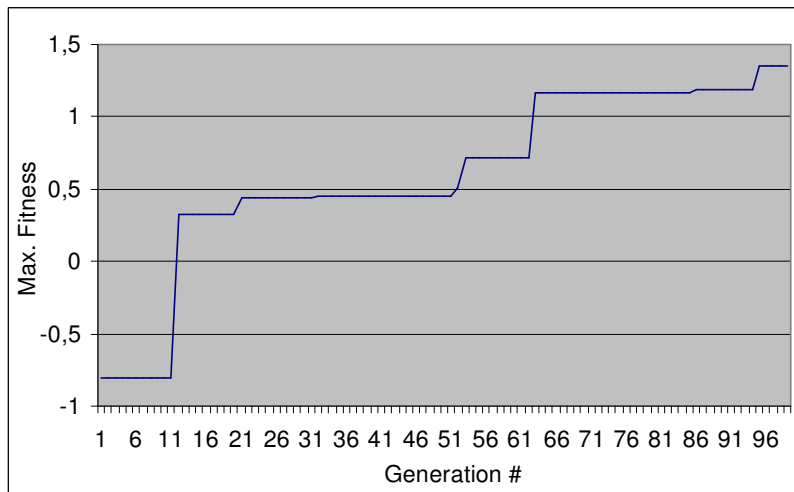


Fig. A 18: Maximum Fitness for 20 pairs using the broadband primary excitation.

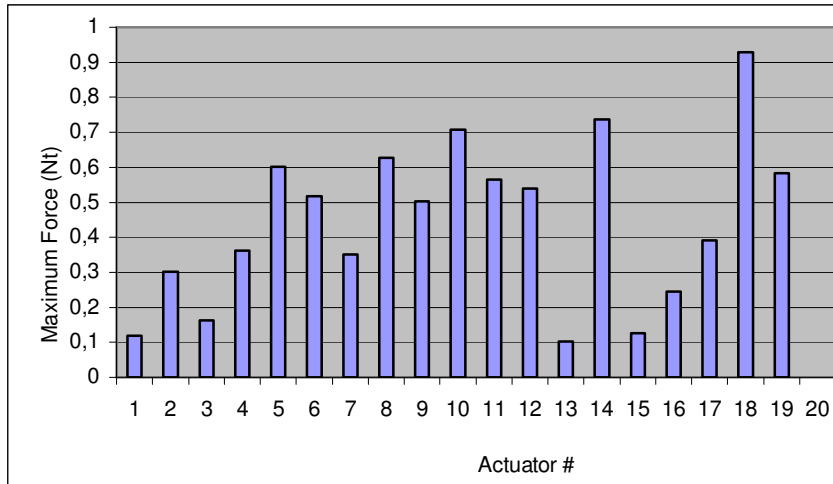


Fig. A 19: Magnitude of the maximum forces for 20 pairs , using the broadband primary excitation.

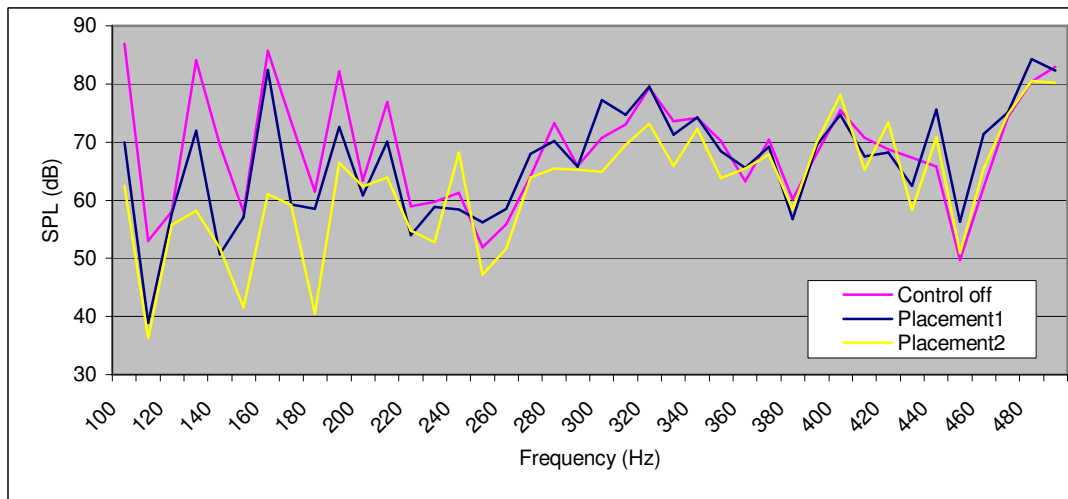


Fig. A 20: Average SPL in all microphones (32) with and without control for 20 pairs, using the broadband frequency excitation.

In the case of 20 pairs and broadband frequency excitation, the convergence of the GA algorithm for the “placement 2” case is presented in Fig. A18. Regarding the maximum force needed it has been found about 0,9 Nt (Fig. A19). In Fig. A20 the noise reduction results are presented. Using “placement2” the improvement is significant at low frequencies in the range between 100 and 240 Hz. At 100 and 130 Hz the improvement is up to 25 dB. Beyond 240 Hz no significant changes have been noticed. Using “placement1” an improvement of the SPL reduction is noticed in the range between 130 and 250 Hz. Nevertheless above 250 Hz the results don’t show any significant improvement.

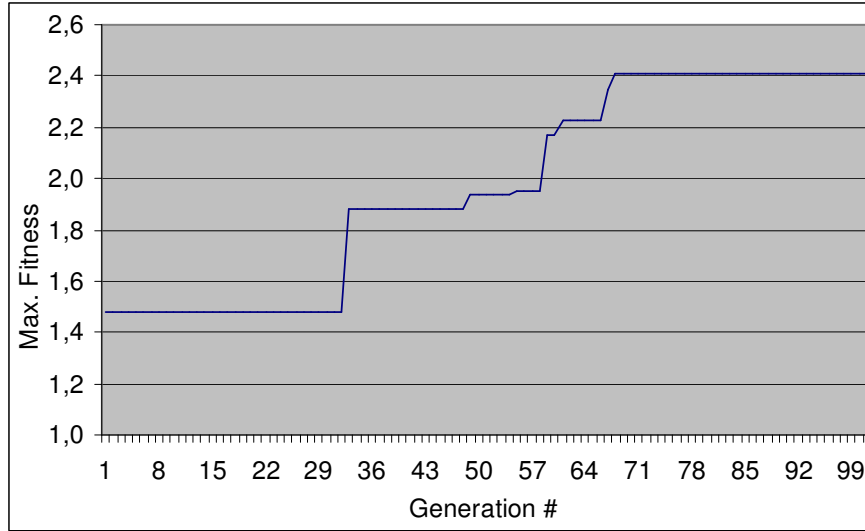


Fig. A 21Maximum Fitness for 30 pairs using the broadband primary excitation.

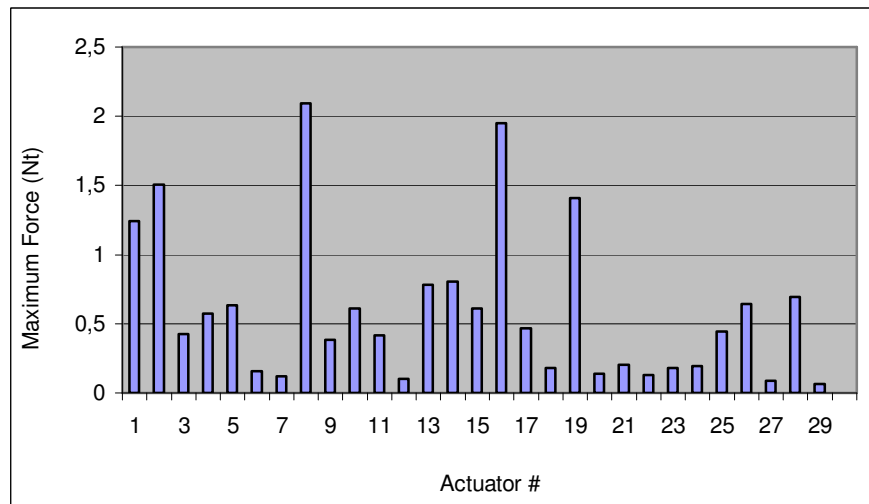


Fig. A 22Magnitude of the maximum forces for 30 pairs , using the broadband primary excitation.

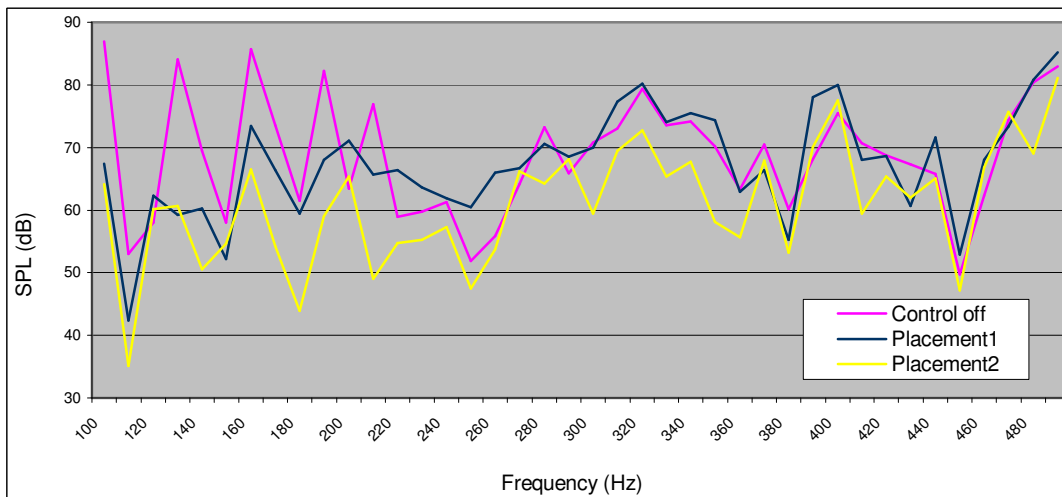


Fig. A 23 Average SPL in all microphones (32) with and without control for 30 pairs, using the broadband frequency excitation.

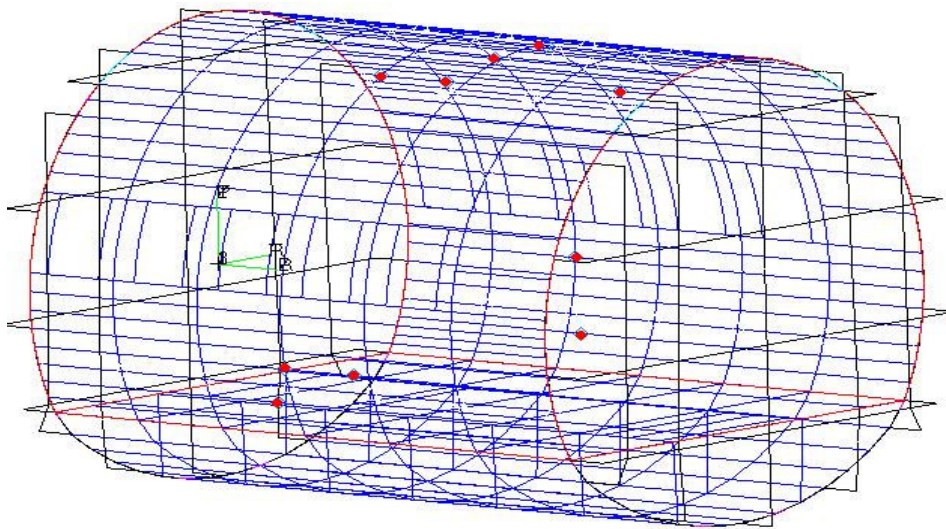
	Low Frequency Excitation			Broadband Excitation		
	10 pairs	20 pairs	30 pairs	10 pairs	20 pairs	30 pairs
400	10,4	13	10	5,5	7,7	8,6
126	2,2	1,8	1	4,1	6,1	7,6

Table A 1" Comparison Table between 400 and 126 candidate points.

Finally in Fig. A21, A22 and A23 the results for 30 pairs and broadband frequency excitation are presented. The convergence of the GA algorithm is presented in Fig. A21. After the 70th generation no significant improvement can be noticed. Regarding the maximum force needed it has been found about 2 N (Fig. 22). In Fig. A23 the noise reduction results are presented. Using placement2 the improvement is significant at low frequencies in the range between 100 and 390 Hz. Using "placement1" the range of significant SPL reduction is limited between 100 and 210 Hz. In addition, in the range between 230 and 280 Hz the SPL has been increased.

Table 1 compares the average SPL reduction in the frequency range of interest (100-500Hz) between the two candidate sets: the candidate set of the present contribution (126 points) and the candidate set of the previous contribution (using 400 points uniformly distributed over the whole structure). A significant difference can be noticed in the low frequency excitation (up to 11 dB in the case of 20 pairs). On the contrary in the case of the broadband excitation the difference is limited. Nevertheless in all cases the new constraints in the placement of the pairs (126 pairs) gives worst results as expected.

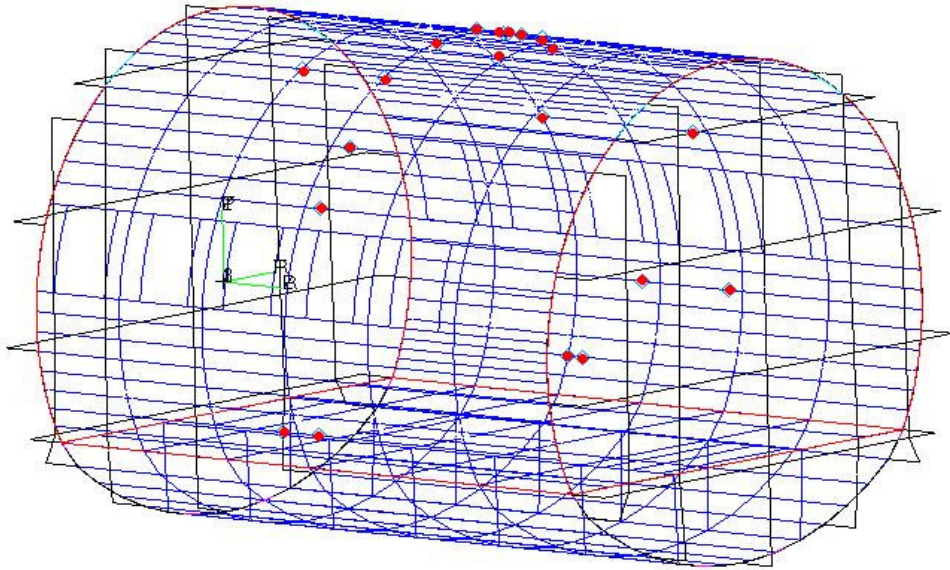
In the next figures the optimal sensor/actuator places are presented. Figs. A24, A25 and A26 depict the "placement 1" positions where the low frequency excitation is supposed. In Figs. A27, A28 and A29 the corresponding "placement 2" positions are depicted for 10, 20 and 30 pairs respectively. A concentration of the actuators in the central frame where the primary excitation is applied was noticed in all cases.



Nodes:

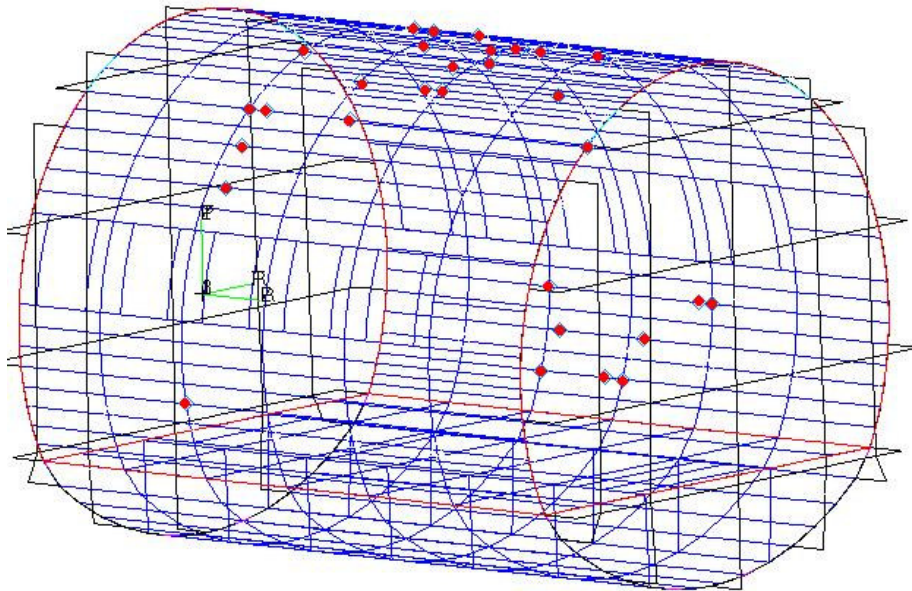
4	187	34	58	22	51	47	45	19	28
78	9	45	0	61	89	77	7	84	63

Fig. A 24: Results with low frequency excitation, using 10 pairs.



										Nodes :
47	52	190		18	19	66	19	15	226	
77	2	2	580	563	392	21	84	37	1	
47	46	184	173	64	90	27	33	52	444	
8	44	32	72	5	79	24	39	8	0	

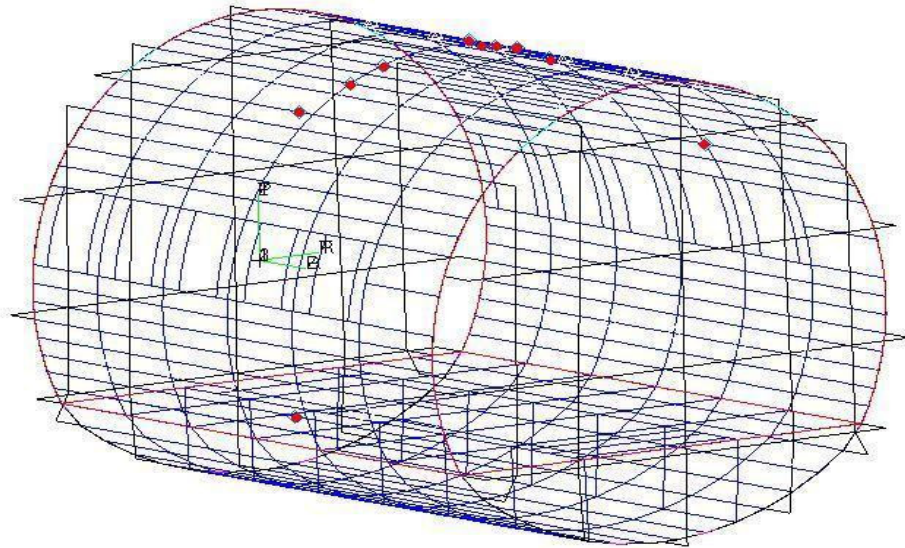
Fig. A 25: Results with low frequency excitation, using 20 pairs.



Nodes:

868	198	854	202	127		560		754	470
4	09	9	04	0	718	1	573	9	0
	193	449	518	148	162	724	906	476	
457	92	8	9	50	35	0	3	0	478
444	741	699	840	329	907	333		273	808
0	6	7	5	1	9	5	580	1	3

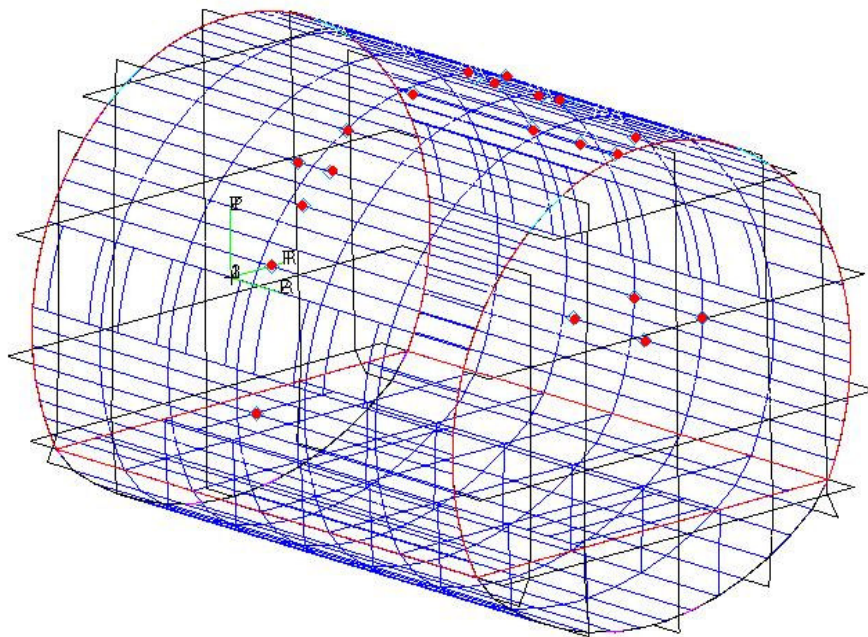
Fig. A 26: Results with low frequency excitation, using 30 pairs.



Nodes:

				125	185		716		189
522	580	435	645	7	63	478	4	718	5

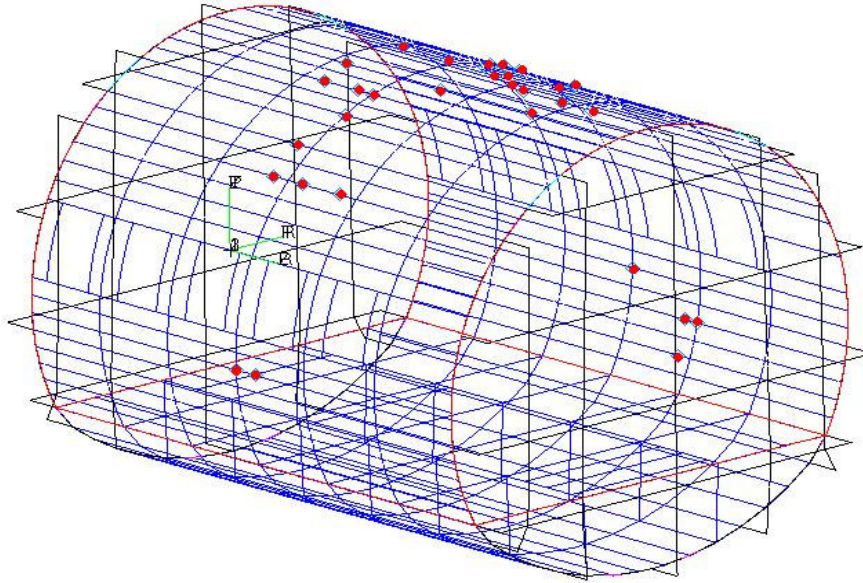
Fig. A 27: Results with broad band frequency excitation, using 10 pairs.



Nodes:

18	15	75	17	17	27	66	46	47	19
50	37	49	389	752	04	21	38	00	809
27	69	19	19	18	17	44	47	12	80
24	97	461	973	563	604	98	8	57	83

Fig. A 28: Results with broad band frequency excitation, using 20 pairs.



Nodes:									
19	52	19	27	20	75	64	58	86	42
142	2	35	24	204	52	5	0	20	90
15	19	81	81	22	47	46	12	43	18
33	461	17	11	61	8	38	57	5	184

17752 7931 19809 4516 2863 2660 4556 1537 1850 18432

Fig. A 29: Results with broad band frequency excitation, using 20 pairs.

In conclusion, in a previous contribution, the results of the algorithm using a large enough “candidate set” that covers the whole structure above the floor level have been presented. After the placement of the first actuator prototypes on the fuselage, some problems have arisen concerning the availability of some specific positions and a new candidate set that excluded several points of the structure has been used. In this contribution the problem of the optimal placement of the sensor/actuator pairs of an active vibration control system has been investigated using the updated candidate set with new constraints.

The selection of the optimal places has been based on a Genetic Algorithm approach. The algorithm selects the optimal places among the candidate set. The optimal actuator forces for a specific combination have been calculated using the least square technique. The fitness function was related with the average acceleration reduction in all candidate points (124). Two types of excitation were supposed: a low frequency and a broadband. The excitation force was assumed nodal and was applied in the area where the wings are attached. The GA was applied for configurations of 10, 20 and 30 pairs of sensors/actuators. The simulation results were very encouraging and have shown a high reduction in the SPL level especially at low frequencies. Nevertheless in all cases the new

constraints in the placement of the pairs (126 pairs) give worst results comparing with the previous investigation with a larger candidate set (400 pairs) as expected.

OPTIMAL POSITIONING APPROACH PROPOSED BY UNINA-DPA

In order to select among the many possible set of control actuators configurations an optimisation activity was required. The used optimisation method is based on “genetic” algorithms: it is well known that they represent a quite fast, not deterministic approach for selection among many possible solutions of a problem whose effectiveness can be measured by a “score”. Genetic algorithms are quite effective if compared to other deterministic approaches since they permit to investigate solutions depending by discrete variables often avoiding to converge in local minima or maxima of the score value. The first characteristic is particularly interesting for this work since 126 actuators potential locations were selected on frames or stiffeners of the two middle bays of the mock-up (figure A30); as a consequence their positions are not represented by continue variable. The authors developed the genetic algorithm code in MATLAB environment: it included a first data input where the numerical responses data base were loaded. The number of possible actuators location defines the “genetic code” that is therefore represented by the integer numbers range between 1 and 126; each actuator represent a gene and each chromosome is a combination of a fixed number of genes. The number of genes constituting a chromosome represents the number of control actuators we want to employ in our system. When the code starts it creates a population of a certain number of chromosome where genes are randomly combined, or in other words, it defines a certain number of possible control actuator locations combination; for each combination (or chromosome) it evaluates the “score”.

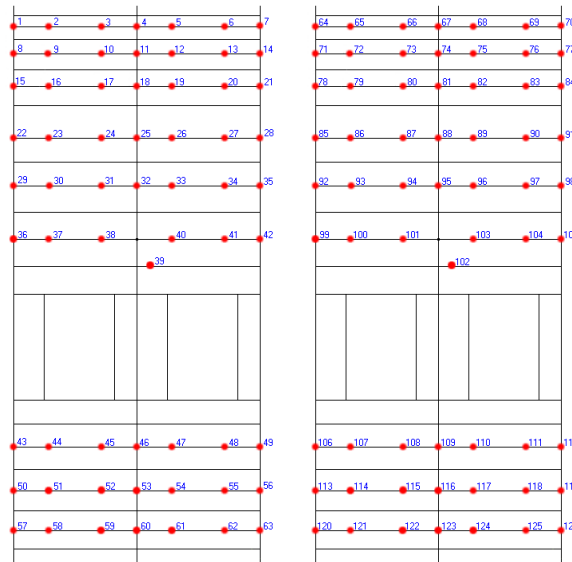


Fig. A 30: The potential control actuator locations (two middle bays – left and right side)

The score chosen for the scopes of this work has been defined as:

$$Score = \frac{1}{|\{p\}^T \{p\}|}$$

where $\{p\}$ represents the vector of the controlled interior noise field in the selected control points. The vector $\{p\}$ is obtained as combination of noise disturb field (primary field) and noise field produced by the control actuators:

$$\{p\} = \{p_p\} + [P]\{F_c\}$$

where $[P]$ is the pressure transfer function matrix obtained as mentioned in the previous chapter and $\{F_c\}$ are the optimal control forces evaluated using the pseudo-inverse approach for the selected chromosome. The values of control forces vector $\{F_c\}$ are obtained by employing the equation reported in the previous paragraph; within that formulation the matrix \underline{R} will be represented by the acceleration or noise Frequency Response Function evaluated in the selected structural or acoustic nodes respectively if an ASAC or ANC approach has been selected. As mentioned above the performance indicator employed as the genetic algorithms score maintains the same formulation whatever control approach has been chosen, since the final goal remains the reduction of interior noise. Following are presented the results obtained by considering as primary disturb the two reference force spectra presented in the MESEMA Deliverable2.1-1. For each disturb field 30 and 50 control actuators configurations have been investigated to be selected among the 126 locations considered within the two middle bays of the mock-up. The ASAC approach has been employed and a final comparison between the best obtainable results employing ASAC and ANC approach has been carried on. Figure A31 presents the selected location for the acoustic sensors where the score was evaluated and the acceleration sensors employed for the ASAC approach. Following the main results related to the 30 control actuators configuration are reported since no main advantages in terms of interior noise reduction have been found employing 50 actuators.

It is possible to notice the good predicted performances in terms of noise reduction related to the final control actuator configuration selected by the optimisation algorithm up to 400Hz.

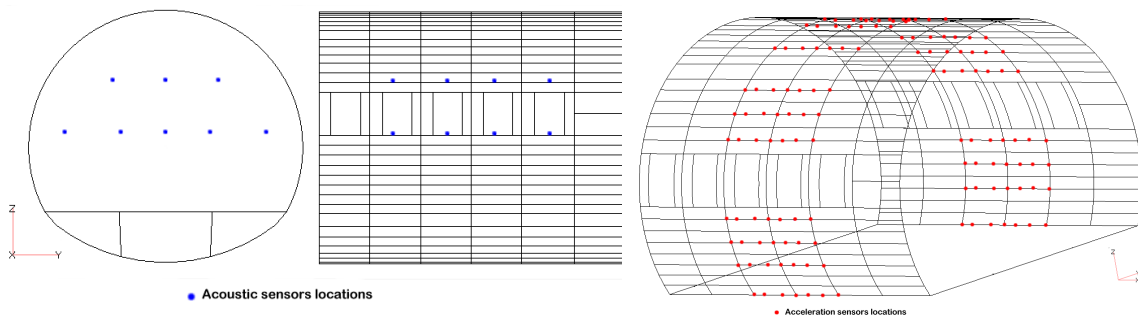


Fig. A 31:Acoustic and acceleration sensors locations

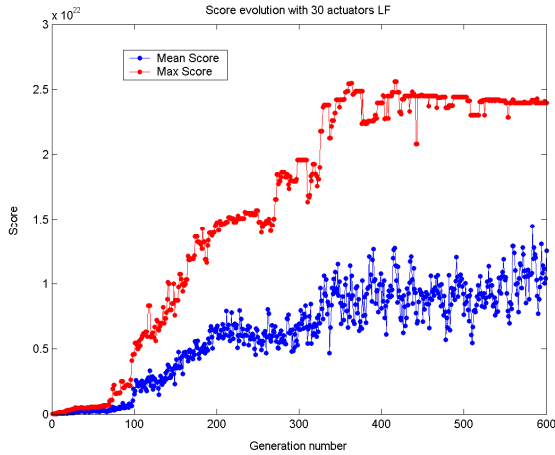


Fig. A 32: “Score” for ASAC approach – low frequency disturb force field

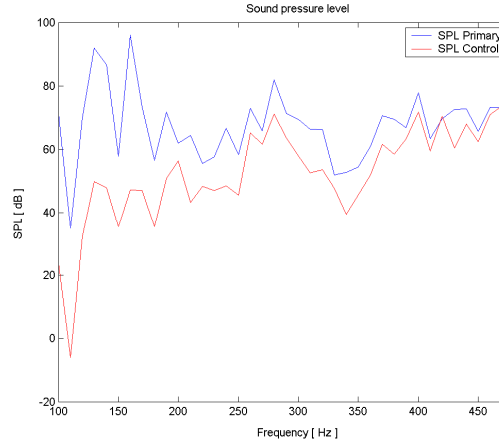


Fig. A 33 Mean interior noise reduction for the optimal actuators configuration – l. f. disturb force field

A very important parameter representing one of the main targets that the authors had to meet was the maximum control force value required from the actuators: this parameter represent in fact a key point of the design of the actuators that will be developed within the MESEMA consortium. Next figure present these values for each one of the 30 control actuators placed in their optimal locations. Part of the analysis results was obviously the optimal actuators placement configuration and their distribution among stiffeners and frames of the fuselage mock-up. Finally, in order to get a picture of the noise and vibratory controlled field a F.E. frequency response has been carried on for the full model including disturb field and control forces.

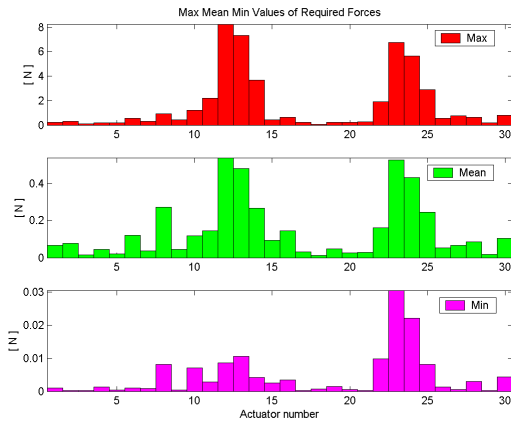


Fig. A 34: Required control force values for the control actuators in their optimal configuration

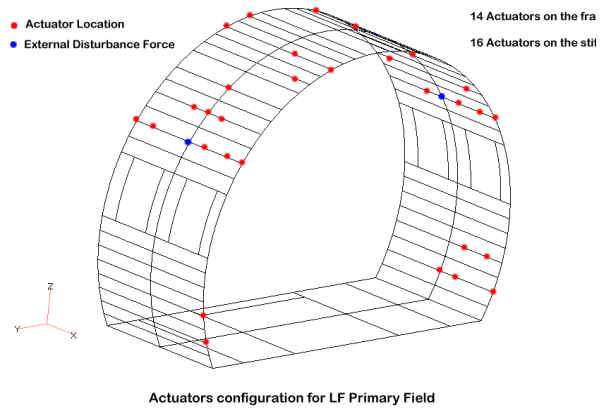


Fig. A 35: Optimal actuators placement configuration – low frequency disturb force field

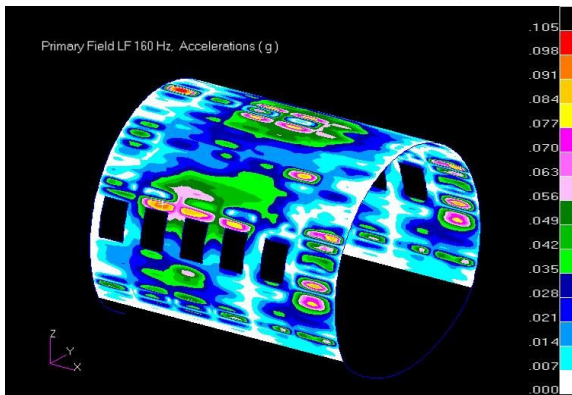
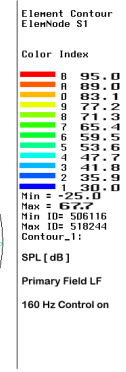
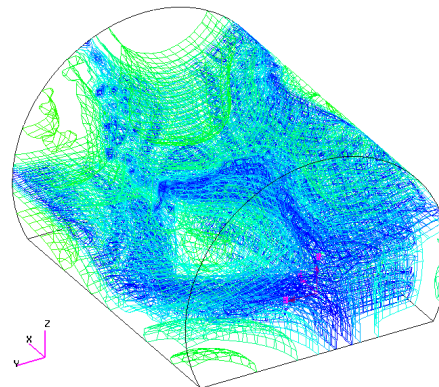
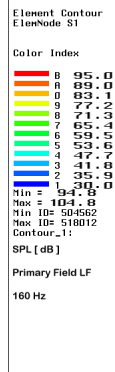
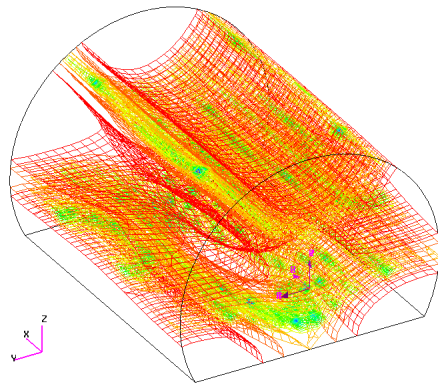


Fig. A 36: Uncontrolled noise and acceleration field at 160Hz – low frequency disturb

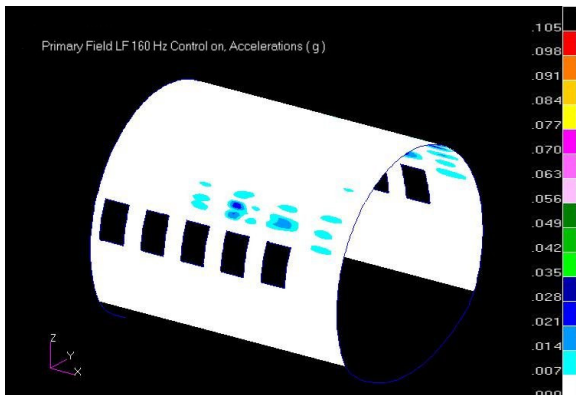


Fig. A 37: Controlled noise and acceleration field at 160Hz – low frequency disturb

In figures A35 and A36 the results are presented at the frequency of 160Hz where maximum performances were achieved. It is possible to notice how the noise reduction obtained is globally distributed at low frequency within the all interior volume and corresponds to a reduced vibratory field at the same frequency, as expected within the ASAC control approach. Among the main obtained results it is interesting to present those obtained simulating an ANC control approach. By considering again 30 control actuators the following figure presents the mean noise reduction related to the “low frequency” disturb field. Better performances at high frequency (above 400Hz) can be noticed if compared to those previously presented for the ASAC approach. Those performances anyway take in account only the selected noise control points where the score is evaluated. Coming to the global picture of the noise field it easy to recognise that, a part from the points mentioned above, the acoustic pattern with control on is not reduced at all but there is only a redistribution of acoustic energy inside the air volume.

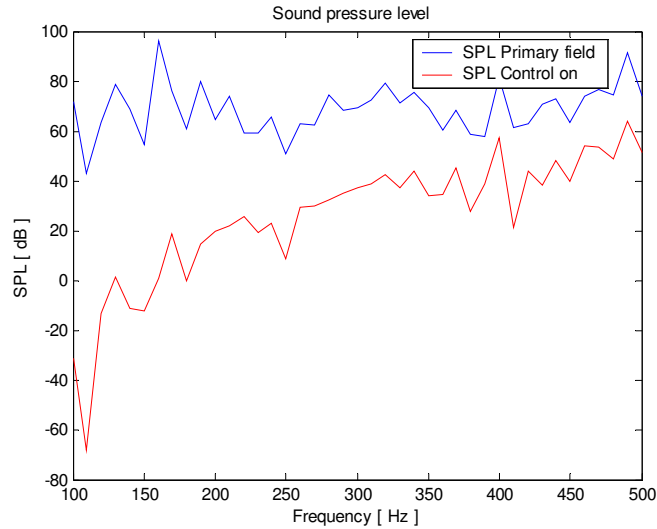


Fig. A 38: Mean interior noise reduction for the optimal actuators configuration - ANC approach – l. f. disturb force field

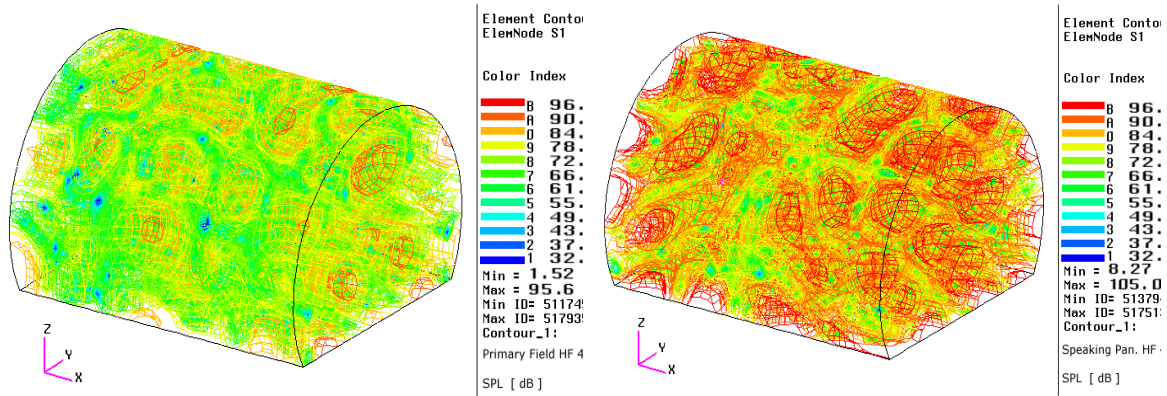


Fig. A 39: Uncontrolled noise field at 400Hz – ASAC approach – low frequency disturb

Fig. A 40: Controlled noise field at 400Hz – ASAC approach - low frequency disturb

Summary of results

Results of the simulation activity permitted to fix the number of required actuators (30 instead of the original number of 50) in order to achieve the best theoretical performances reducing the overall system weight. Furthermore the optimal placement configurations were investigated associated to the control force values; it was demonstrated that reducing the number of actuators did not affect negatively their required performances that remained almost unmodified. Finally comparison between ASAC and ANC approach permitted to demonstrate that they both present the same limits in terms of maximum control frequency; ANC promised good control performances at higher frequencies, but only in the chosen control location, without ensuring an overall noise reduction. Many of these results were expected, since they are strictly related to the patterns of noise and vibration fields within cylindrical structural as far as to their characteristics wavelength, but the presented study permitted to quantify the control parameters based on the availability of a reliable numerical model. Further studies will be carried on in order to keep in account the influence of the actuators own

dynamics on the overall structure as far as to investigate the advantages of installing control actuators in more than two bays, treating as a consequence a wider part of the structure.

CONCLUSIONS

The resulting final configuration presented in Fig. 2 consisted of a trade off among the following considerations:

- 1) Optimal control configurations obtained for low-frequency excitation has been considered for the positioning of the actuators couples on the frames structural element;
- 2) Optimal control configuration obtained by UNI-Na DPA for high-frequency excitation has been considered for the positioning of the actuators on stiffeners;
- 3) A further optimisation/arrangement of few actuators locations has been necessary for keeping into account “operative limitations” that resulted from the mounting process (available space for mounting reduced locally by the presence of rivets or non-structural components that were not modeled in the Finite Element Model).

APPENDIX B – NOISE CONTROL ALGORITHM

This appendix reports the activities carried out by DII-SUN and LFME for selecting the most appropriate control algorithm for noise reduction.

APPENDIX B - NOISE CONTROL ALGORITHM BASED ON AN EXPERT SYSTEM PROPOSED BY LFME

The contribution of the Laboratory of Fluid Mechanics & Energy (LFME) of the University of Patras (UNPA) to subtask 2.1.3 comprised in the development of a new active noise controller design. As presented at the 30 month meeting in Sorrento the controller concept is based on the GASS project (In the framework of the EU project “A Generic Active Vibration Control System of Surfaces” (GASS – Contract No: BRPR-CT96-0243). LFME has developed and tested a Black-box type controller for Vibration Control based on Artificial Neural Networks and Genetic Algorithms. In the framework of WT2.13 of MESEMA project LFME has adapted/modified this controller in order to achieve noise reduction inside the fuselage. The main advantage of the proposed algorithm is that it doesn’t use any apriori knowledge about the structural behavior but it is adaptive on any variation of the load and of the structure.

The operation of the controller consists of two stages:

In the first stage an Artificial Neural Network (ANN) is trained in order to provide a model which substitutes the FRFs between the actuators and the microphones. In order to

create the ANN model the actuators are driven by the controller using randomly created vibration patterns in the frequency range of interest. The created vibration patterns of actuators and the resulting noise patterns (which are collected by the microphones) form the exemplar patterns for the training and validation of the ANN. For steady state condition (e.g. Level flight) the ANN can be determined once, at the beginning of the level flight, and used for the rest of the flight.

In varying conditions (e.g. take off or landing) assuming adequate computing power of the controller the ANN can be adapted continuously over predetermined time intervals (e.g. 15 seconds). In the second stage, using the model provided by the ANN, the Genetic Algorithm searches for the optimal vibration input patterns to the actuators which will lead to the maximum noise reduction at the microphones. The efficiency of the controller is determined only by the accuracy of the ANN model. The accuracy of the ANN model , for its determination over a predefined time interval (e.g 30sec-2min) depends directly on the available computational power of the controller (i.e. multiplicity of excitation/noise patterns).

DESCRIPTION OF THE EXPERT SYSTEM

The basic steps of the proposed controller, are:

1. In the first step, the primary noise field, is acquired by the sensor network.
2. The primary noise field is analyzed by FFT, and the information derived is the frequencies of the most dominant spectrum components (global peaks) and the measured values (acoustic pressure) by all sensors at these frequencies.
3. The third step comprises the (random) excitation of the vibrating structure, at each of the selected frequencies and for each actuator separately. The corresponding amplitudes and phase differences are randomly set. The excitation signals of this step comprise, along with the response of the system, the exemplar patterns for the ANN's training and validation performed in the next step. Therefore, this step is repeated until the desired number of patterns is generated.
4. An ANN is trained in this step, using the exemplar patterns created in step 3. The outcome of this step, are the weights and biases of each neuron of the ANN, which are stored in a file. With the use of these values, the ANN is capable of predicting the magnitude reduction of of the noise field, given the amplitude and phase of the excitation signal that is driven to each actuator. The trained ANN is then used by the GA in the next step, as a model of the vibrating structure.
5. In this step, a Genetic Algorithm is executed and determines the optimal signals i.e., frequency, amplitude, phase, for each actuator, that will produce to the maximum reduction of the noise field.
6. Finally, in this step, the actuators are being driven by the optimal excitation signals that the GA determined, while at the same time, the residual field can be monitored in the frequency domain.

ANN MODELLING OF THE STRUCTURE

In order for the Genetic Algorithm to work a model of the system (the vibrating structure) is required. This model is implemented by an Artificial Neural Network (ANN). The ANNs offer a powerful way to model almost every system, without need for information about the system itself. In order to build an ANN model all is needed is a collection of excitation signals which are send to the structure and the response of the structure to these signals (which response is measured through an acquisition system).

The procedure for the use of the ANN in an application has four steps:

1. Selection of the ANN that will be used. In this step the parameters of the architecture of the ANN are defined. These parameters are the number of layers that will be used the number of neurons in each layer, the activation functions, and the algorithm that will be used for the training of the ANN. All these terms, along with the detailed description of the following two steps (training and validation of the ANN) are discussed in the third part of this report where basic aspects of the ANN theory are presented.
2. Training of the selected ANN. This step comprises of two substeps. First several sets of training data are collected. Each training data set consists (in the general case) of an input vector and a vector of the output data which correspond to the input. In the second substep the training of the ANN takes place. During the training process, the ANN adapt its set of biases and weights according to the rules defined by the selected training algorithm (also referred to as learning algorithm or learning rule), in order to achieve a specified error goal between the desired output of the training set and the approximation which is produced by the ANN.
3. Validation of the ANN. After the convergence of the training procedure, a new data set is presented to the ANN. This data set has the same structure with the training data set i.e. it consists of an input vector and a corresponding output vector. The ANN predicts the output and the error between the desired output and the prediction given by the ANN is recorded. This error should be less than or equal to the error goal used during the training procedure, in order to accept this set of biases and weights. If this error is greater than the error goal then the training procedure starts all over until a set of biases is produced that during the validation achieves an error less than the error goal.
4. Application of the ANN. After a successful validation the set of biases and weights produced comprise the required model of the system.

Although the above described procedure seems straight forward, its application requires besides a good knowledge of the theory of the ANNs and a very good understanding of the physics of the problem under consideration. The knowledge of the theory of ANNs helps to select the most appropriate type of the ANN and the algorithm that should be used for its training. The knowledge of the physics of the problems on the other hand is required in order to develop an efficient ANN architecture. It should be mentioned at this point that a specified ANN architecture may be used in many different

applications. However its performance and efficiency depends on the specific application. It may converge within short time with high accuracy (small error goal) for one application, and converge after long time, or even fail to converge for another application.

This report gives in section 7 (Appendix 1) the basic theory related to the ANNs and in section 3.1 describes the parameters which are used in the current application, and how the above mentioned procedure (from the selection until the application of the ANN is implemented).

Description of the current application

In the current application, an ANN is used to simulate the vibrating structure. In order for this to be achieved the input of the ANN are the signals which would be driven to a specific actuator, and the outputs of the ANN are the corresponding signals which will be monitored by all sensors (microphones). Provided that the analysis is done in the frequency domain the total number of ANNs is calculated by the number of frequencies of interest (peaks of the primary disturbance field) multiplied by the number of actuators.

The ANNs used are feedforward networks, with two hidden layers (leading to a total of four layers). As mentioned in the Appendix 1, where the theory of ANNs was presented, the number of neurons in the input and the output layers, are defined by the application at hand. Each ANN has as input the signals (amplitudes, phases) which would be used for the excitation signals, and as outputs the from the sensors at the selected frequency. The output of the ANN is formed by the frequency response (amplitude and phase) of each sensor.

As already mentioned, the ANN is used by the Genetic Algorithm, embedded in the Expert System as a model of the vibrating structure. The Expert System will work only for specific frequencies. The primary field is detected and the dominant frequencies (the frequencies with the largest amplitudes) are selected. Then, only these frequencies are used for the excitation signals. Thus, the ANN needs only to work for these frequencies. For the creation of the training set each actuator is excited at all these frequencies.

Training subroutine

The training procedure has the following inputs:

1. the number of layers used in the network
2. an array holding the number of neurons in each layer
3. the number of patterns which will be used for the training
4. the training set split into two matrices, one holding the input the other holding the target output
5. the parameters which control the training procedure, namely
 - a) the initial value for the learning rate (recall that the algorithm adjust the learning rate according to the performance of the network)
 - b) the error goal (i.e. the error that the network must achieve in order to stop the learning procedure)
 - c) the maximum number of iterations that could be done during the training procedure (in which iterations the weights and biases are adapted)
 - d) the factors for the adaptation of learning rate, namely the factor for increment, the factor for decrement and the tolerance of the errors between to successive iterations.
 - e)

6. the name of the file where the weights and biases of the converged ANN will be stored.
7. various auxiliary matrices required by the subroutine. The subroutine reinitializes these matrices to zero before their use.

The outputs of the subroutine are two matrices

1. the first holding the weights of the trained ANN
2. the second holding the biases of the ANN

The training algorithm used by this subroutine is the Back Propagation learning algorithm as described in the Appendix 1, which utilizes the momentum term and the variable learning rate technique.

THE DEVELOPED GA

The GA that was developed for the problem at hand, according to the general description and the layout that was presented above, is applied in the following steps:

1. Initially the optimization parameters are encoded
2. The initial random population is created
3. The fitnesses of the strings of the initial population are estimated
4. The operators are applied to the population
5. The fitnesses of the offspring population are estimated
6. Each pair of parents and the corresponding pair of offspring are compared with the old and the best two individuals are selected for the new population. This process continues for all pairs.

As it can be seen from above, the first step that is performed is the encoding of the parameter space, i.e., the independent variables of the problem is transformed into a string. This string is used by the GA as the optimization parameter.

For the problem at hand, the following encoding was selected: the string has a total value of $(6 * \text{number_of_actuators})$ "genes" which are actually positions in a 1D array. Each string is divided into substrings, each one corresponding to each actuator. The first gene of the substring is devoted to the available frequency values for the actuator and the gene represents a specific frequency. The next 3 genes are devoted to the phase values of the actuators taking values from 1 to 360 with step 1. The next two genes are devoted to the amplitude of the actuator taking 100 values between the smaller and the largest value available.

In the second step of the application of the GA, the initial population is created randomly. The genes that represent the frequencies can take values in the range of 1 to

the number of frequency peaks, each value corresponds to a different frequency that is read from the array that contains the frequency values.

The third step in the application of the GA is the calculation of the fitness of each string. This will be done after the proper fitness function has been defined. In order for this to be achieved, the objective of the GA has to be expressed in a mathematical relationship.

The objective of this GA is to find the proper combination of frequency, amplitude and phase for all actuators that are placed on the vibrating surface to create a secondary noise that will be able to reduce the effect of the primary field that the vibrating surface is subjected to, thus resulting in a residual field with reduced vibration amplitudes at the selected frequencies.

In order to achieve this, a correct fitness function has to be defined that will be able to provide us with the necessary information, which in our case is: does the string that was produced by the GA give a good reduction?

From the above it is evident that in order to apply this fitness functions, there had to be some kind of function that would take as input information from the string that was created and it would give as output a measure of the reduction that is accomplished with the given string values. The role of that function here is played by the ANN.

The ANN provides a model of the vibrating surface to be controlled, thus for any given combination of frequency, amplitude and phase for an individual actuator, the ANN predicts the response of the vibrating surface at each sensor location.

Therefore the fitness function that is used is the following:

$$\sum_{i=1}^k \sum_{j=1}^m \frac{P_{i,j}}{R_{i,j}}$$

Where k is the number of frequencies, m is the number of sensors, $P_{i,j}$ is the Primary field of the sensor j at the frequency i and $R_{i,j}$ is the residual field after the control of the sensor j at the frequency i .

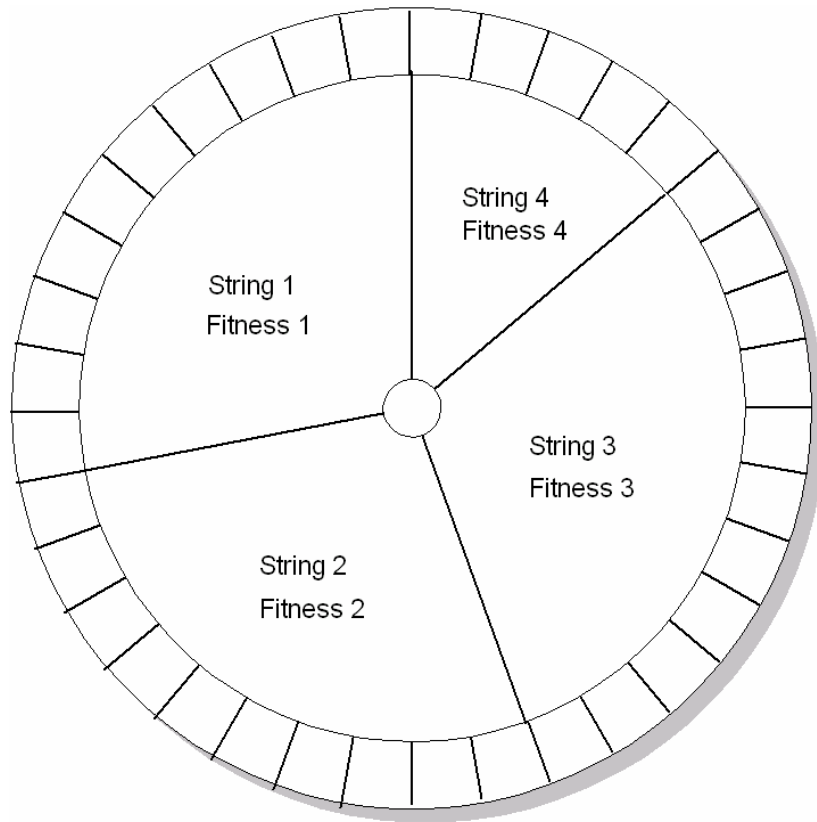
Since the desired response of the plate to a given string should tend to give small residual field, then the best strings are the ones that have larger fitness values.

In the fourth step, the reproduction, crossover and mutation operators are applied:

- **Reproduction.** The fitness function F is used in the classical "roulette" wheel (figure 1) reproduction operator that gives higher probability of reproduction to the strings with better fitness.
- **Crossover.** When the crossover operator is applied, depending on the random number that has been selected for the crossing point, all genes to the left of the crossing point are exchanged.

Mutation. This operator is applied to each gene and it alters its content, with a small probability.

The mutation operator is applied to each gene of each string separately. As mentioned above, the mutation operator is actually a random number that is selected and depending if it is in the predefined limit, it changes the value of a gene also randomly.



Population of 4 Strings
 Fitness 3 > Fitness 1 > Fitness 2 > Fitness 4

Fig. B 1: Mechanical Model for the reproduction operator

In the fifth step the fitness of the offspring is calculated as mentioned above.

In the sixth and final step both parent and offspring populations are compared in pairs, which means that the offspring are compared with their corresponding parents, from which they were created. After the comparison has been made, the two strings with the best fitness, of both parents and offsprings, are selected to “inhabit” the new population for the next generation.

From the application of these operators to the population, a new population is created, as it was mention earlier. The generation of the new populations, from the old ones, continues in a similar manner, until a maximum number of predefined generations has been reached.

SIMULATION RUNS

The proposed control algorithm has been evaluated using experimental data from an aircraft skin panel (fig. 2) available at DII-SUN laboratory. A set of three piezoceramic actuators (ACX Qp20n) and three PCB accelerometers (1V/g) has been used in combination with a dSPACE DS1005 rapid prototyping control system (16-bit A/D channels 12-bit D/A channels). Time domain series of the sensor and actuator signals were provided in .mat files format. The following data has been used:

- The primary noise disturbance at the three sensors (2 seconds duration).
- The response of the sensors (acceleration m/sec²) for random actuator excitation. The actuators had random amplitude and phase at the dominant frequencies of the primary disturbance field. The duration of the excitation was 2 seconds for each actuator.

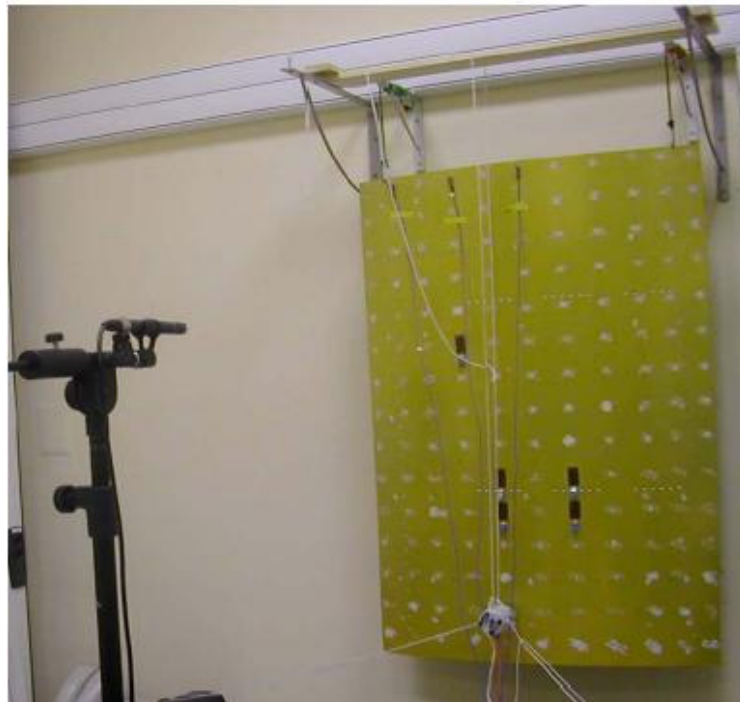


Fig. B 2: the aircraft skin panel used in the simulations.

The spectrum of the primary disturbance field has three peaks at 160, 320 and 440 Hz respectively (freq1, freq2 and freq3). The data from the random excitation of each actuator was windowed using a hamming window and was transformed by a 512 points FFT. From these frequency domain data a training set was formed. It consisted of 9 subsets each subset correspond to a specific actuator (among the three) activated at a specific frequency (among the 160, 320 and 440 Hz). 9 back-propagation ANNs have been trained using these data sets. The convergence of the training algorithm is depicted in figure 3 where the mean square error of each training is presented.

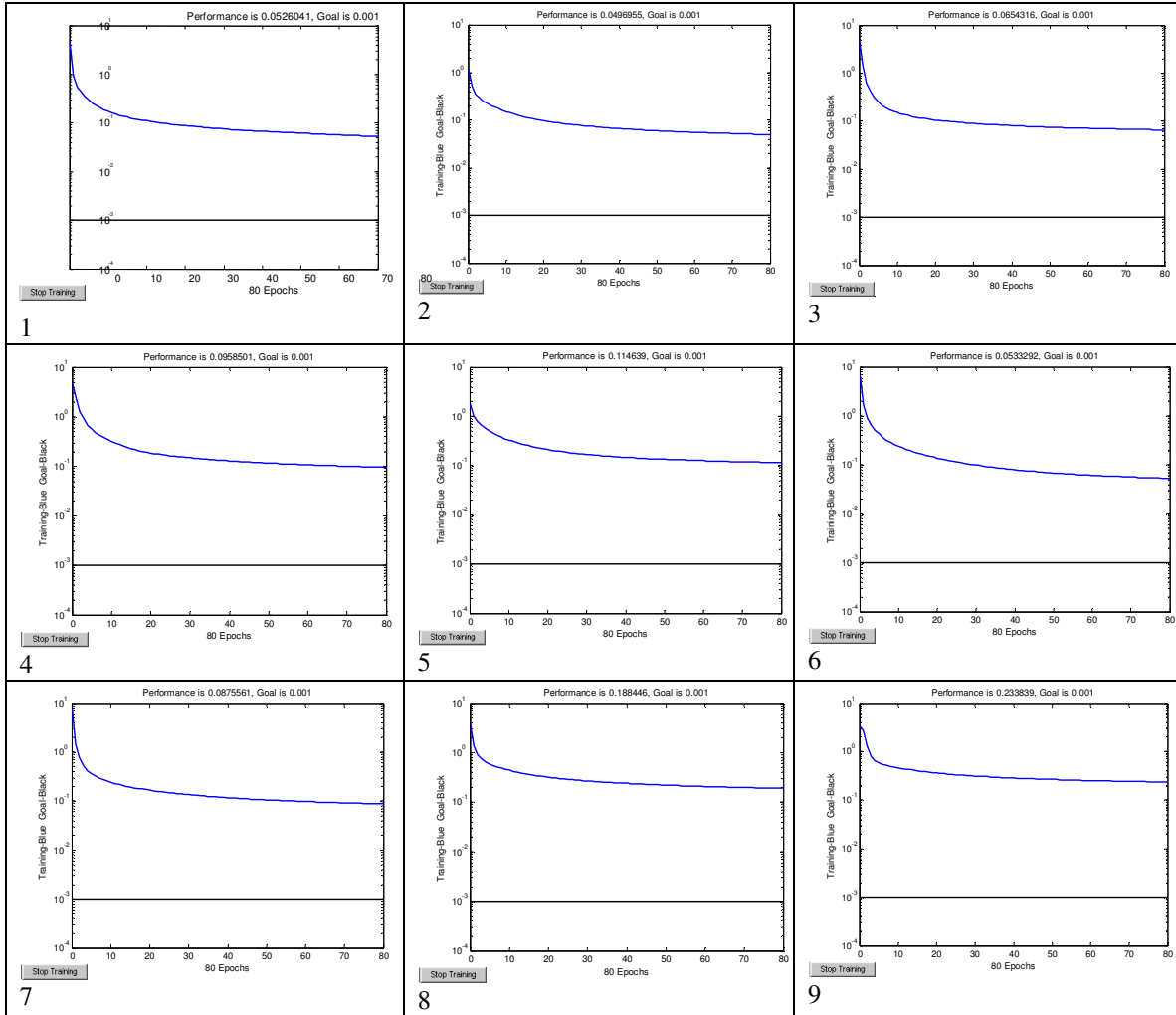


Fig. B 3: The Mean Squared Error for each sub-ann

In the next step the Genetic Algorithm has estimated the optimal actuator signals in order to minimize the residual signal at the sensors. In this report two approaches have been tested. In the first it was assumed that each actuator is activated at only one frequency while in the second approach each actuator is simultaneously activated at the three dominant frequencies of the primary disturbance field. Both approaches have been evaluated in 5 simulations with different primary fields. After 50 generations the results of both approaches are depicted in figures B4 to B13.

The results of the first simulation are presented in figures B4 and B5. In figure B4, the results of the first approach where each actuator activates at only one frequency are depicted. The results are not very satisfactory and we notice that in most of the cases the residual field (after the application of the controller) is larger than the primary vibration field. This can be explained from the fact that the algorithm can focus on a specific frequency giving good results for the specific frequency while the rest of the frequencies are not represented at any actuator.

On the other hand the simultaneous activation at all frequencies of interest at all the actuators is most effective giving very encouraging results. From figure B5, we notice the

almost perfect elimination of the primary disturbance at all the sensors (except sensor2 at the 320 hz).

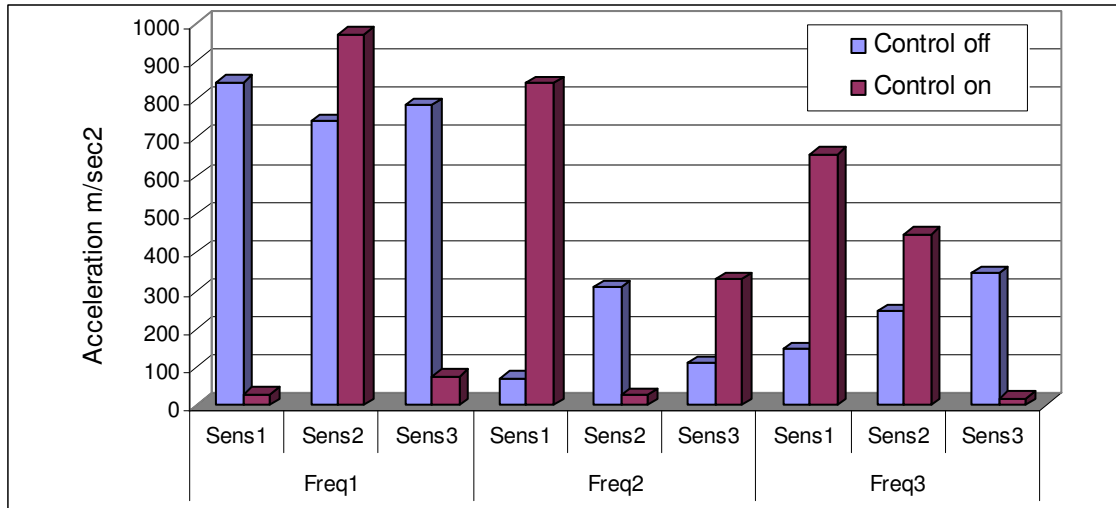


Fig. B 4: Results of the 1st approach where each actuator activates at only one frequency.

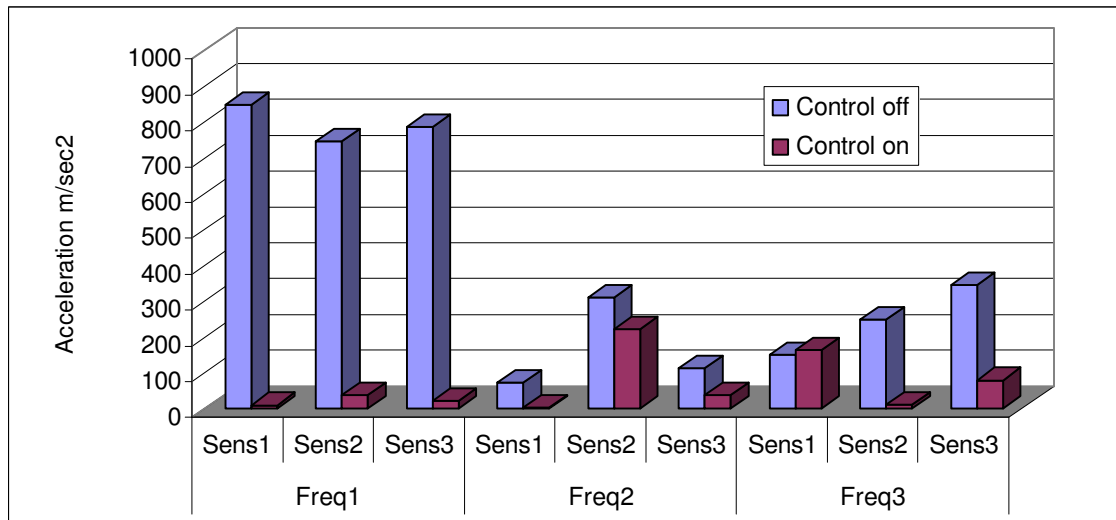


Fig. B 5: Results of the 2nd approach where each actuator activates at all the three frequencies.

The results of the second simulation with different primary excitation, are presented in figures B6 and B7. In figure B6, the results of the first approach where each actuator activates at only one frequency are depicted. The results are once again not very satisfactory and we notice that the “frequency 2” (320 Hz) is not affected at all. On the other hand the second approach gives very good results. From figure B7, we notice the almost perfect elimination of the primary disturbance at all the sensors (except sensor1 at the 320 hz).

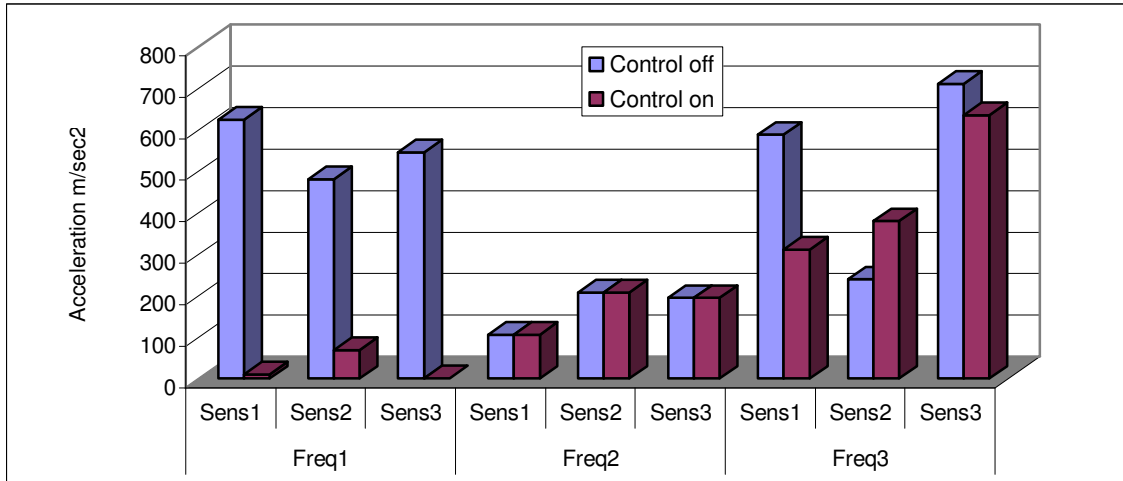


Fig. B 6: Results of the 1st approach where each actuator activates at only one frequency.

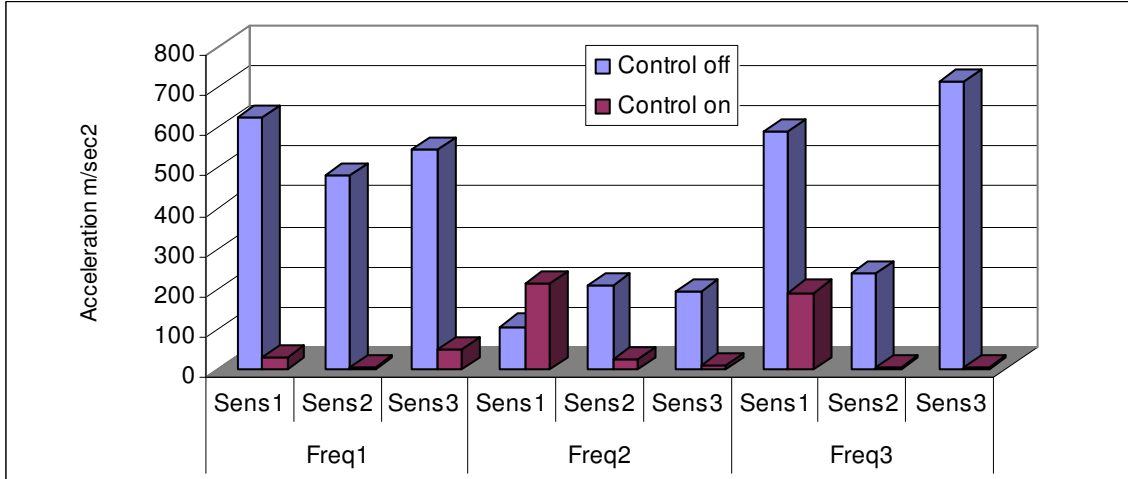


Fig. B 7: Results of the 2nd approach where each actuator activates at all the three frequencies.

Similar results have been achieved in the 3rd simulation. This time in the 1st approach (figure B8) the frequency 3 was not represented while in the frequencies 1 and 2 the reduction was significant. The second approach (figure B9) has shown a very good performance at almost all sensors and in all the frequencies of interest.

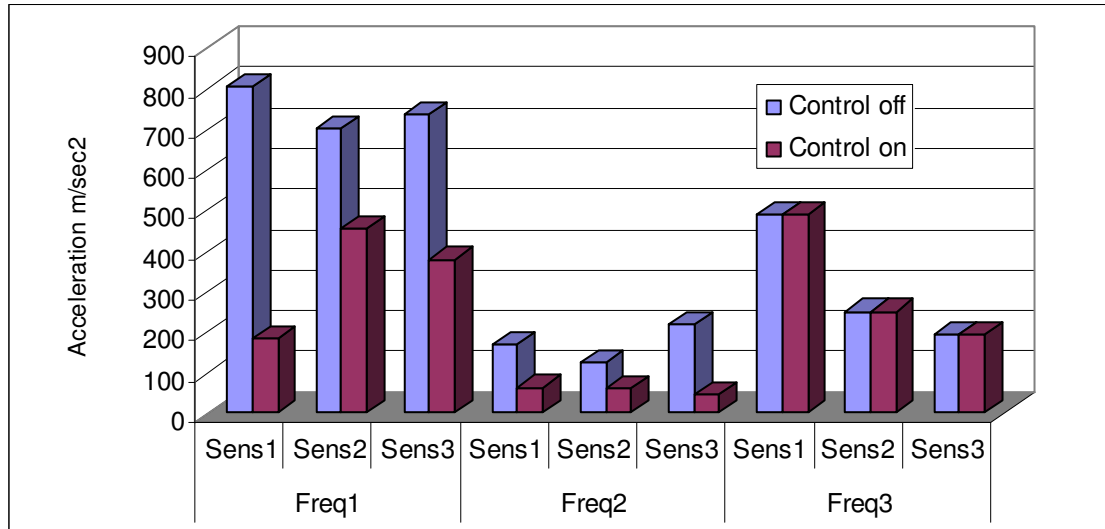


Fig. B 8 Results of the 1st approach where each actuator activates at only one frequency.

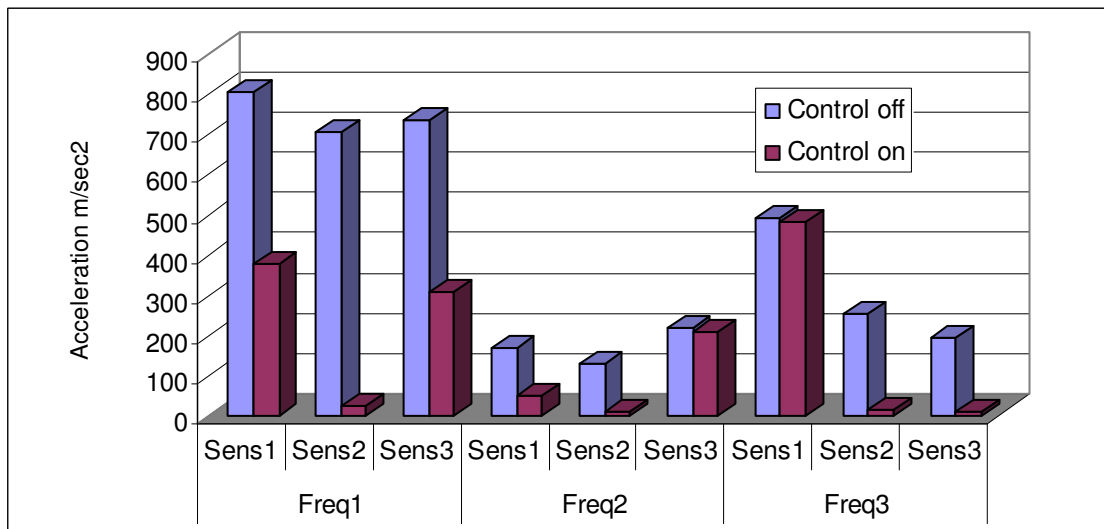


Fig. B 9: Results of the 2nd approach where each actuator activates at all the three frequencies.

Similar results have been achieved in the last two simulations. Using the 1st approach Frequency 3 was still not represented while in the frequencies 1 and 2 the reduction was significant. The second approach still holds the very good performance at almost all sensors and in all the frequencies of interest.

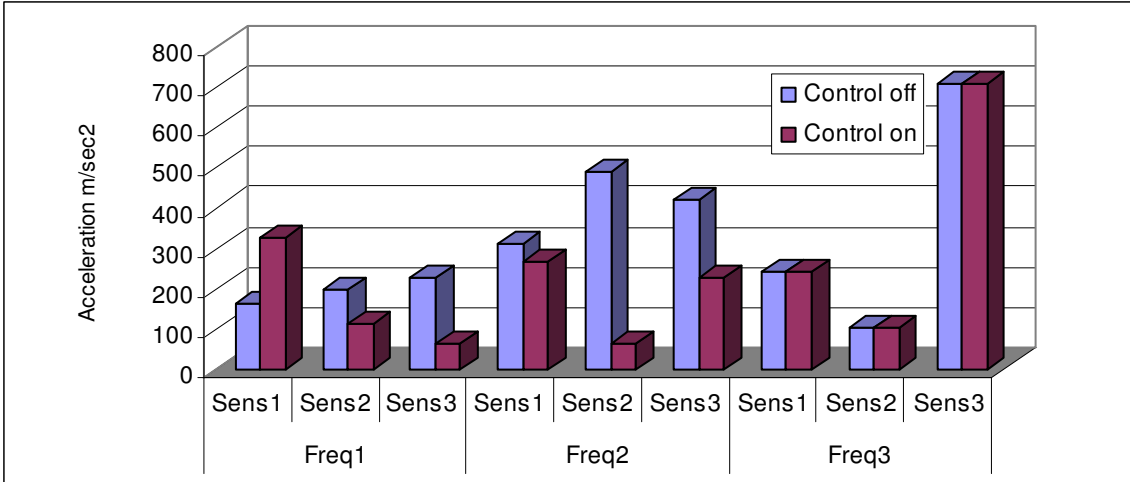


Fig. B 10: Results of the 1st approach where each actuator activates at only one frequency.

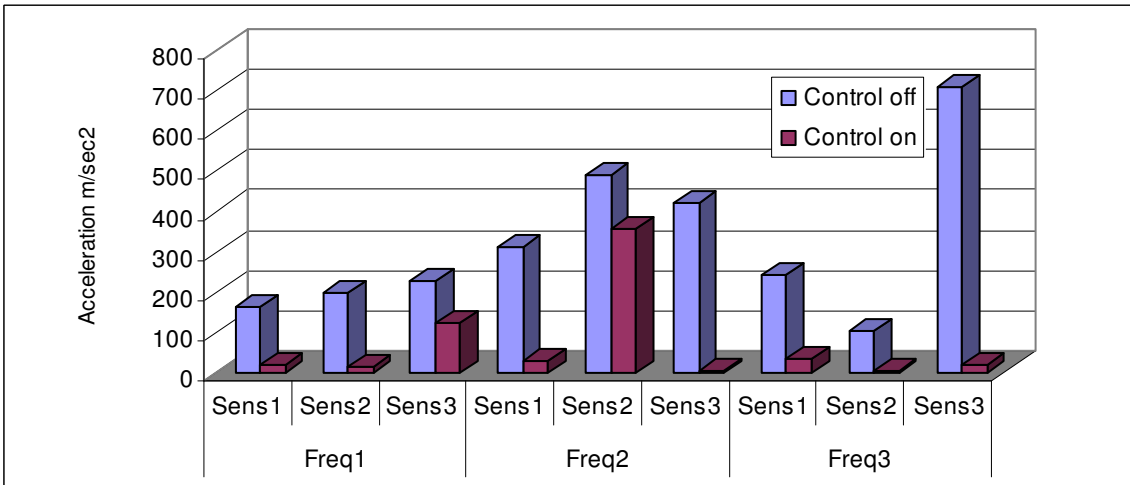


Fig. B 11: Results of the 2nd approach where each actuator activates at all the three frequencies.

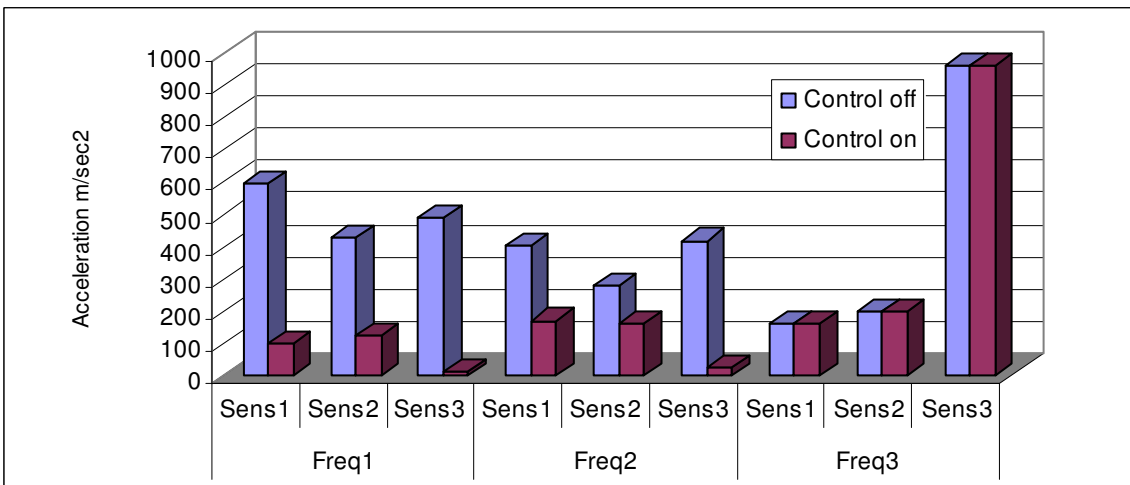


Fig. B 12: Results of the 1st approach where each actuator activates at only one frequency.

In conclusion, in this contribution LFME has presented a controller for the proper activation of the actuators in order to achieve noise reduction inside the fuselage. The main advantage of the proposed algorithm is that it doesn't use any a priori knowledge about the structural behavior but it is adaptive on any variation of the load and of the structure. The presented work is a modification of a previous vibration controller that has been developed and tested by LFME in the framework of GASS project (GASS – Contract No: BRPR-CT96-0243). The controller consists of two stages: in the first stage an Artificial Neural Network (ANN) is trained in order to provide a model which substitutes the FRFs between the actuators and the microphones while in the second stage, using the model provided by the ANN, a Genetic Algorithm searches for the optimal vibration input patterns to the actuators which will lead to the maximum noise reduction. In the report at hand two approaches have been tested. In the first it was assumed that each actuator is activated at only one frequency while in the second approach each actuator is simultaneously activated at the three dominant frequencies of the primary disturbance field. Both approaches have been evaluated in 5 simulations with different primary fields using experimentally derived data. The results were very encouraging especially for the second approach in which very high reduction rates has been achieved.

NOISE CONTROL ALGORITHM PROPOSED BY DII-SUN

DII-SUN has proposed a two level control algorithm, composed by a low-level control for the linearization of actuators behaviour and an high-level control for the noise reduction. A model-following control algorithm, designed on the basis of an experimentally identified dynamic model, has been adopted as the low-level control algorithm in order to overcome the limitation and negative effects of actuators' nonlinearities within the main control system.

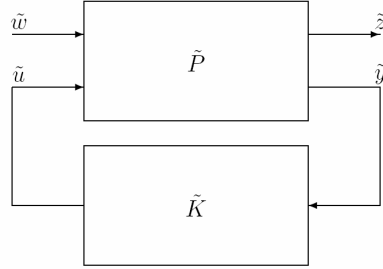


Fig. B 13: Standard control problem

For the high-level control algorithm a model based optimal H_∞ controller has been designed. In the actual implementation low frequencies must be filtered out, otherwise the very low frequency components of the measured signal would saturate the actuators, thus resulting in a very poor control performance. In the application at hand the low frequencies components are due to the rigid-body dynamics, that is immaterial in vibration control and is obviously sensed by an accelerometer, or noise frequencies below 20Hz, to which the human ear is insensitive.

The control problem has been modelled as a standard control problem reported in Fig. B14, where the structure of the plant \tilde{P} can be described by the equations

$$\begin{aligned}\dot{x} &= Ax + \tilde{B}_w \tilde{w} + \tilde{B}_u \tilde{u} \\ \tilde{z} &= \tilde{C}_z x + \tilde{D}_{zu} \tilde{u} \\ \tilde{y} &= \tilde{C}_y x + \tilde{D}_{yw} \tilde{w}\end{aligned}$$

being $x = (x_1^T \ x_2^T)^T \in R^{2n}$ the state vector, $\tilde{u} \in R^m$ the control input, $\tilde{y} \in R^m$ the measured (control) output, $\tilde{w} \in R^{n+m}$ the disturbance (state and measurement disturbances), $\tilde{z} \in R^{n+m}$ the performance output. Moreover, \tilde{D}_{zu} and \tilde{D}_{yw} are assumed full column- and row-rank, respectively. The above hypothesis implies that scaling transformations can be found such that the D 's matrices assume a simpler (normalized) structure. In fact, consider non-singular transformations S_u and S_y , and unitary transformations Q_w , Q_z , all of suitable dimensions, and define scaled variables w , u , z and y by

$$\tilde{u} = S_u u, \quad \tilde{y} = S_y y, \quad \tilde{w} = Q_w w, \quad \tilde{z} = Q_z z$$

it is possible to choose the scaling matrices S_w , S_u , Q_w , Q_z such that

$$D_{zu} = Q_z \tilde{D}_{zu} S_u^{-1} = \begin{pmatrix} 0 \\ I \end{pmatrix}$$

$$D_{yw} = S_y \tilde{D}_{yw} Q_w^H = \begin{pmatrix} 0 & I \end{pmatrix}$$

and the scaled model becomes

$$\begin{aligned} \dot{x} &= Ax + B_w w + B_u u \\ z &= C_z x + D_{zu} u \\ y &= C_y x + D_{yw} w \end{aligned}$$

where $B_w = \tilde{B}_w Q_w^H$, $B_u = \tilde{B}_u S_u^{-1}$, $C_z = S_y \tilde{C}_z$, with

$$A = \begin{pmatrix} 0 & I \\ -\Omega & -\Lambda \end{pmatrix},$$

$$B_w = \begin{pmatrix} 0 & 0 \\ B_{2w} & 0 \end{pmatrix}, B_u = \begin{pmatrix} 0 \\ B_{2u} \end{pmatrix},$$

$$C_z = \begin{pmatrix} 0 & B_{2w}^T \\ 0 & 0 \end{pmatrix},$$

$$C_y = \begin{pmatrix} 0 & B_{2u}^T \end{pmatrix},$$

$$\Omega = \text{diag}(\omega_1^2, \dots, \omega_n^2), \Lambda = \text{diag}(2\zeta_1\omega_1, \dots, 2\zeta_n\omega_n)$$

A selection of the disturbance matrix B_{2w} is proposed in order to design a strongly stabilizing H_∞ controller with a set of m zeros at the origin, so as to guarantee bandpass properties to the controller

$$B_{2w} = (\alpha\Lambda + B_{2u}B_{2u}^T)^{1/2}$$

where $\alpha > 0$ is a scalar coefficient to be suitably selected. The matrix B_{2w} is composed by two terms: the first weights disturbances in the range of B_u , while the other tries to consider also off-range terms, in particular by weighting the system natural modes. Note that all the modes are weighted, and thus H_∞ design will try to reduce structural peaks due to vibration modes and to increase robustness with respect to *matched* disturbances (i.e. in the range of the control input matrix). With this choice of the disturbance matrix, a stable H_∞ controller is derived with bandpass frequency shape. The controller has the form

$$K_\infty(s, \gamma) = -\frac{\gamma^2}{\gamma^2 - 2} B_u^T (sI - A_\infty)^{-1} B_u$$

where

$$A_\infty = \begin{pmatrix} 0 & I \\ -\Omega & -\Lambda_\infty \end{pmatrix}$$

and

$$\Lambda_\infty = \left(1 - \frac{2}{\gamma^2}\right) \Lambda + 2\frac{\gamma^2 - 1}{\gamma^2 - 2} \sqrt{\frac{\gamma^2 - 1}{\gamma^2}} B_{2u} B_{2u}^T.$$

EXPERIMENTAL RESULTS WITH THE TEST ARTICLE

The proposed algorithm has been tested on the lab-scale test article shown in Fig. B2. The performances in terms of vibration reduction are presented in Fig.B15, while the results of the active noise control are reported in Fig. B16.

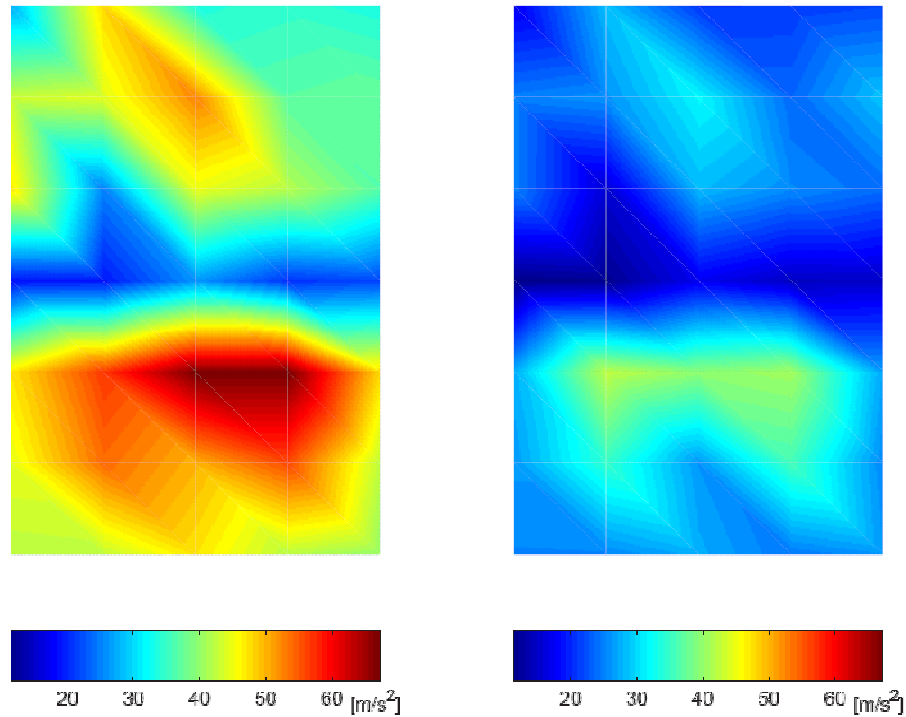


Fig. B 14: Active vibration control

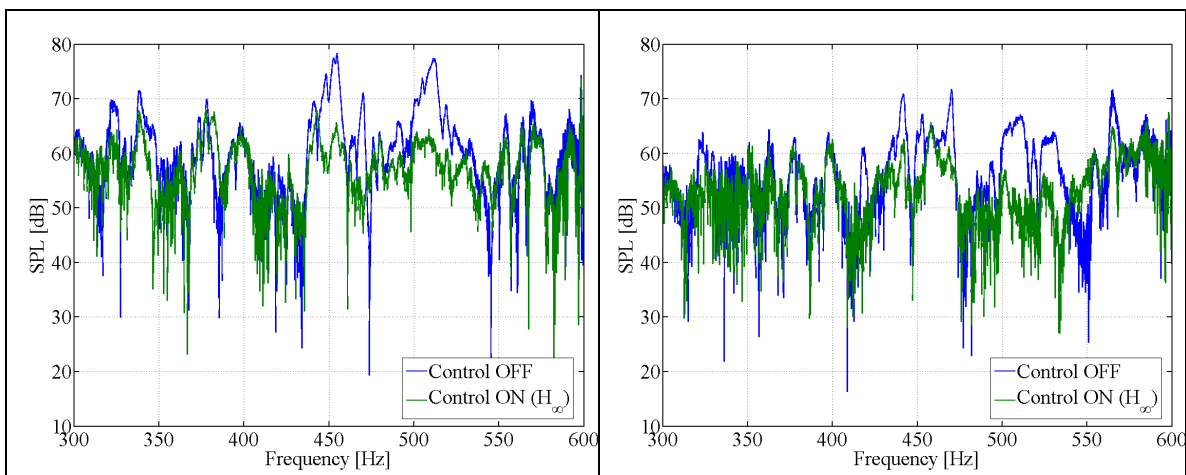


Fig. B 15 Noise reduction

SELECTION OF FINAL NOISE CONTROL ALGORITHM

As agreed with all the partners involved in Task 2.1, the selection of the final noise control algorithm to implement on the full-scale mock-up has been made according to the results obtained on the lab-scale test article and taking into account the specific features of each algorithm. In particular, the approach proposed by DII-SUN has been selected with the following motivations:

- a PC-based implementation of the LFME’s algorithm could be feasible but further investigation is need for a real-time implementation
- due to the actual complexity of input data handling procedures it will be hard for LFME to set up and provide a “user friendly” version of the algorithm before the end of the project
- the LFME’s algorithm has been tested only with a tri-tonal primary field and not with a broadband disturbance as required by the specifications
- the simulations of the LFME’s algorithm have been performed only for a feedforward active vibration control with no experimental testing